

THE UNIVERSITY OF HULL

**INVESTIGATION OF A SUPER PERFORMANCE
DEW POINT AIR COOLER AND ITS APPLICATION
IN BUILDINGS**

being a Thesis submitted for the Degree of Doctor of Philosophy

at the University of Hull

by

Peng XU

MSc Beijing University of Civil Engineering and Architecture

BEng Shandong Jianzhu University, China

August 2017

CONTENTS INDEX

CONTENTS INDEX	I
PUBLICATIONS	VI
ACKNOWLEDGEMENTS	IX
ABSTRACT	X
LIST OF FIGURES	XII
LIST OF TABLES	XVI
ABBREVIATIONS.....	XIX
NOMENCLATURE	XXI
CHAPTER 1: INTRODUCTION	1
1.1 RESEARCH BACKGROUND	1
<i>1.1.1 Demands for Sustainable Building Cooling</i>	<i>1</i>
<i>1.1.2 Evaporative Cooling Technology</i>	<i>4</i>
1.2 RESEARCH OPPORTUNITY, AIM AND OBJECTIVES.....	7
1.3 RESEARCH METHODOLOGY	9
1.4 RESEARCH NOVELTIES.....	12
1.5 THESIS STRUCTURE	14
CHAPTER 2: LITERATURE REVIEW	16
2.1 CHAPTER INTRODUCTION	16
2.2 BASIC CONCEPT AND THEORY, CLASSIFICATION AND PERFORMANCE EVALUATION STANDARDS OF EVAPORATIVE COOLING TECHNOLOGY.....	17
<i>2.2.1 Basic Concept and Theory of Evaporative Cooling</i>	<i>17</i>
<i>2.2.3 Relevant Technical Criteria and Performance Evaluation Standards</i>	<i>24</i>
2.3 R&D PROGRESS AND PRACTICAL APPLICATIONS OF IEC TECHNOLOGIES.....	32
<i>2.3.1 Overview of R&D works in the IEC Field</i>	<i>32</i>
<i>2.3.2 Theoretical Innovation</i>	<i>33</i>
<i>2.3.3 Research Progress in IEC Technologies</i>	<i>36</i>
<i>2.3.4 Analysis of Dew Point Cooling Research</i>	<i>49</i>
<i>2.3.5 Application and Socio-economic Assessment</i>	<i>85</i>

2.4 POTENTIAL OPPORTUNITIES IN THE DEVELOPMENT OF DEW POINT COOLING.....	87
<i>2.4.1 Structure Optimization of the HMX to Reduce Flow Resistance and Enlarge the Effective Surface</i>	<i>87</i>
<i>2.4.2 New Wetted Material to Promote Evaporation</i>	<i>87</i>
<i>2.4.3 Development of Dedicated Computer Simulation Tools</i>	<i>88</i>
<i>2.4.4 Water Consumption and Contamination</i>	<i>89</i>
<i>2.4.5 Comprehensive Evaluation of the System in Real Climatic Conditions</i>	<i>89</i>
2.5 DEVELOPMENT OF THE DEW POINT IEC TECHNOLOGY IN THE PHD PROJECT.....	89
2.6 CHAPTER SUMMARY.....	90
CHAPTER 3: CONCEPTUAL DEVELOPMENT AND	
COMPUTERISED SIMULATION	92
3.1 CHAPTER INTRODUCTION	92
3.2 SYSTEM DESCRIPTION AND WORKING PRINCIPLE	93
3.3 AIRFLOW ORGANIZATION AND THERMODYNAMIC ANALYSIS OF THE AIR TREATMENT PROCESS	95
<i>3.3.1 Airflow Organization inside the HMX.....</i>	<i>95</i>
<i>3.3.2 Thermodynamic Analysis of the Air Treatment Process</i>	<i>97</i>
3.4 NUMERICAL MODEL SETUP AND MASS AND ENERGY CONSERVATION ANALYSIS... 101	
<i>3.4.1 Numerical Model Setup and Related Assumptions</i>	<i>101</i>
<i>3.4.2 Mass and Energy Conservation Analysis</i>	<i>103</i>
3.5 METHODOLOGY AND PARAMETERS ADOPTED TO EVALUATE THE PERFORMANCE. 107	
3.6 COMPUTER MODEL SET-UP AND VALIDATION	110
3.7 RESEARCH OF HEAT AND MASS EXCHANGING PROCESS IN THE CHANNELS..... 115	
3.8 PERFORMANCE STUDY OF THE PROPOSED IRREGULAR HMX	119
3.9 CHAPTER SUMMARY..... 161	
CHAPTER 4: PROTOTYPE DESIGN AND CONSTRUCTION..... 164	
4.1 CHAPTER INTRODUCTION	164
4.2 DESIGN OF THE HEAT AND MASS EXCHANGER (HMX)..... 164	
<i>4.2.1 Design Conditions</i>	<i>165</i>
<i>4.2.2 Heat and Mass Exchanging Sheets</i>	<i>167</i>
4.3 DESIGN OF THE WATER DISTRIBUTOR, WATER SINK AND CONTROL STRATEGY 170	
<i>4.3.1 Water Distributor.....</i>	<i>170</i>
<i>4.3.2 Water Sink</i>	<i>171</i>
<i>4.3.3 Control Strategy.....</i>	<i>172</i>

4.4 SELECTION OF THE FANS AND PUMP	175
4.4.1 Fans	175
4.4.2 Circulating pump.....	181
4.5 MATERIAL SELECTION, PERFORMANCE AND PROCESS TESTING IN HMX FABRICATION.....	182
4.5.1 Aluminium Plate and Moulding Process	183
4.5.2 Fibrous Fabric	186
4.5.3 Adhesive.....	199
4.6 HMX FABRICATION AND PROTOTYPE ASSEMBLY.....	201
4.6.1 HMX.....	201
4.6.2 Water Distributor.....	205
4.6.3 Fan housing, Louvres and Water Sink	207
4.6.4 Fans, Pump and Control Components	208
4.6.5 Prototype Assembly.....	210
4.7 CHAPTER SUMMARY.....	213
CHAPTER 5: TESTING IMPLEMENTION, RESULTS ANALYSIS AND VALIDATION/UPDATE OF THE COMPUTER MODEL	215
5.1 CHAPTER INTRODUCTION	215
5.2 DESIGN OF THE TESTING RIG.....	216
5.3 EXPERIMENTAL INSTRUMENTS AND TESTING SYSTEM.....	218
5.3.1 Intake Air Regulating System	218
5.3.2 Parameters Measurement System.....	220
5.4 IMPLEMENTATION OF THE SYSTEMATIC TESTING.....	225
5.5 PERFORMANCE TESTING AND RESULTS DISCUSSION.....	227
5.5.1 Performance Testing under Various Climates at Working Air Ratio of 0.44 (Test 1)	227
5.5.2 Identification of the Optimum Working Air Ratio (Test 2)	230
5.5.3 Performance Comparison between the Prototype and the M30 DPC (Test 3).....	232
5.5.4 Performance Testing under Various Intake Air conditions at the Optimum Working Air Ratio of 0.364 (Test 4).....	233
5.5.5 Cases for Different Cooling Outputs at the Optimum Working Air Ratio of 0.364 (Test 5)	234
5.6 VALIDATION AND UPDATE OF THE SIMULATION TOOL	239
5.7 CHAPTER SUMMARY.....	244

CHAPTER 6: ENERGY SAVING, ECONOMIC, AND ENVIRONMENTAL PERFORMANCE ANALYSES	246
6.1 CHAPTER INTRODUCTION	246
6.2 ANNUAL OPERATIONAL PERFORMANCE	247
<i>6.2.1 Application Conditions for Evaluation</i>	<i>247</i>
<i>6.2.2 Weather Profiles and Operational Conditions</i>	<i>248</i>
<i>6.2.3 Hourly Energy-Saving Potential for Summer Cooling Days in Beijing</i>	<i>252</i>
<i>6.2.4 Annual Energy-Saving Potential</i>	<i>258</i>
6.3 LIFE-CYCLE ECONOMIC ANALYSIS.....	263
<i>6.3.1 Capital Cost.....</i>	<i>263</i>
<i>6.3.2 Annual Operational Cost and Saving</i>	<i>264</i>
<i>6.3.3 Annual Maintenance Cost.....</i>	<i>265</i>
<i>6.3.4 Cost Payback Period and Life-cycle Net Cost Saving</i>	<i>267</i>
6.4 LIFE-CYCLE ENVIRONMENTAL BENEFITS.....	269
<i>6.4.1 Greenhouse Gas (GHG) Emission</i>	<i>269</i>
<i>6.4.2 Water Use Issues.....</i>	<i>270</i>
6.5 CHAPTER SUMMARY.....	271
CHAPTER 7: CONCLUSIONS AND FURTHER WORK.....	273
7.1 CONCLUSIONS.....	273
<i>7.1.1 Application of New Materials and New Processes</i>	<i>273</i>
<i>7.1.2 Computer-Aided Design, Optimization and Prediction Tool</i>	<i>274</i>
<i>7.1.3 Numerical Investigation</i>	<i>275</i>
<i>7.1.4 Laboratory Testing</i>	<i>276</i>
<i>7.1.5 Socio-Economic Assessment</i>	<i>277</i>
7.2 PROBLEMS AND FURTHER OPPORTUNITIES	278
<i>7.2.1 Cooler Structure and Manufacture.....</i>	<i>278</i>
<i>7.2.2 Numerical Simulation</i>	<i>279</i>
<i>7.2.3 Experimental Investigation</i>	<i>280</i>
<i>7.2.4 Case Study.....</i>	<i>281</i>
<i>7.2.5 Aware but Uncovered</i>	<i>281</i>
<i>7.2.6 Ideal Cooler</i>	<i>281</i>
REFERENCES	282
REFERENCES FOR CHAPTER 1	282
REFERENCES FOR CHAPTER 2	285

REFERENCES FOR CHAPTER 3	300
REFERENCES FOR CHAPTER 4	301
REFERENCES FOR CHAPTER 5	302
REFERENCES FOR CHAPTER 6	303
APPENDIX 1: PROGRAMME FOR SYSTEM CONTROL IN C- LANGUAGE	305
APPENDIX 2: SIMULATION PROGRAMME IN EES	320
APPENDIX 3: LIFE EXPECTANCY CALCULATION	331

PUBLICATIONS

Book Chapter

1. Xudong Zhao, Xiaoli Ma, **Peng Xu**, Diallo Thierno, Zishang Zhu, and Jinzhi Zhou, Cases of Energy System in a Green Building in UK (Chapter 15), Handbook of Energy Systems in Green Buildings, DOI 10.1007/978-3-662-49088-4_15-1, Springer-Verlag GmbH Germany 2017; pp.1-55.

Journal Publications

1. **Peng Xu**, Xiaoli Ma, Xudong Zhao, Kevin Fancey, Experimental Investigation of a Super Performance Dew Point Air Cooler, *Applied Energy* 203 (2017) 761-777.
2. **Peng Xu**, Xiaoli Ma, Xudong Zhao, Kevin Fancey, Experimental investigation on performance of fabrics for indirect evaporative cooling applications, *Building and Environment* 110 (2016) 104-114.
3. **Peng Xu**, Xiaoli Ma, Thierno Diallo, Xudong Zhao, Kevin Fancey, Deying Li, Hongbing Chen, Numerical investigation of the energy performance of a guideless irregular heat and mass exchanger with corrugated heat transfer surface for dew point cooling, *Energy* 109 (2016) 803-817.
4. **Peng Xu**, Xingxing Zhang, Jingchun Shen, Xudong Zhao, Wei He, Deying Li, Parallel experimental study of a novel super-thin thermal absorber based photovoltaic/thermal (PV/T) system against conventional photovoltaic (PV) system, *Energy Reports* 1 (2015) 30-35.
5. **Peng Xu**, Jingchun Shen, Xingxing Zhang, Xudong Zhao, Yingchu Qian, Case Study of Smart Meter and In-home Display for Residential Behaviour Change in Shanghai, China, *Energy Procedia*, 75 (2015) 2694-2699.
6. **Peng Xu**, Jingchun Shen, Xingxing Zhang, Wei He, Xudong Zhao, Design, Fabrication and Experimental Study of a Novel Loop heat-pipe based Solar Thermal Facade Water Heating System, *Energy Procedia* 75 (2015) 566-571.
7. Xingxing Zhang, Jingchun Shen, Yan Lu, Wei He, **Peng Xu**, Xudong Zhao, Zhongzhu Qiu, Zishang Zhu, Jinzhi Zhou, Xiaoqiang Dong, Active Solar

- Thermal Facades (ASTFs): From concept, application to research questions, *Renewable and Sustainable Energy Reviews* 50 (2015) 32-63.
8. Xingxing Zhang, Jingchun Shen, Wei He, **Peng Xu**, Xudong Zhao, Junyi Tan, Comparative study of a novel liquid-vapour separator incorporated gravitational loop heat pipe against the conventional gravitational straight and loop heat pipes - Part II: Experimental testing and simulation model validation, *Energy Conversion and Management* 93 (2015) 228-238.
 9. Xingxing Zhang, Jingchun Shen, Wei He, **Peng Xu**, Xudong Zhao, Junyi Tan, Comparative study of a novel liquid-vapour separator incorporated gravitational loop heat pipe against the conventional gravitational straight and loop heat pipes - Part I: Conceptual development and theoretical analyses, *Energy Conversion and Management* 90 (2015) 409-426.
 10. Xingxing Zhang, Jingchun Shen, **Peng Xu**, Xudong Zhao, Ying Xu, Socio-economic performance of a novel solar photovoltaic/loop-heat-pipe heat pump water heating system in three different climatic regions, *Applied Energy* 135 (2014) 20-34.

Conference Proceedings and Presentations

- (1) **Peng Xu**, B. Wang, K. Fancey, X. Ma, X. Zhao, Feasibility investigation of a bonding method for fibrous materials and aluminium sheets employed in evaporative cooling systems, 16th International Conference on Sustainable Energy Technologies-World Society of Sustainable Energy Technologies, 17th-20th July 2017, Bologna, Italy.
- (2) **Peng Xu**, Yuting Liu, Xiaoli Ma, Xudong Zhao, Experimental and numerical study on the air flow in the irregular exchanger channels of a counter-flow indirect evaporative cooler, The Belt and Road Initiative International Conference on Sustainable Refrigeration, 19th-21st October 2016, Xi'an, China. (Best paper award)
- (3) **Peng Xu**, Xiaoli Ma, Xudong Zhao, Experimental study on fabrics applied to the wet surface of an indirect evaporative cooler, 15th International Conference on Sustainable Energy Technologies - World Society of Sustainable Energy Technologies, 19th-22nd July 2016, National University of Singapore, Singapore.

- (4) **Peng Xu**, Xiaoli Ma, Yaxuan Xiong, Yongzheng Shi, Deying Li, Xudong Zhao, Numerical Study of Novel Corrugated Heat and Moisture Exchanging Sheets Applied to Counter-Flow Dew Point Air Cooler, 14th International Conference on Sustainable Energy Technologies, 25th-27th August 2015, Nottingham, UK.

Patents

1. Huifeng Bai, Xiangwu Ding, **Peng Xu**, Junming Li, Xudong Zhao, Even liquid distribution of intensive formula, China patent, ZL-2016-2-0563598.X, 2016.11.23 (Authorized).
2. Xudong Zhao, **Peng Xu**, Xiaoli Ma, Kevin Fancey, Junming Li, Xiangwu Ding, Geoff Lockwood, Heat exchanger apparatus, UK patent, GB1617362.7, 2016.10.13 (Filed).

Posters

1. Xudong Zhao, **Peng Xu**, Xiaoli Ma, Kevin Fancey, A Novel Extremely Low-Energy Dew Point Air Cooler, Posters for *the workshop for a Novel Extremely Low Energy Dew Point Air Cooler of Innovate UK Manufacturing Sustainability (with China) Competition Project Jointly funded by Innovate UK/EPSRC/China MOST Project, Hull, 20th February 2017*; *Rushlight Events on cleantech and energy efficiency, London 25th January 2017*.
2. **Peng Xu**, Xudong Zhao, Investigation of a Super Performance Dew Point Air Cooler Applied to Buildings, Poster for *Postgraduate Research Posters at the University of Hull, UK, 20th February 2015*.
3. **Peng Xu**, Xudong Zhao, Simulation Study on Oxy-Fuel Combustion of Manufactured Gas from Coal, Poster for *10th European Conference on Coal Research and its Applications, University of Hull, 15th-7th September 2014*.

ACKNOWLEDGEMENTS

First of all, I would like to express my sincere gratitude to my supervisor, Professor Xudong Zhao. His persistent guidance, encouragement and support have always been with me throughout the whole process of my PhD study. His immense knowledge, enthusiastic involvement and perfectionism in academic set fabulous examples for me. His great ambitions and motivations inspire me to explore further and never stop.

Thanks to the University of Hull for the financial support of International Fee-Bursary. Thanks to Dr Kevin Fancey and Dr Jingsheng Liu for their valuable suggestions during my PhD study. Thanks to Dr Kevin Fancey for his detailed review prior to the publication of each journal paper. Thanks to Dr Xiaoli Ma for her combined efforts in accomplishing the EPSRC/ Innovate UK project. Thanks to the project partners Mr Geoff Lockwood and Mr Jeff Elkins from *ebm-papst UK Ltd.* whose conscientiousness to work deeply impress me. Thanks to the Chinese project partner Mr Xiangwu Ding for his help in prototype manufacturing in China.

Thanks to all the young guys pursuing their PhDs and dreams at Hull along with me during the past memorable four years. Their efforts and excellence impress and inspire me. All the best wishes for them.

I wish to thank Beijing University of Civil Engineering and Architecture, where I got my master degree, grew up to an associate professor and have been servicing ever since 2001. I appreciate the support from the University and all my dear colleagues. I am especially indebted to Professor Suilin Wang, whose recommendation to Professor Xudong Zhao made everything possible.

Finally, I wish to dedicate this PhD thesis to my beloved wife, daughter and parents. I could never have accomplished it without their endless love, continuous support and encouragement.

ABSTRACT

Based on extensive literature reviews, technical opportunities were identified to improve the energy efficiency of a dew point air cooler. This applied research aimed to develop a super-performance dew point air cooler to replace or partly replace the conventional energy-intensive air conditioners applicable to buildings.

This research followed the methodology of combined theoretical and experimental investigation and a procedure of concept formation, validating and updating. A simulation software was developed and validated to investigate the impacts of the geometric configuration and operational conditions on the unit's cooling performance and assist the prototype design. As a result, a novel dew point air cooler prototype, featuring innovative structure of the heat and mass exchanger, application of new materials and new processes, unique water distribution and control scheme and exclusive self-developed simulation software, was constructed and tested under controlled laboratory environment. Two patents were generated, one of which has been authorized by the China State Intellectual Property Office and the other has been filed in the Intellectual Property Office of the United Kingdom.

Under standard testing conditions, i.e. dry-bulb temperature of 37.8°C and the coincident wet-bulb temperature of 21.1°C, the prototype cooler achieved a wet-bulb cooling effectiveness of 114% and dew-point cooling effectiveness of 75%, yielding a significantly high Coefficient of Performance (COP) of 52.5 at the optimal working air ratio of 0.364. The performance testing was also carried out under various simulated conditions representing the climates of hot & dry, warm & dry, moderate, warm & humid and the wet-bulb effectiveness of the prototype kept in the range 112% to 128% and dew-point effectiveness of 67%-76%, giving a COP of 37.4-52.5. Compared to the conventional vapour compression air conditioners which have a COP of around 3, the prototype cooler had 11-17 times higher COP, leading to a reduction in electrical power consumption by around 92% to 94%.

A dedicated case study of the proposed dew point cooler based on conditions in Beijing, a representative city in warm and humid climate, was carried out to predict the annual operational performance, economic rewards, and associated environmental benefits. Compared to the conventional packaged air conditioners, 91.4% of annual power demand could be saved. The annual water consumption is less than 0.3 tonnes to provide the cooling of 2428.1 kWh. And the payback period of static investments would be less than 4 years to replace an equivalent packaged air conditioner.

A significant leap forward has been achieved with this study and this is expected to open enormous global business in the very near future, thus bringing about great economic, environmental and sustainability benefits worldwide.

LIST OF FIGURES

Fig. 1-1: Schematic of IEC cooling.	6
Fig. 1-2: Market profile in relation to the evaporative cooling and dew point cooling.	7
Fig. 2-1: Difference between latent and sensible heat for water.	18
Fig. 2-2: Classification of evaporative cooling systems.	19
Fig. 2-3: Diagram of basic evaporative systems. ^[2.5]	20
Fig. 2-4: Pathways of evaporative cooling in a psychrometric chart. ^[2.6]	21
Fig. 2-5: Cut-away Diagram of a Heat and Mass Exchange Module. ^[2.10]	23
Fig. 2-6: Conceptual psychrometric representation of the staged indirect cooling process with continual purge of secondary/working air. ^[2.11, 2.12]	24
Fig. 2-7: System of a water-side IEC. ^[2.49]	38
Fig. 2-8: Water flow patterns inside an IEC tubular exchanger. ^[2.50]	38
Fig. 2-9: A semi-indirect evaporative refrigerator with tubular exchanger. ^[2.51]	39
Fig. 3-1: 3-D configuration model.	94
Fig. 3-2: 2D-view system design indicating air and water distribution. (Unit: mm)	95
Fig. 3-3: Schematic of airflow and heat and mass transfer.	96
Fig. 3-4: Airflow layout in the proposed HMX.	98
Fig. 3-5: Heat and mass exchange process representing at a psychrometric chart. ^[3.2]	99
Fig. 3-6: Computational channel.	101
Fig. 3-7: Validation of PA temperature between simulation and the published experimental results.	113
Fig. 3-8: Comparison of experimental and simulation results in various climates.	115
Fig. 3-9: Heat and mass exchange progress in the channels.	118
Fig. 3-10: Profile of the corrugation. (Unit: mm)	120
Fig. 3-11(b): Temperature difference between IA and EA.	123
Fig. 3-11: Performance variation with IA temperature (at constant HR).	124

Fig. 3-12: Performance variation with humidity ratio (at constant IA temperature).....	127
Fig. 3-13: Performance variation with humidity ratio (at constant relative humidity).....	130
Fig. 3-14: Variation of cooling performance with HR at various IA temperature.	141
Fig. 3-15: Performance variation with the air velocity.....	144
Fig. 3-16: Variation of performance with the channel height.	147
Fig. 3-17: Variation of performance with the channel length.	149
Fig. 3-18: Variation of performance with the wave form.....	151
Fig. 3-19: Variation of performance with the equivalent diameter.	153
Fig. 3-20: Variation of performance with working air ratio.	156
Fig. 3-21: Variation of performance with the temperature of inlet water.	158
Fig. 3-22: Variation of performance with the temperature of inlet water.	160
Fig. 4-1: Design state variation of primary air on psychrometric chart.....	166
Fig. 4-2: Schematic drawing of the complex heat and mass exchanger.....	168
Fig. 4-3: Sandwich structure of the exchanging sheet.....	169
Fig. 4-4: 3-view drawing of the heat and mass exchanger.	170
Fig. 4-5: The water distributor.....	171
Fig. 4-6: Design of the water sink.	172
Fig. 4-7: Control logic of water supply	173
Fig. 4-8: Control circuit for water circulation	174
Fig. 4-9: Control circuit for airflow.....	175
Fig. 4-10: Velocity distribution in wet channel at air flowrate of 1128 m ³ /h.	176
Fig. 4-11: Velocity distribution in dry channel at various airflow rate.	177
Fig. 4-12: Performance of K3G225-RE07-03 at a duty point of 625 m ³ /h at 207 Pa.	180
Fig. 4-13: The fit of the supply fans and exhaust fans in the prototype.	181
Fig. 4-14: Trial mould pair. Fig. 4-15: Fractures after mould pressing.	183
Fig. 4-16: Some of the small-scale sheet moulds for trial.....	184
Fig. 4-17: Various failure of fracture.	184

Fig. 4-18: Change of the corrugation form.	185
Fig. 4-19: Final wave form in side view.	185
Fig. 4-20: Manufacture process of the forge and punching moulds.	186
Fig. 4-21: Experimental testing rig set up.	189
Fig. 4-22: Kraft paper wetted area compared with the reference area.....	190
Fig. 4-23: Schematic diagram of the commercial image processing method.	191
Fig. 4-24: Variation of the wicking height with time.....	192
Fig. 4-25: Variation of wicking height growing rate with time.	193
Fig. 4-26: Wicking height at 15 minutes.	193
Fig. 4-27: Water drop on the fabric.....	194
Fig. 4-28: Wetted areas.	195
Fig. 4-29: Diffusion rates.....	196
Fig. 4-30: Evaporation rates.	196
Fig. 4-31: Images of distorted fabrics. (a) sample 6; (b) sample 7.....	197
Fig. 4-32: Adhesive. (a)Silicone glue; (b) Sikaflex®291i.....	200
Fig. 4-33: HMX plates fabrication process.....	201
Fig. 4-34: Material preparation in workshop.....	202
Fig. 4-35: Formation process of the irregular shape exchanging sheets.	203
Fig. 4-36: A finished irregular shape exchanging sheet.....	204
Fig. 4-37: Assembled HMX.....	205
Fig. 4-38: Test and demonstration system of water distributing.....	206
Fig. 4-39: Structural view of the Water distributing system.	206
Fig. 4-40: Water distributor in assembly.....	206
Fig. 4-41: Fan and housing.	207
Fig. 4-42: Louvres on the fan housing.....	208
Fig. 4-43: Water sink in position.	208
Fig. 4-44: components for fan and pump control.	210
Fig. 4-45: Prototype assembly in progress.	211
Fig. 4-46: Prototype equipped with accessories in 3-side view.....	212
Fig. 4-47: Finishing air cooler prototype.....	212
Fig. 5-1: Layout of the piping system in the lab.....	217
Fig. 5-2: Airflow regulation system prior to the entrance.	217

Fig. 5-3: Organization of the air and water flow and measure points deployment.	218
Fig. 5-4: Testing system.	219
Fig. 5-5: Auxiliary equipment to help create required air conditions.....	220
Fig. 5-6: Layout of the measurement instruments and control elements.....	221
Fig. 5-7: Temperature measuring instruments.....	223
Fig. 5-8: Pressure and airflow rate measuring instruments.	223
Fig. 5-9: Power meters.....	223
Fig. 5-10: Piping system.....	228
Fig. 5-11: The proposed dew point air cooler prototype in demo operation. .	225
Fig. 5-12: Climate characters on the psychrometric chart.....	228
Fig. 5-13: Cooling performance under various climates (Test 1-working air ratio of 0.44).	230
Fig. 5-14: Variation of the temperature drop and cooling capacity with working air ratio.....	232
Fig. 5-15: RH of exhaust air under different working air ratio.	232
Fig. 5-16: Temperature and cooling capacity vs product air flow rate (Riyadh).	235
Fig. 5-17: Effectiveness and COP vs product air flow rate (Riyadh).....	235
Fig. 5-18: Temperature and cooling capacity vs product air flow rate (Kashi).	236
Fig. 5-19: Effectiveness and COP vs product air flow rate (Kashi).	237
Fig. 5-20: Temperature and cooling capacity vs product air flow rate (London).	238
Fig. 5-21: Effectiveness and COP vs product air flow rate (London).....	238
Fig. 6-1: Hourly weather profiles in the cooling season.....	251
Fig. 6-2: Hourly weather profile in two typical cooling days in Beijing, China.	252
Fig. 6-3: Hourly cooling demands and cooling capacity in typical cooling days.	256
Fig. 6-4: Annual cooling time by hour.	259
Fig. 6-5: Cooling load and power consumption with outdoor air temperature.	260
Fig. 6-6: Power consumption by DPC and PAC at same cooling capacity....	262

LIST OF TABLES

Table 1-1: Typical values of COP for some refrigeration cycles. ^{[1.14], [1.15]}	4
Table 2-1: Titled ‘dew point’ cooling case 1	50
Table 2-2: Titled ‘dew point’ cooling case 2	51
Table 2-3: Titled ‘dew point’ cooling case 3	52
Table 2-4: Titled ‘sub-wet bulb’ cooling case 1	53
Table 2-5: Titled ‘dew point’ cooling case 4	54
Table 2-6: Titled ‘M-cycle’ cooling case 1	55
Table 2-7: Titled ‘below wet-bulb’ cooling case 1	56
Table 2-8: Titled ‘regenerative’ cooling case 1	57
Table 2-9: Titled ‘M-cycle’ cooling case 2	58
Table 2-10: Titled ‘M-cycle’ cooling case 3	59
Table 2-11: Titled ‘dew point’ cooling case 5	60
Table 2-12: Titled ‘dew point’ cooling case 6	61
Table 2-13: Titled ‘dew point’ cooling case 7	62
Table 2-14: Titled ‘M-cycle cooling case 4	63
Table 2-15: Titled ‘M-cycle’ cooling case 5	64
Table 2-16: Titled ‘M-cycle’ cooling case 6	65
Table 2-17: Titled ‘M-cycle’ cooling case 7	66
Table 2-18: Titled ‘regenerative’ cooling case 2	67
Table 2-19: Titled ‘M-cycle’ cooling case 8	68
Table 2-20: Titled ‘combined’ IEC case 1	69
Table 2-21: Titled ‘sub-wet bulb’ cooling case 2	70
Table 2-22: Titled ‘M-cycle’ cooling case 9	71
Table 2-23: Titled ‘M-cycle’ cooling case 10	72
Table 2-24: Titled ‘dew point’ cooling case 7	73
Table 2-25: Titled ‘dew point’ cooling case 8	74
Table 2-26: Titled ‘dew point’ cooling case 9	75
Table 2-27: Titled ‘regenerative’ cooling case 3	76

Table 2-28: Titled ‘regenerative’ cooling case 4, 5	77
Table 2-29: Titled ‘dew point’ cooling case 10.....	78
Table 2-30: Titled ‘dew point’ cooling case 11	79
Table 2-31: Titled ‘generative’ cooling case 6	80
Table 3-1: Basic pre-setting parameters for simulation.....	103
Table 3-2: K values and airflow resistance in channels.....	109
Table 3-3: Climate conditions used in comparative simulation research	115
Table 3-4: Pre-set operational conditions for simulation.....	121
Table 4-1: Specification of the selected fan	179
Table 4-2: Specification of the circulating pump	182
Table 4-3: Specification and test certificate of the selected aluminium sheet	185
Table 4-4: Specifications of the fabrics under test	187
Table 4-5: Costs of the textile fabrics.....	188
Table 4-6: Wicking height variation with time.....	192
Table 4-7: Moisture diffusion and evaporation testing results	195
Table 4-8: Summary of the performance of the tested fabrics.	198
Table 4-9: Percentage increase in performance relative to Kraft paper.	199
Table 4-10: Properties of Sikaflex®291i.....	201
Table 4-11: Specification of fans, pump and controllers.....	209
Table 5-1: Major components in the intake air regulation system.	220
Table 5-2: Individual components in the supply and discharge air delivery system.	221
Table 5-3: Specification of the major measurement instruments.	224
Table 5-4: Testing conditions (Test 1)	229
Table 5-5: Test results (Test 1).....	230
Table 5-6: Comparison of the prototype system with the M30.....	233
Table 5-7: Performance under various climatic conditions.....	234
Table 5-8: Validation with test results under various PA flow rate.	242
Table 5-9: Validation with test results under various climatic conditions.	243
Table 6-1: Hourly cooling load and power consumption (16 th June 1999)....	254
Table 6-2: Hourly cooling load and power consumption (17 th July 1999)....	257

Table 6-3: Hourly cooling load and power consumption (17 th July 1999).....	258
Table 6-4: Validation of the calculating temperature and summary of service hourage.	259
Table 6-5: Cooling performance and power consumption under various outdoor temperature.	261
Table 6-6: Capital cost breakdown of the prototype DPC.....	263
Table 6-7: Annual operating costs of DPC and PAC.....	265
Table 6-8: The volume of evaporated water all year round.....	267
Table 6-9: Cost payback period and life-cycle net cost saving.	269
Table 6-10: Environmental benefits of the proposed DPC.....	271

ABBREVIATIONS

<i>AC</i>	<i>Air Conditioning</i>
<i>ANSI</i>	<i>American National Standards Institute</i>
<i>ASHRAE</i>	<i>American Society of Heating Refrigerating and Air</i>
<i>CDC</i>	<i>Computing & Data Centre</i>
<i>CEN</i>	<i>The European Committee for Standardization</i>
<i>CFD</i>	<i>Computational Fluid Dynamics</i>
<i>CNY</i>	<i>Chinese Yuan</i>
<i>COP</i>	<i>Coefficient of Performance</i>
<i>CPT</i>	<i>Cost Payback Time</i>
<i>DB(T)</i>	<i>Dry Bulb temperature</i>
<i>DEC</i>	<i>Direct Evaporative Cooling</i>
<i>DEVap</i>	<i>Desiccant-Enhanced eVaporative Cooling</i>
<i>DPC</i>	<i>Dew Point Cooling/ Cooler</i>
<i>DPE</i>	<i>Dew Point cooling Effectiveness</i>
<i>DP-IEC</i>	<i>Dew Point Indirect Evaporative Cooling</i>
<i>DP(T)</i>	<i>Dew Point temperature</i>
<i>DX</i>	<i>Direct eXpansion</i>
<i>EA</i>	<i>Exhaust Air</i>
<i>EC</i>	<i>Evaporative Cooling</i>
<i>EER</i>	<i>Energy Efficiency Ratio</i>
<i>EES</i>	<i>Engineering Equation Solver</i>
<i>EF</i>	<i>Exhaust Fan</i>
<i>FEM</i>	<i>Finite Element Method</i>
<i>FR</i>	<i>Flow Rate</i>
<i>GBP</i>	<i>Great Britain Pound</i>
<i>GHG</i>	<i>Greenhouse Gases</i>
<i>HVAC</i>	<i>Heating, Ventilation and Air Conditioning</i>
<i>HMX</i>	<i>Heat and Mass eXchanger</i>
<i>HR</i>	<i>Humidity Ratio</i>
<i>IA</i>	<i>Intake Air</i>
<i>IAQ</i>	<i>Indoor Air Quality</i>
<i>IDEC</i>	<i>combined Indirect and Direct Evaporative Cooling</i>
	<i>Indirect Evaporative Cooling/</i>
<i>IEC</i>	<i>International Electrotechnical Commission</i>
<i>IM</i>	<i>Iterative Method</i>
<i>ISO</i>	<i>International Standardization Organization</i>

<i>LCA</i>	<i>Life-Cycle Assessment</i>
<i>LD</i>	<i>Liquid Desiccant</i>
<i>LMTD</i>	<i>Log Mean Temperature Difference</i>
<i>M-cycle</i>	<i>Maisotsenko thermodynamic cycle</i>
<i>NTU</i>	<i>Number of Transfer Units</i>
<i>OECD</i>	<i>Organization for Economic Co-operation and Development</i>
<i>PA</i>	<i>Product Air</i>
<i>PV</i>	<i>PhotoVoltaic</i>
<i>PAC</i>	<i>Packaged Air Conditioner</i>
<i>R&D</i>	<i>Research and Development</i>
<i>REC</i>	<i>Regenerative Evaporative Cooling/ Cooler</i>
<i>RH</i>	<i>Relative Humidity</i>
<i>RHMX</i>	<i>Regenerative Heat and Mass eXchanger</i>
<i>SF</i>	<i>Supply Fan</i>
<i>WA</i>	<i>Working Air</i>
<i>WAR</i>	<i>Working-to-intake Air Ratio</i>
<i>WBE</i>	<i>Wet Bulb cooling Effectiveness</i>
<i>WB(T)</i>	<i>Wet Bulb temperature</i>

NOMENCLATURE

a	chord length of the basic computational element, m
A	heat and mass transfer area of computational element, m ²
COP	Coefficient of Performance, -
C_P	specific heat capacity, kJ/kg·°C
De	equivalent diameter, m
Dh	hydraulic diameter, m
en	latent heat, kJ/kg
g	gravity acceleration, m/s ²
h	convection coefficient, W/(m ² ·°C)
h_m	mass transfer coefficient, m/s
H	height, m
hum	humidity ratio, kg/kg
i	enthalpy, kJ/kg
l	length, m
l_0	thermal entry length, m
Le	Lewis number, -
Nu	Nusselt number, -
n	number, -
P	pressure, Pa
ΔP	pressure drop, Pa
ΔP_f	frictional pressure loss, Pa
ΔP_{local}	local pressure loss, Pa
$Q_{cooling}$	cooling capacity, kW
Q_m	mass flow rate, kg/s
Pr	Prandtl number, -
Re	Reynolds number, -
s	area, m ²
T	temperature, °C
T_f	airflow temperature, °C
u	air velocity, m/s
W	electric power, kW
x	distance, m

Subscripts

air	air
air,wet	wet air
dp	dew point

<i>dry</i>	dry channel
<i>dry,in</i>	inlet of dry channel
<i>dry,out</i>	outlet of dry channel
<i>f</i>	airflow
<i>fan</i>	fan
<i>in</i>	inlet
<i>out</i>	outlet
<i>pump</i>	pump
<i>vap</i>	evaporated water
<i>vapour</i>	water steam
<i>w</i>	channel wall
<i>water</i>	water
<i>wb</i>	wet-bulb
<i>wet</i>	wet channel
<i>wet,in</i>	inlet of wet channel
<i>wet,out</i>	outlet of wet channel
Greek	
λ	heat conduction coefficient, W/(m·°C)
α	thermal diffusivity, m ² /s
λf	coefficient of friction resistance, -
ζ	coefficient of local resistance, -
σ	surface wettability factor, -
Δ	difference between two states, -
μ	dynamic viscosity, kg/(m·s)
ρ	density, kg/m ³
φ	working air fraction over intake air, -
ε	cooling effectiveness, -
η	efficiency, -

CHAPTER 1: INTRODUCTION

1.1 Research Background

1.1.1 Demands for Sustainable Building Cooling

With the growth of population and the process of urbanization, total energy consumption in the world keeps arising, especially in the developing countries e.g. China and India. Serious atmospheric and environmental problems caused by the extensive use of fossil energy, such as global warming, greenhouse gas (GHG) emission, climate change, ozone layer depletion and acid rain, have become inevitable, serious and urgent across the world.

World energy demand is projected to grow by 34% (1.4% p.a.) from 2014 to 2035, with 95% of the growth coming from non-OECD countries. Energy consumption in China is expected to grow by about 48% in the meantime and account for 25% of global energy consumption in 2035 from 23% in 2014. [1.1]

Six major types of GHGs are addressed by the Kyoto Protocol: CO₂, CH₄, NO₂, HFCs, PFCs and SF₆. As the largest contributor to the greenhouse effect and relatively low cost of emission accounting, CO₂ is the first chemical that is to be regulated by all ETSs (Emissions Trading System) in the world. [1.2]

The successful outcome of the 2015 United Nations Climate Change Conference COP 21 (the 21st session of the Conference of the Parties), which was held in Paris, France from 30th November to 12th December 2015, has raised hopes and expectations of concerted global efforts to tackle climate change. [1.3] The

expected key result was the negotiation of the Paris Agreement, a global agreement to set a goal of limiting global warming to less than 2°C compared to pre-industrial levels. The agreement calls for zero net anthropogenic greenhouse gas emissions to be reached during the second half of the 21st century. [1.4] Renewable energy is vital to steer the energy system to the low-carbon future envisioned in the Paris Agreement.

From global point of view, the building sector accounts for more than 30% of the total primary energy consumption and approximately 40% in the EU, e.g. 46.7% in the UK in 2013. [1.5- 1.8].

The growing demand for improved thermal comfort in the building environment led to the wide spread implementation of heating, ventilation, and air-conditioning (HVAC) systems. HVAC has become the major energy user in a building, accounting for 50% of the energy consumption in buildings and 20% of total energy consumption in developed countries, while in some developing countries, such as China, the energy consumption of HVAC accounted for 50-70% of energy consumption in buildings. [1.9, 1.10] Cooling, ventilation and refrigeration has accounted for 36.5% of the electrical consumption in commercial buildings in the USA. [1.11]

Air-conditioning, representing an important function of the HVAC system, is also becoming increasingly crucial for many European buildings, particularly those public types e.g. office blocks, supermarkets, sport centres, airports, factories etc., owing to the recent frequent warm spells, improved building insulation and growth of in-house heat generating appliances.

On the other hand, with the coming of the Big Data Era, Computing & Data Centres (CDCs), which house computer systems and associated components, such as telecommunications and database systems, have emerged in large

numbers in the past decades and swells either in numbers or scales in recent years. In Europe, there are currently 1174 collocation data centres that are scattered across 27-member states of the EU [1.12], and consume more than 100 TWh of electricity each year. In China, the capacity of the CDCs has reached 28.5 GW in 2013 [1.13, 1.14], consuming 549.6 TWh of electricity each year. CDC becomes a significant and growing component of electricity demand all over the world. In 2010, the total electricity used in CDCs was around 1.3% of the world total energy consumption, while figures in Europe and China were 1.4% and 1.5% [1.14-1.16] respectively.

Air-conditioning systems in data centres should work full time all over the year to remove the waste heat generated inside with the operation of different energy-intensive devices. The cooling system is one of the largest parts in electricity consumption in data centres, and takes up around 25%-50% of all electricity use. [1.17]

Therefore, it is crucial to improve the energy performance of HVAC systems, either for human comfort or facilities operation, to reduce building energy and carbon emissions.

To achieve the EU 2020 goals for buildings [1.18], i.e., (1) increasing energy efficiency to achieve a reduction of 20% of total energy use (below 2005 levels); (2) increasing use of renewable energy contributing to 20% of total energy use (11.5% above 2005 contribution), and (3) reducing 20% greenhouse gases relative to 1990 emissions (14% below 2005 emission), seeking for routes to reduce fossil fuel consumption and increase utilization of natural or renewable energy during air conditioning process is of particular importance.

1.1.2 Evaporative Cooling Technology

The air conditioning market is currently dominated by mechanical vapour compression refrigeration systems. This type of system consumes significant amounts of electricity, a high-grade energy, owing to the use of the compressor and therefore, is neither sustainable nor environmentally friendly [1.19]. It is vital and urgent to develop energy-efficient and sustainable cooling systems, suitable for the building application, to gradually substitute the conventional energy-intensive and CFC-refrigerant-used vapour compression refrigeration systems which dominates the current corresponding cooling markets. [1.29]

In a wide range of alternatives, e.g. absorption, adsorption, desiccants and ejector cooling, evaporative cooling systems utilize the latent heat of water evaporation, i.e. a kind of natural energy existing in the atmosphere, to perform air conditioning for buildings with very high energy efficiency against the conventional mechanical compression refrigeration. The typical values of Coefficient of Performance (COP), index of cooling capacity (W) divided by power consumption (W) to rate the system efficiency, for conventional vapour-compression systems and alternative systems are summarised for contrast in **Table 1-1**.

Table 1-1: Typical values of COP for some refrigeration cycles. [1.14], [1.15]

Refrigeration cycle	Vapour-compression	Absorption	Adsorption	Desiccants	Ejector	Thermoelectric	Evaporative
COP	2-5	0.6-1.0	0.2-0.8	0.5-1.5	0.3-0.8	0.5-1.0	15-20

Absorption and adsorption cooling, as a potential alternative to conventional mechanical vapour compression systems, remove the need for the power-intensive compressor, but require high temperature vapour or water, thus limiting their application to occasions where high temperature heat source is available. Further, relatively complex system configurations containing

pressurised and de-pressurised components in the absorption and adsorption systems reduces their attraction to people [1.20] for practical applications.

Evaporative air cooling is a technology that uses the thermodynamic process of water evaporation to cool the air. It is the process in which sensible heat is extracted from air and converted in latent heat without changing the enthalpy value.

Over the past decades, evaporative cooling, utilizing the principle of water evaporation for heat absorption, has gained growing popularity for the use in air conditioning [1.21, 1.22], owing to its simple structure and good use of the latent heat of water, a recyclable/ renewable energy existing in the natural environment. Direct Evaporative Cooling (DEC) keeps the product air in direct contact with water, causing evaporation of the water and reduction of temperature of the air simultaneously. Thus, the vaporised water, in form of vapour, is added into the air, which often creates wetter air conditions and causes discomfort to the residents.

With an air-to-air exchanger, to avoid adding moisture into the product air and remaining transfer of sensible heat through the wall, that is what we call Indirect Evaporative Cooling (IEC). Wet-bulb temperature of the working air is the limit that the intake air could be cooled. In an IEC unit, the evaporation-aided plate-stacked heat exchanger is the core component that comprises numerous exchanging plates, each having a dry surface on one side and wet surface on the opposite side. On integration, the wet surface of a plate is opposite to the wet surface of the other adjacent sheet to formulate a wet channel for the wet airstream to come across; similarly, the dry surface of a plate is opposite to the dry surface of the other adjacent plate, formulating the dry channel to let the dry airstream travel across.

During operation, the primary (product) airstream enters the dry channel and the secondary (working) airstream enters the adjacent wet channel, whilst the water is sprayed to the wet channel wall from the upper side. In this way, the primary airstream is cooled by the evaporation of the water from the wet surface, which creates a temperature difference enabling heat transfer to take place between the two airstreams. Thus, the primary airstream is cooled at the constant moisture content toward the wet-bulb temperature of the intake primary airstream; whereas the secondary airstream is gradually saturated and heated when moving along the flow path, and finally discharged to ambient.

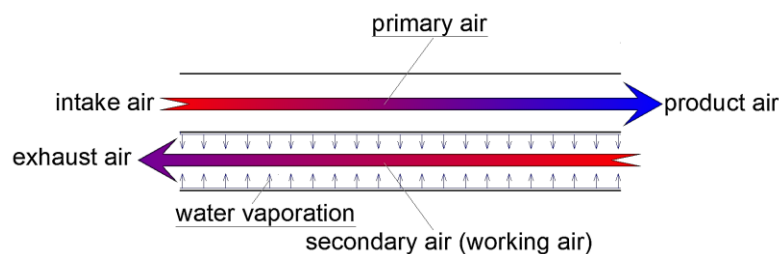


Fig. 1-1: Schematic of IEC cooling.

In reality, instead of working independently, IECs are often applied jointly with other cooling devices to form hybrid cooling systems, e.g. (1) indirect/direct evaporative cooling (IEC/DEC) mode; (2) IEC/cooling coil or direct-expansion (DX) refrigeration system; (3) IEC/DEC/ cooling coil or direct expansion refrigeration system; and (4) Desiccant/IEC/DEC System, which can offer better comprehensive cooling performance and cost efficiency under various climate conditions. [1.23]

In terms of commercial opportunity, it could be predicted that the worldwide evaporative cooling market would experience a fast growth over the next ten years (from £5.5 billion in 2013 to £20 billion in 2024) [1.23-1.25] and the dew point cooling market will also experience a very fast growth (from £1 billion in 2013 to £6 billion in 2024) [1.23] as illustrated in **Fig. 1-2**, whilst the worldwide

air conditioning market continues to grow (from £55 billion in 2013 to £95 billion in 2024 [1.24, 1.25],

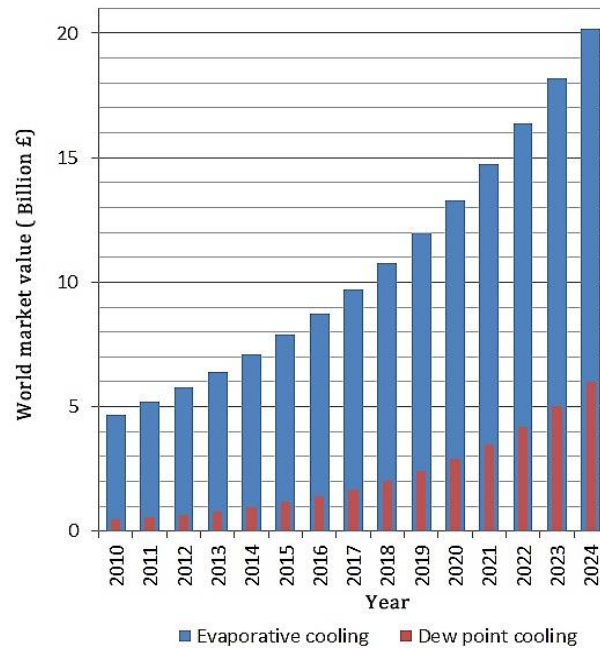


Fig. 1-2: Market profile in relation to the evaporative cooling and dew point cooling.

1.2 Research Opportunity, Aim and Objectives

Over the past decades, great progress has been made both in IEC technology R&D and in its commercial application. However, there is still potential for further technical progress, especially in HMX structure and water distribution on wet surface.

In terms of heat exchanger for the IEC, the structures of the existing HMX are mainly based on the plane-plate stacked form, considering their merits of easy making and cost effective. However, this structure is not the most favourite form as the heat and mass exchanging space is not used effectively and the temperature of secondary air is not low enough to remove more heat from the

primary air. Contrast to the common structure of plane transfer surface, corrugated or irregular shape would greatly improve the heat transfer efficiency, if desirable structure design would be developed and the fabricating cost could be under control.

In terms of materials, water permeability, which greatly influences water distribution across the wet surface, would be the primary factor to be considered under the premise of structural strength and fabrication convenience. Unfortunately, the progress that has been made is still far from satisfactory. [1.26, 29-34]

Most of the existing dew point products share a common feature adopting the cross-current airflow, which is not regarded as the best flow pattern in terms of heat exchange. Counter-flow arrangement would be preferable as it can create higher temperature reduction (logarithmic average) between the two adjacent airstreams and higher efficiency. A comparative study of cross-flow and counter-flow HMXs based on M-cycle for dew point cooling was conducted. Both configurations were theoretically and experimentally investigated to indicate the counter-flow exchanger offered greater (around 20% higher) cooling capacity, as well as greater (15-23% higher) WBE and DPE, but less energy efficient (10%) due to the increase of flow resistance, with equal physical size and under the same operational conditions. [1.27]

The overall aim of the PhD research is to address the above identified technical possibilities and develop a novel dew point air cooling unit along with a dedicated computer software which is able to assist in system and detailed structure design, operation optimization and results prediction. This expects to increase energy efficiency (COP) by around 40% and cooling effectiveness by

around 20%, over the existing DPCs. To enable achieving the aim, the research has set out four specific **objectives** addressed as below.

1) To develop a conceptual design for the dew point air cooling unit with the targets of increasing the heat transfer rate between the dry and wet airstreams by around 25%, decreasing the unit's electricity consumption by around 10%, and limiting the cost increase to less than 10%, relative to the existing DPCs.

2) To develop the components' performance data and computer simulation model to optimise the configuration of the dew point air cooling unit and predict its operational performance, thus demonstrating (or tuning) the above addressed technical targets from theoretical point of view.

3) To design, construct and test a prototype dew point air cooling unit in controlled lab environment and validate the established computer simulation model using the experimental data, thus examining whether the modelling-derived performance data can be realised and suggest the follow-on measures.

4) To carry out economic, environmental and regional acceptance analyses of the dew point air cooling unit, thus examining the cost target and other social-economic measures related to the new unit.

1.3 Research Methodology

This research is a typical applied, creative research targeted to develop a new dew point air cooling unit. It should follow a procedure of (a) concept formation and (b) concept approval or adjustment. The approaches for processing the scientific and technological works are (1) conceptual development (for **objective**

1); (2) performance data and computer simulation model development (for **objective 2**), (3) experimental testing and simulation model validation (for **objective 3**), and (4) economic, environmental and regional acceptance analyses (for **objective 4**). **Approach (1)** is for concept formation, while **approaches (2)-(4)** coming together are to prove or adjust the established concept by the combined efforts of theoretical, experimental and social-economic analyses. These approaches, are briefed as follows.

□ **Approach to objective 1 – Conceptual development of the new dew point air cooling unit**

This approach is designed to develop a conceptual design for the new unit, which, compared to the existing dew point air coolers, has potential to achieve higher heat transfer rate (around 25%), and lower electricity consumption (around 10%). The steps towards this include (1) completing the sketch drawings of the individual components and the integrated unit; (2) delivering the components list and estimate their potential performance variation in terms of material type and geometrical size; and (3) determining the method of the components connection, and analysing the associated aesthetical and cost matters related to the unit construction. This approach will enable developing a concept on how such a unit is structured.

□ **Approach to objective 2 – Developing the components' performance data and computer simulation model to optimise the configuration of the unit and predict its operational performance.**

This approach is designed to demonstrate (or tune) the technical targets set for the new unit in **Approach 1** from theoretical point of view. The steps towards this include (1) measuring the critical performance data of the system components; (2) developing and running a computer simulation model to analyse the cooling output, power input, fluid flow and heat transfer occurring in the unit,

which will enable (a) determination of the operational performance data of the unit under different operational conditions; (b) determination of the optimum geometrical sizes of the system components and whole unit; (c) recommendation of the optimal system operational conditions; (d) identification of the potential increase in energy efficiency (COP) and cooling effectiveness of the new unit relative to existing DPCs. This approach will enable demonstrating (or tuning) the unit's technical performance data addressed in **Approach 1** and allow data validation to be undertaken in **Approach 3**, by using the experimental measures.

□ **Approach to objective 3 – Design/construction/testing of the unit and validation of the computer simulation model using the experimental data.**

This approach is designed to examine whether the modelling-derived performance data of the new unit can be realised and suggest the follow-on measures. The steps towards this are (1) designing and constructing a 4-kW rated dew point air cooling unit; (2) testing its performance and operational characteristics under the laboratory condition, and in particular, determining the energy efficiency and cooling effectiveness of the new unit; and (3) verifying (or modifying) the computer simulation model developed in **Approach 2**. Thus, the energy saving rate and cooling effectiveness increase ratio of the new unit relative to the existing DPCs will be determined. This approach will enable refining or validation of the simulation results (in particular, energy efficiency and cooling effectiveness) derived from **Approach 2** and development of a validated computer simulation model and an experimental prototype. Further, it will suggest the potential measures to improve the performance of unit for use in future commercial development of the technology.

□ **Approach to objective 4 – Economic, environmental and regional acceptance analyses of the new dew point air cooling unit.**

This approach is designed to examine (prove or tune) the cost target and other social-economic measures related to the new unit. This will involve collection of the technical, economic, environmental and life-cycle data relating to the new DPCs, and evaluation of the economic and environmental impact of the technology and analyses of its adaptability to the climate. This approach will allow understanding of the potential benefits and impact of utilizing the new dew point air cooling units to replace the conventional air conditioner, in terms of potential power saving, carbon emission reduction, life cycle cost, and payback period etc., thus enabling evaluation of the non-technical features of the technology.

1.4 Research Novelties

The proposed dew point air cooling unit has the following innovative features.

I. Innovative structure of the heat and mass exchanger

- (1) The heat exchanger has a dedicatedly designed and innovate structure that enables increased heat transfer area between dry and wet airstreams and thus increased cooling output of the unit. The irregular and unique unibody exchanging sheet, including the corrugated part, is able to self-support and remove any supporting guide in the channels and thus greatly decrease the airflow resistance between the exchanging sheets.
- (2) The self-contained counter-flow regenerative HMX enables more efficient heat exchanging between the airstream in adjacent dry and wet channels than common cross-current ones.

The invention *Heat exchanger apparatus* has been filed by UK Intellectual Property Office. (GB1617362.7)

II. Application of new material and new process

The application of the functional fabric bonded onto the exchanging sheet by the self-developed process is a new trial in air cooling unit and is able to enhance the diffusive wetting capability and thus increase the cooling output of the unit and lower the demand for circulating water and associated power consumption.

III. Innovative water distribution and control scheme

The exclusive water distribution design and effective control of circulating water flow help to reduce the pump power consumption and contribute in the increase of the COP.

The patent *Even liquid distribution of intensive formula* (CN205718642U) has been authorized by China State Intellectual Property Office.

IV. Exclusive self-developed simulation software

Based on the investigation of heat/mass transfer and airflow dynamic, the dedicated simulation software is able to assist in conceptual design, structure optimization, and operational parameters prediction with high reliability not only for the proposed cooler but also suitable for the common plane-plate-stack ones.

Combination of the above four initiatives into a single unit is a new trial in DPC development that enables significant increase in energy efficiency and cooling effectiveness.

1.5 Thesis Structure

Chapter 1 – Introduction: this briefly describes the research background, significance, objectives, methodology and novelties.

Chapter 2 – Literature review: this involves an extensive review of the existing IEC technologies, including basic theory, research methodology, evaluation standards, R&D processes and practical applications, and intensive review of the dew point cooling technologies. The current research status and technical barriers regarding IEC technologies are examined. As a result, potential opportunities for future development are identified.

Chapter 3 – Conceptual development and computerised simulation: this describes the basic working principle of the proposed system and dedicatedly develops a set of simulation routines to investigate the impacts of the geometric configuration and operational conditions on the unit's cooling performance. Through running the simulation tool, appropriate design and operational parameters are recommended, and the optimum geometry and capacity of the relevant system components are determined. These results are subsequently applied to the prototype design and experimental testing.

Chapter 4 – Prototype design and construction: this describes the detailed system and major components design, process of material selection and trial, and system integration during the construction of a 4-kW rated prototype cooler.

Chapter 5 – Testing implement, results analysis and validation/update of the computer model: this describes series of laboratory-based experiments and evaluates the prototype cooler under six typical outdoor weather conditions, which respectively represents the climates of hot & dry, warm & dry, moderate,

warm & humid and the standard testing condition. The test results verify the originally developed simulation tool and make further update to a higher level of accuracy.

Chapter 6 – Energy saving, economic, and environmental performance analyses: this discusses the proposed cooler’s annual performance, energy payback periods, and carbon emission reduction issues throughout a consecutive period of a whole cooling season in a typical meteorological year in Beijing (typical warm & humid climate). It addresses the feasibility of such an air cooler in replacing the conventional packaged air conditioner by assessing both economic and environmental benefits.

Chapter 7 – Conclusions and further work: this concludes the major observations and experience during the whole research process, including application of new materials and new processes, development of computer-aided design, optimizing and predicting tool, numerical investigation, laboratory measurement, and socio-economic assessment. Opportunities and challenges involved in structure design and manufacture, numerical simulation, experimental investigation, case study and other aware but uncovered issues in the research are discussed for further development of the technology. Consequently, an ideal but realizable model is depicted.

All the above chapters are systematically connected and intended to tell the complete story of the development process of a super performance dew point air cooler and give practical and valuable suggestions.

CHAPTER 2: LITERATURE REVIEW

2.1 Chapter Introduction

Owing to the continuous progress in technology innovation, particularly the M-cycle development and associated heat and mass transfer and material optimisation, the IEC systems have obtained significantly enhanced cooling performance and energy efficiency in recent decades. This chapter carries out a comprehensive literature review of R&D progress and the practical application in evaporative cooling, intending to base the following research work on a strong scientific foundation. The research gaps are identified by critical analysis to suggest the future research opportunities. The major approaches are briefly given as follows:

- (1) Present the fundamental principle of evaporative cooling and the basic forms in practice.
- (2) Describe the evaluation standards relating to the technical, economic and environmental performance of evaporative cooling systems.
- (3) Illustrate a comprehensive literature review into the R&D progress and practical applications of EC devices.
- (4) Identify the potential opportunities for further research and development of IEC technology.
- (5) Discuss the opportunities for the PhD research.

This part of work provides the foundation for the entire investigation and helps to: (i) identify the technical barriers existing in current IEC technologies; (ii) establish the scientific methods for IEC research; (iii) develop new research topics; and (iv) set up the research direction for the subsequent chapters.

2.2 Basic Concept and Theory, Classification and Performance Evaluation Standards of Evaporative Cooling Technology

2.2.1 Basic Concept and Theory of Evaporative Cooling

Moisture evaporation is a natural process of liquid state water transforming to a gaseous state, i.e. vapour or steam, while there is a partial pressure difference at the interface between the two phases. It is also one of the fundamental water cycles in nature that takes place everywhere and in any time. Frescoes from about 2500 B.C. indicate that the ancient Egyptians noticed and made use of the phenomenon that moisture evaporation could offer cooling effect, to cool the water in porous jars by fanning from outside. [2.1]

With science developing, the essence of phase transformation was gradually discovered and people tried to make better use of the energy conversion during this process. Indeed, now it is very clear that latent heat is a must that accompanies the occurrence of evaporation and the latent heat of vaporization for water is so huge that it could significantly change the temperature of liquid water of which the specific heat capacity is the greatest amongst common materials. The latent heat of water is 2257 kJ/kg [2.2], comparing to the refrigerant R134a of 215.9 kJ/kg, at their respective boiling point and 1 atm pressure. [2.3] **Fig. 2-1** demonstrates the big difference between the latent and sensible heat for water. All the mechanical vapour compression refrigeration systems operate on the principle of phase change between liquid and gaseous states to move heat from one place to another. There is potential for water to be a very high efficiency natural refrigerant merely in the view of its latent heat.

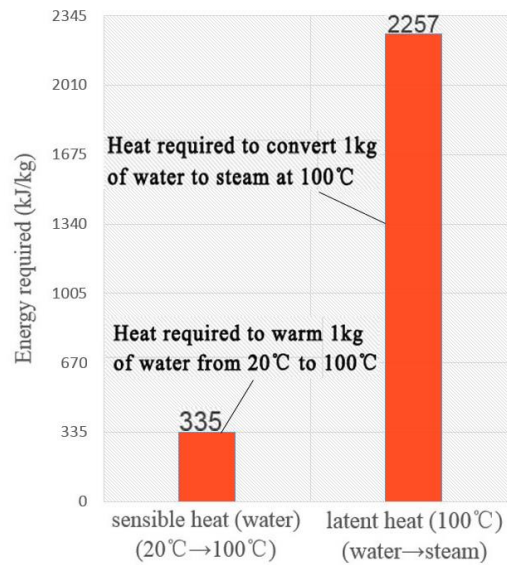


Fig. 2-1: Difference between latent and sensible heat for water.

Unlike the conventional mechanical vapour compression refrigeration system, in which the refrigerant circulates in a close loop and experiences the phase transformation, evaporative cooling makes use of water which is a natural refrigerant and performs phase change by natural vaporization into the air in open space without direct recycle. Therefore, there is no need for energy intensive vapour compressor and chlorofluorocarbon refrigerant which threatens the atmospheric ozone layer.

2.2.2 Classification of Evaporative Cooling Technology

The latent heat to drive the evaporation could originate from various media. In building cooling application, besides the most common medium to be cooled, i.e. the air, water is another practical alternative. Thus, the evaporative cooling technology could be grouped into two main categories according to the media being cooled, i.e. air-side and water-side evaporative cooling, and the cooling units are commonly known as evaporative air cooler and evaporative chiller respectively. [2.4]

By using natural evaporation, moisture goes into the air and increases the air humidity ratio. By means of a heat exchanging wall, water evaporation occurs at

one side of the wall and the latent heat to evaporate the water could be drawn off the wall from the other side. As per whether the water contacting with the cooled air, evaporative technology could be classified into direct evaporative cooling (DEC) and indirect evaporative cooling (IEC). Accordingly, the evaporative cooling systems present in three basic forms, as shown in **Fig. 2-2** and **Fig. 2-3**: 1) direct evaporative cooler, in which the product fluids (water or air) are in direct contact with the water to be evaporated; 2) indirect evaporative coolers, where an exchanging wall separating the product fluids (water or air) from the working air to evaporate the water; 3) hybrid system combined direct and indirect evaporative coolers and/or with other cooling cycles.

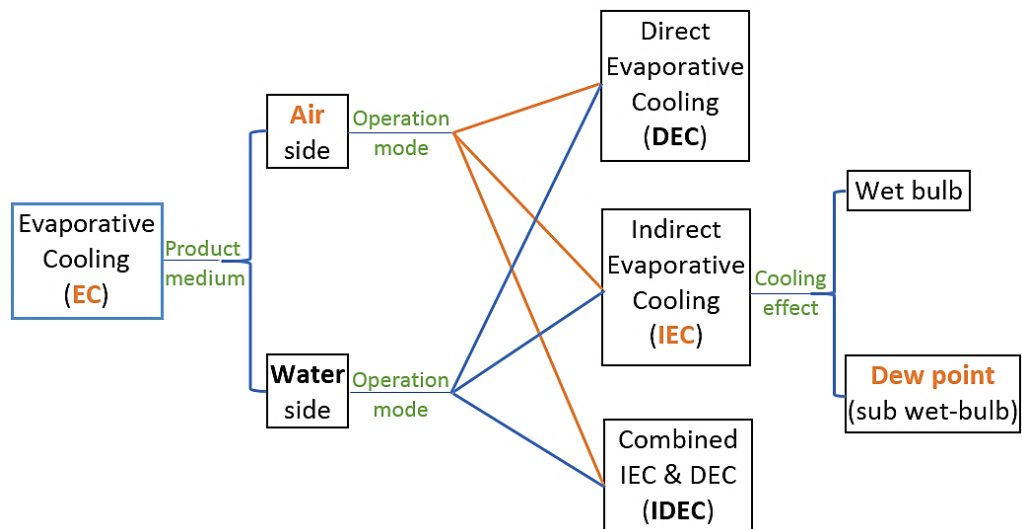


Fig. 2-2: Classification of evaporative cooling systems.

Thereinafter, an outline of the evaporative cooling technology is given based on the evaporative air cooler and the focus will be on IEC technology relating to the following research.

Direct Evaporative Cooling (DEC)

As shown in **Fig. 2-3(a)**, in a DEC unit, ambient air passes through a space in which it contacts intimately with water either in a form of fine droplets or saturating a porous medium. The water evaporates into the air, absorbs heat, adds

moisture and thereby makes it cooler and moister. Theoretically, the evaporation process would not stop until the cooled air reaches the saturation state. However, in practice, the relative humidity cannot always achieve 100% but a few percentage points less because of the practical limitations of the systems. Achieving 90% to 95% of the wet-bulb temperature is often the target for direct cooling performance and the corresponding air state is named as *apparatus dew point*. The real DEC process is often along the pathways **1** and **3** in a psychrometric chart as shown in **Fig. 2-4**. It is an “adiabatic cooling” process for the only heat exchange involved occurs between the intimately contacting air and water.

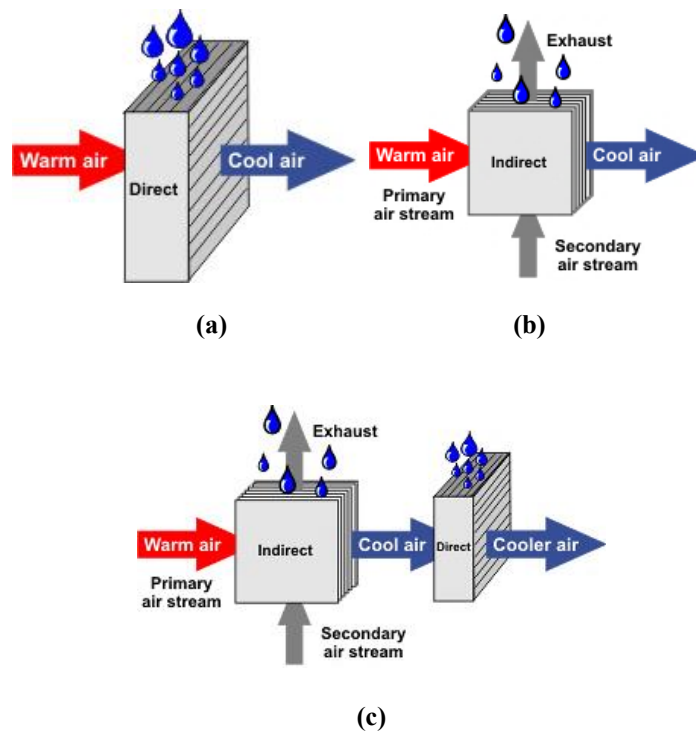


Fig. 2-3: Diagram of basic evaporative systems. ^[2,5]

(a) direct; (b) indirect; (c) indirect/direct.

Along the DEC pathway **1**, the air enters the system at temperature of 37°C, relative humidity (RH) of 20%, and humidity ratio (HR) approximately of 8 g/kg and leaves the system at temperature of 21°C and HR of 14 g/kg. The air has

thus been cooled and humidified. At the end of the process, the relative humidity of the leaving air rises to 90%.

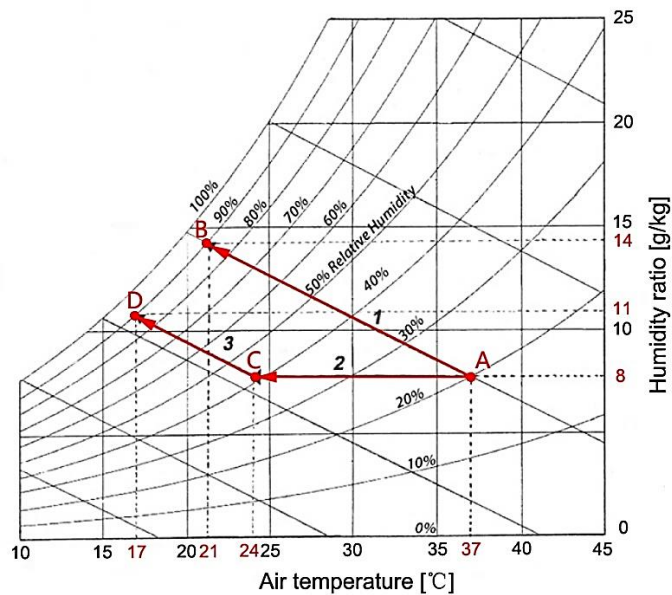


Fig. 2-4: Pathways of evaporative cooling in a psychrometric chart. ^[2.6]

Indirect Evaporative Cooling (IEC)

The latent heat of evaporation can also be employed to cool other media besides the air accommodating the vapour. A heat exchanging wall (membrane or plate) is introduced to separate the cooled media, e.g. water to be used in coils system or the other airstream to avoid adding moisture into it, from the working air which evaporates water and absorbs the heat.

In an indirect evaporative air cooler, as shown in **Fig. 2-3(b)**, the typical process of heat and mass exchange involves two airstreams: one primary/product airstream and the other secondary/working airstream. The IEC process evaporates water and shifts heat from the secondary/working airstream, without adding moisture to the primary/product air. A heat exchanging wall, of which hydrophilic treatment is generally employed with one side to enlarge the contact area between the water and air, is used to separate the secondary/working air from the primary/product air.

At a psychometric chart, the IEC process is a horizontal line moving left across the chart. Without moisture being imported to the primary/product air, the secondary/working air is eventually discharged from the building for it has usually been humidified to nearly saturated state. Theoretically, the air can be cooled to the same wet-bulb temperature as it could be in a DEC process. However, in a real IEC process, the wet-bulb temperature is hard to reach owing to the inefficiencies of the heat exchanger.

As shown in **Fig. 2-4**, along the IEC pathway **2**, the air enters the system at state **A**, i.e. $T_{db}=37^{\circ}\text{C}$, $\text{RH}=20\%$ and $\text{HR}=8\text{ g/kg}$, and is sensibly cooled to the final state **C**, i.e. $T_{db}=21^{\circ}\text{C}$, $\text{RH}=40\%$ and $\text{HR}=14\text{ g/kg}$. As the moisture in the air remains constant while temperature falls, the relative humidity of product air (PA) increases from 20% to 40%. The presence of the additional heat exchanger causes the final PA temperature some degrees higher than in DEC systems ($T_C=24^{\circ}\text{C}$ instead of $T_B=21^{\circ}\text{C}$ in **Fig. 2-4**).

For both DEC and IEC technologies, the thermodynamic wet-bulb temperature, which is the lowest temperature attainable through thermodynamic processes without additional energy, is the targeted temperature to be achieved.

Indirect/Direct Evaporative Cooling (IDEC)

In circumstances where by merely DEC or IEC, the required PA temperature cannot be realized, the relay mode is usually considered to have the both systems operate jointly. The primary air is successively cooled by IEC and DEC to a lower level than when each is used alone. As illustrated in **Fig. 2-4**, along IEC pathway **2** and DEC pathway **3**, the product air finally reaches state **D**, i.e. $T_{db}=17^{\circ}\text{C}$, $\text{RH}=90\%$ and $\text{HR}=11\text{ g/kg}$, with less moisture added relative to DEC process (state **B**). It is obvious that the lowest final PA temperature in the three is attained by the IDEC system.

Dew Point Cooling (DPC) based on M-cycle

Tests indicate that a solo conventional IEC heat exchanger could achieve only around 60% of wet-bulb cooling effectiveness (i.e. ratio of the primary air temperature drop to the wet-bulb temperature depression.) under the specified testing condition [2.7, 2.8], which is too low to provide effective cooling for the conditioned building space. To enhance the cooling effect, i.e. air temperature drop, part of the product air is re-introduced to be the working air and thus lower wet-bulb temperature could be achieved. Such a novel thermodynamic cycle, known as the M-cycle [2.9], was proposed to operate a HMX.

Fig. 2-5 [2.10] demonstrates the structural schematic of a staged M-cycle HMX and **Fig. 2-6** [2.11, 2.12] illustrates the air cooling process in the HMX in a psychrometric chart. As there is technical potential in M-cycle to cool the airflow well below its wet-bulb temperature and even approaching to the dew point, this IEC technology, usually employing M-cycle, is also called dew point cooling (DPC). The tests indicate that the M-cycle based heat exchanger could obtain a wet-bulb cooling effectiveness (WBE) of around 80% and dew-point cooling effectiveness (DPE) of around 50% under the specified testing condition [2.8, 2.10], which is around 20% higher than that of the conventional IEC.

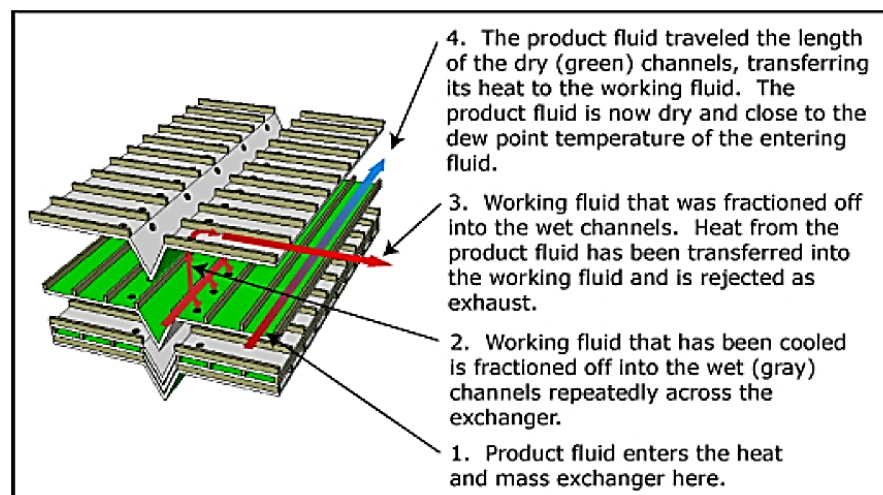


Fig. 2-5: Cut-away Diagram of a Heat and Mass Exchange Module. [2.10]

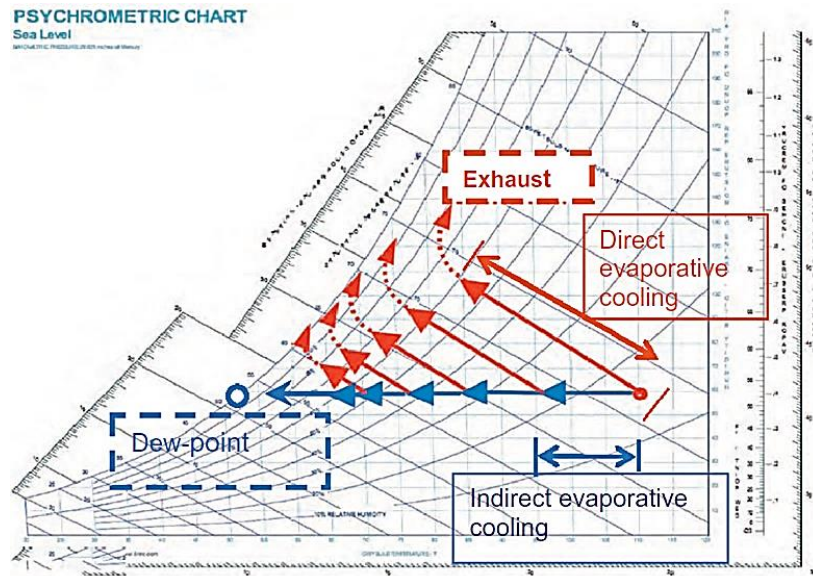


Fig. 2-6: Conceptual psychrometric representation of the staged indirect cooling process with continual purge of secondary/working air. [2.11, 2.12]

2.2.3 Relevant Technical Criteria and Performance Evaluation Standards

Technical and Product Standards

Even though evaporative cooling is regarded as the oldest form of cooling either for air or water, there existed no standard method for testing and evaluating evaporative coolers in the world until 1974, Indian Standard *Evaporative Air Cooler* [2.13] was published. Thereafter, Canada (1983 [2.14]), Australia (1987 [2.15]), Saudi Arabia (1997 [2.16]), Iran (1998, [2.17]), the United States (2001 [2.18, 2.19]) and other countries, e.g. China (2010 [2.20]), have established standards of evaporative cooling air conditioner in succession [2.21]. However, there are still no ISO, IEC or CEN standards published for evaporative coolers up to now.

Among the several available national/regional standards for evaluating the performance of evaporative cooling devices, the Australian and American standards are mostly referred.

To standardize the methods for evaluating the commercial evaporative cooling products, the Australian standard AS 2913 *Evaporative Air Conditioning Equipment* was first published in April 1987. This standard, from a technical point of view, prescribed a basis for rating the performance of evaporative air conditioning equipment in terms of airflow, evaporation efficiency and electricity consumption. Performance requirements for the commercial products, test methods and test procedures are specified. [2.15] It is worth mentioning that it suggested the calculation of cooling capacity and some specifics for nominal test conditions, such as inlet dry-bulb temperature of 38°C, inlet wet-bulb temperature of 21°C and room dry-bulb temperature of 27.4°C, which are widely referred by the subsequent standards developed in different countries thereafter.

Nowadays, the most comprehensive and mostly referred standards are the American standards, i.e. ANSI/ASHRAE standard **133** *Method of Testing Direct Evaporative Air Coolers* which dates from 1986 and **143** *Method of Test for Rating Indirect Evaporative Coolers* from 1989. The evaporative cooling technical Committee (TC5.7), which was set up by the American Society of Heating, Refrigerating and Air-Conditioning Engineers (ASHRAE), is responsible to specially develop standards for establishing consensus for both test methods for commercial use and performance criteria to guide the industry. The most updated version of the ANSI/ASHRAE standards for evaporative cooling in operation are ANSI/ASHRAE Standard 133-2015 *Method of Testing Direct Evaporative Air Coolers* and 143-2015 *Method of Test for Rating Indirect Evaporative Coolers*. There is also a pending proposed Standard 212P *Method of Test for Determining Energy Performance and Water-Use Efficiency of Add-On Evaporative Pre-Coolers for Unitary Air Conditioning Equipment*.

The Standard 143-2015 *Method of Test for Rating Indirect Evaporative Coolers* [2.22] provides recommended practices and accurate measurement procedures

for testing IEC devices under laboratory conditions to obtain rating information and is regarded as the essential reference in the following experimental research.

Technical Parameters for Performance Evaluation

The following indicators, i.e. temperature drop, wet-bulb depression, dew-point depression, pressure differential, wet-bulb cooling effectiveness, dew-point cooling effectiveness, cooling capacity, coefficient of performance (COP) and water consumption rate, are generally employed and will be adopted in this thesis to evaluate the cooling performance, energy efficiency and environmental impact of the DPC system. The operational parameters which affect the final cooling effect include intake air states of temperature and humidity, air velocity and flow rate, working-to-intake air ratio, etc.

(1) Temperature drop

Temperature drop is defined as the difference between the states of intake air (IA) and product air (PA). It depicts the effect the intake air being cooled under a certain condition.

(2) Wet-bulb depression

Wet-bulb depression is used to indicate how the air approaches to the state of adiabatic saturation. It is defined as the difference between the dry-bulb and wet-bulb temperatures of an airflow. [2.22]

(3) Dew-point depression

Similar to the wet-bulb depression, dew-point depression is the difference between the dry-bulb and dew-point temperatures of an airstream and describes the extend how the air approaches to its dew point.

(4) Pressure differential

Pressure differential refers to the pressure drop along the airflow pathway due to friction and velocity. [2.22] It relates closely to the power consumption of the fans which are the main components consuming electricity in an IEC system.

(5) Wet-bulb cooling effectiveness/saturation efficiency

Ideally, after sufficient exchange of heat and mass during a direct evaporative process, the dry-bulb temperature of the leaving airflow would equal to the wet-bulb temperature of initial entering air. However, in practice, the efficiency of heat and mass exchange is hard to reach 100%. Therefore, wet-bulb cooling effectiveness (WBE) is employed to demonstrate the saturation efficiency of an airstream after an EC stage. It is also introduced to evaluate the integrative effect of the heat and mass transfer in an IEC unit and defined as a quotient [2.22] in **Eq. [2-1]**, in which the numerator is the temperature drop and the denominator is the wet-bulb depression.

$$\varepsilon_{wb} = \frac{T_{db,in} - T_{db,out}}{T_{db,in} - T_{wb,in}} \quad [2-1]$$

Where,

ε_{wb} - Wet-bulb cooling effectiveness/saturation efficiency;

$T_{db,in}$ - Entering primary air dry-bulb temperature, °C;

$T_{wb,in}$ - Entering secondary air wet-bulb temperature, °C;

$T_{db,out}$ - Leaving primary air dry-bulb temperature, °C.

For commercial products, a reference value of the saturation efficiency is often given by the manufacturer under design conditions as per the exchanger size and material. Therefore, the outlet air temperature could be calculated with **Eq. [2-**

1] under given inlet air condition. While in operation, the saturation efficiency (WBE) is also a function of other operational parameters e.g. the airflow rate.

(6) Dew-point cooling effectiveness

Like dew-point depression, the dew-point cooling effectiveness is a dedicated indicator applicable to evaluate the cooling performance of a HMX employing dew point cooling technology, the advanced form of IEC.

Being precooled in an IEC unit, the entering air could reach by moisture evaporation a so-called state of sub wet-bulb, with temperature not only lower than its original wet-bulb but towards dew-point temperature. Similarly, dew-point cooling effectiveness (DPE) is defined in accordance with the wet-bulb effectiveness to rate the entire cooling effect, as **Eq. [2-2]** in which the numerator is the temperature drop and the denominator is the dew-point depression.

$$\varepsilon_{dp} = \frac{T_{db,in} - T_{db,out}}{T_{db,in} - T_{dp,in}} \quad [2-2]$$

Where,

ε_{dp} - Dew-point cooling effectiveness;

$T_{dp,in}$ - Entering primary air dew point temperature, °C.

(7) Cooling capacity

In an IEC unit, the product air experiences merely sensible cooling process. Therefore, the cooling capacity of an IEC unit can be evaluated by the sensible cooling of product air [2.22] as **Eq. [2-3]**. This cooling capacity definition will be used in the following research.

$$Q_{cooling} = \frac{c_{p,a} \rho_a V (T_{db,in} - T_{db,out})}{3.6} \quad [2-3]$$

Where,

Q_{cooling} - Cooling capacity, W;

$c_{p,a}$ - Specific heat of air at constant pressure, kJ/(kg·°C);

ρ_a - Density of air, kg/m³;

V - Airflow rate of product air, m³/h;

$T_{db,in}$ - Dry-bulb temperature of entering primary air, °C;

$T_{db,out}$ - Dry-bulb temperature of leaving primary air (i.e. product air), °C.

To keep consistent with the definition of cooling capacity for DEC units and highlight its superiority in cooling performance, the IEC cooling capacity sometimes is expressed also in form of total cooling capacity including latent and sensible cooling as **Eq. [2-4]**.

$$Q_{\text{total}} = \frac{\rho_a V (i_{db,in} - i_{db,out})}{3.6} \quad [2-4]$$

Where,

Q_{total} - Total cooling capacity including latent and sensible cooling, W;

$i_{db,in}$ - Specific enthalpy of entering (primary) air, kJ/kg;

$i_{db,out}$ - Specific enthalpy of leaving (primary) air, kJ/kg.

(8) Total power

Total power consumed by the system to perform evaporative cooling is the sum of the power provided to the fans for primary and secondary air, recirculating pump and the appurtenances. [2.22]

(9) Coefficient of performance (COP)/ Energy efficiency

Other than wet-bulb and dew-point effectiveness which are indices to respectively describe how the product air approaches to its original adiabatic and

psychrometric saturation states, coefficient of performance (COP) [2.23] is an index to evaluate the system efficiency in terms of energy utilization. It is defined as the result of output cooling capacity divided by the input total power as **Eq. [2-5]**.

$$\text{COP} = \frac{Q_{\text{cooling}}}{W} = \frac{c_{p,a}\rho_a V(T_{ab,in} - T_{ab,out})}{3.6W} \quad [2-5]$$

Where,

W - Measured total power consumption, W .

(10) Water evaporation rate and water consumption rate

Water consumption associated with evaporative cooling is an important common concern for the public, especially in the regions under hot and dry climate i.e. scarcity of water resources.

The water turning into the exhaust airflow by evaporation is the effective part to directly perform cooling activity and could be calculated by taking account of the moisture increase from inlet to outlet of the working air as **Eq. [2-6]**.

$$V_{evp} = \frac{1000V_2\rho_{a,2}}{\rho_w} (w_2 - w_1) \quad [2-6]$$

Where,

V_{evp} - Water evaporation rate, L/h;

V_2 - Secondary airflow rate, m^3/h ;

$\rho_{a,2}$ - Mean density of secondary air, kg/m^3 ;

ρ_w - Water density, kg/m^3 ;

w_1 - Inlet humidity ratio of secondary air, kg/kg ;

w_2 - Outlet humidity ratio of secondary air, kg/kg .

However, excess water, more than directly involved in evaporation, is essential in practice to keep a desirable evaporation performance against mineral build-up, scaling, fouling and possible algae growing on the soggy evaporation media and maximally realise the fully wetting of the evaporation media.

When the dissolved mineral content in the cycling water reaches a certain level, more water is required to be introduced to dilute by bleeding off part of the existing water in the system. However, the relationship between water hardness and bleed rates is so complex that no national or international standards available up to now, to propose a general equation to calculate the bleeding water consumption rate.

An ideal evaporative cooler, with full heat and mass exchange and operating on distilled water, would consume 1.5 L water to generate 1 kWh cooling, based on the theoretical calculation of latent heat in phase transformation. This represents a lowest limit associated with water consumption rate without excess drain water.

(11) Working-to-intake air ratio/ secondary-to-primary air ratio

In IEC systems, the primary airstream is separated from the secondary airstream by the moisture-tight heat exchanging sheet or membrane. The secondary air evaporates water and cools the primary air at the other side of the heat exchanging wall. Usually, more secondary air could accommodate more moisture to evaporate and produce more cooling. Especially, when the total amount of the primary and secondary air is constant, e.g. in a regenerative system, the proportion of the secondary air, being working medium, determines the cooling performance of the IEC unit.

Secondary-to-primary air ratio is also called working-to-intake air ratio for regenerative IEC systems, and abbreviated as *working air ratio*. Working air

ratio is defined to describe the ratio of working airflow rate to total intake airflow rate as **Eq. [2-7]**.

$$\varphi = \frac{V_{EA}}{V_{IA}} \quad [2-7]$$

Where,

φ - working air ratio;

V_{IA} - Intake airflow rate, m³/h;

V_{EA} - Working (commonly exhaust) airflow rate, m³/h;

2.3 R&D Progress and Practical Applications of IEC Technologies

2.3.1 Overview of R&D works in the IEC Field

With the continuous progress in technology innovation and research deepening, particularly the development of M-cycle [2.24], the IEC systems have obtained significantly enhanced cooling performance in recent decades and attracted more attention in various application fields and regions. Many researchers have been attracted by its cooling performance, especially its energy efficiency which is much more than that of the conventional vapour compression refrigeration. Many comprehensive review papers [2.25-2.37] have been published and intended to help explore the potential in R&D development and introduce new application fields by forming hybrid systems.

The research work on IEC technologies mainly exists in the following aspects:

1) research methodology and theory innovation, e.g. introducing the concept of entransy, entropy and exergy to analyse and evaluate the energy efficiency of the IEC system [2.38-2.46]; 2) the technical progress in IEC technologies, e.g. M-cycle, regenerative IEC and dew point cooling; 3) in-depth studies on the heat

and mass exchanger, e.g. HMX structure, flow pattern and application of new material as the wetted media; 4) hybrid system combining other technologies, especially the dehumidification assisted IEC; 5) engineering demonstration and application in extensive fields and feasibility study, e.g. data centres; 6) energy saving, economic and environmental analysis, and climatic adaptability assessment.

2.3.2 Theoretical Innovation

Thermodynamic methodologies have been introduced in recent years to analyse and optimize the system efficiency not only in view of the first thermodynamic law but also the second law considering the entransy dissipation and exergy destruction.

Chen et al [2.38] introduced a new approach based on entransy theory to tackle the coupled heat and mass transfer process, analyse and optimize the evaporative cooling system in 2010. Some new concepts, e.g. moisture entransy, moisture entransy dissipation and thermal resistance based on moisture entransy dissipation (TRMED), were firstly introduced. The endothermic ability of humid air is described with the moisture entransy. The loss of the endothermic ability, i.e. the irreversibility was measured with the moisture entransy dissipation. A new index, i.e. the moisture entransy dissipation rate divided by the squared refrigerating effect output rate, was defined as new thermal resistance to evaluate the performance of an EC system. Two DEC cases were analysed with the proposed concepts to demonstrate the applied value of the new theory.

Chen et al [2.39] further demonstrated the application of the new concepts in direct/indirect evaporative cooling processes. The validated results proposed that other than enthalpy, the new defined moisture entransy represents the endothermic ability of humid air, and TRMED is an essential factor for the system performance. The case study suggested a way leading to better cooling

performance by either enlarging the thermal conductance or reducing the temperature potential of the humid air, i.e. lowering the system TRMED.

Based on the entransy theory, Yuan and Chen [2.40] proposed a global optimization method to improve the energy efficiency of IEC systems. The study was based on the analysis of the process irreversibility and evaluated by the entransy dissipation. The theoretical relationship between the user demands and the physical structure of the HMX and operating parameters of the air and water involved was established to perform the optimization with the dedicated equation groups. A case study on an IEC system was conducted to demonstrate that the optimal performance of the system depended much more on the global optimization rather than the detailed parametric analysis.

Santos et al [2.41] applied exergy analysis along with the normal energy analysis to the evaporative cooling process. The authors did not agree the conventional evaluation methodology by saturation effectiveness could reflect the irreversibility process of the heat and mass transfer within the HMX and suggest the optimum working conditions. As a supplementary to the mass and energy analysis, an exergy analysis and the second law of thermodynamics efficiency were investigated with the object of an air washer. The results indicated that the optimal state of intake air for a desirable thermal comfort did not accord with that for optimum thermodynamic performance. The authors suggested that the energy and exergy analyses should be conducted simultaneously in optimizing the comprehensive performance of an EC system.

Farmahini-Farahani et al [2.42] performed exergy analysis based on experimental results. The evaporative cooling systems of direct, indirect and two-stage indirect/direct under various climatic conditions in Iran were experimentally investigated and exergy balances were established to present the exergy efficiency and the process irreversibility. The authors suggested that it was necessary to integrate the second law of thermodynamics into account when

evaluating the comprehensive efficiency of an evaporative cooling system. Further, the authors recommended the optimal climatic conditions for three EC systems perspective from the exergy efficiency.

Caliskan et al [2.43] compared the performance of M-cycle and other three conventional IEC systems in terms of combined energy and exergy analyses. Sustainability index, which is directly relates to exergy efficiency and exergy destructions, was introduced to evaluate the sustainability of the system. The results proved the superiority of M-cycle over the other three conventional IEC systems under different dead temperatures (i.e. reference temperature) from the points of exergy efficiency and system sustainability.

Zhang et al [2.44] intended to propose a proper theoretical tool for AC system performance optimization. The similarities and distinctions between exergy and entransy analyses were investigated. Based on the investigation of exergy destruction and entransy dissipation in mixing and heat transfer process, relating formulas were deduced to present the numerical relationship among various parameters. Exergy destruction and entransy dissipation were employed to identify the principal factors limiting system performance and the results indicated the contribution of reducing exergy destruction or entransy dissipation to the improvement of system performance. The authors suggested different theoretical parameters for different technical purposes, i.e. entransy for transfer process and exergy for heat-work conversion process.

Zhang et al [2.45, 2.46] further applied the exergy and entransy analyses to the humid air handling process in evaporation and dehumidification. Case studies aiming to reduce the unmatched exergy destruction implied that raising the water temperature was more effective than higher air temperature to promote the moisture evaporation.

The investigation into the literatures on IEC and relevant technologies in the recent decade shows that the irreversibility of the heat and mass transfer and the impact of exergy destruction and entransy dissipation on system performance has attracted the researchers' attention. They intended to develop comprehensive methods to evaluate and assist optimizing the IEC system, combining the application of the first and second laws of thermodynamics. The concept of new thermal resistance based on moisture entransy dissipation (TRMED) and sustainability index were proposed based on the second law analyses. Although they have been validated and employed into applied case studies by the authors themselves, the new concept and approaches have not been discussed and adopted extensively in the worldwide IEC research up to now. However, it proposed a promising way to explore the in-depth mechanism inside IEC process from the point of the second law of thermodynamics.

2.3.3 Research Progress in IEC Technologies

Although it was proposed early in 1976 by Dr Maisotsenko via patent application [2.47], the conception of M-cycle aroused the researchers' interests in IEC application since the *Coolerado*® Corporation launched the commercial products around 30 years later. [2.48] The increasing research interest concerning IEC keeps constant especially after 2010, which could be seen from the increased number of published peer-review research papers from more than 20 countries worldwide. [2.30]

The recent development of IEC technologies can be summarized into the following aspects: 1) the development and validation of research methods, including numerical simulation, experimental investigation and combined experimental research based on validated simulation model; 2) variety of product, i.e. common air-side IEC (air cooler) and water-side IEC (water chiller); 3) optimization of HMX configuration and the system operation, including plate-stack exchanger and tube exchanger, flow pattern of count-flow and cross-flow

and various wetted media; 4) hybrid systems combined with other techniques, e.g. desiccant, heat pipes, PV etc.; 5) enlarged application fields, e.g. data centres, gas turbines, and associate performance and economical assessment.

After a brief overview relating to the technique progress in the aforementioned various aspects. The literature review in this section will focus on the material acting as wetted and evaporating media and the investigation, either numerically or experimentally, into the sheet-stack HMX inside to help develop a super performance dew point cooler.

Water-side IEC (water chiller)

Other than the conventional product of cool air, Xie and Jiang [2.49] developed an IEC system to produce cold water for terminal air conditioning use. The authors intended to increase the cooling delivery efficiency by water instead of comparatively huge amount of airflow, especially for applications in large scale public buildings in hot and dry climate. The established system is illustrated in **Fig. 2-7**. The intake air is firstly pre-cooled with a sensible heat exchanger and then directly contacts with the spraying water in the padding tower to produce cold water by evaporative cooling process. The field tests showed that the product water could achieved sub-wet bulb temperature of the inlet air with a COP value of 9.1 after 5 years normal running. However, the research followers on this system are few in terms of published journal paper in English since it appeared in 2010.

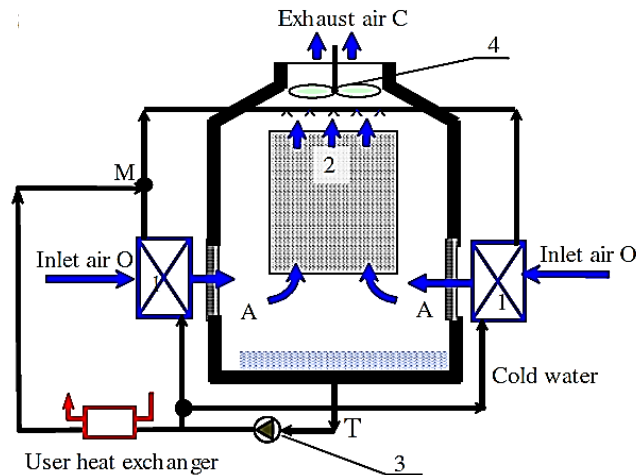


Fig. 2-7: System of a water-side IEC. [2.49]

Tubular exchanger

As an IEC air cooler, the moisture evaporation could take place inside or outside of the tube, which separates the product airflow from the working air with the solid wall.

R. Armbruster and J. Mitrovic [2.50] carried out experiments research on evaporative cooling of a freely falling water film among horizontal tubes. Under different water flow rate, the water flow between the tubes presented three basic patterns, i.e. droplets, columns, or a liquid sheet as shown in **Fig.2-8**, at moderate tube spacing. The authors developed an empirical equation to calculate the evaporative cooling performance based on the experimental results. This work could be regarded as a fundamental research for IEC application with tube structure HMX.

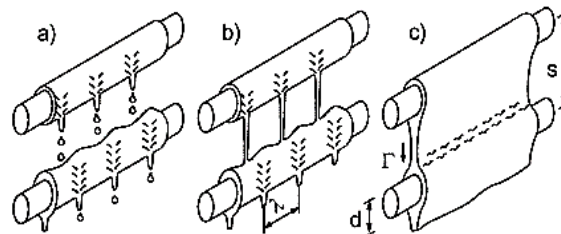


Fig. 2-8: Water flow patterns inside an IEC tubular exchanger. [2.50]

a) droplets; b) columns; c) liquid sheet.

Martinez et al [2.51, 2.52] introduced a semi-indirect evaporative refrigerator which was made of standing solid porous ceramic pipes as shown in **Fig. 2-9**. The primary and secondary airflow was separated by the ceramic wall and water down flowed and evaporated along the inner wall. The primary air swept across the outer surface of the tubes and allowed some vapour in due to the permeability of the porous wall. Depending on the air humidity, it could act as a sensible or enthalpy exchanger. One of the applicable conditions recommended by the authors was hot and humid climate.

Considering the geometric configuration, publications relating to the tubular HMX employed in IEC applications have been rarely observed in recent years.

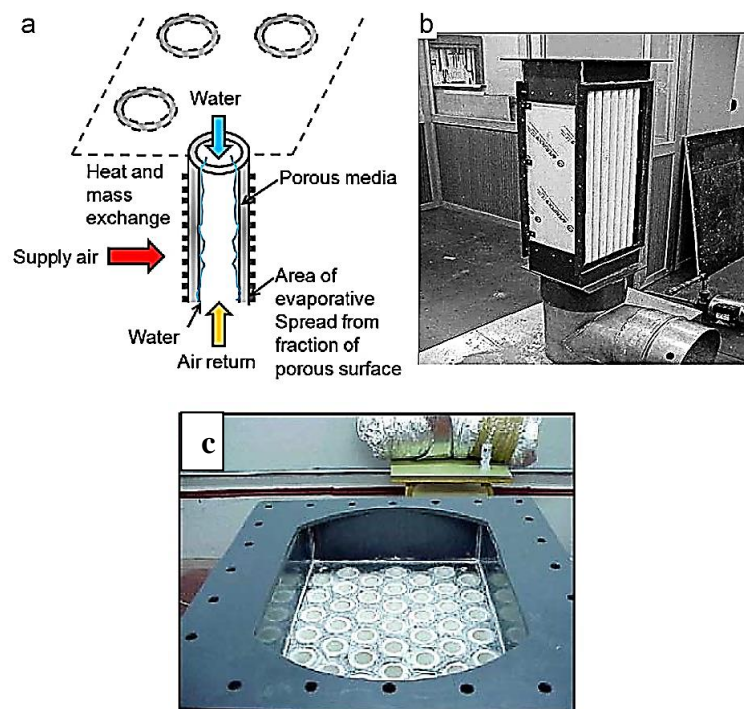


Fig. 2-9: A semi-indirect evaporative refrigerator with tubular exchanger. ^[2.51]

- a) schematic of the heat and mass transfer inside a porous ceramic pipe;
- b) experimental prototype; c) above view of the ceramic pipe exchanger.

Hybrid system (desiccant enhanced IEC, DEVap)

With the technical innovation and progress, the IEC technologies have raised increasing concerns and been regarded to be able to lead a promising way,

independently or by being integrated into hybrid systems, towards better energy-efficient air conditioning in either building or data centre applications. [2.53-2.63] Besides sporadic applications in recent years integrated with e.g. heat pipes [2.64, 2.65], inlet air cooling of gas turbine [2.66], nocturnal radiative cooling [2.67], cooling/reheating treatment [2.68], most research interests are drawn in the hybrid systems combined desiccant process to enhance the evaporative cooling effect and climatic adaptability.

Independent control of the air temperature and humidity in building air conditioning application presents a promising way for better comprehensive energy efficiency. [2.69-2.74] Moreover, the pre-treatment by cooling and dehumidification to the inlet air in the IEC system allows the working air to be able to show enhanced cooling potential in the working channel. Therefore, the desiccant-enhanced evaporative air conditioning (DEVap) is regarded as a desirable hybrid system and attracts increasing concerns in relating research fields. Among the three general forms, i.e. membrane dehumidification [2.75-2.79], solid [2.80-2.83] or liquid [2.84-2.97] desiccant hybrid systems, liquid desiccant based IEC system dominates the relevant research.

The common used liquid desiccants include calcium chloride, lithium chloride, lithium bromide, tri-ethylene glycol, and a mixture of 50% calcium chloride and 50% lithium chloride. Owing to the difference of partial vapour pressure between the air and the surface of the liquid desiccant solution in high concentration, desiccants absorb moisture of the inlet air and complete the pre-humidification. When the solution is diluted by the absorbed moisture, it is sent to regeneration process to release the moisture by heating with an external low-grade heat resources. The air is dehumidified with the desiccant dehumidifier and its temperature is lowered by the evaporative cooler. In desiccant based evaporative cooling techniques, latent and sensible loads are separately removed using desiccant dehumidification system and cooling unit, respectively.

The recent concerns mainly focus on the research method, equipment and system configuration, energy saving and economic assessment of various applications. The progress in the liquid desiccant enhanced IEC hybrid system helps remove the limitation of humid climates to the IEC application, and create indoor thermal comfort with desirable energy efficiency.

Material for evaporating surface

Researches aiming to improve the IEC performance are numerous. In addition to optimize the HMX geometry to enhance the heat and mass transfer rates, research interests have also shown in evaporating medium (wet surface material) [2.98-2.105]. This is because the properties of the heat/mass exchanging medium, i.e. its moisture wicking ability, diffusivity and evaporation ability, can greatly affect the wetted area as well as the moisture diffusion and evaporation rate, and therefore affect cooling efficiency and performance of evaporative cooling systems.

Bruno [2.98] constructed a flat-plate cross-flow heat and mass exchanger, which used a special medium with high water retention and wickability characteristics to form the wet channel, and a moisture impervious membrane for the dry channel. Tests indicated that the exchanger had a dew point effectiveness of 75%, which was comparatively low under the given operational condition.

Velasco et al. [2.99] carried out an experimental study into a polycarbonate based IEC heat exchanger, which benefited from low cost and weight, with no corrosion problems; the limitations caused by low thermal conductivity were reduced by minimising plate thickness. The results showed that higher outdoor air temperature or airflow rate facilitated to enhance the system cooling performance.

A wide range of materials have been commonly used as the heat/mass exchanging medium, and may be classified as metal, fibre, ceramic, zeolite and carbon types. Metal types include metal forms, metal wools, sintered metals and wickered metal plates/tubes. Fibre types include paper board, cloth (wood or glass) fibres. Ceramic types include silicon carbide/silicon carbide composites, zirconia ceramics, zirconia-toughened aluminium, zirconium dioxide, aluminium oxide, and aluminium nitride and polystyrene composites. Zeolite types include porous ceramics, molecular sieves and synthetic polymers, and carbon fibres refer to carbon composites and activated carbon. Zhao et al. [2.100] conducted a comparative study on the above types of materials as potential heat and mass transfer media used in IEC systems, and the results showed that thermal properties of the materials, i.e., thermal conductivity and water-retaining capacity (porosity), had little impact on system heat/mass transfer, and therefore, these two parameters had low key roles in terms of material selection. Instead, shape formation/holding ability, durability, compatibility with water-proof coatings, contamination risk as well as cost, were more important concerns in this regard.

Some natural fibres have been investigated for their evaporating cooling effect [2.101-2.104].

Maurya et al. [2.101] comparatively studied three types of cooling pad made of aspen fibre, cellulose, and coconut coir, based on summer weather conditions in Bhopal, India. The results showed that the saturation efficiency at the air velocity of 0.5 m/s was highest for aspen material at 80.99% compared to 69.58% for the cellulose and 68.15% for the coconut coir. The performance of coconut coir was very close to the cellulose pad in water soaking ability. The saturation efficiency of the pad depended upon the wetted surface area because a higher wetted surface area causes greater evaporation of water into air, thereby decreasing the air temperature.

Kulkarni et al. [2.102] reported a theoretical performance study of an evaporative cooler with different cooling pad shapes and materials. The performance of rectangular, cylindrical, and hexagonal shapes of evaporative cooler pads, based on rigid cellulose, aspen, corrugated paper, and high-density polyethylene (HDPE) were theoretically analysed. It was found that the highest saturation efficiency was 91% for the hexagonal pad of aspen material and the lowest value of 72.4% was obtained for the rectangular pad of cellulose material under the simulated working conditions.

Soponpongpiat [2.103] studied the evaporative cooling efficiency and pressure drop of wetted recycled HDPE and rice husk pads in an EC system. A commercial wetted pad was also tested for comparison. It was found that the rice husk pad gave an average saturation efficiency of 55.9%, while recycled HDPE of 29.1% under the testing conditions. However, the pressure drop across the rice husk and recycled HDPE pads was significantly higher than that of the commercial wetted pad.

Faleh [2.104] studied the cooling performance of an evaporative cooler by using cooling pads made of different materials such as jute, luffa and palm fibre. As reference, a widely used commercial Aspen-wood excelsior wetted pad was evaluated as well. The experiment was set with a flow velocity through the cooling pads at 2.4 m/s. In conclusion, the study showed cooling efficiency of the cooling pads made of various materials as follow: 62.1% for jute, 55.1% for luffa, 49.5% for the commercial cooling pad and 38.9% for palm fibre. The results from the cooling efficiency degradation indicated that luffa had an overall advantage over the other fibres. Palm fibres and the commercial material demonstrated a significant reduction in the cooling efficiency, while jute showed the highest deterioration. However, if the jute surface could be treated to offer higher mould resistance characteristics, it would be the best alternative.

Cloth fabrics, which exhibit large capillary force and avoid bacterial growth with proper treatment, are potentially highly effective media for evaporative cooling. However, relatively few reports of this type of materials can be found in evaporative cooling applications. Niyomvasa et al. [2.105] performed experimental studies to compare two types of cooling pad made from a curtain fabric and a raw cotton fabric. It showed that the average difference in temperatures between inlet and outlet were 2.9°C and 1.7°C for the curtain and raw cotton fabrics, respectively. The average saturation efficiency was found to be 54.8% for the curtain fabric, and 33.2% for the raw cotton fabric.

A variety of fabric samples weaved from various moisture-wicking fibres are intended to be tested in the following chapters as for the capability of moisture wicking, diffusivity rate, evaporation rate and mechanical processability to explore a new way to prompt the moisture evaporation and reduce the water recirculating.

HMX and system configuration

In recent development of IEC technologies, the HMX structure has been dominated by various sheet-stacked forms with different material assisting moisture evaporation and heat transfer. The airflow patterns mainly included cross-flow and counter-flow. The research methodologies covered the experiment-based, simulation-based and combined experiment and simulation works.

In terms of the experimental research, *Coolerado*® (USA) developed a cross-flow heat exchanger with perforated holes on the flow paths. A test indicated that this type of exchanger could obtain the wet-bulb and dew-point effectiveness of around 80% and 50% under the specified operational condition [2.106], which is around 20% higher than those of the conventional IEC heat exchangers.

Riangvilaikul et al [2.107] conducted an experimental investigation into a novel dew point evaporative cooling system, indicating that the wet-bulb and dew-point effectiveness were in the range 92% to 114% and 58% to 84%, under the pre-set operational condition.

Chen et al [2.108] presented an experimental investigation to evaluate the performance of a plate type air cooler under four working modes, i.e. dry/wet mode and low/high air humidity. The wet operation mode relating to IEC application improved the cooling capacity significantly both in sensible and latent aspects. Condensation was observed under high humidity inlet condition, which led to the decrease in sensible efficiency but increase in latent efficiency and total heat transfer rate. Under the IEC mode, the highest COP of the air cooler achieved 9.0 when condensation occurred.

Antonellis et al [2.109] experimentally studied the performance of a cross-flow IEC system under different operating conditions of data centres with special concern on water flow rate. The test results indicated that the water flow rate influenced the cooler performance heavily and the wet-bulb cooling effectiveness varied in range of 50-85% as per the operating conditions and system setup.

In terms of the computer simulation and combined modelling and experiment, Tuisidasani et al [2.110] studied the relation between the COP and air velocity for a tube type HMX using both modelling and experimental methods, indicating that the maximum COP of the IEC unit was 22 at the primary air velocity of 3.5 m/s and the secondary air velocity of 3 m/s, leading to 10.4°C of primary air temperature drop.

Guo et al [2.111] numerically investigated the thermal performance of a cross-flow IEC cooler in regard to air velocity, channel width, inlet relative humidity and the wettability of the evaporating surface. It was concluded that smaller

channel width, lower inlet RH of the secondary air, higher wettability and higher working air ratio contributed to a higher cooling effectiveness.

Zhao et al [2.112] conducted a numerical study into a novel counter-flow flat-plate HMX for dew point cooling, indicating that cooling effectiveness and energy efficiency of the exchanger were largely dependent on the dimensions of the airflow passages, air velocity and working-to-intake air ratio, and less dependent on the temperature of the feed water.

Zhan et al [2.113] carried out a comparative study into the M-cycle counter-flow and cross-flow flat-plate HMXs, indicating that the counter-flow exchanger offered around 20% greater cooling capacity, 15%-23% higher dew-point and wet-bulb effectiveness, but 10% lower COP. Further, Zhan et al [2.114] conducted a numerical study into a cross-flow dew point cooling HMX, indicating that the average air velocities in dry and wet channels should be less than 1.77 m/s and 0.7 m/s respectively, the optimum working-to-product air ratio was 50%, the channel's length-to-height ratio should be in the range 100 to 300, while its height should be in the range 4 mm to 6 mm.

Hasan [2.115] developed an analytical model based on a modified ϵ -NTU method aiming to achieve sub-wet-bulb temperature by indirectly pre-cooling the working air. The modification to the normal sensible heat exchanger mainly existed in the potential gradients, transfer coefficient, heat capacity rate parameters and assuming a linear saturation temperature-enthalpy relation of air. The application to predict the cooling performance succeed in a case of a regenerative IEC unit.

Cui et al [2.116] presented a computational fluid dynamics (CFD) study into the counter-flow HMX, in order to analyse the impacts of operational conditions and geometrical parameters on the cooler's performance. The discrepancy regarding to temperature distributions and outlet air conditions provided by the model was

found to be within $\pm 10\%$. The simulation results indicated that cooling effectiveness of the exchanger was increased with lower air velocity, smaller channel height, larger channel length-to-height ratio, and higher working-to-intake air flow ratio. Cui et al [2.117] developed a modified log mean temperature difference (LMTD) method for predicting thermal performance of the present M-cycle counter-flow and cross-flow HMX. The results were found to be within $\pm 8\%$ discrepancy when compared to experimental data.

Chen et al [2.118] noticed the condensation problem occurring in dry channels when the IEC system was applied under humid climate. The authors developed analytical models, which were validated by the published results, to distinguish the three condensation states, i.e. non-condensation, partially condensation and totally condensation states. Further, the authors incorporated the analytical models into TRNSYS to predict an IEC hybrid cooling system's performance in a field study in Hongkong for validation.

Lin et al [2.119] presented a numerical study of a dew point cooling system with counter-flow configuration. The study found the saturation point of working air occurring at a fixed point regardless of the inlet air conditions, the minimum intensity point of water evaporation at 0.2 to 0.3 m from the entrance and the overall heat transfer coefficient above $100\text{w}/(\text{m}^2\cdot\text{K})$ in wet channel of the unit.

Moshari and Heidarinejad [2.120] presented a numerical simulation to the cross- and counter-flow Regenerative Evaporative Coolers (REC) and a cross-flow IEC cooler and associated experimental validation. The results showed that the counter-flow REC could achieve 30% higher wet-bulb effectiveness than the cross-flow type of the same size. When increasing the working air ratio from 0.2 to 0.9, the wet-bulb effectiveness of the cooler increased by 10%-20%.

Moshari et al [2.121] numerically compared three different configurations for two-stage systems, i.e. IEC/IEC to find out the optimal structural design as for

wet-bulb effectiveness under various Iran climatic conditions, i.e. hot-dry, hot-semi-humid, hot-humid, moderate-dry and moderate-humid. The authors intended to accurately compare water evaporation rate among different evaporative coolers by proposing a definition of Dimensionless Water Evaporation Rate (DWER). The DWER decreased with the increase of the primary airflow rate whereas water consumption increased in either a counter-flow regenerative evaporative cooler or a common IEC unit.

Sohani et al [2.122] presented a numerical model for simulating the performance of the dew point coolers with an M-cycle cross-flow HMX. This model employed a novel data handling neural networking method to carry out the statistical works. The features of the proposed system were optimised for twelve diverse climatic conditions, based on Koppen–Geiger’s classification.

Pandelidis et al [2.123] developed a two-dimensional HMX model and investigated eight different types of M-Cycle HMXs used in dew point cooling. The simulation results were compared with the testing data, in order to find a solution to improve the HMX performance. Pandelidis et al [2.124] described the optimization process of a cross-flow M-cycle dew point air cooler using both the single-parameter and multi-parameters methods. The multi-parameters optimization method, based on the analysis of the Harrington function of desirability, could give satisfactory results, and thus enabled the identification of the optimal operational and geometrical conditions for the HMX and the determination of the optimum climatic conditions for its effective operation.

Riangvilaikul and Kumar [2.125] presented a numerical study of a counter-flow heat exchanger, which involved the numerical simulation of the heat and mass transfer processes within the flow channels, and experimental validation [2.107]. Reasonable agreement was achieved between the numerical and experimental results, giving 5%-10% of deviation in terms of the outlet air temperature and

cooling effectiveness, respectively. The dew-point effectiveness of the unit was in the range 0.58 to 0.84, higher than the cross-flow exchanger.

Kabeel et al [2.126] numerically and experimentally investigated the performance of a novel indirect evaporative cooler with internal baffles. The effect of the inlet conditions (inlet air temperature and humidity ratio) was studied and the results showed that for five cooler configurations under different inlet air conditions, the outlet air temperature decreased with the increasing number of baffles.

Lin et al [2.127] proposed a transient model for a counter-flow dew point cooling system, indicating that the dynamic behaviour of the dew point evaporative cooler was crucial in achieving an efficient cooling. It was also found that the proposed transient model could predict the product air temperature with a maximum discrepancy of 4.3%.

2.3.4 Analysis of Dew Point Cooling Research

By intensive literature review of the IEC technology progress over the last decade, it is found that M-cycle and regenerative pre-cooling are the two most commonly used approaches to realize dew point cooling, which stands for the cutting-edge technology in evaporative cooling. To develop the proposed dew point cooler, the significant papers and technique reports which feature dew point cooling, regenerative and M-cycle, in the past ten years have been extensively and intensively reviewed and tabulated in **Tables 2-1 to 2-31** to facilitate comparison as per the publishing year, research methodology, assumptions for modelling, flow pattern, wetted media, HMX configuration and conclusions. The tables follow the chronological order, intending to reflect the research progress.

Table 2-1: Titled ‘dew point’ cooling case 1

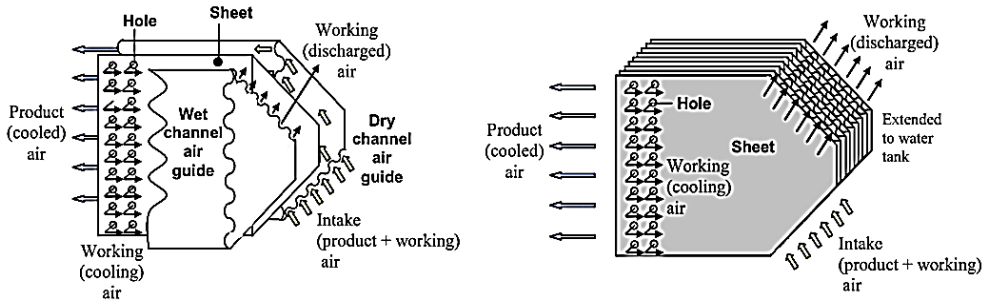
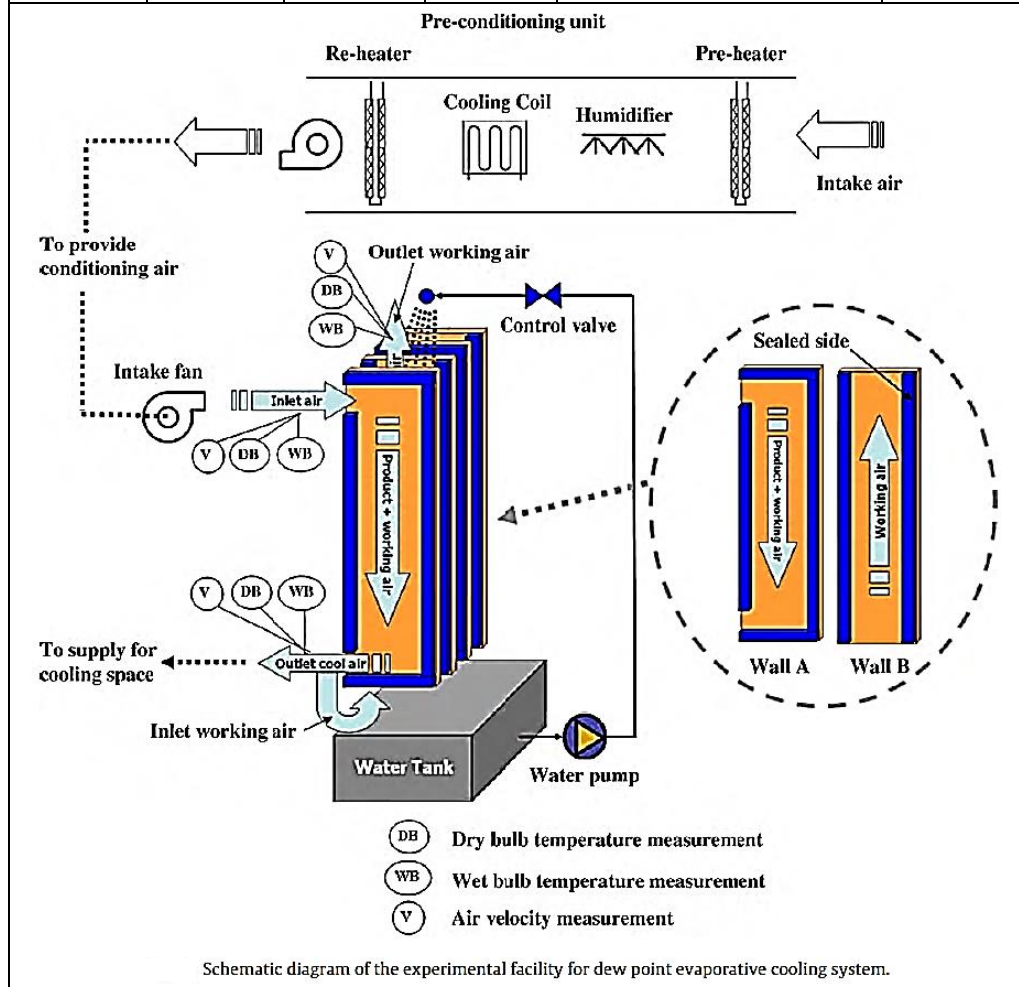
Ref.	Year	First author	Nation	Methodology	
[2.112]	2008	Zhao	UK	Numerical, based on Newton iterative method with EES software	
Assumptions					
1) Heat transfers vertically to the separating plate, and no heat flow occurs along the airflow direction; 2) Airflow across the channel is uniform; 3) Water travels vertically to the airflow; 4) Wet wall is entirely saturated; 5) Air is incompressible.					
Flow pattern	Configuration				
	Channel gap (mm)	Channel length (mm)	Channel width (mm)	Material	Plate thickness (mm)
Counter	10	1000	-	Polygonal sheets	0.5
 <p style="text-align: center;">The polygonal stack exchanger configuration.</p>					
Conclusions					
1) Cooling effectiveness (DPE/ WBE) and energy efficiency are largely dependent on the dimensions of the airflow passages, air velocity and working air ratio, and less dependent on the water temperature; 2) IA velocity should be controlled at 0.3–0.5 m/s; 3) Channel height should be 6 mm or less and the channel length should be 200 times of the height; 4) working air ratio should be around 0.4.					

Table 2-2: Titled ‘dew point’ cooling case 2

Ref.	Year	First author	Nation	Methodology	
[2.107]	2010	Riangvilaikul	Thailand	Experimental	
Flow pattern	Configuration				
	Channel gap (mm)	Channel length (mm)	Channel width (mm)	Material	Plate thickness (mm)
Counter	5	1200	80	Polymer sheets (dry) /cotton sheet coated with polyurethane (wet)	0.5



Conclusions

1) When IA temperature more than 30°C, IA velocity should be kept below 2.5 m/s to obtain WBE greater than 100%; 2) WBE varies not much during continuous operation under the real ambient conditions.

Table 2-3: Titled ‘dew point’ cooling case 3

Ref.	Year	First author	Nation	Methodology
[2.125]	2010	Riangvilaikul	Thailand	Numerical, based on finite difference model
Assumptions				
1) The velocity and properties of all fluids are uniform; 2) Adiabatic condition for the outer surface and no heat loss of working air at the inlet of wet channel; 3) Heat transfer of process air is only in the direction normal to the parallel wall; 4) Wet surface is entirely saturated; 5) Thermal conductivity of the wall and temperature difference of wall surfaces between dry and wet side are neglected.				
Flow pattern	Configuration			
	Channel gap (mm)	Channel length (mm)	Channel width (mm)	Material
Counter	5	1200	80	Polymer sheets (dry) /cotton sheet coated with polyurethane (wet)
<div style="display: flex; justify-content: space-around;"> <div style="text-align: center;"> <p>(a)</p> </div> <div style="text-align: center;"> <p>(b)</p> </div> </div> <p style="text-align: center;">The dew point evaporative cooling system and (b) two types of the wall.</p>				
Conclusions				
1) WBE is less sensitive ranging between 106% and 109% for the same inlet condition; 2) Suggested design parameters: IA velocity below 2.5 m/s, channel gap less than 5 mm, channel length larger than 1 m and working air ratio around 0.35-0.6.				

Table 2-4: Titled ‘sub-wet bulb’ cooling case 1

Ref.	Year	First author	Nation	Methodology	
[2.145]	2010	Hasan	Finland	Numerical	
Assumptions					
1) Cooler is well insulated from its surroundings; 2) Thermal conduction in the wall and water film in the x-direction is neglected; 3) Heat and mass transfer coefficients inside each passage are constant.					
Flow pattern	Configuration				
	Channel gap (mm)	Channel length (mm)	Channel width (mm)	Material	Plate thickness (mm)
Counter/parallel	3.5	500	500	-	0.5
<p>a</p> <p>b</p> <p>(a) Indirect evaporative air cooler, (b) Dividing a cooler into elements.</p>					
Conclusions					
Four types of coolers are studied: three two-stage coolers (a counter-flow, a parallel-flow and a combined parallel-regenerative flow) and a single-stage counter-flow regenerative cooler.					

Table 2-5: Titled ‘dew point’ cooling case 4

Ref.	Year	First author	Nation	Methodology	
[2.98]	2011	Bruno	Australia	Experimental	
Flow pattern	Configuration				
	Channel gap (mm)	Channel length (mm)	Channel width (mm)	Material	Plate thickness (mm)
Counter	-	-	-	-	-
<p style="text-align: center;">Schematic of heat exchanger of dew point cooler.</p>					
Conclusions					
<p>1) Counter-flow indirect evaporative cooler can supply air at a temperature comparable to refrigeration systems at higher thermal efficiencies; 2) Unlike refrigeration systems, the energy efficiency increases with outdoor temperatures, and so the cooler can contribute to reducing the peak electrical load.</p>					

Table 2-6: Titled ‘M-cycle’ cooling case 1

Ref.	Year	First author	Nation	Methodology	
[2.114]	2011	Zhan	UK	Numerical, based on finite-element approach with EES	
Assumptions					
<p>1) Heat and mass transfer is in steady state. Cooler enclosure is the system boundary; 2) Wet surface of the fibre sheet is completely saturated. The water vapour is distributed uniformly within the wet channel; 3) A temperature gradient for the channel cross-section is zero. Heat transfer in the separating plate is considered in the vertical direction only; 4) Within the working fluid, the cross stream convective heat transfer is considered as the dominant mechanism of heat transfer; 5) Each element has a uniform wall surface temperature. Temperature difference between dry and wet sides of the wall can be ignored; 6) Air is incompressible.</p>					
Flow pattern	Configuration				
	Channel gap (mm)	Channel length (mm)	Channel width (mm)	Material	Plate thickness (mm)
Cross	4	400-1200	-	-	0.24
<div style="display: flex; justify-content: space-around;"> <div style="text-align: center;"> <p>(a) Structure view</p> </div> <div style="text-align: center;"> <p>(b) Air flow distribution in the dry/wet channels.</p> </div> </div> <p style="text-align: center;">Schematic of the heat and mass exchanger in ISAW TAC-150. (a) Structure view. (b) Air flow distribution in the dry/wet channels.</p>					
Conclusions					
<p>1) The recommended average air velocities in dry and wet channels should be less than 1.77 m/s and 0.7 m/s, respectively; 2) Reducing the channel height leads to an increase in cooling capacity or WBE but decrease of the system COP. Channel height should be set to no more than 4 mm; 3) Increasing the channel length leads to improved cooling effectiveness but reduced system COP. Dimensionless channel length should be controlled between 100 and 300; and 4) System performance is highly dependent on the climatic conditions.</p>					

Table 2-7: Titled ‘below wet-bulb’ cooling case 1

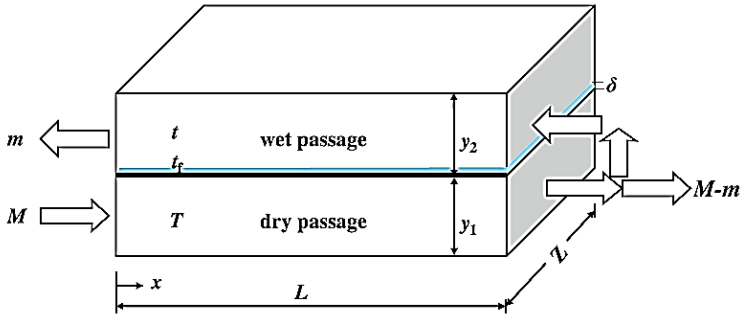
Ref.	Year	First author	Nation	Methodology	
[2.115]	2012	Hasan	Finland	Numerical	
Assumptions					
1) Cooler is well insulated to the surrounding; 2) Longitudinal thermal conduction in the wall in the x-direction is neglected; 3) Heat and mass transfer coefficients inside each passage are constants; 4) Reynolds analogy is valid and the Lewis number is unity; 5) Liquid side of the air–water interface offers a negligible resistance to heat transfer so that the interface temperature is saturated at the water film temperature.					
Flow pattern	Configuration				
	Channel gap (mm)	Channel length (mm)	Channel width (mm)	Material	Plate thickness (mm)
Counter	3.5	500	500	-	1.5
 <p style="text-align: center;">A single stage counter flow regenerative air cooler.</p>					
Conclusions					
1) Modified analytical model for indirect evaporative coolers could be based on the ϵ -NTU method for sensible heat exchangers when proper adjustments are made by redefining the potential gradients, transfer coefficient, heat capacity rate parameters and assuming a linear saturation temperature–enthalpy relation of air. 2) the modified ϵ -NTU method is universal and is applicable to any type of indirect evaporative cooler (regenerative, counter-flow and parallel-flow).					

Table 2-8: Titled ‘regenerative’ cooling case 1

Ref.	Year	First author	Nation	Methodology	
[2.128]	2013	Bellemo	Denmark	Numerical- EES	
Assumptions					
1) Adiabatic with the surroundings; 2) Airflow distributes evenly among the channels; 3) Heat conduction in the flow direction is neglected; 4) Heat transfer in the vertical direction is neglected; 5) Water distribution is homogeneous; 6) Hygroscopic foils adhere to the plates perfectly; 7) Hygroscopic foils are modelled as layers of water with negligible thermal resistance.					
Flow pattern	Configuration				
	Channel gap (mm)	Channel length (mm)	Channel width (mm)	Material	Plate thickness (mm)
Counter	3	1380	-	Hygroscopic foils	0.25+0.10
<p style="text-align: center;">DPC structure (external side view on the left as shown by Janssen and Uges (2010), internal front view on the right - dimensions in [mm])</p>					
Conclusions					
1) Realistic performances correspond to an area effectiveness coefficient of 0.55 owing to inhomogeneous water distribution. 2) The model enables calculations of the required amounts of water and electricity. 3) Net cooling capacity is maximized for a recirculation fraction around 30%. 4) Inlet humidity ratio has the strongest influence on the supply temperature. 5) Supply temperature also decreases with decreasing inlet temperature and flow rate, but to a lower extent. 6) Effectiveness alone is not sufficient to evaluate the DPC performance: it may increase either by increasing supply temperatures or decreasing temperature differences between inlet and outlet.					

Table 2-9: Titled ‘M-cycle’ cooling case 2

Ref.	Year	First author	Nation	Methodology	
[2.141]	2013	Rogdakis	Greece	Numerical	
Assumptions					
1) Equality of cross section area; 2) Reflectance of recirculation zone length; 3) Whole cooling device is fully isolated; 4) Saturation of the wet surfaces (uniformly wetted); 5) Stability of mass flows (incompressible and constant through each channel); 6) Thin layer boundaries and thermal conduction can be neglected; 7) Neglect of thermal radiation; 8) Both evaporative walls of working stream are at the same temperature.					
Flow pattern	Configuration				
	Channel gap (mm)	Channel length (mm)	Channel width (mm)	Material	Plate thickness (mm)
Counter	-	-	-	-	-
<p style="text-align: center;">Final configuration of the proposed geometry (three -layer counter-flow cooler, with precooling zone and reverse working flow; cross section and side views)</p>					
Conclusions					
1) Geometries are of lower water consumption than of standard plate geometry, while they produce fresh air at about 21°C and consume less than 2 kg of water per cooling kWh. 2) M-cycle based models are directly comparable to standard cycle geometry. Product air temperature is a little higher than that of standard geometry (1.0°C - 1.5°C), but the low water consumption renders the developed cylinder geometry.					

Table 2-10: Titled ‘M-cycle’ cooling case 3

Ref.	Year	First author	Nation	Methodology	
[2.129]	2014	Rogdakis	Greece	Experimental and numerical, MathCAD software	
Assumptions					
-					
Flow pattern	Configuration				
	Channel gap (mm)	Channel length (mm)	Channel width (mm)	Material	Plate thickness (mm)
Cross	-	-	-	-	-
<p style="text-align: center;">Configuration of plate Maisotsenko heat and mass exchanger.</p>					
Conclusions					
<p>1) Efficiency does not depend on the ambient conditions, but PA temperature is strongly affected by the humidity of the region. 2) Specific water consumption under normal mode varies (under common ambient conditions) between 2.5 kg/kWh-cooling and 2.8 kg/kWh-cooling.</p>					

Table 2-11: Titled ‘dew point’ cooling case 5

Ref.	Year	First author	Nation	Methodology	
[2.130]	2014	Jradi	UK	Experimental and numerical, based on a fully implicit accurate finite difference scheme with Matlab	
Assumptions					
1) Mass and heat transfer process is adiabatic and in steady state; 2) Temperature of the interface between the working air and the water film is equal to the water temperature; 3) Wet channel surfaces are completely saturated with a uniform distribution of water film across the channel surface; 4) Thermal resistance of the wall separating two adjacent channels is negligible; 5) Air velocity and thermal properties are uniform within a single control volume.					
Flow pattern	Configuration				
	Channel gap (mm)	Channel length (mm)	Channel width (mm)	Material	Plate thickness (mm)
Cross	5	500	-	Fibre sheets coated with polyethylene (dry) /fibrous material(wet)	0.5
<p style="text-align: center;">Schematic diagram of the proposed dew point evaporative cooler.</p>					
Conclusions					
1) Cooling effectiveness is directly proportional to the IA temperature and channel length; 2) Cooling effectiveness is inversely proportional to the intake air velocity, channel height and supply to intake air ratio.					

Table 2-12: Titled ‘dew point’ cooling case 6

Ref.	Year	First author	Nation	Methodology	
[2.116]	2014	Cui	Singapore	Numerical, CFD, ANSYS FLUENT	
Assumptions					
1) Outer surface is insulated; 2) Air flow in each channel is fully developed and laminar; (3) One-dimensional; 4) Water droplets are evenly distributed on the entire surface of wet channel, and 5) Airflow is steady and incompressible.					
Flow pattern	Configuration				
	Channel gap (mm)	Channel length (mm)	Channel width (mm)	Material	Plate thickness (mm)
Counter	6(dry)/ 3(wet)	1000	-	-	0.2
<p style="text-align: center;">Schematic of the novel dew-point evaporative air cooler (one-unit channel pair).</p>					
Conclusions					
Cooling effectiveness is dependent on the IA conditions and the dimension of the airflow passages. 1) IA velocity should be below 1.5 m/s; (2) Channel length should be at least 200 times of the channel height; 3) Product channel height would be less than 10 mm; (4) Working channel height would be about half of the product channel height; and 5) Product to working air ratio should be smaller than 1.5.					

Table 2-13: Titled ‘dew point’ cooling case 7

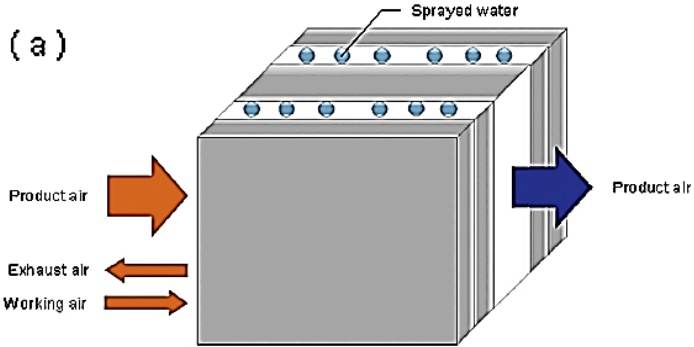
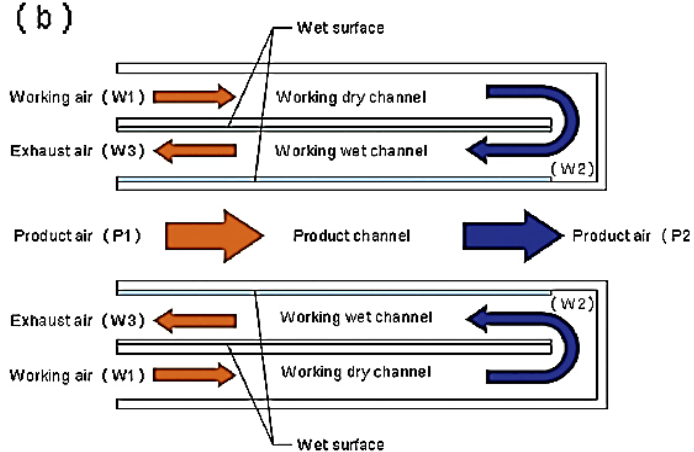
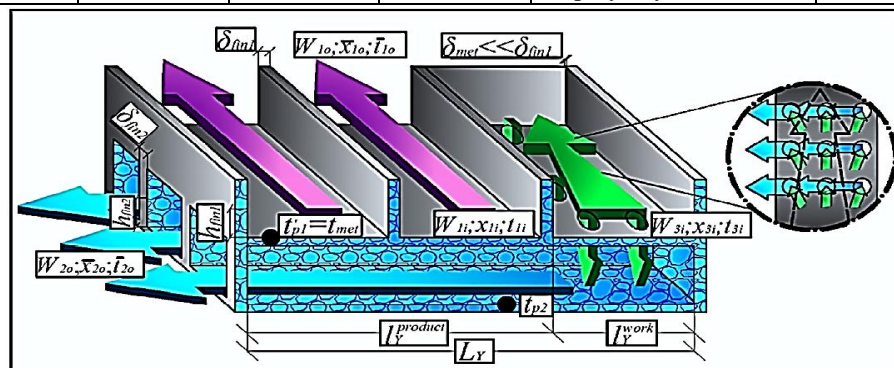
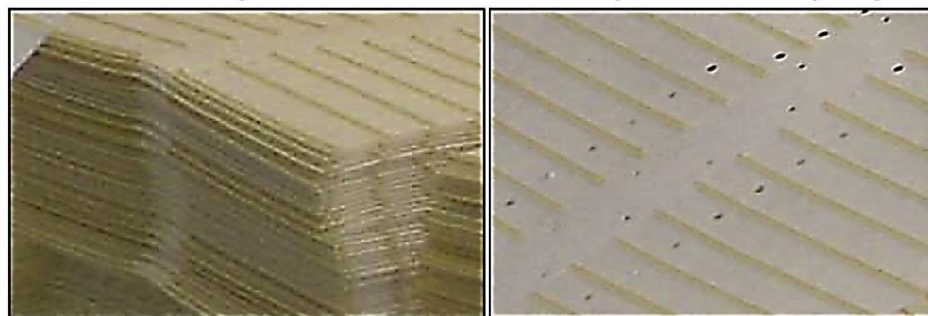
Ref.	Year	First author	Nation	Methodology	
[2.131]	2014	Cui	Singapore	Numerical, modified LMTD method, CFD	
Assumptions					
1) No heat transferred to the surroundings; 2) One-dimensional process; 3) Water droplets are even on the entire surface of wet channel; 4) Airflow is steady and incompressible.					
Flow pattern	Configuration				
	Channel gap (mm)	Channel length (mm)	Channel width (mm)	Material	Plate thickness (mm)
Counter	6(dry)/ 3(wet)	1000	-	-	0.2
<p>(a)</p>  <p>(b)</p>  <p style="text-align: center;">Schematic of the novel dew point evaporative air cooler. (a) One-unit channel pair (b) plan view.</p>					
Conclusions					
<p>1) Room return air being working air, the cooling effectiveness could be effectively increased. 2) Channel dimension markedly impacts the cooling effectiveness. 3) To promote cooling effectiveness, it is suggested that the channel length should be at least 200 times of the working channel height. 4) IA velocity being more than 1.5 m/s, WBE would increase by 10-20% for a cooler with ribs installed, compared with one with plain channel.</p>					

Table 2-14: Titled ‘M-cycle cooling case 4

Ref.	Year	First author	Nation	Methodology	
[2.133]	2014	Anisimov	Poland	Numerical simulation based on modified ϵ -NTU model	
Assumptions					
1)Steady state operation; 2) Heat loss to the surroundings is negligible; 3) Airflow is an ideal, incompressible gas mixture of dry air and water vapours; 4) Kinetic properties of airflow and water film are constant and equal to bulk average values; 5) Driving force of mass transfer is a gradient of moisture content (partial vapour pressure); 6) Longitudinal molecular diffusion of water vapour in air and longitudinal heat conduction along the wall as well as inside the fluids in the direction of airflow are negligible; 7) Consumed water rate corresponds to sufficient evaporation and keeping up the material of plates in hygroscopic saturated condition.					
Configuration					
Flow pattern	Channel gap (mm)	Channel length (mm)	Channel width (mm)	Material	Plate thickness (mm)
Cross	3.2	-	24; fin width 1.9	(wet) porous material (cellulose fibre)/ (dry) coated with impervious material (e.g. metal foil or polyethylene)	0.4



Maisotsenko cycle HMX structure characteristics: wet and dry channel's structure respectively.



Conclusions

1) Heat and mass transfer performance strongly depends on IA temperature and humidity, geometrical size of the channels, type of plate-fin surface, uniformity of water distribution, IA velocity, secondary to primary air mass flow ratio, but depends less on the conductive conductance through the fin; 2) Heat exchanger can be relatively long in the direction of product airflow, while its length in the direction of secondary air flow should not become excessive; 3) Primary to secondary air flow rate ratio should be close to 1, while velocity values in channels should remain relatively low; 4) DPE as well as WBE is not an adequate indicator for indirect evaporative air cooler performance; 5) In some cases (e.g. high IA relative humidity) DPE can increase while specific cooling capacity rate of the HMX becomes lower. 6) An optimized design of the M-cycle heat exchanger is a compromise between DPE and cooling capacity.

Table 2-15: Titled ‘M-cycle’ cooling case 5

Ref.	Year	First author	Nation	Methodology	
[2.132]	2014	Anisimov	Poland	Numerical simulation based on modified ϵ -NTU model	
Assumptions					
1) Steady state operation; 2) Heat loss to the surroundings is negligible; 3) Airflow is an ideal, incompressible gas mixture of dry air and water vapours; 4) Kinetic properties of air flow and water film are constant and equal to bulk average values; 5) Driving force of mass transfer is a gradient of moisture content (humidity ratio or partial vapor pressure); 6) Longitudinal molecular diffusion of water vapor in air and longitudinal heat conduction along the wall as well as inside the fluids in the direction of air flow are negligible; 7) Consumed water rate corresponds to sufficient evaporation and keeping up the material of plates in hygroscopic saturated condition; 8) Even distribution of water film in channels.					
Flow pattern	Configuration				
	Channel gap (mm)	Channel length (mm)	Channel width (mm)	Material	Plate thickness (mm)
Counter/cross	4	0.5	0.5	0.5 mm wet porous material and 0.02 mm coating impervious material	0.5+0.02
Different versions of the air flow arrangement in the M-Cycle heat and mass exchangers. (a) Modified counter-flow HMX. (b) Regenerative HMX. (c) Regenerative HMX with perforation. (d) Cross-flow HMX. (e) Modified cross-flow HMX.					
Conclusions					
1) Performance strongly depends on IA temperature and humidity, value of the NTU number, IA velocity and secondary to primary air mass flow ratio. 2) Modified counter-flow HMX shows the highest temperature effectiveness, but its structure is used ineffectively, which results in the lowest value of specific cooling capacity. 3) Temperature effectiveness of the cross-flow M-Cycle HMX is similar to the counter-flow M-Cycle HMX, while its specific cooling capacity is higher and construction is easier to design, therefore cross-flow M-Cycle HMX seems to be the most reasonable unit for commercial purpose.					

Table 2-16: Titled ‘M-cycle’ cooling case 6

Ref.	Year	First author	Nation	Methodology	
[2.134]	2014	Anisimov	Poland	Experimental and numerical simulation based on modified ϵ -NTU model	
Assumptions					
1) Driving force of mass transfer is a gradient of absolute humidity; 2) Airflow is treated as an ideal non-reacting gas mixture of dry air and water vapours; 3) Kinetic properties of air flow and water film are constant, equalled to bulk average values; 4) Longitudinal molecular diffusion of water vapor in air and longitudinal heat transfer at the expense of thermal conductivity are negligible; 5) No wall, air and fluid thermal and moisture diffusivity in the flow directions; 6) Channel factor affinity for moisture is variable and depends on the IEC construction; 7) Consumed water rate corresponds to sufficient evaporation and keeping up the material of plates in hygroscopic saturated condition; 8) Passage geometry is uniform throughout the heat exchanger; 9) Passage walls are impervious to mass transfer; 10) Water film temperature, sensible heat transfer coefficient and Lewis factor depend on the IEC operating conditions.					
Flow pattern	Configuration				
	Channel gap (mm)	Channel length (mm)	Channel width (mm)	Material	Plate thickness (mm)
Cross	3.2	-	24; fin width 1.9	(wet) porous material (cellulose fibre)/ (dry) coated with impervious material (e.g. metal foil or polyethylene)	0.4
Photo of the dry plate; (b) photo of the wet plate; (c) wet and dry channels in the exchanger; (d) infra-red photo of the supply part of the exchanger; (e) infra-red photo of the exhaust part of the exchanger; (f) measuring points inside the dry part of the exchanger; (g) measuring points inside the wet part of the exchanger.					
Conclusions					
Dry and wet-bulb effectiveness do not vary much during continuous operation under real range of ambient air condition changes. To make this device commercially viable to humid climates, the assistance of desiccant dehumidifier or hybrid devices using both IEC and mechanical compression systems should be studied.					

Table 2-17: Titled ‘M-cycle’ cooling case 7

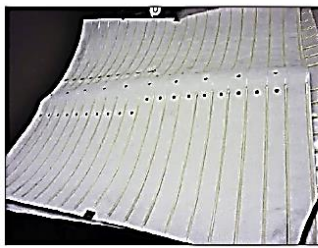
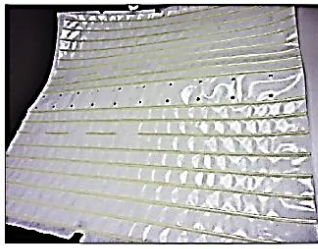
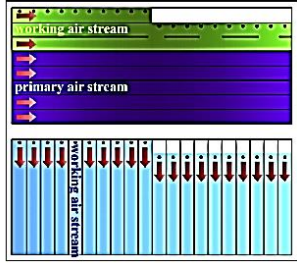
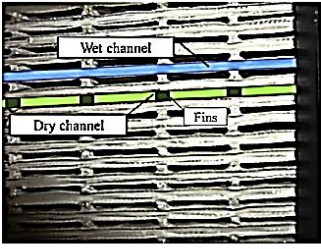
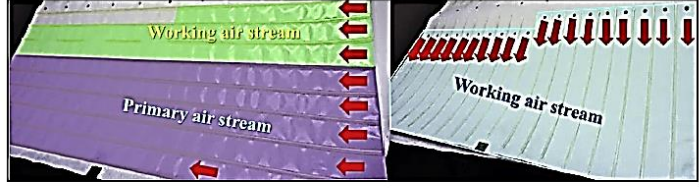
Ref.	Year	First author	Nation	Methodology	
[2.123]	2015	Pandelidis	Poland	Numerical simulation based on modified ϵ -NTU model	
Assumptions					
1) Negligible heat loss to the surroundings; 2) Operation in the steady state; 3) Driving force of mass transfer is a gradient of humidity ratio; 4) Airflow is an ideal, incompressible gas; 5) Longitudinal molecular diffusion of water vapour in air and longitudinal heat conduction along the wall as well as inside the fluids in the direction of air flow are negligible; 6) Consumed water rate corresponds to sufficient evaporation and keeping up the material of plates in hygroscopic saturated condition; 7) Temperature of the water film, sensible heat transfer coefficient and the Lewis factor depend on the operating conditions; 8) The channel walls are impervious.					
Flow pattern	Configuration				
	Channel gap (mm)	Channel length (mm)	Channel width (mm)	Material	Plate thickness (mm)
Cross	3.2	-	24	-	0.4
<div style="display: flex; flex-wrap: wrap;"> <div style="width: 50%;"> <p>(a) </p> <p>(b) </p> </div> <div style="width: 50%;"> <p>(c) </p> <p>(d) </p> <p>(e) </p> </div> </div> <p style="font-size: small;">Matsosenko Cycle HMX structure characteristics. (a) Wet channel sheet, (b) Dry channel sheet, (c) Flow scheme in dry and wet channel, (d) View on the entrance part of the exchanger, (e) Air flow scheme on primary and working air plates.</p>					
Conclusions					
1) The performance of the M-Cycle units depends on the IA temperature. 2) The effectiveness of considered devices depends on the operational parameters, such as working air ratio and airflow rate. 3) The hole arrangement and size of the working and primary part in the dry channels have significant impact on cooling efficiency.					

Table 2-18: Titled ‘regenerative’ cooling case 2

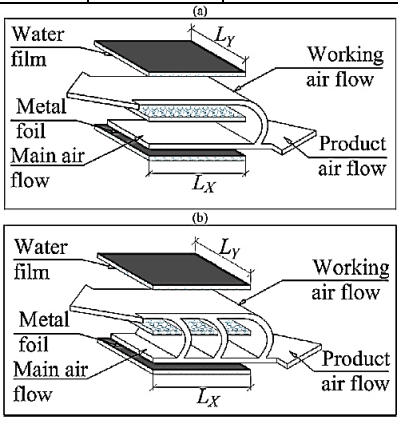
Ref.	Year	First author	Nation	Methodology	
[2.135]	2015	Pandelidis	Poland	Numerical simulation based on modified ϵ -NTU model, Pascal language	
Assumptions					
1) Heat exchange with the surrounding is negligible; 2) Operation in the steady state; 3) Air is an ideal, incompressible gas; 4) Consumed water rate corresponds to sufficient evaporation and keeping up the material of plates in hygroscopic saturated condition. 5) Driving force of mass transfer is a gradient of humidity ratio. 6) Kinetic properties of air stream and water are constant and equal to bulk average values; 7) Water film temperature, sensible heat transfer coefficient and Lewis factor depend on the operating conditions.					
Flow pattern	Configuration				
	Channel gap (mm)	Channel length (mm)	Channel width (mm)	Material	Plate thickness (mm)
Counter	5	1200	80	-	0.5
 <p style="text-align: center;">Analyzed exchangers: (a) typical regenerative HMX, (b) perforated regenerative HMX.</p>					
Conclusions					
1) Energy efficiency is affected by geometrical parameters: length, height and shape of the channels, as well as IA velocity and the working air ratio. 2) Channels in the regenerative air coolers should be relatively low-pitched. 3) Increasing of the channel length results in lower outlet temperature, therefore the HMXs should be relatively long. 4) Most effective channel shape for the regenerative indirect evaporative air coolers is triangle. However, it is hard to obtain even water distribution on the triangle fins, therefore it may be reasonable to use the flat channels instead. 5) Perforated regenerative exchangers show higher temperature efficiency than the typical regenerative units for the working air ratio higher than 0.45, due to the more effective distribution of the air flow in the wet channels.					

Table 2-19: Titled ‘M-cycle’ cooling case 8

Ref.	Year	First author	Nation	Methodology	
[2.136]	2015	Pandelidis	Poland	Numerical simulation based on modified ε -NTU model	
Assumptions					
1) Heat exchange with the surrounding is negligible; 2) Operation in the steady state; 3) Air is an ideal, incompressible gas; 4) Consumed water rate corresponds to sufficient evaporation and keeping up the material of plates in hygroscopic saturated condition; 5) Driving force of mass transfer is a gradient of humidity ratio; 6) Kinetic properties of air stream and water are constant and equal to bulk average values; 7) Water film temperature, sensible heat transfer coefficient and Lewis factor depend on the operating conditions.					
Flow pattern	Configuration				
	Channel gap (mm)	Channel length (mm)	Channel width (mm)	Material	Plate thickness (mm)
Cross	3	-	25	Cellulose fibre (wet) covered with polyethylene (dry)	0.2
<p style="text-align: center;">M-cycle heat and mass exchanger structure. (a) Air flow distribution. (b) Important elements of the exch</p> <p style="text-align: center;">Schematic visualization of analyzed exchanger.</p>					
Conclusions					
1) Increasing the dry working air portion of the exchanger results in improving exchanger performance; 2) Increasing the dry working air portion of the exchanger at a cost of primary air portion is justified when it allows obtaining higher cooling performance. For lower airflow rates, the working air ratio should be kept at level 2:6, in order to improve the system COP, while for the higher air flow rates this proportion should be equal 1:7. 3) It is important to keep even airflow distribution inside the wet channels. 4) Uneven distribution leads to significant decreasing in cooling performance (higher outlet temperatures, lower cooling capacity and the COPs of the system); 5) It is important to find effective ways of maintaining the even airflow in the working air channels, such as using different size of the holes in the plate or more efficient hydraulic schemes of the system.					

Table 2-20: Titled ‘combined’ IEC case 1

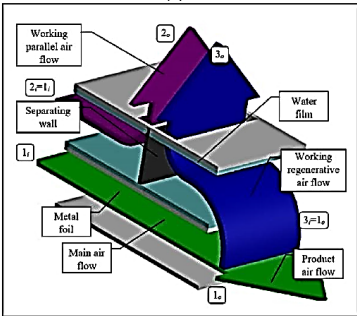
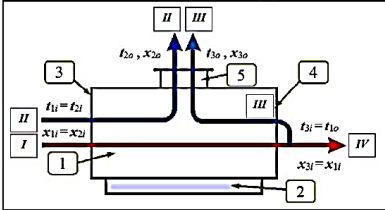
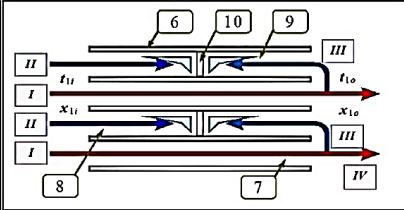
Ref.	Year	First author	Nation	Methodology
[2.137]	2015	Anisimov	Poland	Numerical simulation based on modified ϵ -NTU model
Assumptions				
1) No heat transferred to the surroundings; 2) One-dimensional process; 3) Water are even on the entire surface of wet channel; 4) Airflow is steady and incompressible.				
Flow pattern	Configuration			
	Channel gap (mm)	Channel length (mm)	Channel width (mm)	Material
Counter/parallel	5	1200	80	-
<div style="display: flex; justify-content: space-around;"> <div style="text-align: center;"> <p>(a)</p>  </div> <div style="text-align: center;"> <p>(b)</p>  </div> <div style="text-align: center;"> <p>(c)</p>  </div> </div> <p style="text-align: center; font-size: small;">General scheme of analyzed indirect evaporative air cooler [21]: (a) general scheme; (b) top view of the exchanger; (c) side view of the exchanger.</p>				
Conclusions				
1) For higher parallel airflow rate, it may achieve lower COP; 2) Impact of the operating factors on the energy efficiency is established; 3) Optimization study allows to establish the Pareto-optimal performance of the novel HMX; 4) The proposed optimal design of the novel heat exchanger is a compromise solution obtained from the analysis of selected individual quality criterion: DPE, specific cooling capacity per cubic meter of the HMX structure and the system COP.				

Table 2-21: Titled ‘sub-wet bulb’ cooling case 2

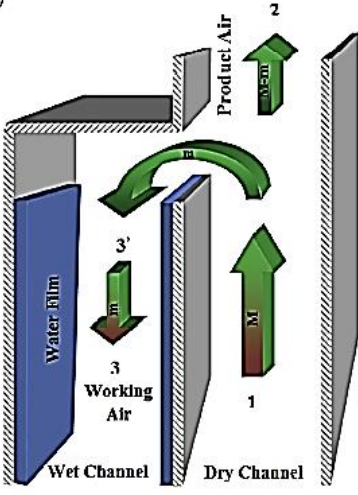
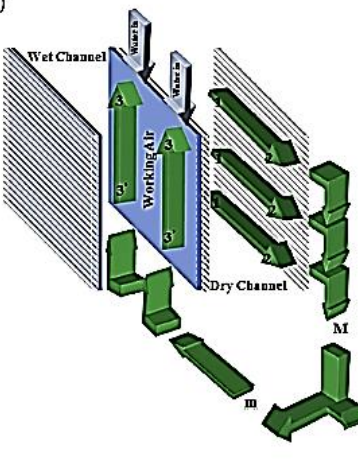
Ref.	Year	First author	Nation	Methodology	
[2.120]	2015	Moshari	Iran	Numerical with Finite Difference Method, iterative method in MATLAB.	
Assumptions					
1) The process is steady-state; 2) System is isolated and no internal heat generation occurs in channels; 3) Constant specific heat of the fluid, air and vapour; 4) Air is an incompressible gas; 5) Spray water is circulated in a closed-loop; 6) No conduction in the water layer in the flow directions; 7) Heat and mass transfer effects between water droplets and air in the wet channel are negligible.					
Flow pattern	Configuration				
	Channel gap (mm)	Channel length (mm)	Channel width (mm)	Material	Plate thickness (mm)
Counter/cross	7	500	500	-	0.3
<p>(a)</p>  <p>(b)</p>  <p style="text-align: center;">Geometry for REC, (a) counter-flow configuration, (b) cross-flow configuration.</p>					
Conclusions					
1) Counter-flow REC has higher cooling ability in comparison with cross-flow REC and four-stage IEC. 2) PA temperature decreases as the working air ratio increases.					

Table 2-22: Titled ‘M-cycle’ cooling case 9

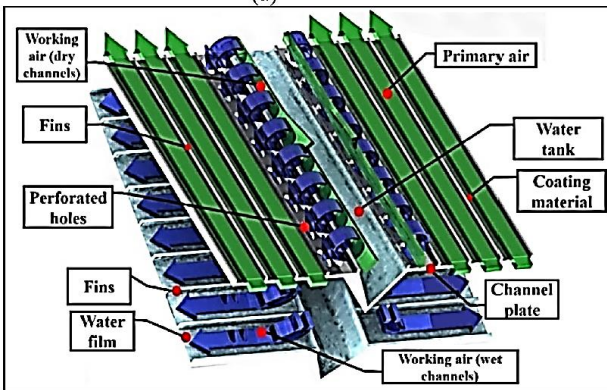
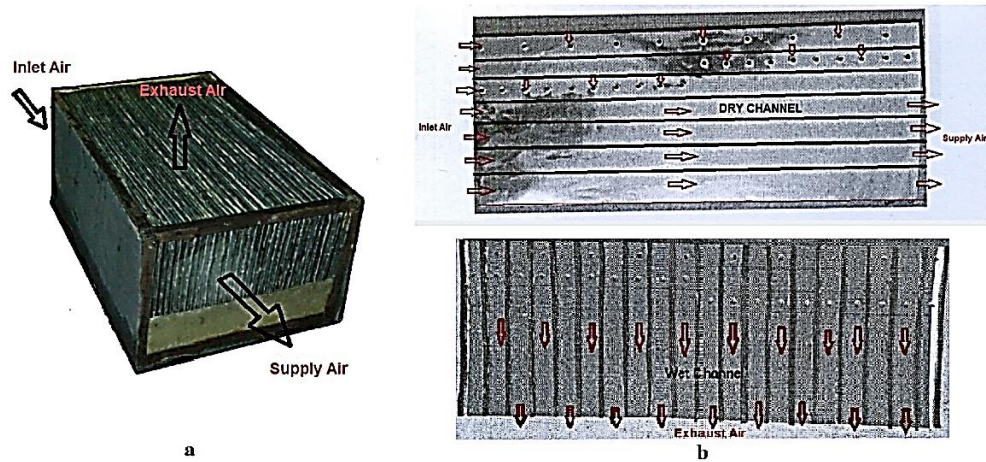
Ref.	Year	First author	Nation	Methodology	
[2.124]	2016	Pandelidis	Poland	Numerical	
Assumptions					
1) No heat transferred to the surroundings; 2) One-dimensional process; 3) Water are even on the entire wetted surface; 4) Airflow was steady and incompressible.					
Flow pattern	Configuration				
	Channel gap (mm)	Channel length (mm)	Channel width (mm)	Material	Plate thickness (mm)
Cross	3	500	250	-	-
<div style="display: flex; justify-content: space-around;"> <div style="text-align: center;"> <p>(a)</p>  </div> <div style="text-align: center;"> <p>(b)</p>  </div> </div> <p style="text-align: center; font-size: small;">Cross-flow Maisotsenko cycle heat and mass exchanger. (a) Scheme of the unit. (b) Photograph of the unit.</p>					
Conclusions					
1) The optimization was performed with two methods: single-parameter and multi-parameter compromise method. The single parameter optimization lead to the unsatisfactory results, due to the different trends shown by the quality criteria under identical variation of input parameters. The multi-parameter optimization was based on analysis of the Harrington function of desirability. 2) The results of optimization allowed establishing optimal range of operational and geometrical conditions for the presented exchanger and establishing the optimal climate conditions for its effective operation.					

Table 2-23: Titled ‘M-cycle’ cooling case 10

Ref.	Year	First author	Nation	Methodology	
[2.140]	2016	Khalid	Pakistan	Experimental	
Flow pattern	Configuration				
	Channel gap (mm)	Channel length (mm)	Channel width (mm)	Material	Plate thickness (mm)
Cross	4	508(dry)/203(wet)	25	Aluminium sheets coated with Felt (a fibrous material)	0.175+0.3



Schematic of Maisotsenko cycle: (a) Structure view; (b) Distribution of air in the dry and wet channels.



a



b

Attaching of guides to aluminum sheets: (a) Dry channel; (b) Wet channel.

Conclusions

1) DPE and WBE vary in the range of 62–85% and 92–120% respectively with IA temperature variation from 25 to 45 °C at different humidity ratio ranging from 11 g/kg to 19 g/kg; 2) Overall performance of the improved design is found 5% more efficient in terms of WBE compared to the previous systems.

Table 2-24: Titled ‘dew point’ cooling case 7

Ref.	Year	First author	Nation	Methodology	
[2.119]	2016	Lin	Singapore	Numerical, Newton Raphson iteration with MATLAB	
Assumptions					
1) Adiabatic boundary with the surrounding; 2) Fully wetted surface covered by the saturated and stagnant water film within the wet channel; 3) Airflow is steady, and the dry air density is constant; 4) Properties are uniform within each control volume, and the kinetic properties of the fluid are constant; 5) Transverse heat conduction of water film is neglected; 6) Thermal mass of wick material is not considered.					
Flow pattern	Configuration				
	Channel gap (mm)	Channel length (mm)	Channel width (mm)	Material	Plate thickness (mm)
Counter	5	1000	100	-	-
<p style="text-align: center;">Schematic diagram for a single-stage dew point evaporative cooler with counter-flow configuration.</p>					
Conclusions					
1) Saturation point of the working air occurs at a fixed point regardless of the IA conditions, and it is mainly influenced by the working air ratio and channel height; 2) Intensity of the water evaporation approaches a minimum at 0.2 to 0.3 m from the entrance; 3) Wet channel can be separated into two zones, and the overall heat transfer coefficient is above 100 W/(m ² ·K) after the water film temperature becomes higher than the working air temperature.					

Table 2-25: Titled ‘dew point’ cooling case 8

Ref.	Year	First author	Nation	Methodology	
[2.127]	2016	Lin	Singapore	Numerical, Unsteady-state analysis, transient model, objective cell elements and control volume	
Assumptions					
1) System is well insulated and no heat exchange with the surroundings; 2) Influence of pressure difference along the airflow is neglected; 3) Wick-material surface is covered with a layer of stagnant and saturated water film; 4) Channel plate is integrated with the water film in the transient modelling and temperature difference is neglected; 5) Bulk average values of air and water properties are used for each control volume, and the dry air density is constant; 6) Dimensionless number and other air transport properties appearing in the model are calculated using the transient temperature and humidity of the air streams.					
Flow pattern	Configuration				
	Channel gap (mm)	Channel length (mm)	Channel width (mm)	Material	Plate thickness (mm)
Counter	5	1000	100	-	-
<div style="display: flex; justify-content: space-around;"> <div style="text-align: center;"> <p>(a)</p> </div> <div style="text-align: center;"> <p>(b)</p> </div> </div> <p style="text-align: center;">System configuration of dew point evaporative cooling: (a) cross-flow; and (b) counter-flow.</p>					
Conclusions					
1) Response trend and settling time are markedly dependent on the IA temperature, humidity and velocity; 2) Settling time of the transient response ranges from 50 s to 300 s when the system operates under different IA conditions; 3) Average transient WBE (1.00-1.06) of the system is observed to be higher than the steady state WBE (1.01) in the range of study.					

Table 2-26: Titled ‘dew point’ cooling case 9

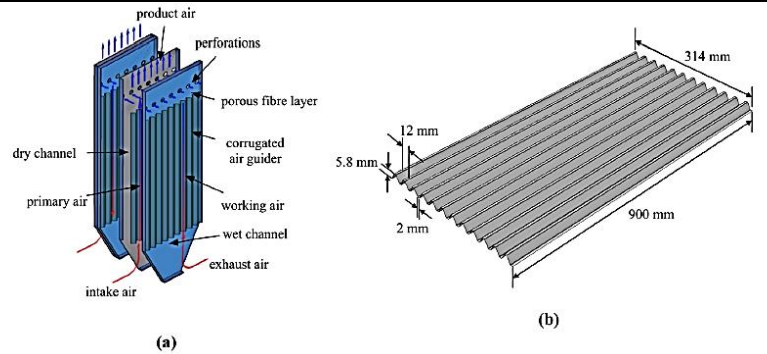
Ref.	Year	First author	Nation	Methodology	
[2.139]	2016	Ham	Korea	Numerical, Finite difference model, Python Language	
Assumptions					
1) All the heat and mass transfer processes are steady-state; 2) The DPHX (Dew Point Evaporative Heat eXchanger) is thermally isolated; 3) The water sprayed into the wet channel is circulated and evenly distributed within the channel; 4) The temperatures of the interfacial wall, water film, and the saturated water-air interface layer are identical; 5) The transversal wall thermal resistance is negligible because of its small thickness (0.2 mm); 6) The conduction heat transfer coefficient of the interfacial wall is infinity; 7) Condensation occurs in the dry channel if the air temperature reaches its dew point temperature; 8) Airflow is in the longitudinal direction and is not mixed vertically; 9) Thermal properties of air and water within a node are uniform.					
Flow pattern	Configuration				
	Channel gap (mm)	Channel length (mm)	Channel width (mm)	Material	Plate thickness (mm)
Counter	3	-	-	Composite fibre made of polyethylene phthalate sheets and paper	-
Conclusions					
1) Systematic energy performance of DPHX with a LD (Liquid-Desiccant) unit (LD + DPHX) is evaluated in the summer design condition and compared to that of the VAV (variable-air-volume) system and DP-IEC with an LD unit (LD + DP-IEC). 2) The simulation results show that the LD + DPHX can reduce source-weighted energy by 15% compared to the LD + DP-IEC by reducing the size of the LD unit and fans.					

Table 2-27: Titled ‘regenerative’ cooling case 3

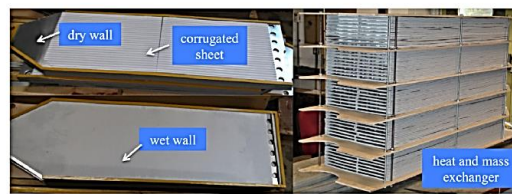
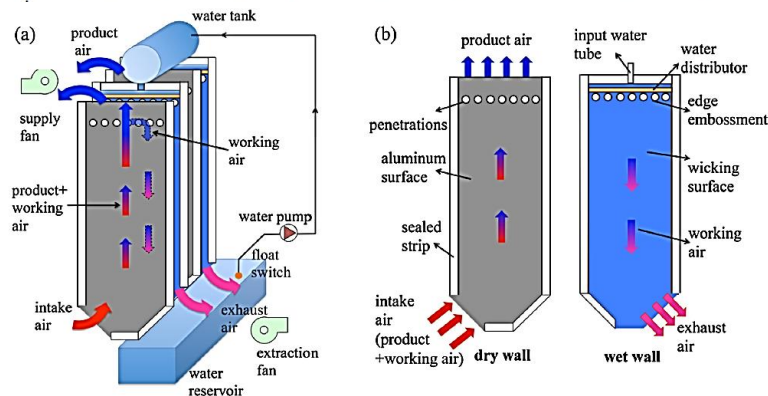
Ref.	Year	First author	Nation	Methodology	
[2.89]	2016	Fakhrabadi	Iran	Numerical, the simplified conjugate gradient method (SCGM), genetic algorithms and the gradient-based optimization algorithms	
Assumptions					
1) Airflow is incompressible and steady; 2) Longitudinal heat conduction and mass diffusion are negligible; 3) No heat transferred to the surroundings; 4) Channel height is small compared to the channel width, thus the model can be considered one dimensional; 5) Airflow along the channel is fully-developed and laminar; 6) Specific heat and mass transfer coefficients are constant; 7) Due to low diffusion rates, Reynolds analogy is valid and the Lewis number is equal to one; 8) Air-water interface temperature is equal to the water film temperature, due to a negligible thermal resistance of the water film.					
Flow pattern	Configuration				
	Channel gap (mm)	Channel length (mm)	Channel width (mm)	Material	Plate thickness (mm)
Counter	4-6	0.4-0.6	-	-	-
<p style="text-align: center;">(a) (b)</p> <p style="text-align: center;">Schematic of (a) a regenerative heat and mass exchanger; (b) a liquid-to-air membrane energy exchanger.</p>					
<p style="text-align: center;">Schematic of the hybrid LD-regenerative evaporative air conditioner and the computational elements used for numerical simulation.</p>					
Conclusions					
<p>1) Raising the channel length and reducing the channel height both increase the optimal RCC as well as the required fan power. Channel length and the channel height should be selected between 0.4-0.6 m and 0.004-0.006 m, respectively. 2) IA temperature and humidity ratio have substantial impacts on the optimal RCC. A 10°C increase in the IA temperature decreases the optimal RCC by 36%, and a 0.006 kg water/kg dry air rise in the IA humidity ratio reduces the optimal RCC by 53%. 3) Optimized values of the working-to-product air flow ratio are significantly affected by the inlet air temperature. Under the reference IA temperature (35°C), the optimized values of the working-to-product air flow ratio are approximately fixed and around 0.4 for different IA humidity ratios, and for a wide range of exchanger’s geometric parameters. 4) Only IA condition has a significant impact on PA temperature of the optimized RHM. Under the reference IA condition, the PA temperatures of the optimized RHM are almost constant at about 18.2°C for different channel lengths under various channel heights.</p>					

Table 2-28: Titled ‘regenerative’ cooling case 4, 5

Ref.	Year	First author	Nation	Methodology	
[2.143, 2.144]	2016, 2017	Duan	China	Experimental	
Flow pattern	Configuration				
	Channel gap (mm)	Channel length (mm)	Channel width (mm)	Material	Plate thickness (mm)
Counter	6	900	314	Aluminium film (dry)/ cellulose-blended fibre (wet)/ reactive hydrophilic adhesive with triangular air guider	0.25



Schematics of proposed regenerative evaporative cooler (a) configuration of dry and wet channels (b) geometry of corrugated sheets



(c)

Graphs showing schematics of (a) the developed counter-flow REC system, (b) the heat exchanging walls with corrugated air guiders and (c) images of the heat exchanging walls and HMX fabricated in laboratory.

Conclusions

1) WBE is significantly enhanced through either ways of increasing inlet wet-bulb depression or reducing IA velocity, or alternatively by increasing working air ratio; 2) Cooling capacity and EER of cooler is rapidly increased by means of increasing inlet wet-bulb depression or increasing IA velocity, or reducing working air ratio instead; 3) Cooling effectiveness reduces by less 5% while feed water temperature increased from 18.9°C to 23.1°C; 4) Apparent acceleration in water evaporation rate is gained from increasing inlet wet-bulb depression or air velocity.

Table 2-29: Titled

‘dew point’ cooling case 10					
Ref.	Year	First author	Nation	Methodology	
[2.138]	2017	Jafarian	Iran	Numerical, group method of data handling-type neural network (GMDH-type neural network), C++	
Assumptions					
1) Fluids are Newtonian and air is ideal gas; 2) Airflows are laminar and thermophilically properties are constant; 3) Water film sensible thermal capacitance is neglected and the air at the plate surface in the exhaust airflow channel is thermodynamically in equilibrium with water film; 4) Common wall and half part of each channel is chosen as the calculation domain. Simplifying continuity, momentum and energy conservation equations for air streams using mentioned assumptions based on calculation domain and coordinates; 5) Velocity on the walls and normal gradient of all parameters on symmetry line are equal to zero; 6) Inlet conditions are imposed by ambient and inlet conditions of exhaust channel are equal to outlet conditions of supply channel; 7) Thermal boundary condition on the separating wall is neither temperature constant nor flux constant; 8) Water evaporation absorbs heat from both channels, meaning sum of heat fluxes of the two channels on the wall is equal to the absorbed heat by evaporation; 9) Air in direct contact with the water is assumed thermodynamically in equilibrium and the water vapour pressure is calculated using the Goff-Garth expression.					
Flow pattern	Configuration				
	Channel gap (mm)	Channel length (mm)	Channel width (mm)	Material	Plate thickness (mm)
Counter	1.85(dry)/2(wet)	560	430	Polyethylene, and a wicking material	0.25+0.3
<p style="text-align: center;">Schematic top view of a channel pair in a dew-point indirect evaporative cooling system.</p>					
Conclusions					
1) Present a GMDH-type model and multi-objective optimization of an indirect dew-point evaporative cooler (M-cycle); 2) For each climate, a separate optimization is needed because the system reaches the optimum point under different values for design and operating parameters at each climate. Hence, there is no unique optimized system that could be implemented at all categories of weathers.					

Table 2-30: Titled ‘dew point’ cooling case 11

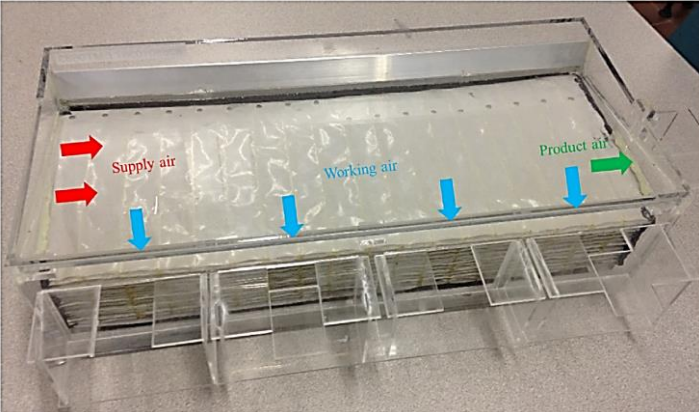
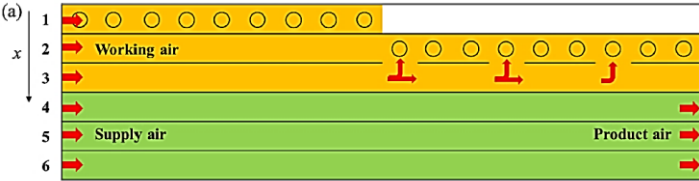
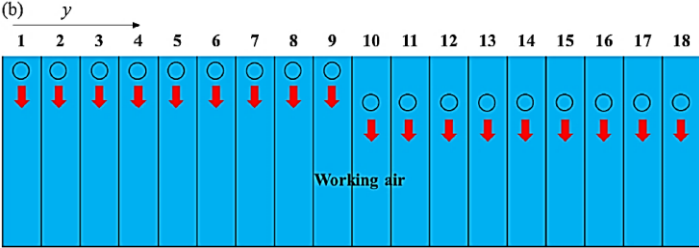
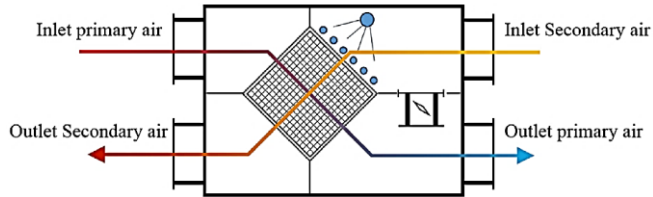
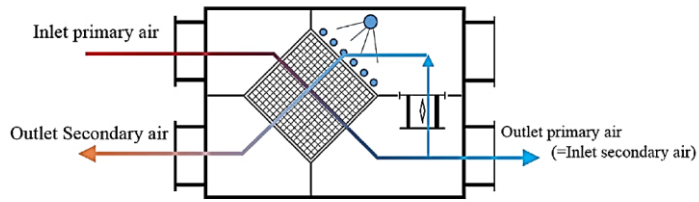
Ref.	Year	First author	Nation	Methodology	
[2.146]	2017	Lin	Singapore	Simulation, transient model	
Assumptions					
1) Supply air and working air are evenly distributed into each channel or hole; 2) Physical properties inside each control volume are uniform; 3) Negligible heat transfer between the cooler and the environment; 4) Wet channel surface is fully covered by a layer of water film, and the water surface is saturated.					
Flow pattern	Configuration				
	Channel gap (mm)	Channel length (mm)	Channel width (mm)	Material	Plate thickness (mm)
Cross	3	-	22	-	-
					
<p>(a)</p>  <p>(b)</p>  <p style="text-align: center; font-size: small;">Flow arrangement of the cross-flow dew point evaporative cooler: (a) dry channel layer; and (b) wet channel layer.</p>					
Conclusions					
1) Maximum discrepancy between the simulation results and experimental data is within $\pm 3.0\%$; 2) Overall WBE and DPE of the cross-flow cooler can reach 1.25 and 0.85 at moderate humidity; 3) Respective WBE, cooling capacity and COP of the cross-flow system are 0.86, 2.2 kW and 4.6 under humid ambient air condition; 4) Dehumidification of the supply air enables the cooling capacity and energy efficiency to be improved by 70–135%.					

Table 2-31: Titled ‘generative’ cooling case 6

Ref.	Year	First author	Nation	Methodology	
[2.142]	2017	Kim	Korea	Experimental	
Flow pattern	Configuration				
	Channel gap (mm)	Channel length (mm)	Channel width (mm)	Material	Plate thickness (mm)
Cross	5	380	380	Corrugated polyethylene film (dry)/ fibre fabricated with polyethylene phthalate sheets and paper (wet)	0.2

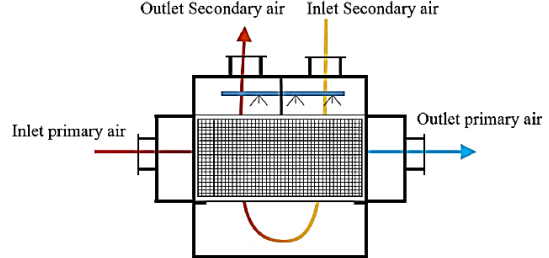


(a) General IEC mode (mode-1)

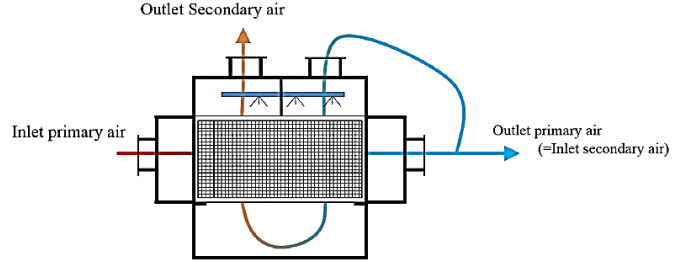


(b) Regenerative IEC mode (mode-2)

IEC1 configuration and operation modes.



(a) General IEC mode (mode-1)



(b) Regenerative IEC mode (mode-2)

IEC2 configuration and operation modes.

Conclusions

1) IEC performance in general operation mode is higher than that of the IEC operating in the regenerative cooling mode in terms of cooling capacity, wet-bulb effectiveness, and supply air temperature; 2) Typical cross-flow type IEC is better suited than the regenerative cross-flow IEC for use in a 100% outdoor air system; 3) Regenerative IEC mode contributes to increasing system efficiency in summer days by conditioning the process air with a portion of the preconditioned air instead of hot and humid ambient air.

By analysing the recent research progresses worldwide, valuable conclusions could be drawn and these are briefed below.

(1) Research methodologies

A few researchers developed the cooler prototype and carried out experimental investigation. Most of the published works were conducted by numerical simulation and further validated by published experimental data of others. Besides few transient models, most of the simulation work stayed at static simulation and the usual methods for modelling were finite difference analysis and modified ε -NTU model. The equations could be solved based on Newton iterative method with various commercial software e.g. EES and MATLAB.

EES (Engineering Equation Software) is a general commercial equation solver that is easy to master but able to solve coupled non-linear algebraic and differential equations describing the heat and mass transfer inside the HMX. EES includes a library of thermodynamic and transport properties for air and vapour which is conveniently called in calculation program. It could be the principal tool for the development of simulation and optimization software.

(2) Assumptions

Assumptions for modelling are similar, mainly including the following:

- a) adiabatic system and no heat exchange with the surroundings;
- b) ideal and incompressible gas;
- c) laminar flows and constant thermochemical properties;
- d) one dimensional heat transfer and no longitudinal heat conduction;
- e) negligible thermal resistance of the wall separating two adjacent channels;
- f) fully developed and laminar airflow;
- h) Lewis factor of one;
- h) uniform physical properties within each computational cell;
- i) fully wetted evaporating surface.

Owing to the EES inbuilt library of thermodynamic and transport properties for air and vapour, thermochemical properties under a certain condition are convenient to attain. Therefore, the assumption of “*constant thermochemical properties*” is not necessary. The state of flow and heat transfer in the entrance region will be considered. Therefore, the assumption of “*fully developed laminar airflow*” in the channels is not applicable. The wetted state of the evaporating surface is an essential item to evaluate the moisture diffusivity of the fibrous material and the recirculating water demand. Therefore, the assumption of “fully wetted evaporating surface” will not be adopted in the following numerical modelling.

(3) Flow pattern

Counter, cross and parallel flow patterns were all extensively investigated and compared in the references. The results showed that counter flow could help achieving the best cooling performance among the three flow patterns.

Consequently, the counter-flow pattern will be given priority in the following design of airflow organization.

(4) HMX configuration

Thickness of the exchanging sheets was mostly in range of 0.2-0.5 mm, and the channel gap between 3 and 5 mm while channel length varied from 0.3 m to 1.4 m. It is worth noting that under many circumstances, guiding bars or sheets were positioned in the narrow channels to keep shape of the soft exchanging sheets. Thus, it is no doubt to increase the airflow resistance in the channels.

The conclusions from the published work offer valuable information for structural design of the HMX.

(5) HMX material

In consideration of anti-corrosion issues under warm and humid environment, most of the mentioned dry-side materials were non-metallic, like polymer sheets and polyethylene coating, and few adopted aluminium. For even water distribution and better retainability, cotton, felt, paper and cellulose were taken as the wetted media to evaporate moisture.

Aluminium possesses much better thermal conductivity than polymer sheets and sufficient stiffness to make it possible to remove the guiding bars or sheets supporting the soft polymer, which will contribute to reducing flow resistance and lowering the fans power consumption. Moreover, aluminium is corrosion resistant under the cooler operation environment.

The moisture-wicking and quick-drying fibrous textile owns excellent properties of moisture shifting and evaporating, which can help accelerate the moisture evaporation and lower the recirculating water.

The combination of aluminium thin sheet and functional fabric gives a promising way to achieve excellent thermal conductivity and moisture evaporation. The key in the following development is to find a feasible approach to bond the two materials together for long-lasting operation under warm and moist conditions.

(6) Valuable conclusions

a) Wet-bulb and dew-point cooling effectiveness and energy efficiency are largely dependent on the dimensions of the airflow passages, air velocity and working-to-intake-air ratio, and less dependent on the water temperature;

b) Suggested design parameters: intake air velocity below 2.5 m/s, channel gap less than 5 mm, channel length larger than 1 m and working air ratio around 0.35-0.6.

c) Unlike refrigeration systems, the energy efficiency increases with outdoor temperatures, and so the cooler can contribute to reducing the peak electrical load.

d) Cooling effectiveness, either wet-bulb or dew-point effectiveness, alone is not adequate to evaluate the IEC unit's performance. An optimized design of the M-cycle heat exchanger is a compromise between cooling effectiveness and cooling capacity.

e) Saturation point of the working air occurs at a fixed point regardless of the inlet air conditions, which is mainly influenced by the working air ratio and channel height, and intensity of the water evaporation approaches a minimum at 0.2 to 0.3 m from the entrance.

f) Regenerative IEC mode can contribute to increasing system performance by conditioning the process air with a portion of the preconditioned air instead of hot and humid ambient air.

g) Feed water temperature has little impact on cooling effectiveness.

(7) Issues not well addressed

a) Wet side material

The wetted condition of the evaporating surface is essential for the cooling effect. However, few details of wet side material and water distribution effects were addressed.

b) Recirculating water demand

A certain flow rate of recirculating water helps to keep the evaporating surface evenly wetted and consumes power. However, few information was presented in the published papers.

c) COP

Although CFD technology was introduced to help analyses the flow condition, results relating to fans as well as the pump power consumption were seldom seen. Therefore, it is hard to evaluate the energy efficiency of the whole IEC unit.

These findings from the literature review will be seriously considered and be based to develop the proposed dew point cooler. The undressed issues will be paid special attention to reveal the truth.

2.3.5 Application and Socio-economic Assessment

With the technological progress and marketing promotion, numerous new IEC products and successful case study could be found at the website of IEC leading companies, e.g., *Munters*®, *Coolerado*®, etc. The application domains cover but not limit to public building, campus, industry, subway station, industry, data centre. To break through the climatic limitation especially in humid regions, the research interests in recent years are more focused on the hybrid systems with pre-dehumidification and relevant application potential and economic evaluation.

Kim et al [147] investigated the energy saving potential by integrating a liquid desiccant system into an I/DEC-assisted 100% outdoor air system and showed that the proposed hybrid system consumed 51% less cooling energy compared to the conventional VAV system. The authors also explored later [148] the energy saving potential by replacing the I/DEC with an M-cycle or a dew point IEC. The simulation results showed an enhancement of 41% in cooling capacity.

Chen et al [149] introduced partial circulation air, other than the common 100% fresh air in IEC system, and quantitatively evaluated the energy saving potential of a hybrid system consisting of liquid desiccant and regenerative IEC. The results showed 23.5% energy saving could be achieved under Hong Kong

climate and the desiccant-assisted IEC could be a promising scheme for energy efficient air conditioning in hot and humid regions.

Jaber [150] assessed the economic and environmental feasibility of IEC unit based on the hourly climatic data in Mediterranean, maritime and desert regions. The Life Cycle Cost, Payback Period and environmental assessment revealed the IEC is a promising technology in Mediterranean and European climate regions.

Duan et al [2.144] performed an experimental-based evaluation of energy saving potential of a counter-flow regenerative dew point cooler based on hourly weather data under various climates in China. The results indicated that the application of such dew point air cooler could cover 93-100% annual cooling demand in north-western China, 84-96% in northern China and 53-72% in south-eastern and south-western regions under comparable physical dimension with the conventional packaged unit air conditioner. And the annual energy saving ratios were 53-59%, 41-45% and 13-28% respectively in north-western, northern, south-eastern and south-western regions of China.

Caliskan et al [151] comprehensively assessed the thermodynamic performance of M-cycle IEC by energy and exergy analyses. To evaluate the benefits and negative impacts on the society, e.g. environmental damage, a sustainability index method relating to exergy efficiency was proposed to help understand the sustainability aspects of the system. As a result, for M-cycle IEC under the optimum operation, the maximum exergy efficiency could be 19.14%, i.e. sustainability index of 1.24, at a reference temperature of 23.88°C.

2.4 Potential Opportunities in the Development of Dew Point Cooling

The extensive literature reviews help identify the opportunities to develop dew point cooling technology in the following aspects.

2.4.1 Structure Optimization of the HMX to Reduce Flow Resistance and Enlarge the Effective Surface

The common HMX structures are based on stacked exchanging sheets in the IEC application. The narrow flow channel and the in-built supporting and guiding components bring large flow resistance and deteriorate the system energy efficiency. Although plenty of published works have presented suggestions for the optimization of structural parameters, innovations in the basic structure of narrow channels separated by supporting elements have not been found.

The exchanging sheets employed to form the HMX in the reviewed publications are all flat form to facilitate the airflow organization. Thus, the space in the HMX has not been effectively used indeed. Corrugated exchanging sheet might be a better option to enlarge the effective exchanging area, although there will be challenges in reasonable airflow organization.

Excellent structural design should be able to enlarge the internal exchanging area as much as possible while guiding desirable airflow to reduce the flow resistance.

2.4.2 New Wetted Material to Promote Evaporation

Most of the published works assumed that the surfaces of wet channel were evenly and entirely wetted by circulating water. Only a few opaquely mentioned the wetted material were cotton, composite fibre, paper, cellulose-blended fibre or hygroscopic foils etc. with few evidence for the actual wetted details.

Based on the investigation of the physical properties of such materials, it is found there may exist difficulties to realize perfect water distribution across the channel surface, especially for the common vertical channels. It is hard for some aforementioned materials, e.g. cotton, to release the absorbed moisture, leading to the deteriorative evaporation performance. For other materials, e.g. cellulose-blended fibre, it is not easy to diffuse the small water stream to desirably large area and the remedial actions may raise the volume of water flow, which leads to increased pump power consumption and degenerative system energy efficiency, i.e. COP.

The desirable material should be able to effectively wick and diffuse the contacted moisture and be easy to release the absorbed moisture to the unsaturated air. The application of new wetted material might markedly enhance the energy performance of the system.

2.4.3 Development of Dedicated Computer Simulation Tools

Various numerical models, e.g. finite-differential models, modified ε -NTU modes, genetic algorithms and neural network etc., were developed and could be solved with numerous commercial software, e.g. EES, MATLAB, C++, etc. Although most of the models were declared being validated by published data, it is hard to guarantee the reliability without dedicated physical prototype and exhaustive experimental data.

Most of the numerical investigations were based on static models. Only very few researches have been found trying to explore the transient process of heat and mass exchange inside the HMX. Development of reliable and solvable transient models will help approach to the in-depth mechanism and the structural and operational optimization of the system.

2.4.4 Water Consumption and Contamination

Water consumption and flow rate of circulating water were seldom discussed in the published papers. Water consumption relates to the bleed-off scheme to maintain the purity and hygiene of the circulating water. The required minimum flow rate of circulating water, which relies on the effective water distribution across the channel wall, refers to the pump power consumption.

Microorganism breeding in the narrow and moist wet channel environment is an inevitable problem. However, no dedicated in-depth research has been found in the relevant engineering fields.

2.4.5 Comprehensive Evaluation of the System in Real Climatic Conditions

Most of the published socio-economic assessment were based on simulation approaches, although the weather data came from reliable actual records. Few field tracking measurements across a long run were reported. The exergy analyses and sustainability index were proposed but have not been extensively adopted in engineering application.

Tracking measurements of the cooler performance across a long period will monitor the performance stability and help identify the impacts of working water quality on the cooling performance. Comprehensive evaluation based on the second law analysis helps to realize the contribution of technical progress to the social sustainability.

2.5 Development of the Dew Point IEC Technology in the PhD Project

In summary, based on the critical literature review and identified potential opportunities to develop dew point IEC technology, this PhD project would

address the following aspects: (1) developing an innovative HMX structure to facilitate airflow organization along with corrugated exchanging interface to enlarge the effective heat and mass exchanging area; (2) applying a new moisture-wicking and quick-drying fibrous fabric to the wet channel to help diffuse moisture and promote evaporation; (3) adopting aluminium thin sheet to form the channel wall to raise thermal conductivity and remove the supporting elements between the exchanging sheets to reduce the flow resistance; (4) finding an applicable process to bond the fabric with aluminium panel tightly; (5) developing a dedicated water distribution system and water supply scheme to effectively reduce the pump power consumption; (6) developing a dedicated simulation tool to assist structural and operational optimization and performance prediction; (7) constructing a prototype cooler incorporating all the technical innovation and experimentally investigating the cooling performance under various climatic parameters; (8) evaluating the cooler's performance socio-economically through a case study based on local hourly weather data in a typical meteorological year.

2.6 Chapter Summary

An extensive and critical literature review into the research work and practical application of IEC technologies has been carried out. The review work helped to clarify the basic concept and theory, understand the universal evaluation standards and methods, realize the various research interests and status of IEC technical development, identify the potential research opportunities to improve the performance of dew point IEC technology.

The dew point cooling researches in recent decade were analysed in detail. Results of the comparison among the various established works from the aspects

of research methodologies, simulation assumptions, flow patterns, HMX configuration, HMX materials and respective conclusions, helped figure out the issues not well addressed. The identified potential research opportunities for dew point air cooler development mainly exist in the HMX structure optimization to reduce flow resistance and enlarge the effective surface, application of new wetted material to promote evaporation, development of dedicated computer simulation tools, water consumption and contamination investigation and comprehensive evaluation of the system in real climatic conditions.

This PhD project intends to achieve breakthroughs in cooling performance and energy use by incorporating a variety of innovation into a counter-flow regenerative dew point air cooler prototype. The develop scheme includes developing a novel structure bonding the aluminium thin sheet with functional fabric, an innovative HMX structure with irregularly corrugated exchanging sheet facilitating airflow organization, a dedicated water distribution system and water supply scheme, a dedicated simulation tool based on finite differential models, constructing a prototype cooler and experimentally investigating the performance and finally conducting socio-economical evaluation of the proposed cooler.

This part of literature review contributes to (1) illustrating the basic theory and concept; (2) identifying the opportunities to make progress in dew point cooler by referring to the published experience; (3) forming a clear scheme to develop a super performance dew point cooler, and (4) building the research direction for the subsequent chapters.

CHAPTER 3: CONCEPTUAL DEVELOPMENT AND COMPUTERISED SIMULATION

3.1 Chapter Introduction

This chapter proposes a conceptual design for a 4-kW (cooling capacity) rated innovative dew point cooler (DPC) which has potential to achieve higher heat transfer rate (around 25%), lower electricity consumption (around 10%), and less production cost compared to the existing commercial products. The expected technical targets are intended to be achieved by 1) distinct heat and mass exchanger (HMX) design and airflow organization to reduce the flow resistance; 2) enhancement of evaporation by applying the moisture-wicking and quick-drying fibrous material; 3) reliable water distribution and pump operation control; 4) corrugated sheets to enlarge the heat and mass exchanging area. The dedicated numerical modelling is developed and the computerized simulation is carried out to investigate the impacts of the geometric configuration and operational conditions on the unit's cooling performance. The following work will be presented in this chapter.

- (1) Sketch drawings of the proposed DPC configuration and a list of major components involved.
- (2) Working principle of the integrated system, description of the physical structure and thermodynamic analysis of the air treatment process.
- (3) Numerical model setup and conservation analysis of mass and energy.
- (4) Programming and computerized simulation.
- (5) Computer model validation.
- (6) Simulation results and discussion.

This part of work proposes the concept and preliminary design of a novel DPC, and carries out numerical investigation to explore the rational configuration and technical potential in cooling performance. The simulation work should be able to determine the optimum HMX sizes, predict its operational performance, recommend the applicative conditions, as well as deliver the evidence to finalise the design of the HMX and whole system. The results will be double validated and optimized with the experimental results in **Chapter 6**.

3.2 System Description and Working Principle

The DPC consists of 7 major parts, i.e. 1) supply fans, 2) heat and mass exchanger (HMX), 3) exhaust fans, 4) water sink, 5) circulating pump, 6) water distributor and 7) control panel. In addition, some auxiliary components such as air filters, insulation, encapsulation, water and circuit connection etc. are also incorporated. A 3D general sketch of the proposed cooler is shown schematically in **Fig. 3-1** and **Fig. 3-2** contrastively shows the air and water distribution patterns from the side and front views.

Water is fed onto the fibrous surface of wet channel via a dedicated top water distributor and flows downwards along the wet channel walls. Part of the feeding water evaporates while the remaining falls into the lower water sink. A small DC pump is used to lift the water from the lower sink to the upper water distributor when a certain water level is reached. The feeding speed of the water, either from the main supply or from the circulating pump, is controlled by a solenoid valve, water level detectors and a dedicated logic programme.

Air is drawn into the unit from the down/ front side of the unit with the upper supply fans. It then moves upward across the dry channels, where it is cooled by

the channel walls. Finally, one part of the intake air becomes cooler product air to supply and the other goes into the adjacent wet channels through the perforations at the top end of the exchanging sheets. The force driving the air into the wet channels comes from the lower exhaust fans. The air diverting into wet channels flows downwards and evaporates the moisture along the channel walls acting as working air. At the end of wet channels, the working air close to saturation state leaves together with the excess water down flowing. Finally, the air exhausts by one side of the unit and water drips into the lower sink.

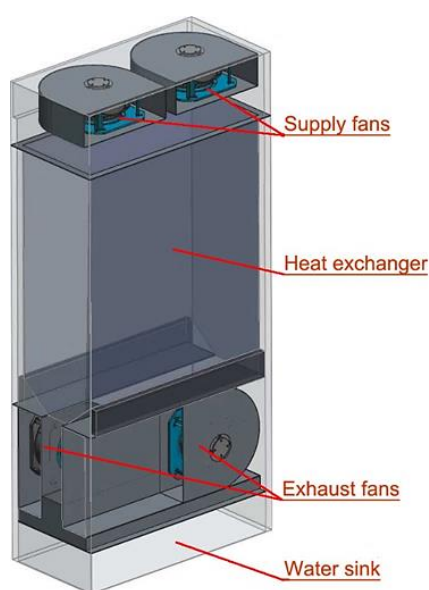


Fig. 3-1: 3-D configuration model.

The wet surfaces of the two adjacent plates are against each other to build a wet channel. Similarly, the dry surfaces of two adjacent plates are against each other to build a dry channel. **Fig. 3-3(a)** illustrates the channels and airflow inside the exchanger.

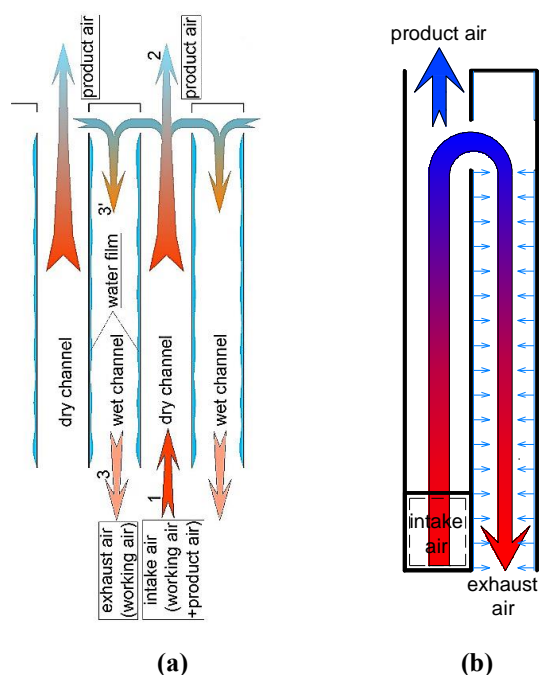


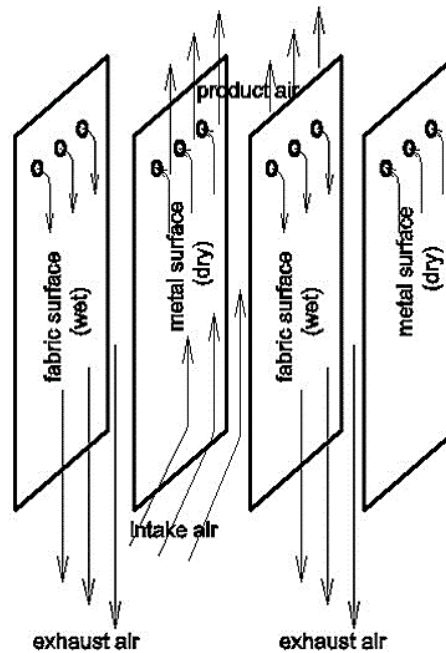
Fig. 3-3: Schematic of airflow and heat and mass transfer.

(a) configuration of the wet and dry channels; (b) process of heat and mass transfer

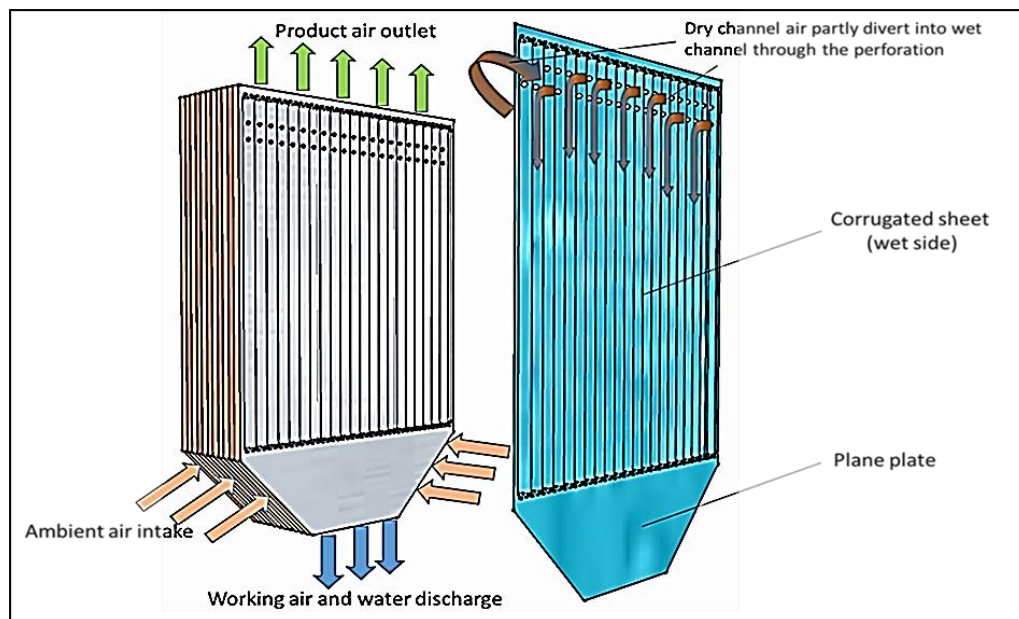
The intake (mostly ambient) air firstly enters the dry channels through the opening on the side-wall, as demonstrated in **Fig. 3-3(b)**, then travels across the dry channels whereby it loses heat to the adjacent wet channels, thus leading to certain temperature drop. At the end of the dry channels, the air is split into two parts: one, called product air, is delivered into the conditioned space to perform cooling; while the remaining part, defined as working air, is diverted into the adjacent wet channels. Within the wet channels, the working air flow backwards, absorbing the heat transported from the adjacent dry channels and receiving the moisture evaporating from the surface of the wet channels, thus completing a heat and moisture transition process from one-part air to another, which leads to the generation of cooled product air.

3.3.2 Thermodynamic Analysis of the Air Treatment Process

In the dry channel, the airflow generally experiences a process of sensible cooling. Under extreme conditions, e.g. high humidity intake air, condensation may occur at the far end of the dry channel. Through the perforations at the end of the dry channel, part of cooled air with same parameters to the product air diverts into the adjacent wet channels other than becoming the final product air and acts as working air in the following process. Along the wet channel, moisture comes into the airflow by natural evaporation under the vapour pressure difference between the wetted surface and airflow, and the airflow is humidified until saturation.



(a)



(b)

Fig. 3-4: Airflow layout in the proposed HMX.

(a) airflow between the exchanging sheets; (b) airflow distribution in 3D view

Fig. 3-4 illustrates the airflow layout within the HMX in a 3D view. Concretely, at the psychrometric chart **Fig. 3-5**, the heat and moisture exchanging process and the change of the airflow parameters along the channels are demonstrated. During operation, the intake (either outdoor or mixture of the outdoor/indoor) air is initially introduced into the dry channels, where it loses heat to the neighbourhood wet channels, leading to a certain temperature drop and change of the states from **1** to **2** in **Fig. 3-5**. At the end of each dry channel, the air is split into two parts, namely product air (PA) and working air (WA). Within the wet channels, WA travels backwards, absorbs heat transferred from the dry channels, receives the moisture evaporated from the surface of the wet channels, resulting in the continuous temperature and moisture growth of the air and change of the air states from **2** to **3**, and eventually discharges to the atmosphere.

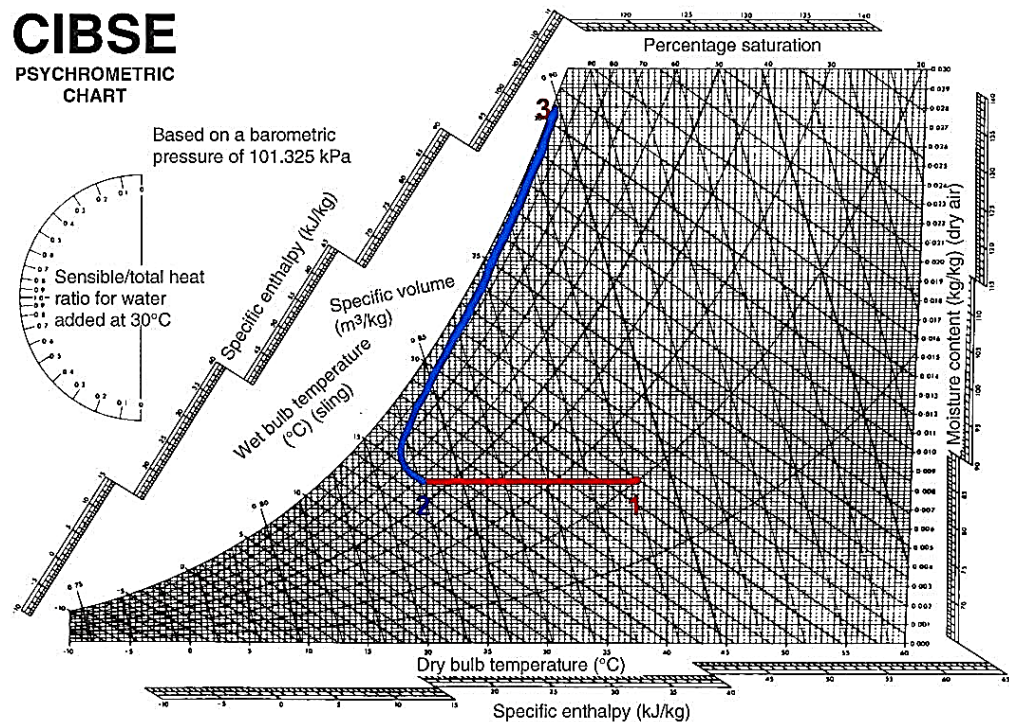


Fig. 3-5: Heat and mass exchange process representing at a psychrometric chart. ^[3.2]

It should be mentioned that the curve from point **2** to **3** in **Fig. 3-5** just demonstrates a general state variation of the air in the wet channel rather than covers all the circumstances. The process from point **2** to **3** starts from the entering of the airflow beyond the perforations in the wet channel. The state of the airflow would depend on the heat exchange between the airflow and the wet wall and the effect of water evaporation from the wet surface. Generally, the saturation degree of the air, which depends on the inlet air state and the cooling effect in the dry channel, and the temperature of the wall, which could possibly be defined by the water flow, influence the water evaporation and heat transfer at the initial stage. In extreme cases, e.g. product air closing to saturation and the temperature of circulating water lower than the relevant condensing temperature, condensation rather than evaporation possibly occurs.

At the initial stage in the wet channel, the temperature of the wet wall is relatively low owing to the inlet water and the airflow releases heat to the wet surface while it absorbs heat due to water evaporation. With the heat exchange along the wet

wall, the water temperature soon overtakes the air temperature and then the both heat flows point to the air together. Therefore, at the initial stage, there is a curve form from point **2** to **3** instead of a totally straight line.

However, unusual cases may occur. For example, in case sufficient cold water, the temperature of which is below the PA dew point, is supplied across the perforation line, condensation will take place in certain distance from the perforation line until the wet surface is heated by the adjacent dry airflow beyond the dew point of the wet air. Another case occurs where the channel is too long for mass exchange in the wet channel under certain intake air state and there is still distance to the wet channel outlet when the airflow becomes saturated. In the last section before exhausting, small quantity of evaporation still occurs just with the wet surface temperature arising, under the enlarged vapour pressure difference between the wet surface and airflow, due to the heat from the adjacent dry airflow. In addition, ‘apparatus dew point’ hints that the state of 100% RH is hard to be achieved in practice due to the limited heat transfer effectiveness.

It is thus clear that the real process of heat and mass transfer either in the dry or wet channel may be complicated as per the various initial conditions. All these special cases should be identified in the simulation program for universal application. Also, the simulation is expected to accurately predict the effective channel length under certain initial conditions to help optimize the structural design.

3.4 Numerical Model Setup and Mass and Energy Conservation Analysis

3.4.1 Numerical Model Setup and Related Assumptions

Following the waveform, the physical space between the exchanging sheets is divided into several identical and independent computational channels. Each computational channel is established by involving a dry semi-channel and its neighborhood wet semi-channel, schematically shown as the pink entity in **Fig. 3-6**. The cross section of the computational channel is sinusoidal waveform as per the corrugation and the whole corrugated surface is the effective exchanging area. The width of a computational channel exactly covers a complete sinusoidal wave of the exchanging sheet.

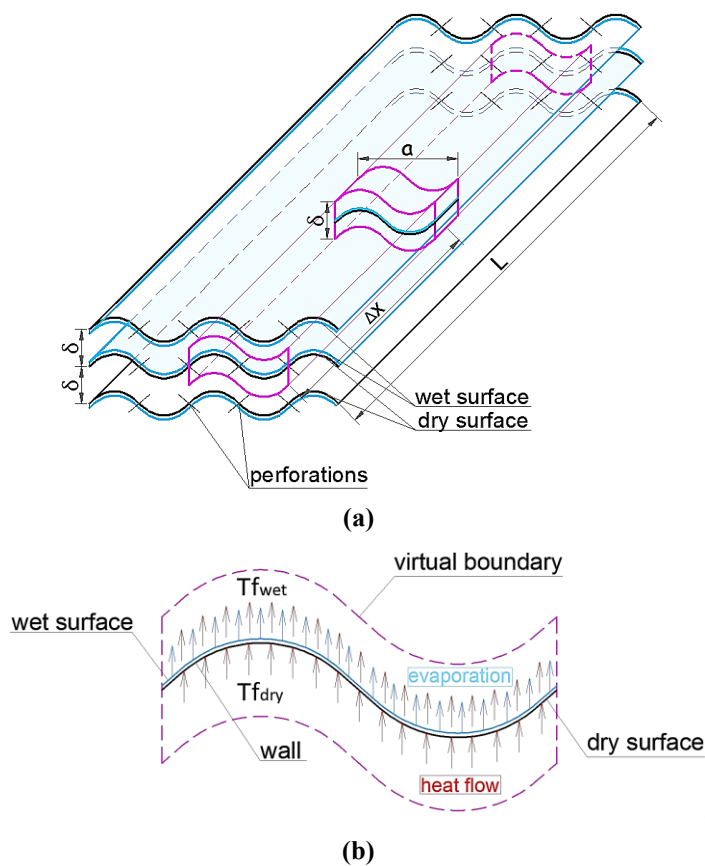


Fig. 3-6: Computational channel.

(a) a computational channel; (b) cross section of a computational channel

The computational channels pack tightly to form a channel array with no space in between. Therefore, if the airflow, either in dry or wet channels, and water distribution on the wet surfaces are even and uniform, the parameters at the adjacent boundaries of each computational channel should be indiscriminate, or in other words, there is no heat and mass transfer between the adjacent computational channels. The computational channels are independent with adiabatic boundaries.

The computational element is considered as the basic unit for simulation. “Finite element” approach is applied to make “differential” treatment to the traditional energy and mass equilibrium equations, thus establishing the relevant differential equations based on each element. Numerous finite elements constitute a computational channel. Within a single computational channel, Newton iteration method is applied to peruse the equilibrium state in terms of heat and mass transfer. To simplify the simulation process and mathematical analysis, the following assumptions have been made:

- 1) The element’s boundary surfaces are adiabatic.
- 2) The exchanger is adiabatic, i.e., no heat transfer occurring between the exchanger body and the surroundings.
- 3) The heat and mass transfer process within the elements is at steady state.
- 4) The heat transfer via the channel walls is in the vertical direction. The convective heat transfer is the dominant mechanism for the heat transfer between the airflow and water film/ channel walls. The channel walls are impervious to water moisture.
- 5) The temperature of the wall and the water is identical at the same point.
- 6) The thermal resistance of the channel wall is negligible, indicating that there is no temperature difference between the dry and wet sides of the wall. [3.3]

- 7) Air is incompressible and the air velocity is uniform within a computational channel.

Along the channel length, each computational channel is divided into numerous computational elements. For the convenience to compare with the referenced experimental results [3.4, 3.5], the typical geometry of the computational element and the whole modular exchanger are pre-set as shown in **Table 3.1**.

Table 3-1: Basic pre-setting parameters for simulation

Parameters	Value
Channel length (m)	1.2
Cross-sectional wave length (equal to the chord) (m)	0.08
Interval between exchanging sheets (m)	0.005
Surface wettability factor	1
Working air ratio	0.33
Velocity of inlet (m/s) \bar{v}	2.4
Temperature of circulating water ($^{\circ}\text{C}$)	16

3.4.2 Mass and Energy Conservation Analysis

For the computational element, the energy and mass equilibrium equations are shown as follows.

(1) Energy balance within a dry element

The air enthalpy difference between the inlet and outlet of a dry element is equal to the amount of heat transferred between the airflow and channel walls.

$$\Delta i_{dry} = C_p \cdot Q_{m,dry} \cdot \Delta T_{f_{dry}} = h_{dry} \cdot (T_{f_{dry}} - T_w) \cdot \Delta A$$

[3-1]

(2) Mass balance in a wet element

The difference of humidity ratio (HR) between the inlet and outlet in a wet element is equal to the amount of water evaporated across the wet surface.

$$\Delta hum_{wet} = h_m \cdot \rho_{air,wet} \cdot (hum_w - hum_{air,wet}) \cdot \sigma \cdot \Delta A \quad [3-2]$$

Where, hum_w and $hum_{air,wet}$ are the humidity ratio of the working air at the wet wall temperature and wet channel air temperature respectively. The difference between hum_w and $hum_{air,wet}$ is the inherent driving force for water evaporation occurring at the wet channel surface. σ is the wettability of the surface material, which is defined as the ratio of the wetted surface area to the total surface area. σ is affected by the water diffusivity of surface material.

The convective mass transfer coefficient between the working airflow and wet channel surface is expressed as a function of the convective heat transfer coefficient and the Lewis number, as follows. [3.6]

$$\frac{h}{h_m} = \rho \cdot C_p \cdot Le^{1-n} \quad [3-3]$$

Whereby, $n=1/3$.

The convective heat transfer coefficient between the airflow and the channel wall along the flow path is a variable, which is mainly determined by the flow regime. Under the low airflow velocity and small channel size condition (i.e. $Re < 2300$), the airflows within both the dry and wet channels are laminar [3.6]. The thermal entry length for the laminar airflow in the dry/wet channel can be expressed as the function of the relevant Reynolds numbers and Prandtl numbers, as follow. [3.7]

$$l_0 = 0.05 \cdot De \cdot Re \cdot Pr \quad [3-4]$$

For the entrance region ($x \leq l_0$), the Nusselt number can be calculated using the following empirical correlation [3.6]:

$$Nu = 1.86 \left(\frac{Re \cdot Pr}{\frac{x}{De}} \right)^{\frac{1}{3}} \cdot \left(\frac{\mu_f}{\mu_w} \right)^{0.14} \quad [3-5]$$

While in the fully developed region ($l_0 \leq x \leq l$), the Nusselt number is constant [3.6]:

$$Nu = 2.47 \quad [3-6]$$

According to the definition of Nusselt number, the convective heat transfer coefficient could be expressed as follows:

$$h = \frac{Nu \cdot \lambda}{De} = 1.86 \left(\frac{Re \cdot Pr}{\frac{x}{De}} \right)^{\frac{1}{3}} \cdot \left(\frac{\mu_f}{\mu_w} \right)^{0.14} \cdot \frac{\lambda}{De} \quad [3-7]$$

(3) Energy balance of the airflow in the wet element

The difference of air enthalpy between the inlet and outlet of a wet element is equal to the sum of the heat transferred from the dry to wet elements and the change of airflow enthalpy in the wet element owing to evaporation, which leads to change in air's humidity ratio.

$$\Delta i_{wet} = C_P \cdot Q_{m,wet} \cdot \varphi \cdot \Delta T_{f_{wet}} = \Delta Q_{wet} + \Delta i_{vapour} \quad [3-8]$$

Where,

$$\Delta Q_{wet} = h_{wet} \cdot (T_w - T_{f_{wet}}) \cdot \Delta A \quad [3-9]$$

$$\Delta i_{vapour} = h_m \cdot \rho_{air,wet} \cdot (hum_w - hum_{air,wet}) \cdot C_{p,vapour} \cdot T_{f_{wet,out}} \cdot \sigma \cdot \Delta A$$

[3-10]

(4) *Conservation of water mass between the inlet and outlet of a wet element*

The variation of the water flow rate between the inlet and outlet of the computational wet element is equal to the amount of water evaporated from the element surface.

$$\Delta Q_{m,water} = h_m \cdot \rho_{air,wet} \cdot (hum_w - hum_{air,wet}) \cdot \sigma \cdot \Delta A$$

[3-11]

(5) *Energy balance in a coupled dry & wet element and variation of the air humidity ratio*

The only heat source supporting all the thermodynamic state change, including water evaporation, temperature rising of airflow and flowing water in the wet element, is the heat transferred from the adjacent dry element.

$$\Delta Q_{dry} = \Delta Q_{wet} + \Delta Q_{vap} + \Delta i_{water}$$

[3-12]

$$\Delta i_{water} = (Q_{m,water,out} \cdot T_{w_{out}} - Q_{m,water,in} \cdot T_{w_{in}}) \cdot C_{p,water}$$

[3-13]

$$\Delta Q_{vap} = h_m \cdot \rho_{air,wet} \cdot (hum_w - hum_{air,wet}) \cdot en_{vapour} \cdot \sigma \cdot \Delta A$$

[3-14]

The latent heat of the evaporated water [4.2] can be expressed as

$$en_{vapour} = 2446 + 1.86T_{water}$$

[3-15]

3.5 Methodology and Parameters Adopted to Evaluate the Performance

The following criteria are commonly used to evaluate the performance of an IEC system: i) cooling capacity; ii) energy efficiency, i.e., Coefficient of Performance (COP); iii) wet-bulb cooling effectiveness; and iv) dew-point cooling effectiveness.

Cooling capacity

According to the formula provided by ASHRAE [3.8], the cooling capacity can be written as:

$$Q_{cooling} = C_p \cdot (T_{dry,in} - T_{dry,out}) \cdot (1 - \phi) \cdot Q_{m,dry,in} \quad [3-16]$$

Coefficient of Performance

Coefficient of Performance (COP) [3.8] is expressed as the ratio of the cooling capacity ($Q_{cooling}$) to the total power consumption (W) of the cooler system:

$$COP = \frac{Q_{cooling}}{W_{fan} + W_{pump}} \quad [3-17]$$

Although actual power consumptions of the fans and pump are affected by numerous operational factors, the following theoretical formulas are often used to estimate their power needs.

The power consumption of a fan can be expressed as follows.

$$W_{fan} = \frac{\Delta P \cdot u \cdot s}{\eta_{fan}} \quad [3-18]$$

Where, ΔP is the pressure drop of the airflow in the dry or/and wet channels, which includes the frictional pressure loss along the channel and the pressure loss from local fittings.

$$\Delta P = \Delta P_f + \Delta P_{local} \quad [3-19]$$

The frictional and local-fitting resistances of airflow [3.9] can be calculated with the following equations.

$$\Delta P_{local} = \zeta \cdot \frac{\rho u^2}{2} \quad [3-20]$$

$$\Delta P_f = \lambda_f \cdot \frac{l}{Dh} \cdot \frac{\rho u^2}{2} \quad [3-21]$$

$$\Delta P = \left(\zeta + \lambda_f \cdot \frac{l}{Dh} \right) \cdot \frac{\rho u^2}{2} = K \cdot \frac{\rho u^2}{2} \quad [3-22]$$

The power consumption of a pump is calculated based on the water circulation rate and water raising height, by using the following equation:

$$W_{pump} = \frac{Q_{m,water} \cdot \Delta P_{water}}{\rho_{water} \cdot \eta_{pump}} \quad [3-23]$$

Based on the technical data from *ebm-papst*, the efficiency of the fan is assumed to be 65% in the following simulation.

Determination of the flow channels' K values by CFD simulation

Owing to the complexity of the heating channel, it is difficult to sort out the local resistance factor ζ and frictional factor λ_f of each element included in the dry and wet channels. In this case, the CFD tool is applied to aid this determination. This

simulation has been undertaken based on laminar flow model by using ANSYS FLUENT 16.1, whereas the pressure-velocity coupling equations are solved by using SIMPLE algorithm. The numerical schemes for pressure and momentum are standard and first order upwind.

The flow domain is considered as three-dimensional. The boundary conditions are depicted below:

- a) A symmetry conditions are imposed on external walls.
- b) “Inlet velocity” boundary is used at the dry air entrance.
- c) “Outflow” condition is used for the dry and wet air outlets. Wet side flow rate weighting is assumed as 0.4.
- d) The surface roughness values on the wet and dry channels are those for fibre and aluminum, as shown in **Table 3-2**.
- e) Geometry variations of the irregular channel at the inlet and outlet, i.e. from-flat-to-corrugated and from-corrugated-to-flat, are taken into consideration, while the air diverting from dry to wet channel via the perforated holes is also considered.

Table 3-2 provides a summary of K values, which have been calculated with the CFD simulation results.

Table 3-2: K values and airflow resistance in channels

u (m/s)	K (-)	onway (Pa)			local (Pa)			ΔP (Pa)
		Dry	Wet	sub-total	Dry	Wet	sub-total	
0.5	256.2	26.0	10.3	36.2	1.1	0.2	1.2	37.5
1.0	132.6	52.1	20.6	72.7	4.3	0.6	4.9	77.6
1.5	91.4	78.3	30.9	109.3	9.6	1.5	11.0	120.3
2.0	70.8	104.7	41.3	146.0	17.0	2.6	19.6	165.6
2.5	58.4	131.2	51.7	182.9	26.5	4.0	30.5	213.3
3.0	49.9	157.6	62.1	219.7	38.0	5.0	43.1	262.7

Wet-bulb cooling effectiveness

Wet-bulb cooling effectiveness (WBE) [3.10, 3.11] is defined as the ratio of the difference between the inlet and outlet product air temperatures to the wet-bulb depression [3.11], i.e. the difference between the inlet air dry-bulb and wet-bulb temperatures, which is expressed as:

$$\varepsilon_{wb} = \frac{Tf_{dry,in} - Tf_{dry,out}}{Tf_{dry,in} - Tf_{dry,in_wb}} \quad [3-24]$$

Dew-point cooling effectiveness

Dew-point evaporative cooling systems can provide the product air at a temperature close to the dew point of the intake air; as such, the dew-point cooling effectiveness [3.10, 3.11] is defined as

$$\varepsilon_{dp} = \frac{Tf_{dry,in} - Tf_{dry,out}}{Tf_{dry,in} - Tf_{dry,in_dp}} \quad [3-25]$$

3.6 Computer model set-up and validation

To enable simulation of the heat and mass transfer processes occurring in the different elements/channels, a dedicated computational algorithm is developed to solve the above equations using the finite element and Newton-iteration method, which is operated under the EES (Engineering Equation Solver) environment [3.12]. The Newton-iteration algorithm [3.13] used for developing the computer model is detailed as follows.

- (a) Entering the geometrical and operational parameters relating to the dry/wet channels, including the channel length/height, number of

computational elements, ratio of the working-to-intake airflow rate, water temperature and intake air condition, e.g. the dry-bulb temperature, relative humidity/ wet-bulb temperature/ humidity ratio, and velocity in the dry channel.

(b) Assuming the start-up temperature for the intake air and the dry channel wall, and determining the thermal-physical properties of the air, i.e., density, specific heat capacity, thermal conductivity, dynamic viscosity and Prandtl number.

- Calculating the Reynolds number and determining the Nusselt number and convective heat transfer coefficient by using Eqs. [3-4] to [3-7].
- Calculating the air temperature at the dry element outlet by using Eq. [3-1], and determining the air temperature at the dry channel outlet.
- Running the model by iteration until the required error allowance for the dry channel air temperature is reached.

(c) Assuming start-up temperatures for the exhaust air and wet channel wall, and determining the thermal-physical properties of the wet air, i.e., density, specific heat capacity, thermal conductivity, dynamic viscosity and Prandtl number.

- Calculating the Reynolds number and determining the Nusselt number and the convective mass transfer coefficient by using Eqs. [3-3] to [3-7].
- Calculating the humidity ratio increment across the element by using Eq. [3-2], and determining the air humidity ratio at the wet channel outlet.

(d) Calculating the air temperature at the wet channel outlet by using Eqs. [3-8] to [3-10].

- Running the model by iteration until the required error allowance for the wet channel air temperature is reached.

- (e) Calculating the water flow rate by using Eq. [3-11].
- (f) Calculating the wall temperature based on the energy balance for the coupled dry & wet elements, by using Eqs. [3-12] to [3-15].
 - Comparing the computed wall temperature with the previously assumed value, and
 - Running the model by iteration until the required error allowance is reached.
- (g) Completion of the model iteration process with reasonably accurate results.
- (h) Calculating the cooling capacity, COP, and wet-bulb and dew-point cooling effectiveness by using Eqs. [3-16] to [3-25].
- (i) Delivering the simulation results and terminating the simulation process.

The computer model can be used for simulation of both the proposed irregular HMX and the referenced plane-plate HMX; the latter is treated as a specific geometrical set-up in the model, i.e. the wave length equalling to the chord for the corrugated geometry. To validate the computer model, the simulation was carried out based on a plane-plate HMX module which had the published experimental results [3.4, 3.5]. These testing data were used to examine the effectiveness and accuracy of the proposed model.

Given the channel interval, length and width of 5 mm, 1200 mm and 80 mm respectively, intake air velocity of 2.4 m/s and working-to-intake air ratio of 0.33, which were the experimental conditions applied in [3.4], the simulation was carried out to generate a series of modelling results. In that the common criteria to evaluate the cooling performance, i.e. wet-bulb cooling effectiveness, dew-point cooling effectiveness, cooling capacity and COP, all depend on the only variable – product air temperature under certain input conditions, the following validation was based on the product air temperature. The simulation results were

compared with the testing data to examine the effectiveness and accuracy of the model, as shown in **Fig. 3-7**.

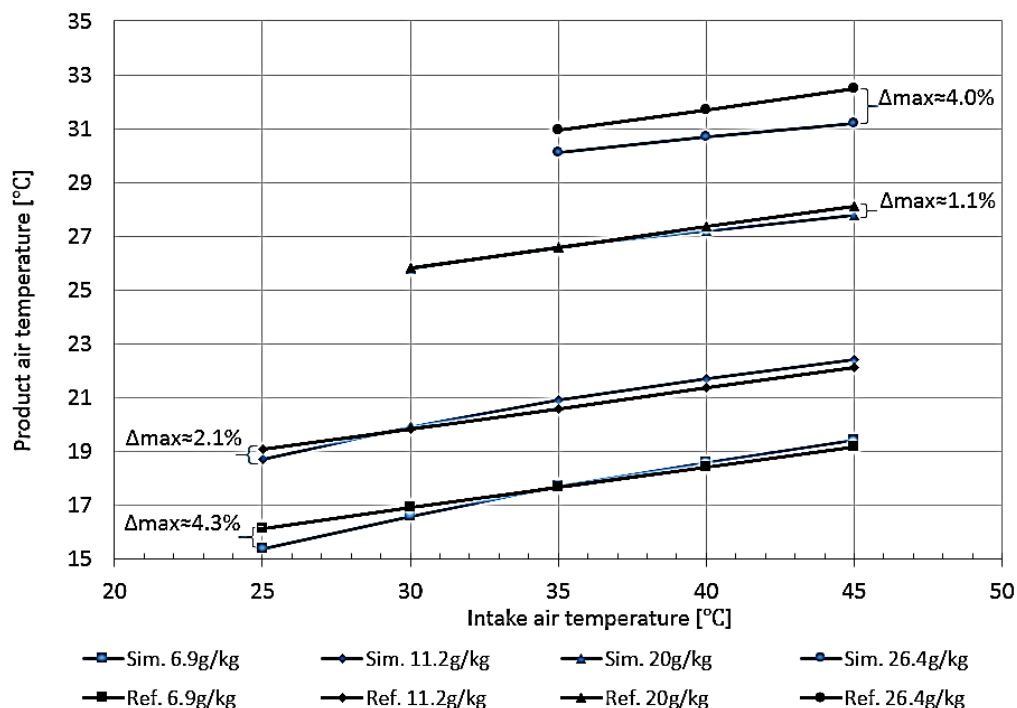


Fig. 3-7: Validation of PA temperature between simulation and the published experimental results.

It is found that at low humidity ratio i.e. 6.9 g/kg, 11.2 g/kg and 20 g/kg, the simulation results agreed with the referenced experimental data with high accuracy, except for one case giving the maximum deviation of 4.3% at the lowest intake air temperature of 25°C and humidity ratio of 6.9 g/kg, as shown in **Fig. 3-7**.

Why did this happen? After continuous detailed pre-conditions comparison between the simulation and the referenced experiment, and analysis of the process value of the simulation, it was found that the water temperature at the wet surface varied in a wide range as per the intake air and water conditions. However, the water condition was not mentioned in the reference. For the referenced experiment, the water was assumed continuously circulating as

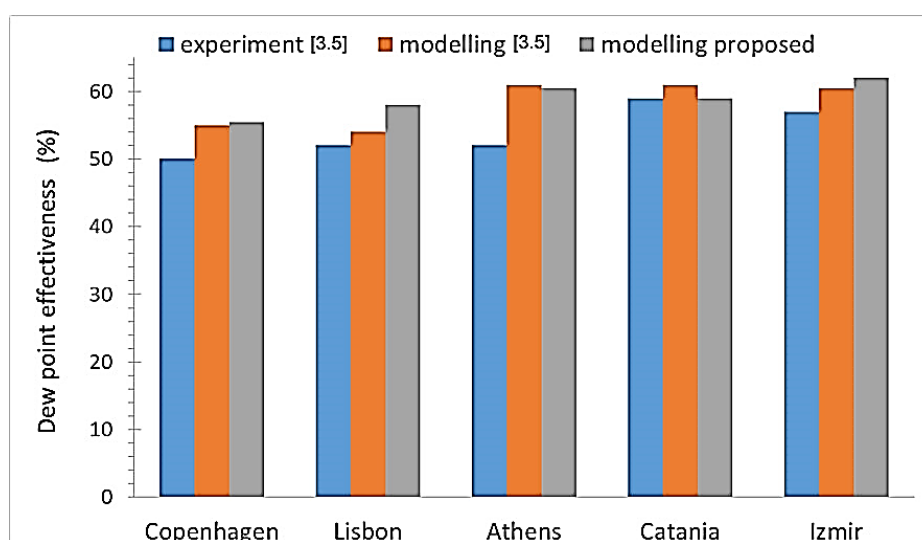
almost all the other references did, i.e. the outlet water temperature being approximately equal to the inlet water temperature. It should be noted that generally there will be several to more than twenty Celsius degree temperature increase for the working water after heat exchanging with the air. This implies that for continuously circulating water the temperature may maintain at a high level, thus removing part of the cooling from the evaporation and leading to an increase of the product air temperature. The specific difference between the outlet and inlet water temperature certainly also depends on the heat loss in the intermediate process, e.g. the volume of the water tank and the insulation of the pipeline and water tank.

In the simulation settings, the inlet water temperature was set at a fixed value as per the main supply temperature, which better reflected the proposed design, i.e. intermittent main water administration and little circulating water. Owing to insufficiency details about circulating water, it was impossible to exactly repeat the referenced experiments by simulation. However, by analysing the variation of water temperature between the outlet and inlet, the desirable tendency agreement and rational deviation suggested that the simulation was reasonable and credible.

For further validation of the reliability, simulation was also conducted under different operational conditions presented in [3.5], i.e. intake air velocity of 0.83 m/s, working air ratio of 0.4 and intake air conditions given in **Table 3-3**. The simulation results were compared with the published experimental data [3.5], giving the derivation profile shown in **Fig. 3-8**. The difference between the modelling and the published results was around 3.1% in average, indicating that the model could achieve a reasonable accuracy in predicting the cooling performance of the dew point cooling HMX.

Table 3-3: Climate conditions used in comparative simulation research

No.	City	County	Dry bulb temperature (°C)	Wet-bulb temperature (°C)	Dew point temperature (°C)	Relative humidity
1	London	UK	28.0	20.0	16.0	48.2%
2	San Pablo	Spain	39.9	25.1	19.2	30.3%
3	Lisbon	Portugal	32.1	19.7	12.9	31.0%
4	Catania	Italy	34.1	21.6	15.5	32.9%
5	Athens	Greece	33.8	20.8	14.1	30.5%
6	Izmir	Turkey	35.5	20.4	12.1	24.4%
7	Copenhagen	Demark	24.0	17.3	13.4	51.5%
8	Helsinki	Finland	26.7	19.1	15.1	48.9%

**Fig. 3-8: Comparison of experimental and simulation results in various climates.**

3.7 Research of Heat and Mass Exchanging Process in the Channels

To further validate the proposed simulation model and investigate the heat and mass exchanging process inside the channels, a series of simulation results was taken to be analysed below. The pre-set general conditions are the same as those in [3.5] and the initial intake air (IA) conditions include temperature of 35°C and humidity ratio of 6.9 g/kg. The simulated product air (PA) temperatures which are marked in **Fig. 3-8** agree well with the experimental data in [3.5]. The

following analysis will focus on the internal heat and mass transfer process along the channels.

Fig. 3-9(a)-(c) presents the dynamic processes of the parameters, i.e. the temperature, relative humidity (RH), humidity ratio (HR) of the air, the temperature of wet surface, the evaporation and heat exchange rate along the dry and wet channel length, based on the dedicated numerical simulation. It should be noted that the processes in dry and wet channels are in opposite direction for the counter-flow pattern, i.e. the start point of the dry channel corresponding to the end point of the wet channel and vice versa. Therefore, the process in dry channel starts at the channel length of **0** while the process in wet channel starts at the channel length of **1.2 m**.

Fig. 3-9(a) shows nothing special along the dry channel, i.e. the relative humidity increases with the air temperature drop. In the wet channel, the air temperature keeps decreasing at the short initial stage within around 0.1m due to the effect of the low temperature entering water, and then maintains increasing along the wet channel being heated by the air in adjacent dry channels. In the extent about 0.4 m from the start point, the air relative humidity in the wet channel rises rapidly from 60% to 95% owing to the water evaporation, then in the rest stage, the relative humidity keeps close to saturation with the evaporation process and the increase of air temperature. The temperature of the wet wall, equalling to the temperature of the water as pre-assumed, keeps ascending with the heat exchanging process with the air in the adjacent dry channel.

Fig. 3-9(b) shows the variation of humidity ratio and evaporation rate in the wet channel along the channel length. The driving force exists in the difference of partial vapour pressure/humidity ratio between the wet surface and the inner air. With the temperature increase, the humidity ratio at saturated state over the wet surface keeps rising and humidity ratio of the wet air ascends due to the process

of evaporation. As for the slight air temperature drop in the initial 0.1m (**Fig. 3-9(a)**), which affects the partial vapour pressure at the same humidity ratio, it could be seen that the evaporation rate reduces while the HR difference even more. Comparing the variation trends between the evaporation rate and HR difference, it could be concluded that the temperature predominates the evaporation process superior to the HR difference in such case.

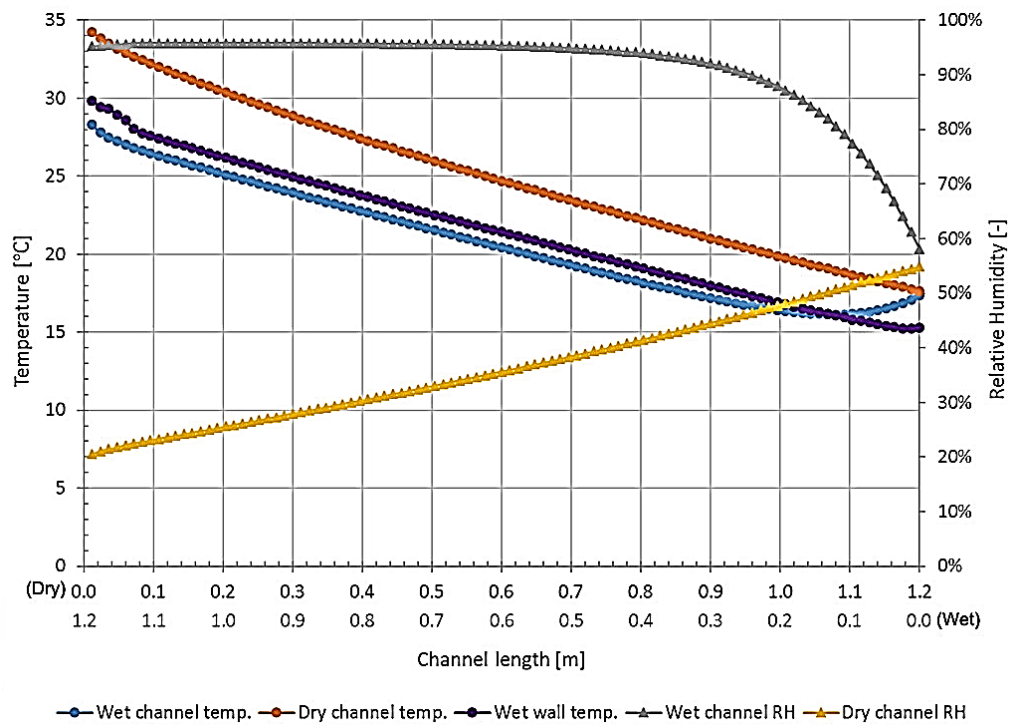


Fig. 3-9(a): Variation of temperature and RH along the channels.

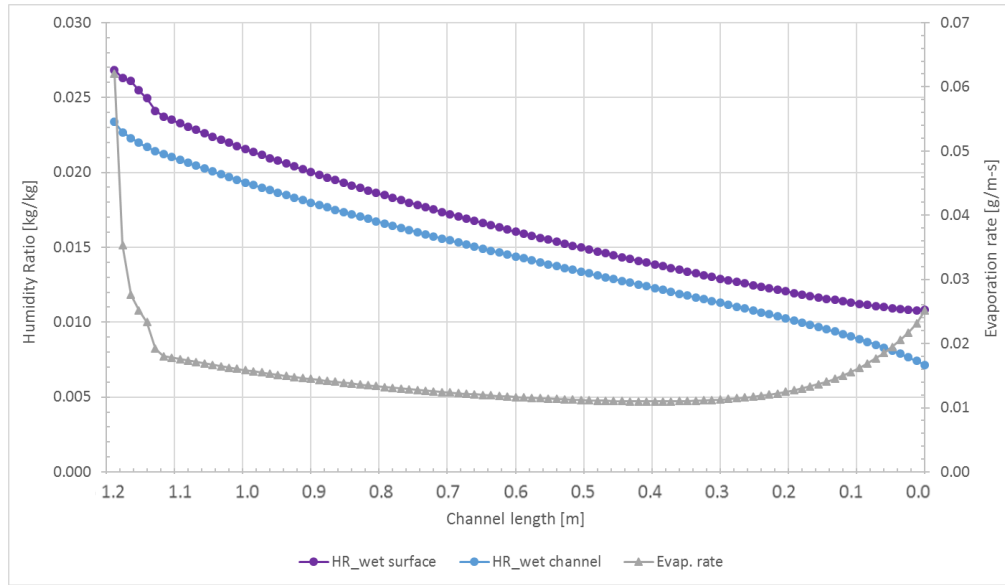


Fig. 3-9(b): Variation of HR and evaporation rate in the wet channel.

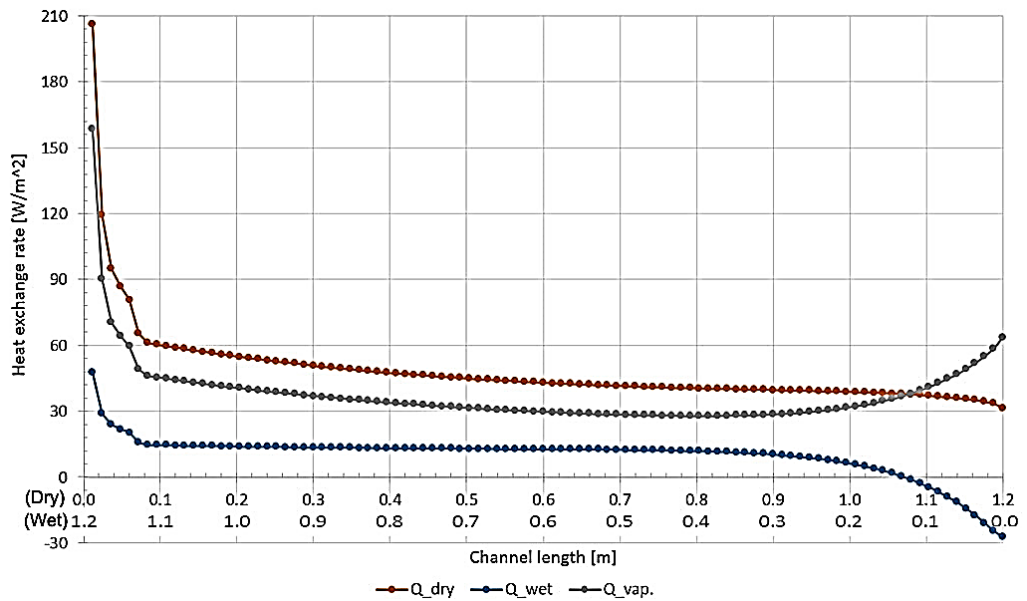


Fig. 3-9(c): Heat exchange along the channel length.

Fig. 3-9: Heat and mass exchange progress in the channels.

Fig. 3-9(c) demonstrates the heat exchanging process along the channel length. Q_{dry} means the heat exchange between the airflow and the wall in the dry channel, Q_{wet} for heat exchange between the airflow and the wall in the wet channel and Q_{vap} for the heat transfer by water evaporation. Within the initial stage of about 0.1 m in the wet channel, the heat flows from the air to the wet

channel wall due to the low temperature of entering water and thus Q_{dry} presents a minus value. Owing to the relatively low evaporation rate in the extent of 0.2 m, Q_{vap} shrinks till the evaporation reaches a normal state with the wall temperature increase. Q_{dry} is the result of the sum of Q_{wet} and Q_{vap} .

The variation processes of the operational parameters in **Figs. 3-9(a)-(c)** accord with the theoretical analysis. It manifests the rationality of the numerical simulation.

3.8 Performance Study of the Proposed Irregular HMX

As previously addressed, the computer model developed in this study can be used to simulate the performance of both corrugated and plane-plate heat and mass exchangers. To further explore the performance potential of the proposed irregular HMX and its superiority over the common plane-plate heat exchanger, the simulation was conducted based on the validated model under the most referenced operation conditions [3.14], i.e. IA wet-bulb temperature of 21.1°C with coincident dry-bulb temperature of 37.8°C and HR of 8.74 g/kg, and the design profile of the irregular exchanger. The results were also parallelly compared with those of the plane-plate one.

The parameter variation for adaptability to the validated model details as follow.

1) In geometry configuration, the exchanging sheet updates to corrugation form with wave length of 13.2 mm and amplitude of 2.77 mm base on a chord of 11.6 mm (**Fig. 3-10**), which was proved by the preliminary material mechanical process tests.

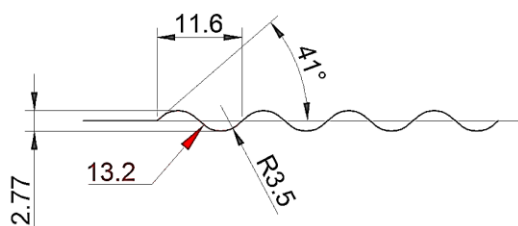


Fig. 3-10: Profile of the corrugation. (Unit: mm)

- 2) The wet surface is covered by fabric material and the rough surface enlarges the effective evaporation area. A factor of 1.5 is applied to the mass transfer area.
- 3) Water distribution control realises intermittent main water supply and less need for the water recirculation. The inlet water temperature is thus fixed at 16°C.
- 4) Power consumption by the water pump is determined by the required water supply rate and operating time. The totally required water supply is assumed 3 times of the water evaporation, i.e. 18 kg/h for a 4-kW cooling rated unit. The pump runs following the mode of per 15-second operation with a 10-minute interval based on the preliminary test experience.

In this section, the performance of the two heat and mass exchangers, i.e. the plane-plate HMX and the proposed irregular HMX with corrugation, is investigated and compared under various IA conditions, including temperature, humidity ratio and velocity, channel dimensions, and operational parameters including the working-to-intake air ratio and water temperature.

The simulation conditions applied to the comparative study are listed in **Table 3-4**.

Table 3-4: Pre-set operational conditions for simulation

Channel length (m)	Channel interval (m)	Channel numbers (-)	Element numbers per channel (-)	Working air ratio (-)	Inlet water temperature (°C)
1	0.005	100	100	0.4	16
DBT of intake air (°C)	WBT of intake air (°C)	Air velocity in dry channel (m/s)	Surface wettability factor (-)	Fan efficiency (-)	Pump efficiency (-)
37.8	21.1	2	1	65%	100%

DBT-Dry bulb temperature; WBT-Wet bulb temperature; Working air ratio- Working-to-intake air ratio.

The IA conditions and geometrical parameters of the heat and mass exchanger are the key factors impacting the performance of evaporative cooling. The simulation results are presented as follows.

3.8.1 Impact of the intake air parameters

(1) *Impact of the intake air temperature*

Keeping the IA humidity ratio at 8.74 g/kg, which corresponds to the referenced operation conditions of IA wet-bulb temperature of 21.1°C and coincident dry-bulb temperature of 37.8°C, impact of the IA temperature on the performance of both the proposed irregular and normal plane-plate HMXs was investigated and the difference between the two exchangers was analysed. The results are shown in **Fig. 3-11(a), (b) and (c)** respectively.

For the both exchangers, increasing the IA temperature led to significant linear increase in the coolers' cooling capacity and COP. What needs illustration is that the calculation of COP depends on the power consumption by the pump and fans, which varies with the operating condition in practice. The practical circulating water volume is usually as large as 20-30 times [3-16] of the evaporative capacity for normal plane-plate HMX owing to the very poor performance moistening the evaporation surface. Large amount of water benefits sensible cooling other than evaporative cooling.

For a mutual basis of comparison, all the mentioned COPs, either for the proposed irregular HMX or the competitive plane-plate one, were calculated based on a water flow rate of 3 times of the actual evaporative capacity, which is just one of the goals to pursue in this project by means of effective evaporation medium and water distribution control. Therefore, the COP value of the competitive plane-plate one may be enlarged by decreasing the power consumption at pump side. Otherwise, it will not change the law based on evaporative cooling.

Moreover, the effective evaporation area of the proposed irregular HMX is multiplied by a coefficient of 1.5 to embody the increment due to the fabric surface other than the smooth water film. The impact of this coefficient will be in detail studied in the following specific section.

Unless there are obvious differences, the following analysis for the simulation results will be applied to the proposed irregular HMX model.

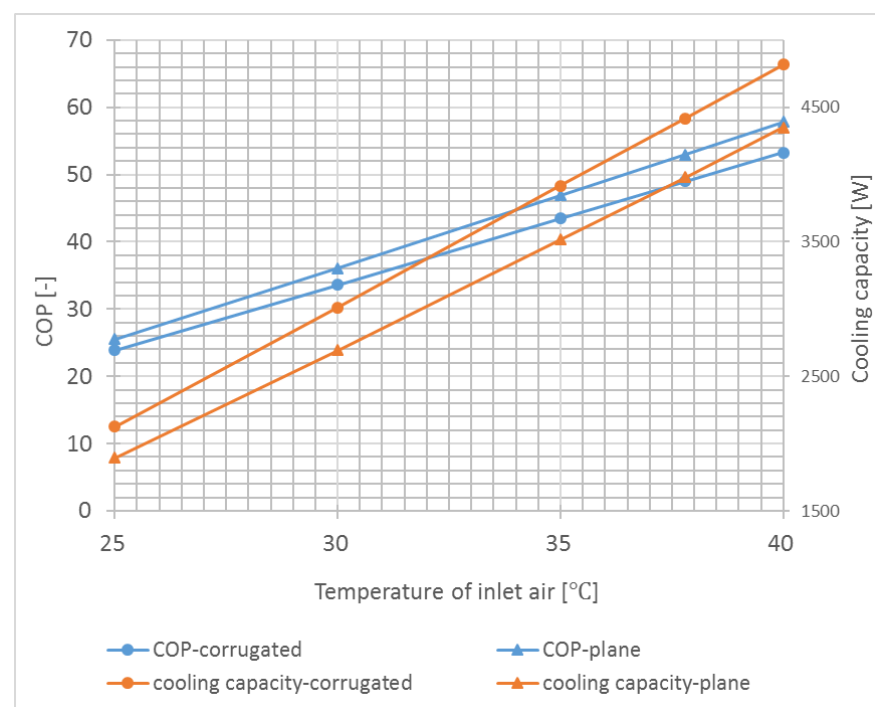


Fig. 3-11(a): Cooling capacity and COP.

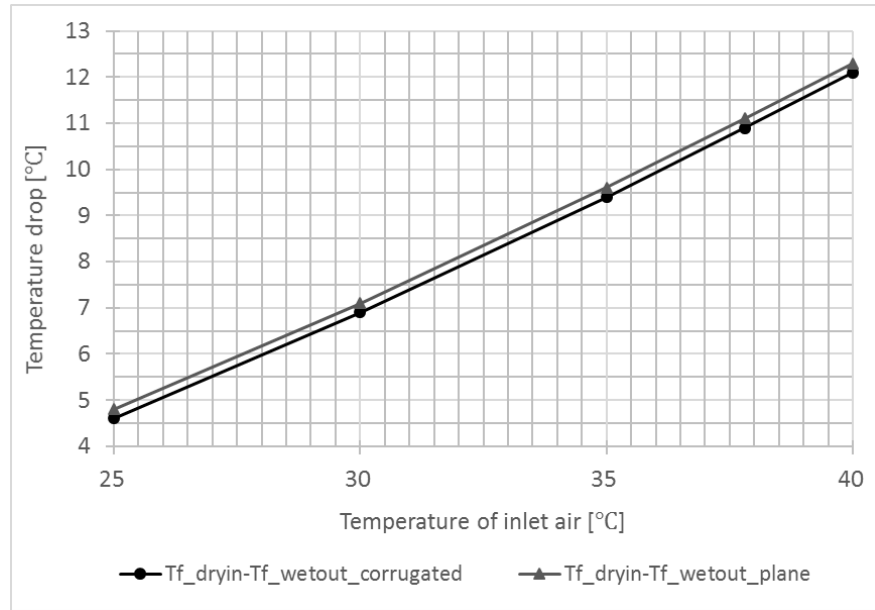


Fig. 3-11(b): Temperature difference between IA and EA.

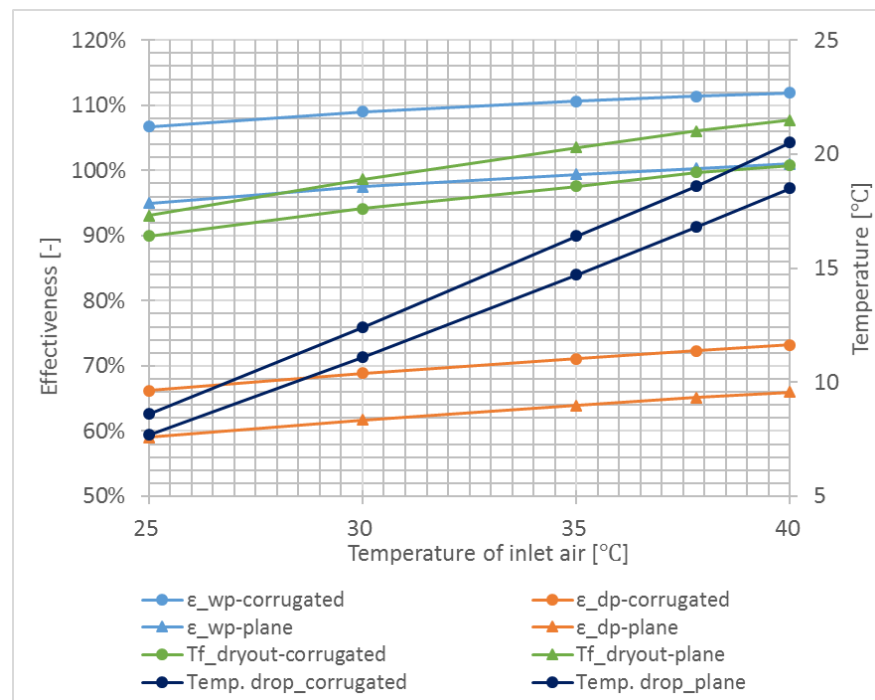


Fig. 3-11(c): Cooling effectiveness and PA temperature.

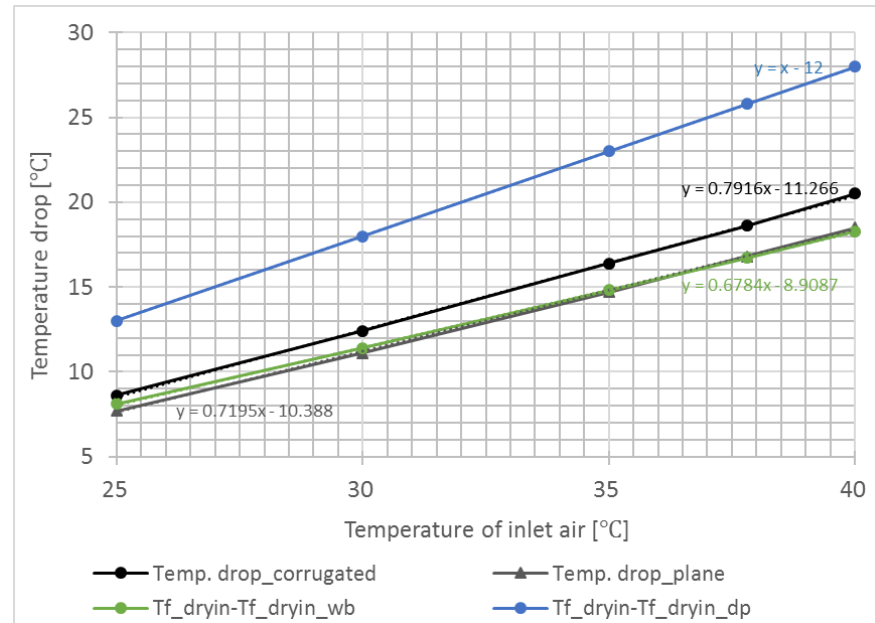


Fig. 3-11(d): Variation of wet-bulb and dew-point temperature

Fig. 3-12: Performance variation with IA temperature (at constant HR).

In **Fig. 3-11(a)**, the cooling capacity and COP increase linearly with the IA temperature, owing to the fact that the increased air temperature could lead to the reduced RH, i.e. the more powerful driving force to evaporate water [3.10]

As a fact, with the increase of IA temperature, the temperature difference between the inlet and exhaust air enlarges coincidentally as shown in **Fig. 3-11(b)**. It means more of cooling capacity by water evaporation lost to the exhaust air (EA). As a result, the evaporation rate and cooling capacity of the exchanger eventually increase without the increase of power consumption.

For the proposed HMX, the wet-bulb cooling effectiveness (WBE) increases from 106.7% to 111.9%, and dew-point cooling effectiveness (DPE) from 66.2% to 73.2% while the temperature drop between IA and PA and the cooling capacity more than double respectively from 8.6°C to 20.5°C and 2126 W to 4819 W. It could be explained in **Fig. 3-11(d)** with the definition of WBE and DPE i.e. Eqs. [3-24] and [3-25], that the difference between inlet dry-bulb and

wet-bulb or dew-point temperature linearly increases with the enlargement of the temperature drop by a similar slope.

The characteristic of cooling capacity rising substantially with the IA temperature benefits the application in building air conditioning, for the internal cooling load generally increases with the outdoor temperature while air humidity ratio basically keeps constant in a day. This bonus will also be talked about in the case study in **Chapter 6**. (In one-day-long time, the moisture contained in the atmospheric air is considered constant at a general location.)

Under the same operational condition, the irregular exchanger shows better performance than the plane-plate one with the similar variation trend of all the indicative performance parameters, i.e. COP, cooling capacity, WBE and DPE versus the outdoor air temperature. The cooling performance of irregular exchanger is 12.3%-10.8% (11.5% in average) larger than that of the plane-plate one in IA temperature range of 25°C-40°C in terms of cooling capacity, WBE and DPE.

Compared to the plane-plate HMX, the irregular type is able to deliver higher cooling capacity and lower PA temperature due to the enlarged area for heat transfer and water evaporation. This leads to more effective heat and mass transfer and thus a more compact physical configuration.

(2) Impact of the intake air moisture content (humidity ratio)

The moisture content within atmospheric air varies with seasons more than days, while in a day, the temperature variation leads to different relative humidity at different moments. To investigate the impact of the IA humidity ratio (HR), in the following section, the IA temperature and relative humidity (RH) are respectively held constant and the variation of the indicative performance parameters with humidity ratio are presented.

The HMX performance in different seasons could be reflected in computational simulation by holding the IA temperature constant at different levels, which could be available in practice by various means e.g. simple heating treatment all year round.

Constant intake air temperature

Keeping the IA temperature at bench level of 37.8°C, impact of the humidity ratio on the performance of both the irregular and plane-plate HMXs was investigated and the difference between the both was analysed. The results are shown in **Fig. 3-12(a)**, **(b)** and **(c)** respectively. One thing to note is that the points on each curve in **Fig. 3-12** correspond to the relative humidity of 10%, 21.4%, 20%, 30%, 40%, 50%, 60% and 70% respectively.

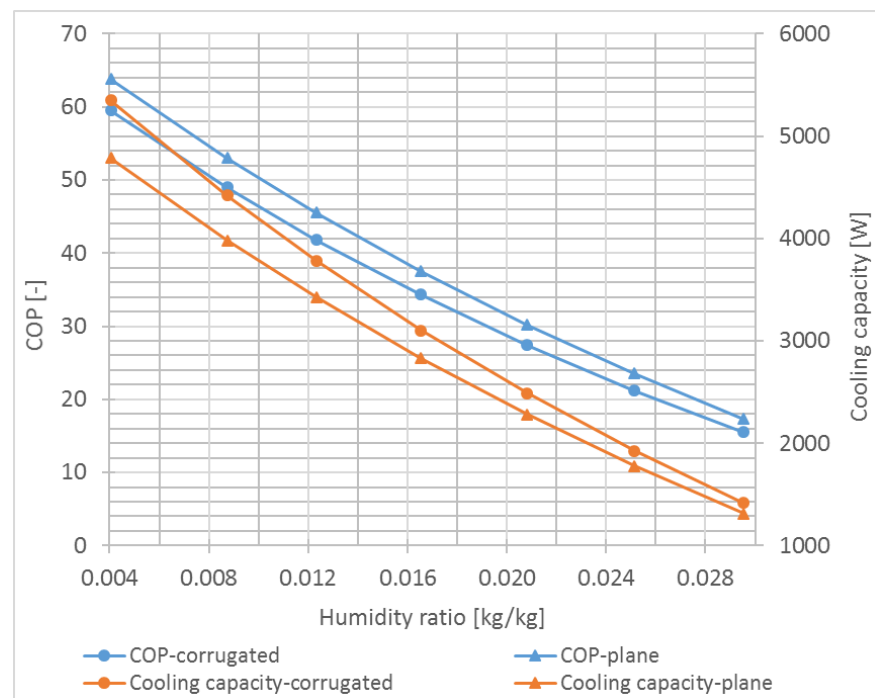


Fig. 3-12(a): Cooling capacity and COP.

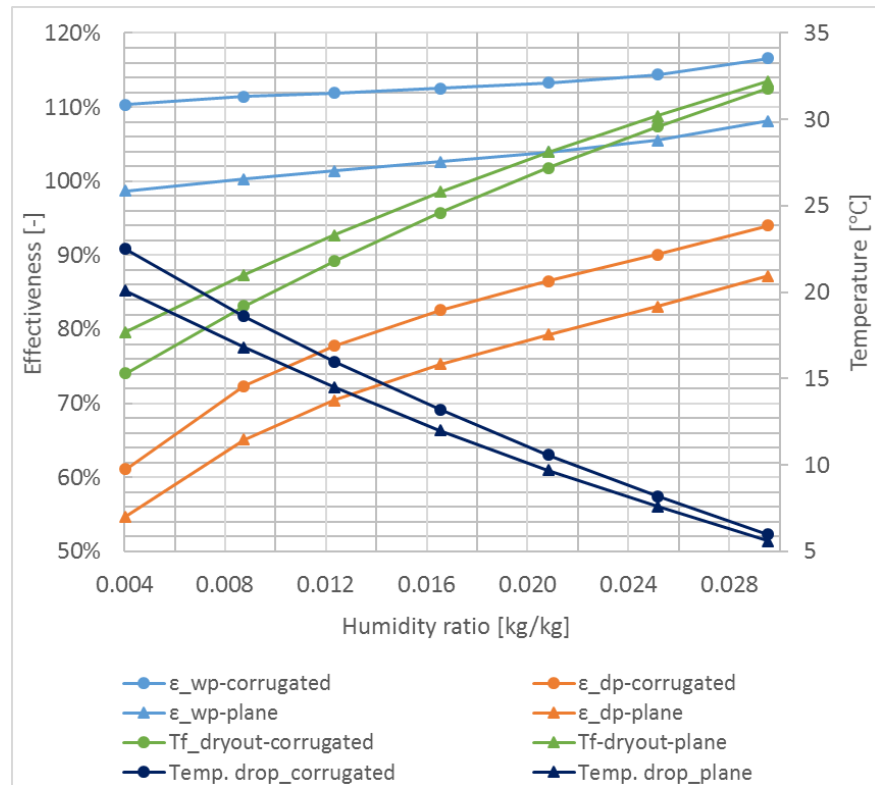


Fig. 3-12(b): Cooling effectiveness and PA temperature.

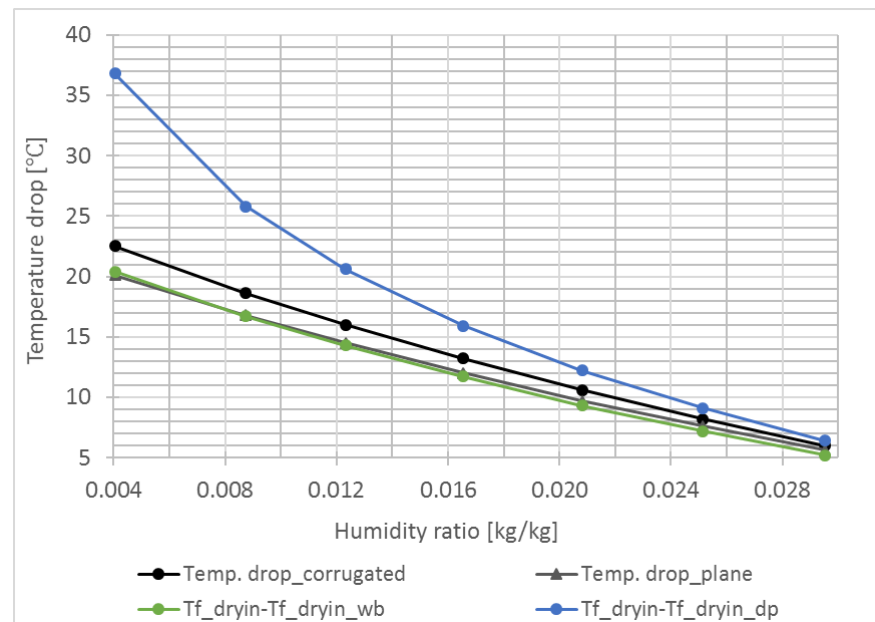


Fig. 3-12(c) : Air temperature drop.

Fig. 3-13: Performance variation with humidity ratio (at constant IA temperature).

It is seen from the **Fig. 3-12(a)** and **Fig. 3-12(b)** that the indicative performance parameters, i.e. COP, cooling capacity, WBE and DPE for the both exchangers, show similar variation trend versus the humidity ratio. The cooling capacities and COPs decrease quickly with the HR increase of the intake air, indicating that the exchangers may present better performance in the cooler seasons owing to the reduced humidity ratio of ambient air. It means that for constant-temperature intake air, e.g. in year-round running air conditioning systems, the performance of the HMX is much better in cool seasons owing to the lower humidity ratio of the ambient air.

Fig. 3-12(c) explains why the dew-point effectiveness rise sharply at low humidity ratio. The dew point corresponding to the state of dry-bulb temperature of 37.8°C and RH of 10% is as low as 1.0°C, which makes a much bigger denominator, i.e. the dew-point temperature depression, to calculate the DPE in Eq. [3-25]. With the increase of humidity ratio, i.e. the relative humidity at same temperature, dry-bulb temperature rapidly approaches to the dew point. In this case, although the cooling capacity greatly decreases, which makes the temperature drop i.e. the numerator to calculate the DPE low, with the increase of dew point, the denominator may shrink even more, which still makes a high value possible.

For instance, the state of dry-bulb temperature of 37.8°C and relative humidity of 70% (HR=29.5 g/kg), corresponds to the dew point of 31.8°C. Although the cooling capacity under such inlet condition is so low that it can only lower the IA temperature about 6°C, it can still present a striking dew-point cooling effectiveness of 94%. The fact manifests that the indicative performance parameter of cooling effectiveness is strongly associated with the inlet air condition. Dew point is a monotropic function of humidity ratio and higher humidity inlet condition may lead to an extremely high dew-point cooling

effectiveness regardless of the awful cooling capacity. Therefore, it makes no sense to talk about cooling effectiveness without regarding the inlet air condition.

Constant relative humidity

Keeping the relative humidity at referenced level of $RH=21.4\%$, impact of the humidity ratio on the performance of both the irregular and plane-plate HMXs was investigated and the difference between the both was analysed. The points on each curve in the **Fig. 3-13** correspond to the IA temperature of 25°C , 30°C , 35°C , 37.8°C and 40°C respectively. The results are shown in **Fig. 3-13(a)**, **(b)** and **(c)** respectively.

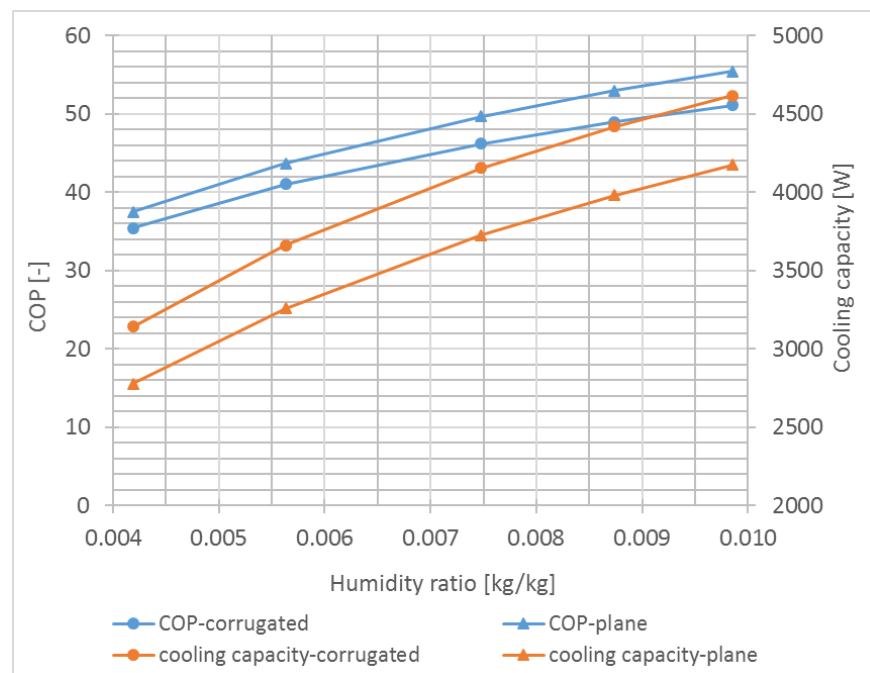


Fig. 3-13 (a): Cooling capacity and COP.

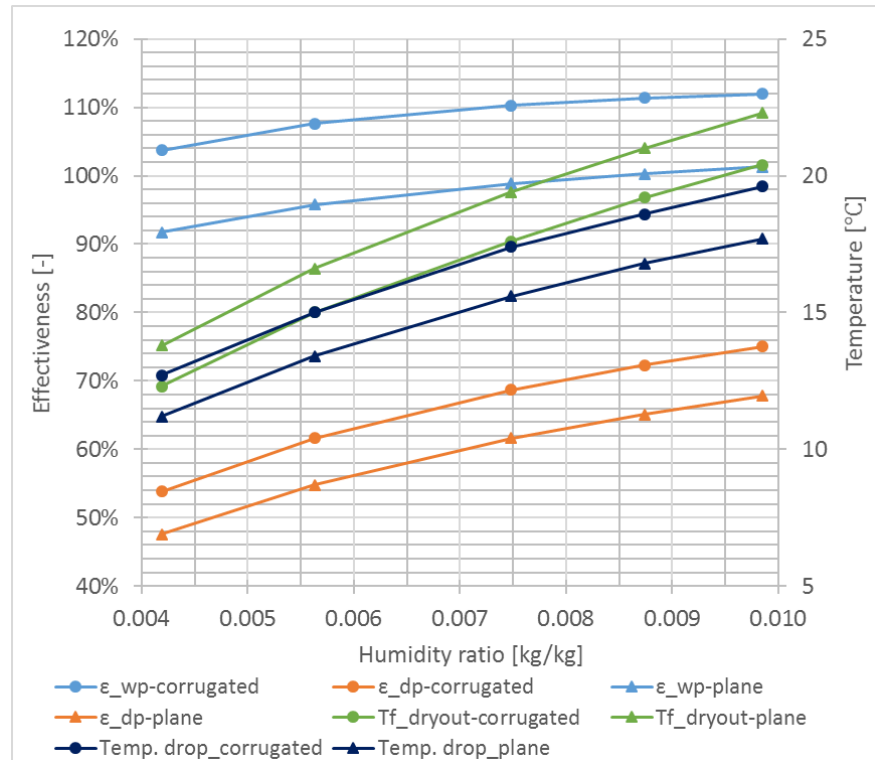


Fig. 3-13(b): Cooling effectiveness and PA temperature.

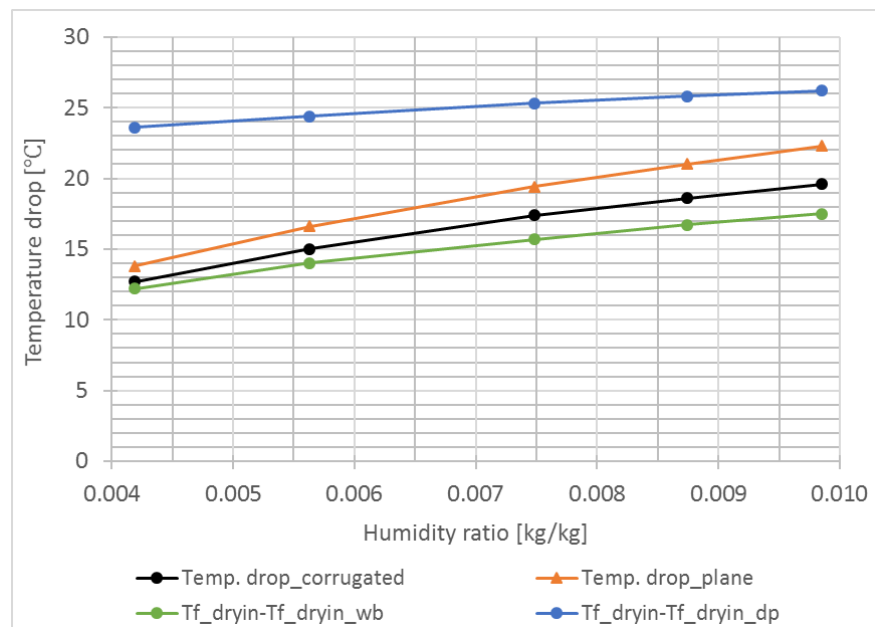


Fig. 3-13(c) : Air temperature drop.

Fig. 3-14: Performance variation with humidity ratio (at constant relative humidity).

It is seen from the **Fig. 3-13(a)** and **Fig. 3-13(b)** that the indicative performance parameters, i.e. COP, cooling capacity, WBE and DPE, for the both exchangers show similar variation trends versus the humidity ratio. **Fig. 3-13(b)** presents the temperature drop sharply enlarges from 12.7°C to 19.6°C with the humidity ratio increasing from 4.19 g/kg to 9.85 g/kg at the same RH of 21.4%, which leads to the fact shown in **Fig. 3-12(a)** that cooling capacity increases by 47%. What is noteworthy is the fact that the increment rate of temperature drop does not equal to that of cooling capacity. The answer lies in the difference of air density between 25°C and 40°C, the influence of which may be unnoticeable and easily ignored but being there with a notable value more than 5%. The increment of COP is a certainty in **Fig. 3-12(a)** since the power consumption stays the same with the increase of cooling capacity.

Fig. 3-13(b) presents the variation trend of cooling effectiveness with humidity ratio. It is obvious that dew-point effectiveness is more sensitive to the HR variation. As for **Fig. 3-12(b)**, the same situation applies. To better understand the impact of IA humidity ratio, more computed results are plotted in terms of each single output parameters as shown in **Fig. 3-14(a)-(k)**. In each graph, series of computed results based on different temperatures, i.e. 25°C, 30°C, 35°C, 37.8°C and 40°C, are plotted by humidity ratio as X-axis and the output parameter, i.e. cooling effectiveness, cooling capacity, PA temperature, COP, as Y-axis. The data points in each curve correspond to the different RH level, i.e. 10%, 21.4%, 30%, 40%, 50%, 60% and 70%. The highlighted red big point stands for the working state corresponding to the referenced IA condition, i.e. dry-bulb temperature of 37.8°C, RH of 21.4% and HR of 8.74 g/kg.

As for the location where the dew point cooler will be applied, humidity ratio of ambient air generally varies with seasons while within one single day it basically keeps constant. However, the environmental temperature varies periodically with time in each day. Consequently, the HR value could stand for the HR level

during a relatively long period, e.g. a cooling month, and the temperature range could partly represent the ambient temperature variation during the working period in a cooling day.

The geographical region with average humidity ratio in the most humid month higher than 12 g/kg generally considered as moist area which is not suitable for the application of evaporative cooling [3.16]. The selected temperature range, i.e. from 25°C to 40°C, is rational for most application scenarios, since under much lower outdoor air temperature natural air cooling is commonly considered more economical than evaporative cooling and ambient temperature over 40°C is rare in practice.

Since there is no change in air and water system corresponding to power consumption, the variation of cooling capacity and COP almost merely associates with temperature drop between the IA and PA. Therefore, the variation tendencies of cooling capacity and COP are similar with that of air temperature drop as shown in **Fig. 3-14(a)-(c)**. In terms of fixed humidity ratio, cooling capacity and COP rise pro rata with the IA temperature. It reflects the operation state of the proposed dew point cooler during the working period in a day.

The lines connecting the operation points at the same RH level tell a fact that with the RH increment, the impact of temperature on the cooling performance fades out. At the RH level of 70%, the difference of cooling capacity at the IA temperature of 40°C and 25°C is 30.5%, while 52.8% at RH=10%. As the relative humidity of the outdoor air anywhere experiences periodical changes with the temperature in each normal day, the varying pattern implies the operation states of the unit at the similar moments i.e. similar RH levels within a day in different seasons with different humidity ratio for one location or at different locations with different temperature levels. In other words, for the application of the

proposed dew point cooler at a location, the cooling performance varies with seasons. The outputs of the cooler in low-RH periods (in a day) vary with the IA temperature (seasons) more than those in higher-RH periods.

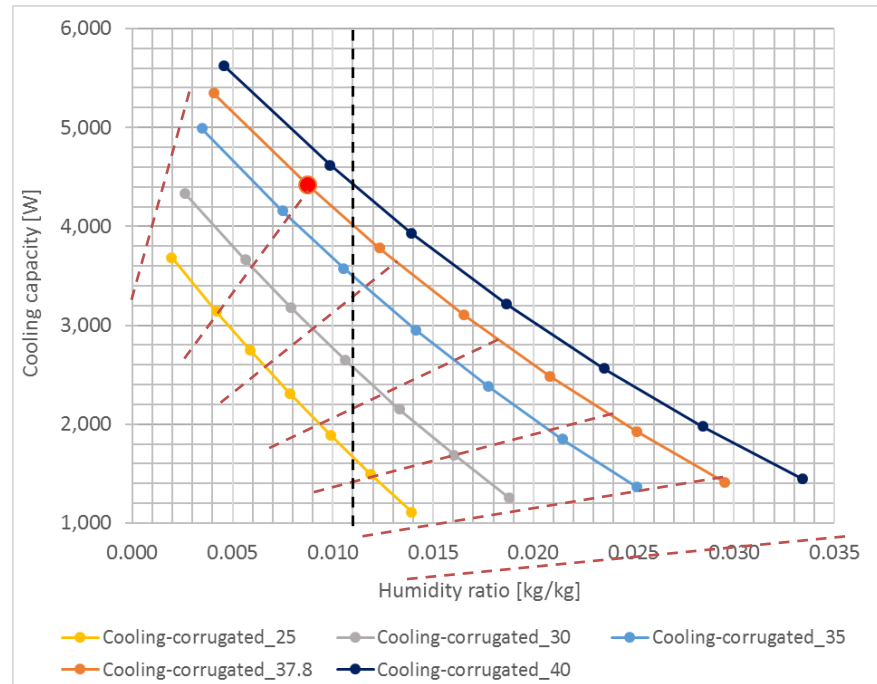


Fig. 3-14(a): Variation of cooling capacity with HR at various IA temperature.

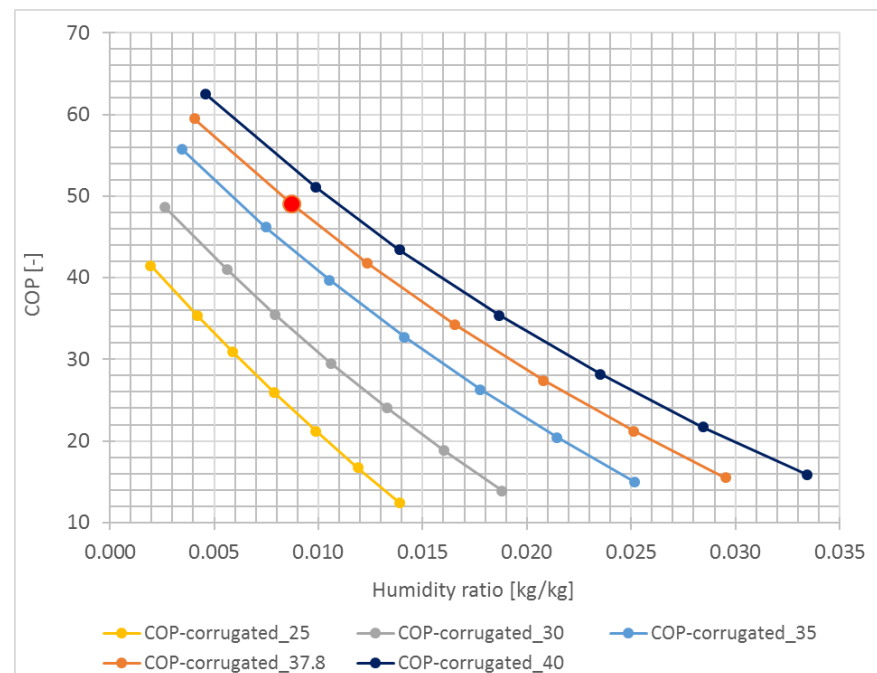


Fig. 3-14(b): Variation of COP with HR at various IA temperature.

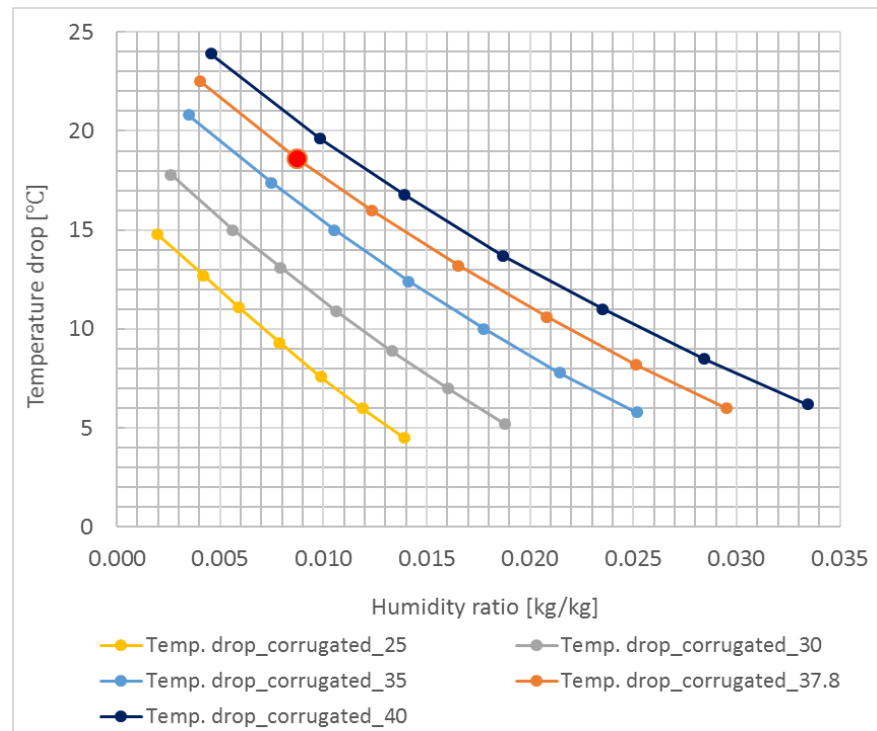


Fig. 3-14(c): Variation of temperature drop with HR at various IA temperature.

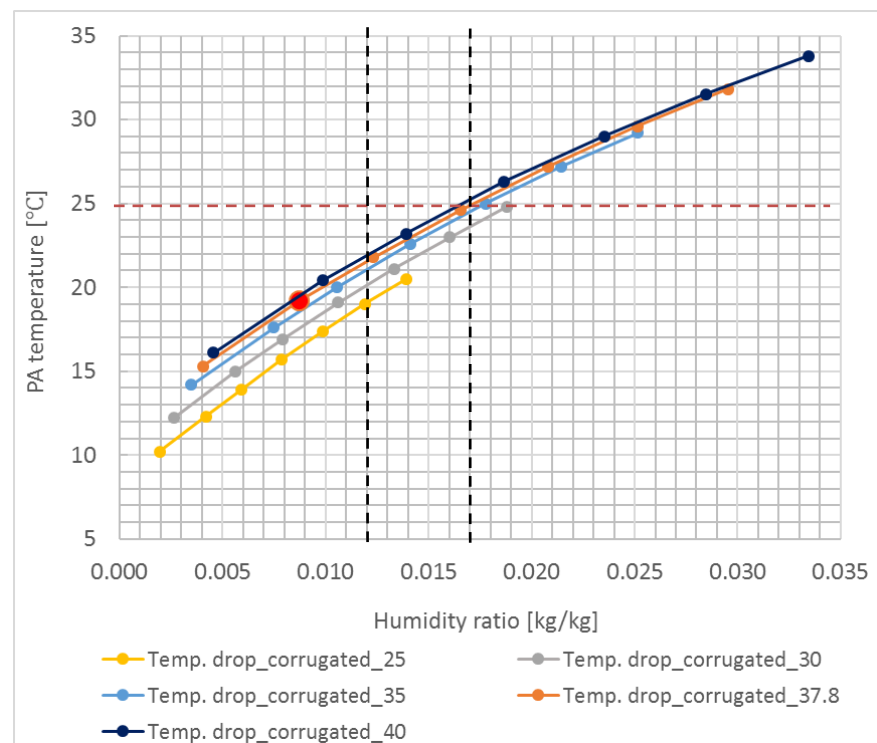


Fig. 3-14(d): Variation of PA temperature with HR at various IA temperature.

Fig. 3-14(d) shows the variation of PA temperature with the temperature and humidity ratio of IA. At a specific humidity ratio, the PA temperature rises with the IA temperature. For example, at humidity ratio of 8.74 g/kg, when outdoor temperature varies from 25°C to 40°C, the PA temperature changes from 16.4°C to 19.5°C. In practice, it means that during a certain day, with the ambient temperature change, the PA temperature cannot stay constant. Basically, the difference of PA temperatures varies proportionally with the difference of IA temperature. Even if the IA temperature rises from 25°C to 40°C, i.e. 15°C increment, the PA temperature just ascends by 3.1°C due to the great promotion of the cooling capacity with the IA temperature.

As for all fresh air systems, if the extreme conditions of PA are defined as temperature of 25 °C and RH of 60%. Merely at the temperature side, it could be seen in **Fig. 3-14(d)** that when HR beyond 0.017 kg/kg, for the case of IA temperature over 37.8°C, the PA temperature will exceed the temperature limit of 25°C. It means that when the HR is as high as 0.017 kg/kg or more, the application of the dew point cooler under the condition of IA temperature of 37.8°C or more, i.e. RH beyond about 40%, will fail to deliver desirable air to the service area. The alternative solution could be either pre-dehumidifying/ pre-cooling the ambient air before it enters the unit or post-dehumidifying/ post-cooling the product air.

In **Fig. 3-14(d)**, product air of HR=0.012 kg/kg at 25°C relates to a higher IA temperature than 40°C. Accordingly, it could be deduced that the temperature may be about 55°C. Therefore, it could be concluded that to supply cool air for indoor air conditioning, the maximum IA temperature could be as high as 55°C, but the humidity ratio must be lower than 0.012 kg/kg. Corresponding to the temperature of 55°C, the RH upper limit is 12% and RH of 29% for 37.8°C.

It could be seen in **Fig. 3-14(e)**, for IA temperature of 37.8°C at HR of 0.017 kg/kg, the RH of the product air will be about 84.5%, which does not meet the requirement for product air. Corresponding to the air state of 25°C and RH of 60%, the HR is 0.012 kg/kg.

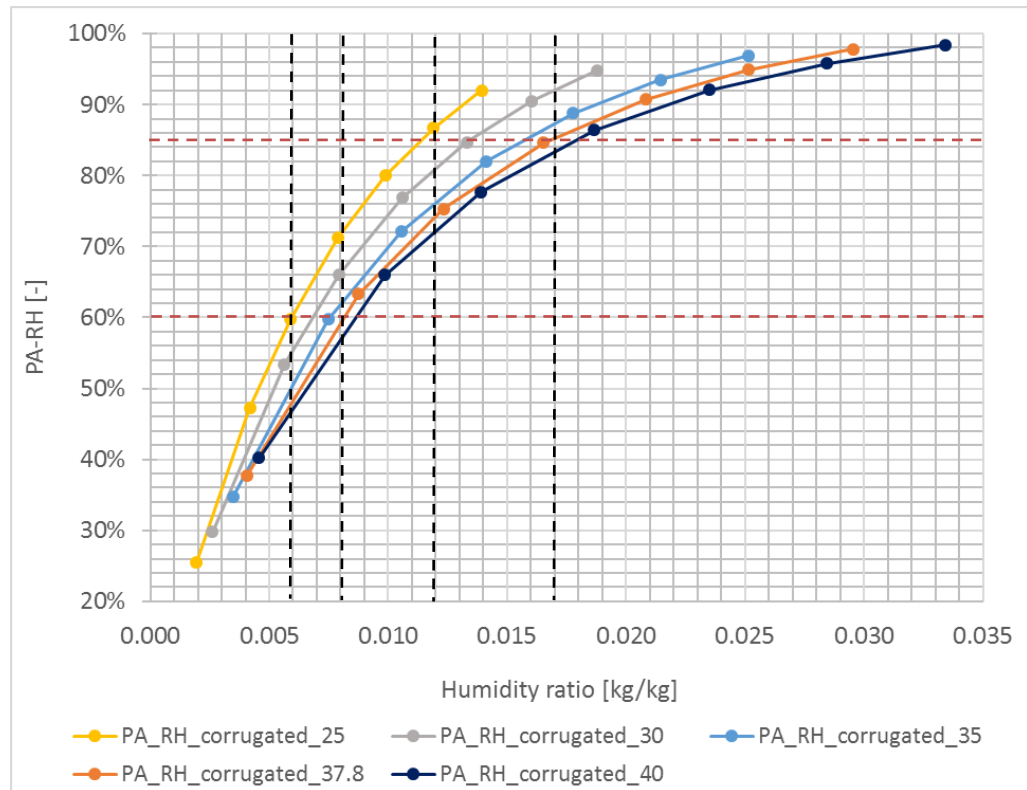


Fig. 3-14(e): Variation of PA relative humidity at various IA temperature.

To meet the requirement for product air of $RH < 60\%$ at 25°C, it could be seen in **Fig. 3-14(e)**, the IA humidity ratio should not exceed the 0.006 kg/kg. For cases of IA temperature beyond 37.8°C, the maximum humidity ratio should be less than 0.0082 kg/kg, i.e. RH no more than 17.5%.

To be sure, the above results are based on the operation condition of air velocity at 2 m/s in dry channels and working air ratio of 0.4, of which the impacts on cooling performance will be discussed in the following sections. Meanwhile, the PA relative humidity is required for the air conditioning system.

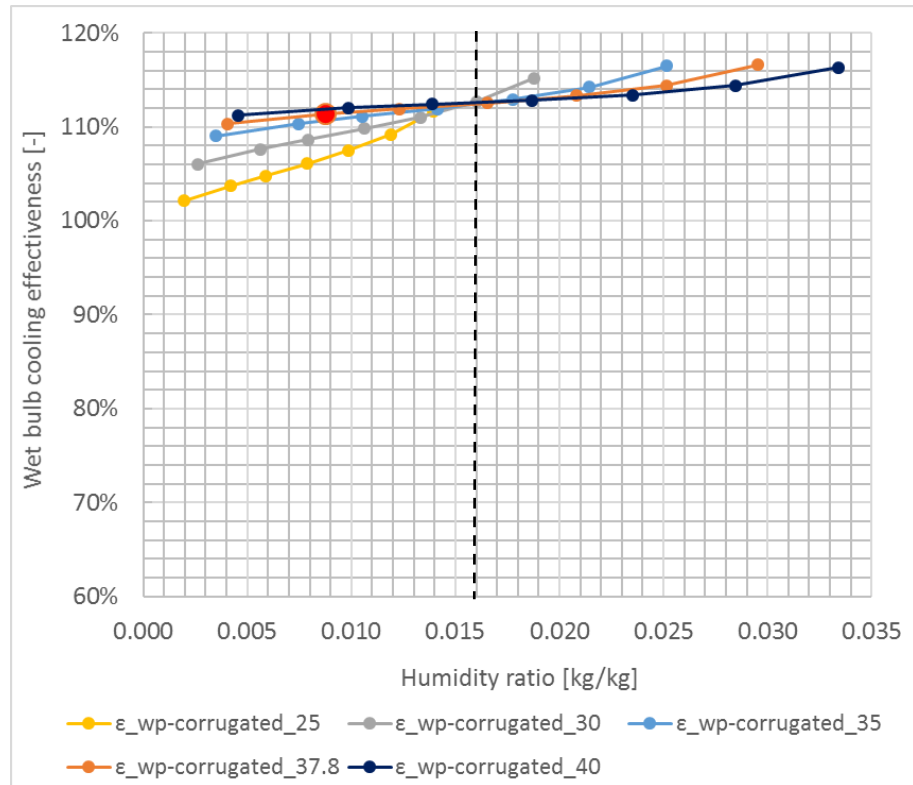


Fig. 3-14(f): Variation of WBE with HR at various IA temperature.

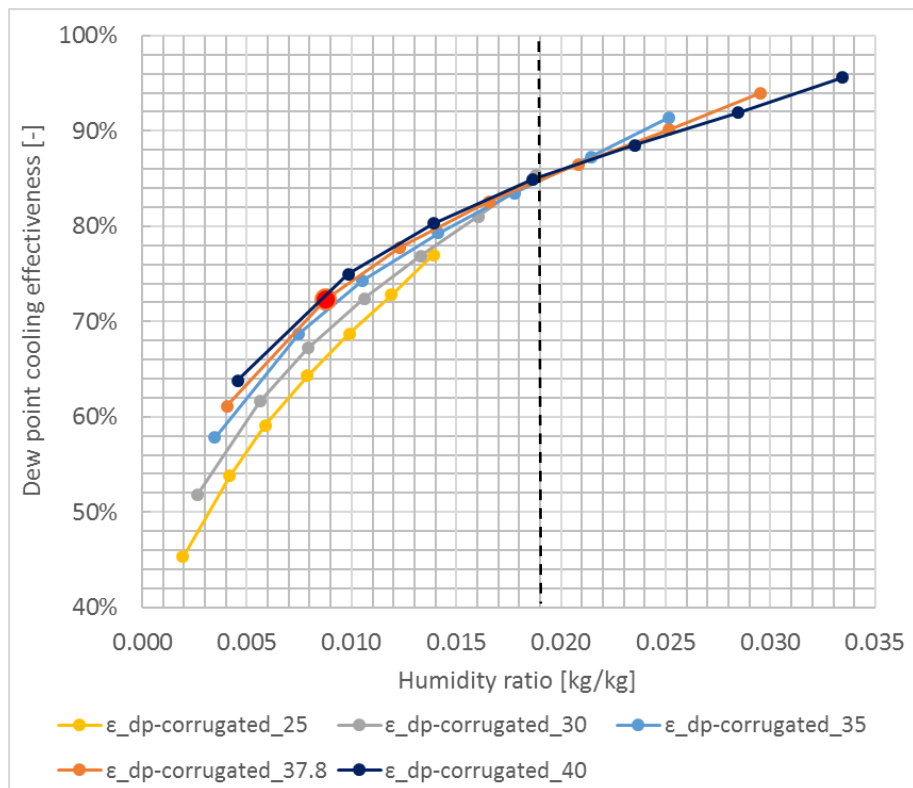


Fig. 3-14(g): Variation of DPE with HR at various IA temperature.

Fig. 3-14(f) and **Fig. 3-14(g)** show that with the increment of IA humidity ratio, the wet-bulb and dew-point cooling effectiveness both increase. At a certain humidity ratio, around 0.016 kg/kg for WBE in **Fig. 3-14(f)** and 0.019 kg/kg in **Fig. 3-14(g)** for DPE, the curves in a range of IA temperature converge at a certain point, i.e. reach a same WBE/ DPE value.

At least two interesting conclusions could be deduced. One clarifies a fact that the cooling effectiveness depends closely on the IA conditions besides the cooler performance. Furthermore, other than higher temperature and lower relative humidity, it is the IA state of lower temperature and higher relative humidity leads to a higher value of cooling effectiveness. For example, in **Fig. 3-14(g)** the IA conditions of 40°C & 40% RH and 30°C & 70% RH present the same DPE value of 87.5%. The other, based on the definition of cooling effectiveness (Eqs. [3-24] and [3-25]), for any IA temperature, the PA temperature and other relevant output parameters e.g. cooling capacity and cooling effectiveness at a specific common humidity ratio e.g. 0.019 kg/kg in **Fig. 3-14(g)**, could be reckoned owing to the simple one-to-one relation between dew-point temperature and humidity ratio. If it has been known for example that the PA temperature is 26.5°C under the conditions of IA temperature of 40°C, and dew-point temperature of 24°C corresponding to the humidity ratio of 0.019 kg/kg, the PA temperature at any IA temperature could be deduced according to the definition of dew-point cooling effectiveness as demonstrated in Eq. [3-26].

$$\frac{Tf_{in} - Tf_{PA}}{Tf_{in} - 24} = \varepsilon_{dp} = \frac{40 - 26.5}{40 - 24} = 0.84375 \quad [3-26]$$

Then the relationship between PA temperature and IA temperature at HR=0.019 kg/kg could be further deduced to a correlation [3-27].

$$Tf_{PA} = 0.16Tf_{in} + 20.25 \quad [3-27]$$

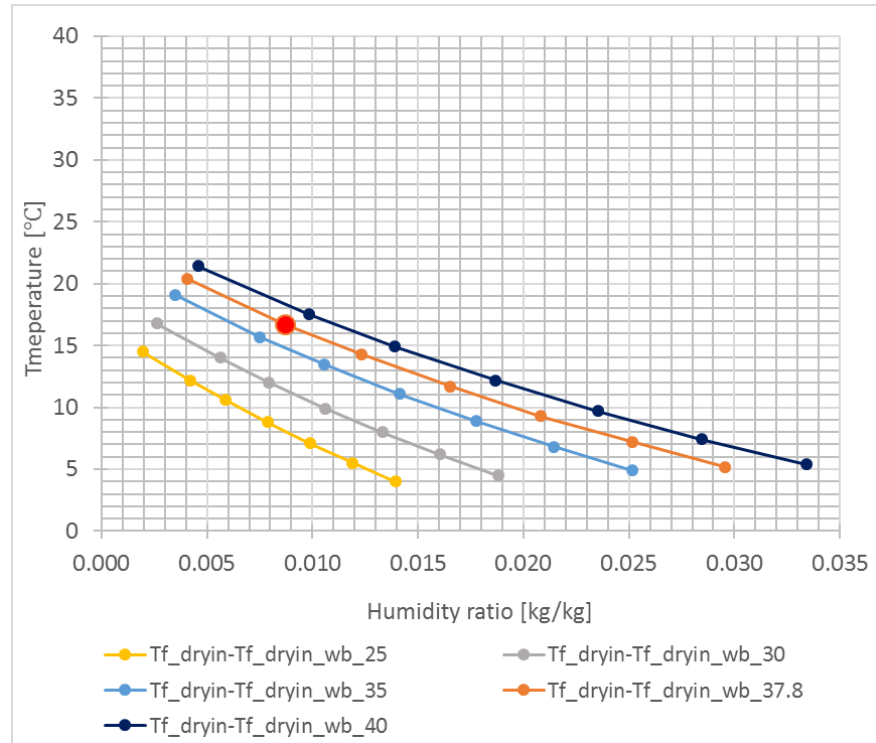


Fig. 3-14(h): Variation of wet-bulb depression with HR at various IA temperature.

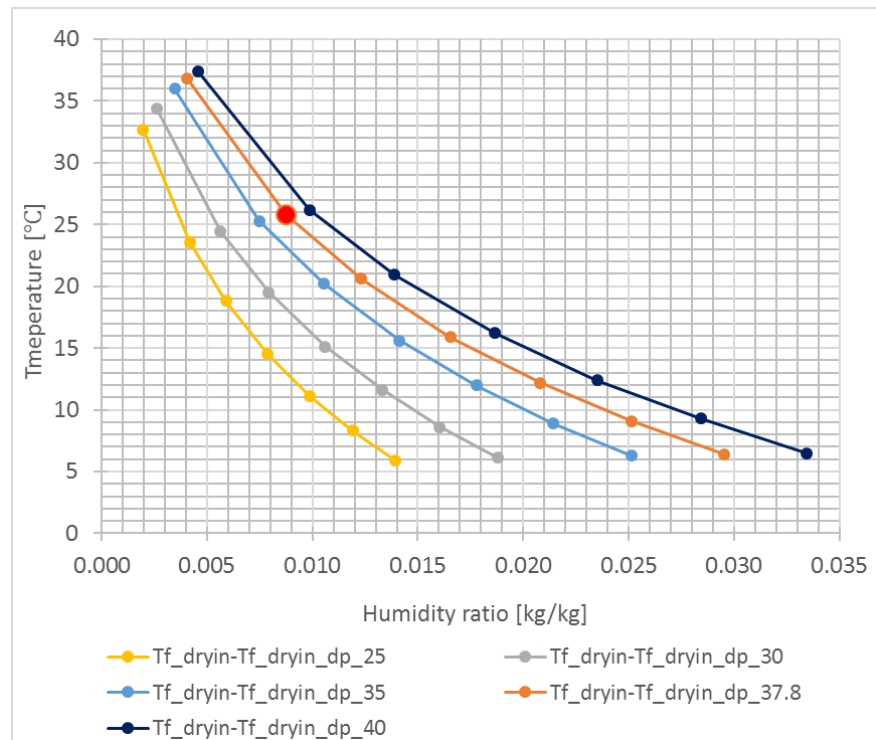


Fig. 3-14(i): Variation of dew-point depression with HR at various IA temperature.

Fig. 3-14(h) and **Fig. 3-14(i)** show the variation tendency of temperature depression, i.e. temperature difference between IA dry-bulb temperature and coincident wet-bulb or dew-point temperature, with the increase of humidity ratio. Attached respectively with curves of temperature drop, i.e. difference between IA temperature and PA temperature, **Fig. 3-14(j)** and **Fig. 3-14(k)** are generated.

Temperature depression is the denominator and temperature drop is the numerator to calculate the cooling effectiveness (Eqs. [3-24] and [3-25]). It is clear in **Fig. 3-14(k)**, with the increase of humidity ratio, the dew-point depression and temperature drop trend to uniformity. In other words, with the increment of humidity ratio, the DPE grows rapidly in low humidity ratio range and finally tends to be the extreme value of 100%. In short, high IA humidity ratio or relative humidity results in high dew-point cooling effectiveness (refer to **Fig. 3-14(g)**). By contrast, in **Fig. 3-14(j)**, the wet-bulb depression and temperature drop maintain a similar variation tendency. With the increase of humidity ratio and the simultaneous shrink of the wet-bulb depression and temperature drop, the wet-bulb cooling effectiveness keeps tenderly growing (refer to **Fig. 3-14(f)**).

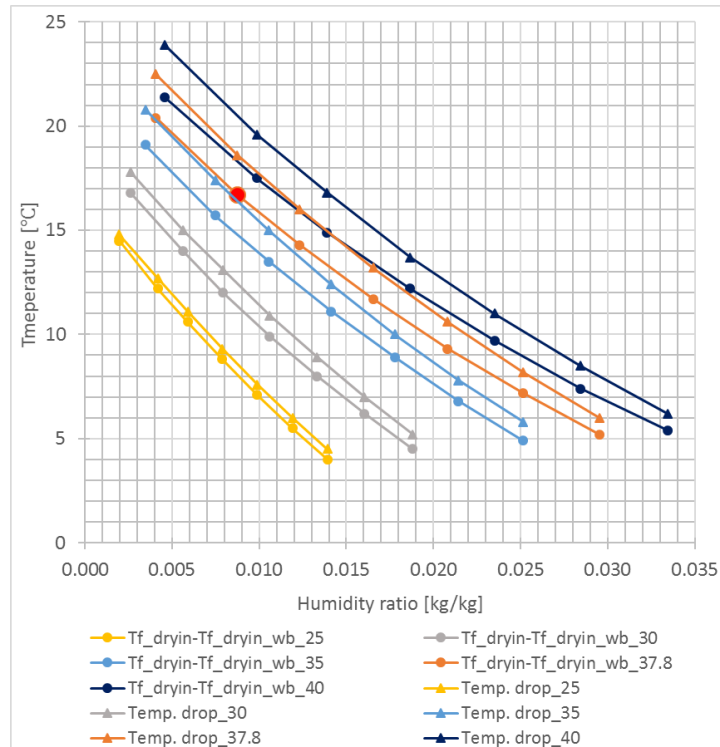


Fig. 3-14(j): Comparison of temperature drop and wet-bulb depression with HR at various IA temperature.

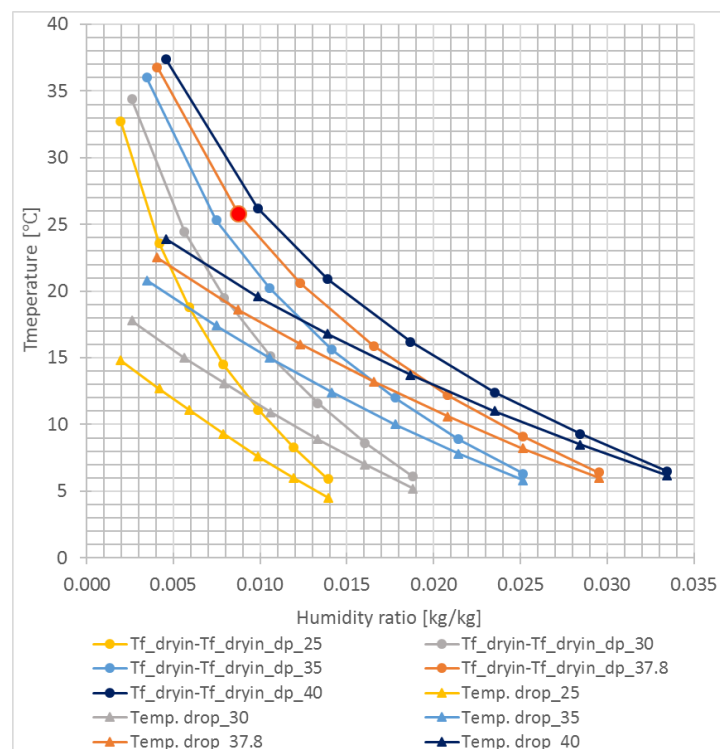


Fig. 3-14(k): Comparison of temperature drop and dew-point depression with HR at various IA temperature.

Fig. 3-15: Variation of cooling performance with HR at various IA temperature.

(3) Impact of the intake air velocity

The air velocity is a factor impacting the flow rate and flow pattern of the air within the channels: the former affects the cooling capacity directly and the latter affects the heat and mass transfer rate which consequently impacts the cooling capacity of the cooler. Furthermore, the airflow rate relates to the operation of the fans. Thus, the variation of air velocity affects the COP value. Impact of the air velocity on the performance of both the irregular and plane-plate HMXs was investigated and the difference between them was analysed. The results are shown in **Fig. 3-15(a)**, **(b)** and **(c)** respectively.

As shown in **Fig. 3-15(a)**, the PA flow rate increases from 188 m³/h to 1128 m³/h by a 500% promotion. At the meantime, cooling capacities of the both exchangers increase with the rise of air velocity, while the irregular type increases some faster than that of the plane-plate one. When the air velocity varies from 0.5 m/s to 3.0 m/s, the cooling capacity of the irregular exchanger varies from 1426 W to 5720 W, which are 2.1% and 14.1% higher than that of the plane-plate type respectively. Merely at the irregular type side, the cooling capacity boosts by 301% while PA flow rate improves by 500%. The reason exists in the decrease of the temperature drop.

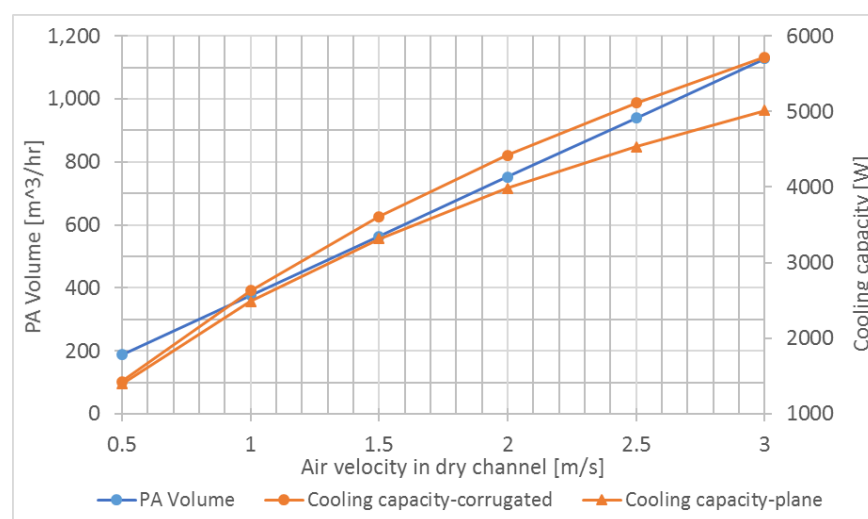


Fig. 3-15(a): Cooling capacity and product air flow rate.

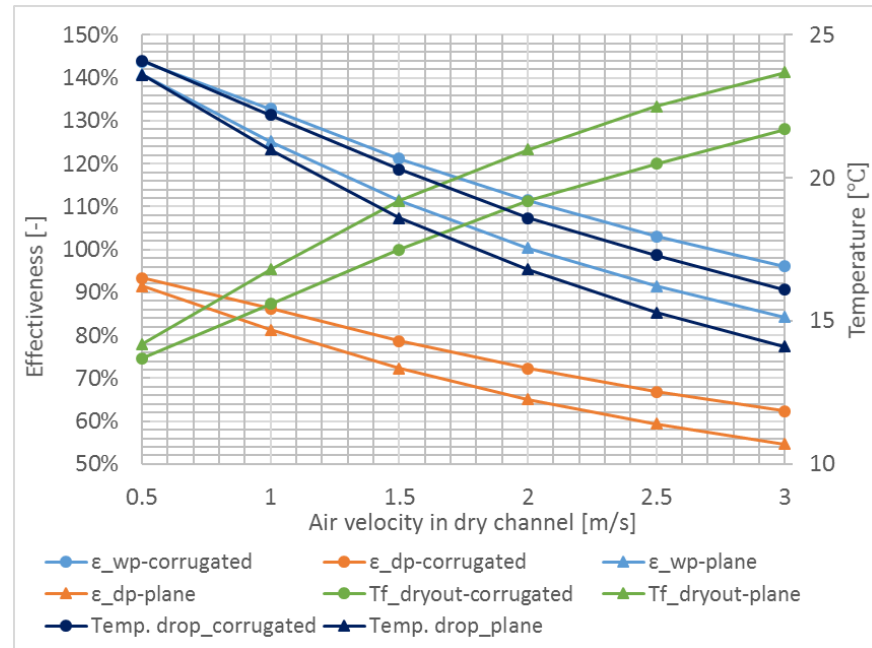


Fig. 3-15(b): Cooling effectiveness and product air temperature.

Fig. 3-15(b) shows the variation of temperature drop with the air velocity. Compared to plane-plate type, the temperature drop of the irregular one is less sensitive to the variation of air velocity. With a 500% lift of air velocity, i.e. from 0.5 m/s to 3.0 m/s, the temperature drop decreases from 24.1°C to 16.1°C by 33.2%. By contrast, the curves of PA temperature for both types show that the impact of air velocity on PA temperature is greater for plane-plate type than for the irregular one. In other words, it implies that comparing to the common plane-plate type exchangers, for the proposed irregular one, it is more feasible to boost cooling capacity by improving airflow rate in practice.

Fig. 3-15(b) also presents the variation of cooling effectiveness, which has been discussed in the above section on the HR impact. From the view of the operational condition, cooling effectiveness weakens with the increase of air velocity owing to the less growth rate of water evaporation. It is different from the impact of humidity ratio, the variation of WBE is more obvious than DPE with the increase of air velocity.

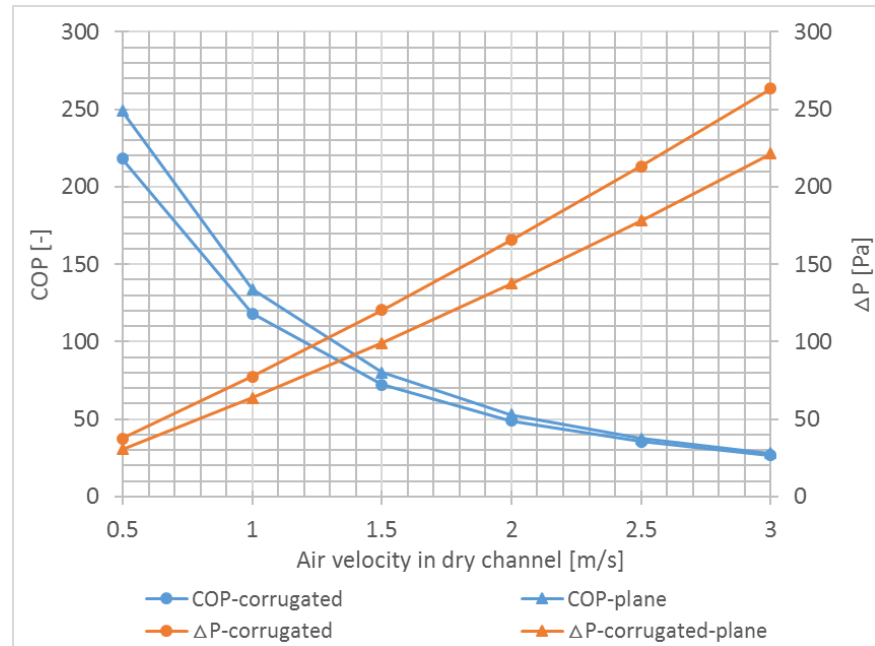


Fig. 3-15(c): Pressure drop and COP.

Fig. 3-16: Performance variation with the air velocity.

Fig. 3-15(c) demonstrates the increase of the total pressure drop with the air velocity. Generally, power consumption by fans is much greater than that by water pump. The pressure drop which associates closely with the fan power consumption influences the COP value greatly. It could be seen at lower air velocity the COP value could be very high owing to the extremely low power consumption by the fans. With the increase of air velocity, the power consumption rises sharply, which results in a rapid decrease of COP value. When the velocity is beyond 2 m/s, the variation of COP slows down since the working conditions of the fans come into relatively steady states. It should be noted that the actual working conditions and power consumption relate to the layout of the fans as well as their performance characteristics. Thus, the curves of COP value are for reference only.

3.8.2 Impact of the channel dimensions

The dimensions of the computational channel, i.e. channel interval and length, may affect both the flow rate and flow pattern, which in turn influence the heat

and mass transfer rate and cooling capacity of the heat and mass exchangers. The form of the corrugated exchanging sheet, i.e. the wave shape and length, relates to the evaporating area and may affect the effective channel length performing water evaporation. The ratio of wave length over channel interval on cross section determines the equivalent diameter, which affects the geometric similarity between the bench computational channel and an objective channel in practice, and accordingly affects the judge on flow pattern and the intensity of heat and mass exchange.

Based on the exchanger stack of 1m (Height)×1 m (Width)×0.348 m (Thickness) and under conditions of IA temperature of 37.8°C, wet-bulb temperature of 21.1%, air velocity in dry channel of 2 m/s and working air ratio of 0.4, impacts of the channel interval, channel length, wave length and equivalent diameter on the performance of the both exchangers were investigated and the difference in cooling performance between the two exchangers was analysed.

(1) Impact of the channel interval

Fig. 3-16(a) shows with the increment of channel interval, the PA temperature rises and the temperature drop decreases greatly. The reason exists in the fact that the airflow rate increases with the channel interval at a fixed velocity. Without corresponding changes in heat and mass exchanging capacity, the cooling effect certainly decreases. However, in **Fig. 3-16(b)**, it presents an increase of the cooling capacity due to the augment of airflow rate and the fact that more air dilutes the partial vapor pressure in wet channel which leads to more water evaporation.

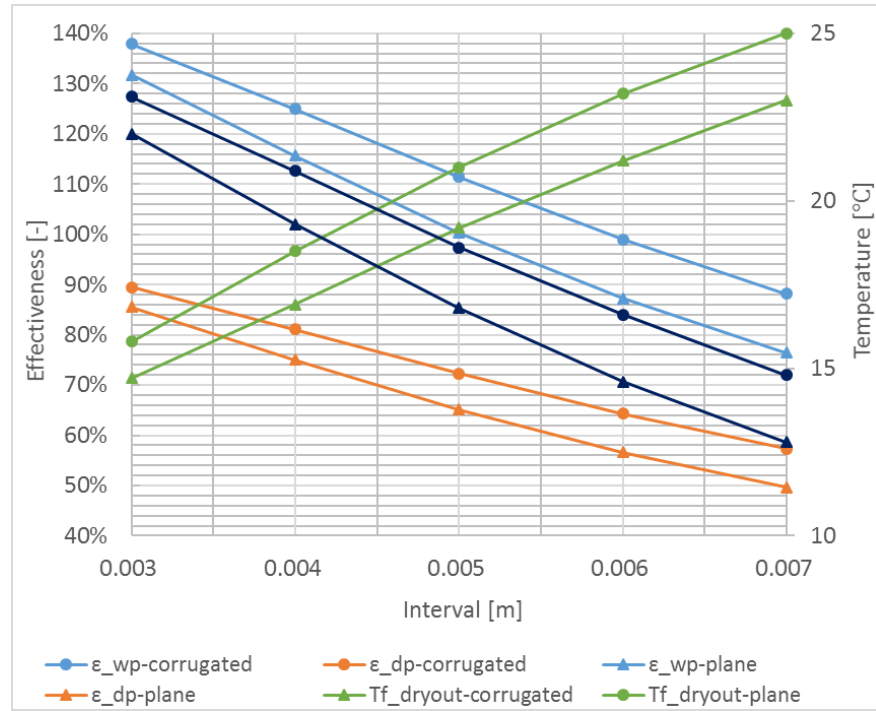


Fig. 3-16(a): Cooling effectiveness and product air temperature.

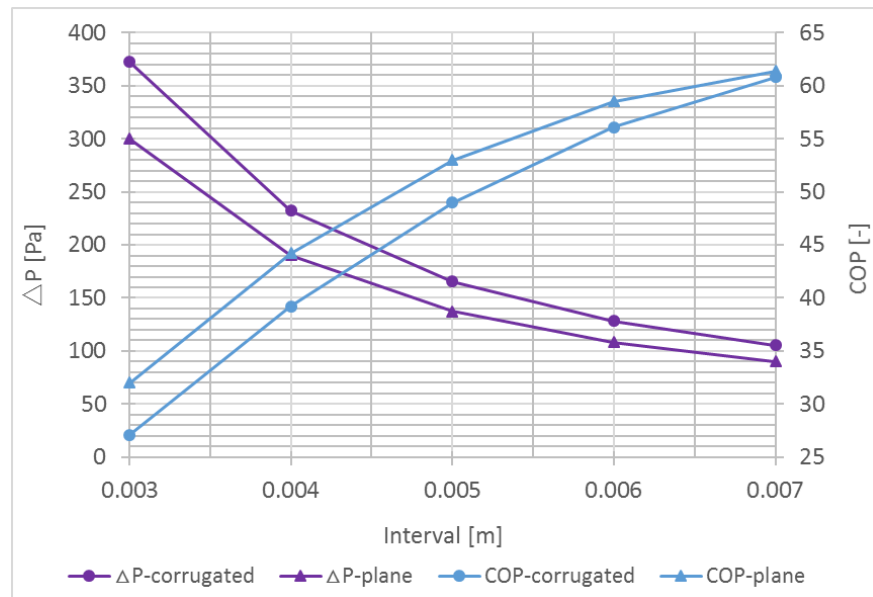


Fig. 3-16(b): Pressure drop and COP.

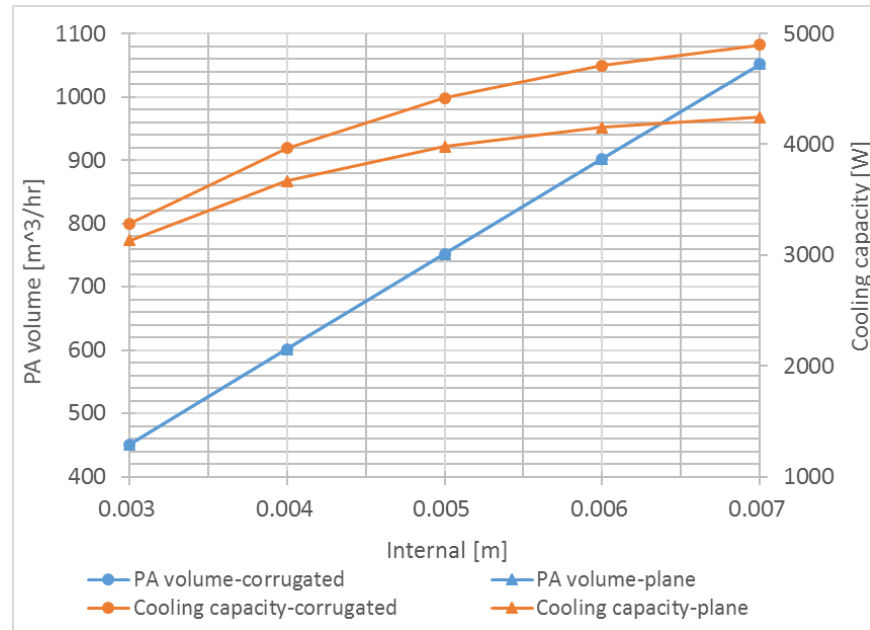


Fig. 3-16(c): Cooling capacity and product air flow rate.

Fig. 3-17: Variation of performance with the channel height.

Another benefit brought by the increase of channel interval is the reduction of flow resistance as shown in **Fig. 3-16(b)** and accordingly the increase of COP value.

In terms of cooling effectiveness, the WBE and DPE both decrease with the augment of channel interval due to the worse cooling performance relating to per unit volume air.

(2) Impact of the channel length

Longer channel length means more sufficient heat and mass exchange. However, the power consumption by fans increases as well to overcome the flow resistance of the air travelling through the channels.

Fig. 3-17(a) shows the variation of cooling effectiveness and PA temperature versus the channel length. It could be seen that the rise tendency of temperature drop slows down with the increase of the channel length. The variation of wet-bulb effectiveness is more than relevant dew-point effectiveness.

Fig. 3-17(b) presents the variation trends of cooling capacity and COP versus the channel length, indicating that cooling capacity increases due to the more heat and mass exchange and the COP decreases when increasing the channel length owing to the increase of airflow resistance as shown in **Fig. 3-17(c)**.

The variation tendency of either temperature drop, cooling capacity or cooling effectiveness suggests that a certain channel length should be guaranteed because it has an essential influence within a certain range. Since the cooling effectiveness reflects the saturated state of wet air, i.e. the completeness of water evaporation in wet channel, **Fig. 3-17(a)** implies the channel length of 1.2 m might be a practical choice considering the increase of material cost and fan power consumption.

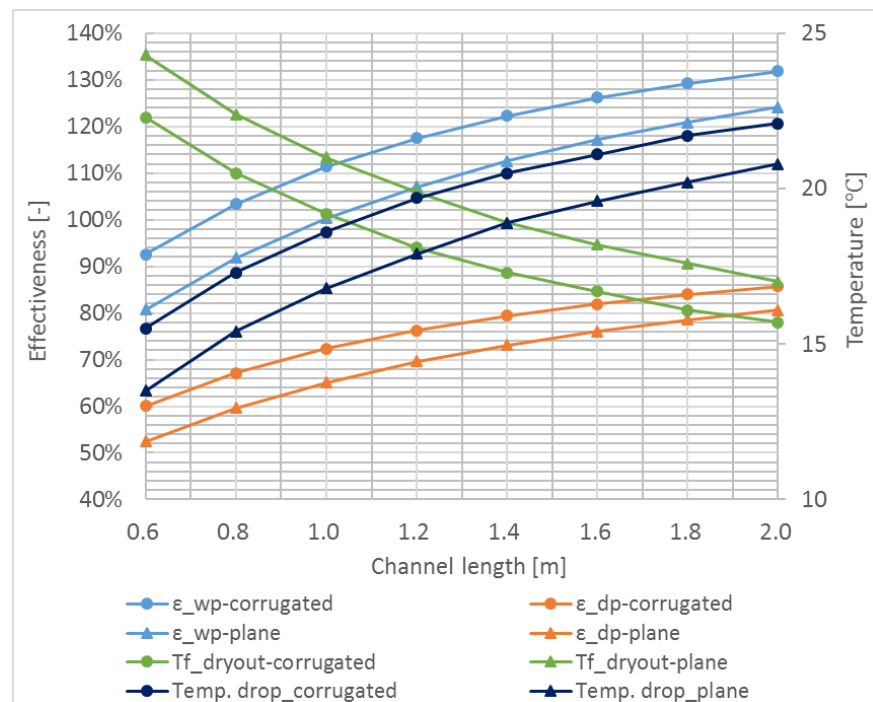


Fig. 3-17(a): Cooling effectiveness and PA temperature.

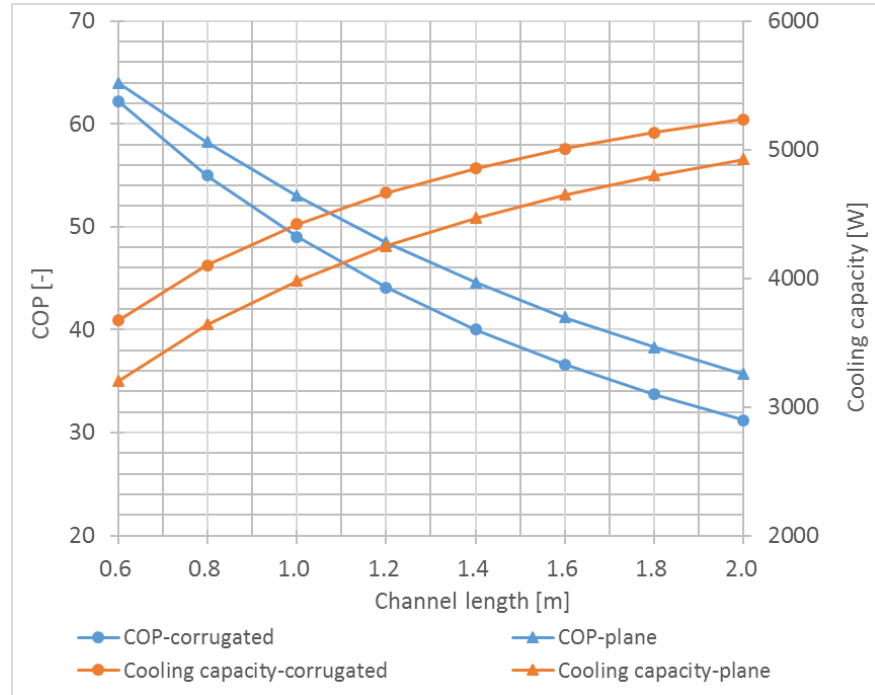


Fig. 3-17(b): Cooling capacity and COP.

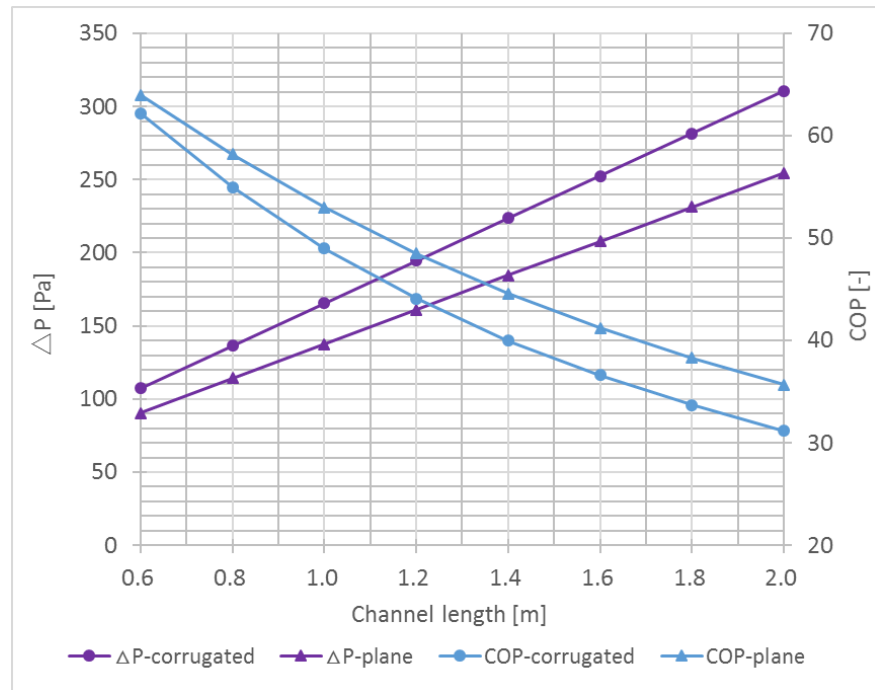


Fig. 3-17(c): Pressure drop and COP.

Fig. 3-18: Variation of performance with the channel length.

(3) Impact of the wave length

The longer the wave length of the corrugated sheet (refer to **Fig. 3-6**), the more exchanging area. However, in practice, the feasibility of shape formation is a problem to be considered for material selection. Therefore, it is necessary to investigate the impact of the wave form. For convenience, a ratio of wave length over the relevant chord is defined as the base for comparison.

It can be seen in **Fig. 3-18(a)**, with the expansion of effective area for heat and mass exchange, i.e. the value of ‘wave/chord’, the PA temperature sharply decreases and the temperature drop and cooling effectiveness increase accordingly. Since the state of intake air keeps constant, the wet-bulb and dew-point cooling effectiveness has the same growth rate with the temperature drop. With doubled exchanging area, the temperature drop as well as cooling effectiveness and cooling capacity (shown in **Fig. 3-18(a)** and **(b)**) realize a promotion of 39%. Nevertheless, the airflow resistance nearly doubles with the doubled surface and COP falls finally by 5.3%, as shown in **Fig. 3-18(c)**.

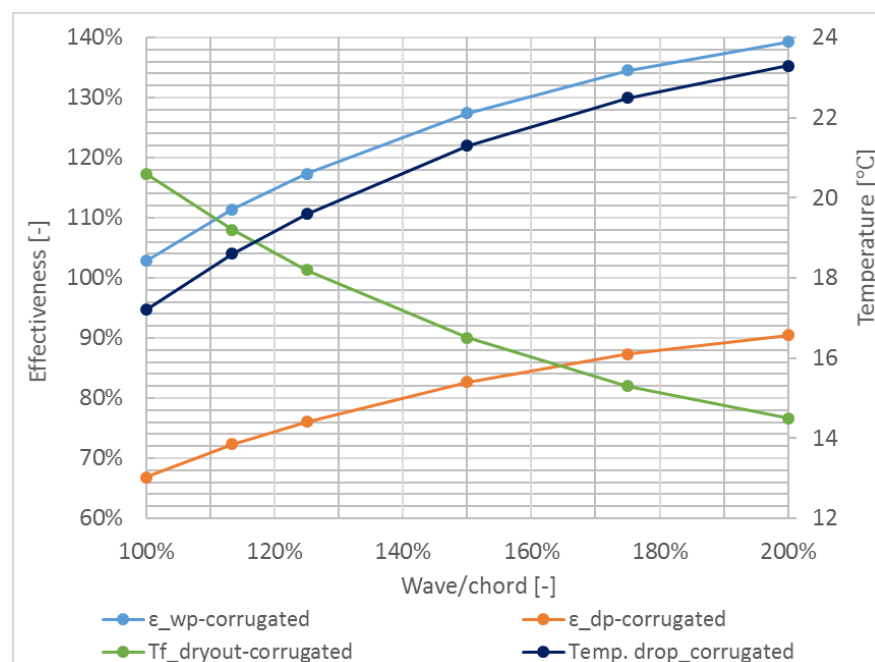


Fig. 3-18(a): Cooling effectiveness and product air temperature.

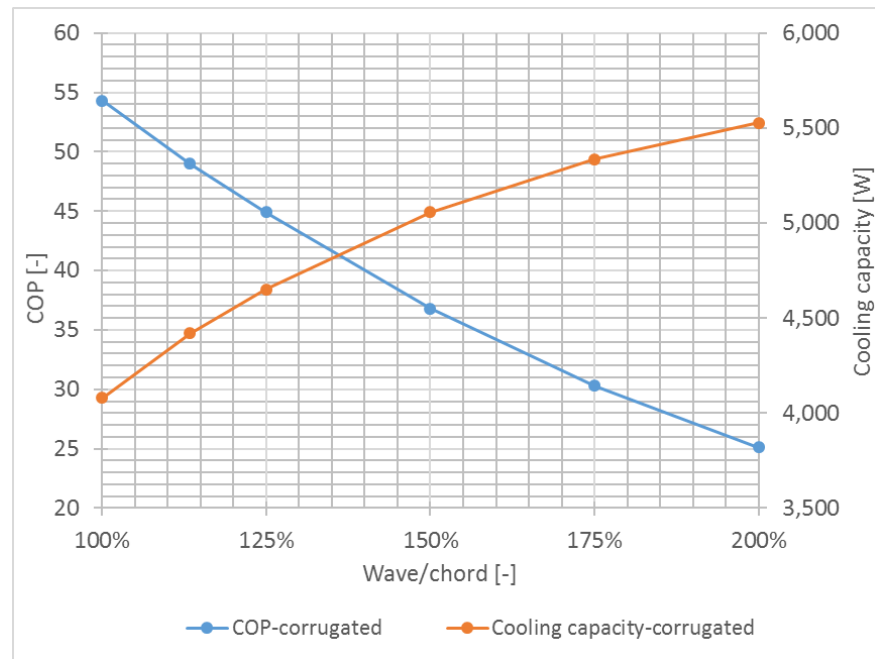


Fig. 3-18(b): Cooling capacity and COP.

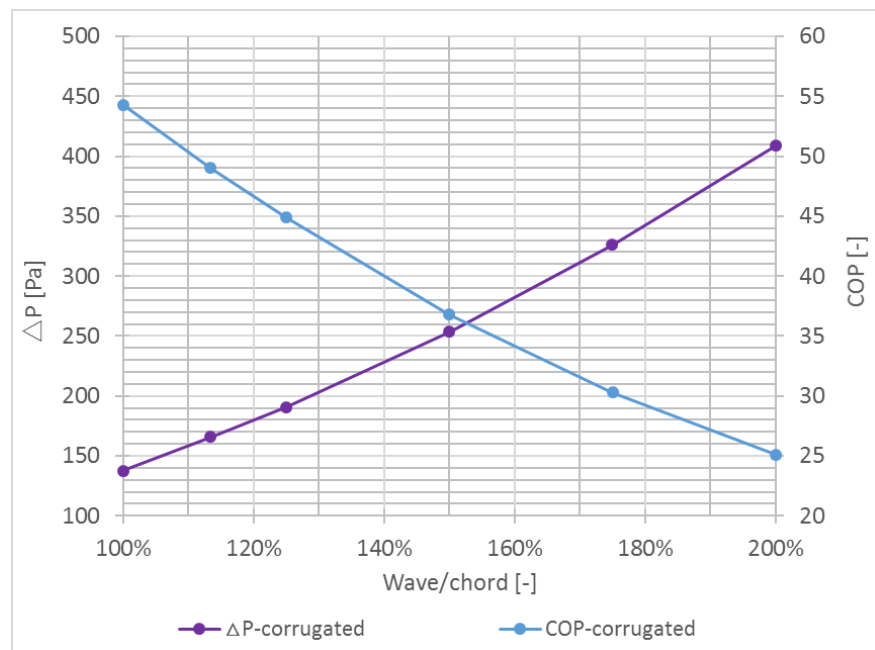


Fig. 3-18(c): Pressure drop and COP.

Fig. 3-19: Variation of performance with the wave form.

(4) Impact of the equivalent diameter

Keeping the channel interval and the corrugation shape constant, the equivalent diameter used for the calculation of flow parameters like Reynolds number varies with the span of the corrugated shape. This section talks about the impact of the selection of computational channel width. Firstly, a basic wave element is defined with a bench chord (i.e. chord0) of 11.6 mm and wave length of 13.2 m (refer to **Fig. 3-10**). The cooling performance will be discussed as per the selection of the computational channel width, i.e. multiple of the chord0. The equivalent diameters of the computational channels differ with the various channel width, i.e. the ratio of “*chord/chord0*”.

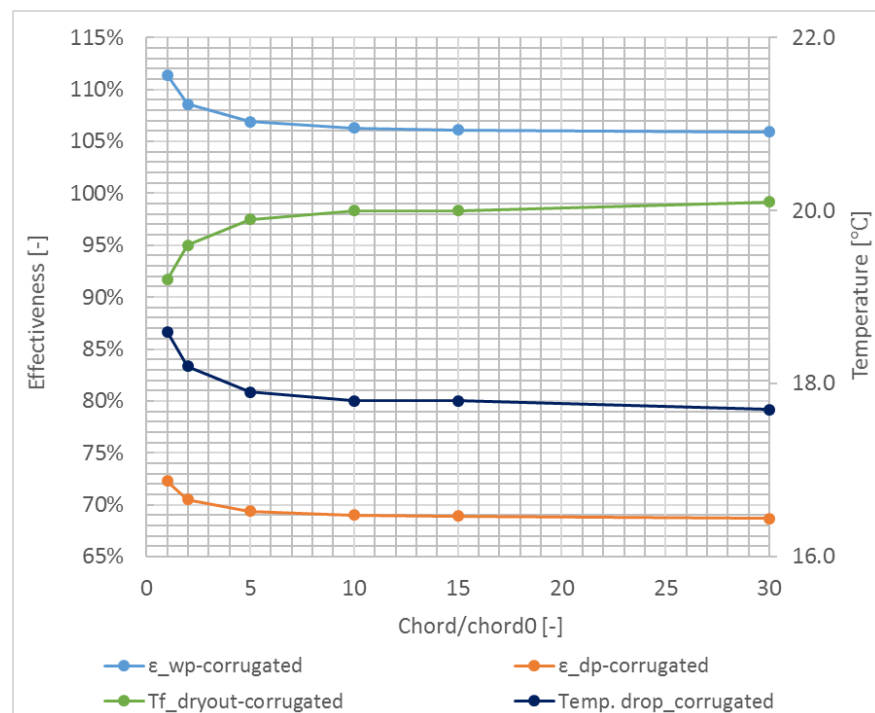


Fig. 3-19(a): Cooling effectiveness and product air temperature.

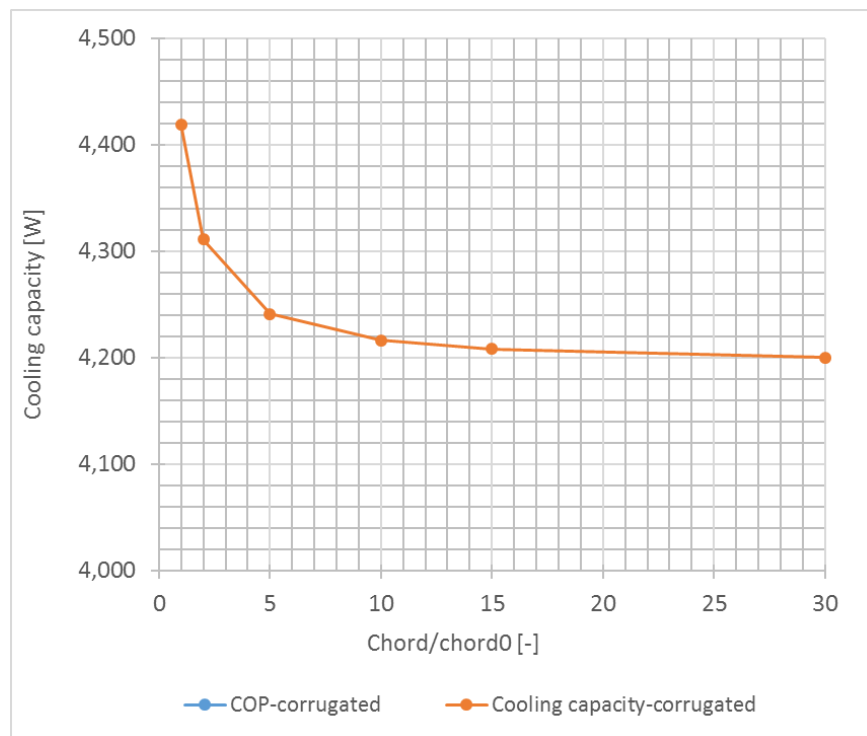


Fig. 3-19(b): Cooling capacity.

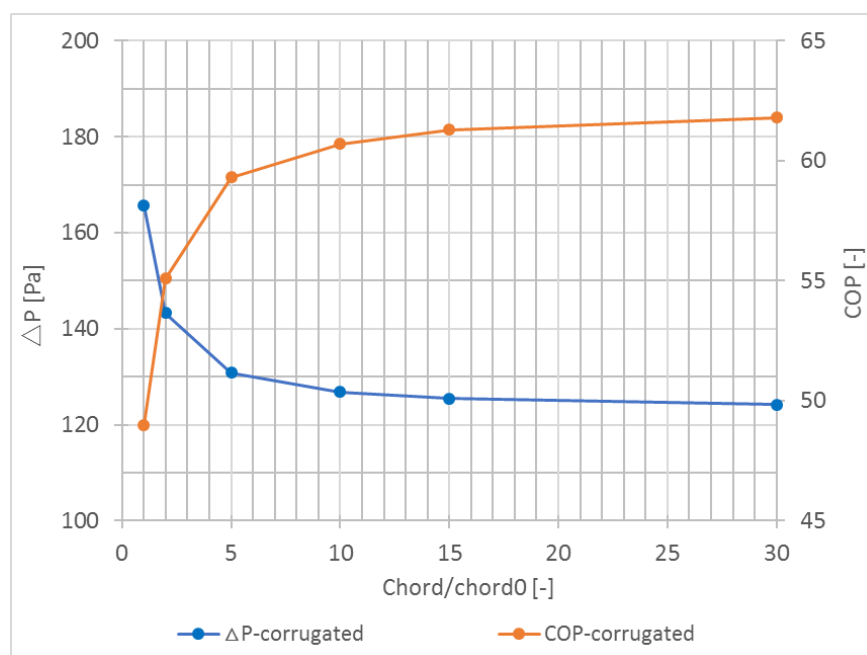


Fig. 3-19(c): Pressure drop and COP.

Fig. 3-20: Variation of performance with the equivalent diameter.

Fig. 3-19(a) shows that the results of PA temperature as well as cooling effectiveness is greatly influenced by the selection of the computational channel width in small scale. When the computational channel width enlarges to over 10 times of the bench chord, i.e. 0.16 m, the simulation results differ little. In terms of cooling capacity, COP and pressure drop, the more reliable *chord/chord0* ratio points to 15, i.e. 0.174 m.

Therefore, it could be concluded that for computer simulation, the minimum computational channel width should be bigger than 0.174 m and the computational channel with 15 waves and the chord of 0.174 m could be a basic element to be employed to conduct reliable simulation for larger scale application.

3.8.3 Impact of the operational parameters

(1) *Impact of the working-to-intake air ratio*

Working-to-intake air ratio is defined as the ratio of working airflow rate in the wet channel to the total intake airflow rate, which is the sum of the working air and product air. Higher working air ratio could enhance the water evaporation in the wet channels, thus enhancing the cooling effectiveness of the heat and mass exchanger. However, this may also lead to the reduced PA flow rate and thus reduce cooling capacity. Therefore, an optimum working air ratio should be in existence to achieve the best balance between the cooling output and cooling efficiency. A dedicated investigation was carried out to optimize the working air ratio and the results are shown in **Fig. 3-20(a), (b) and (c)**.

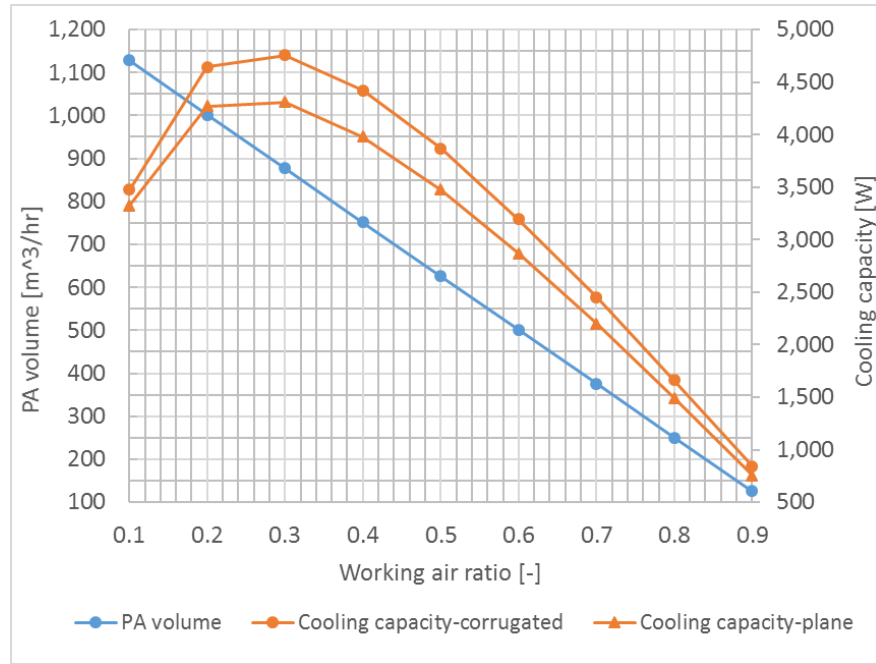


Fig. 3-20(a): Cooling capacity and COP.

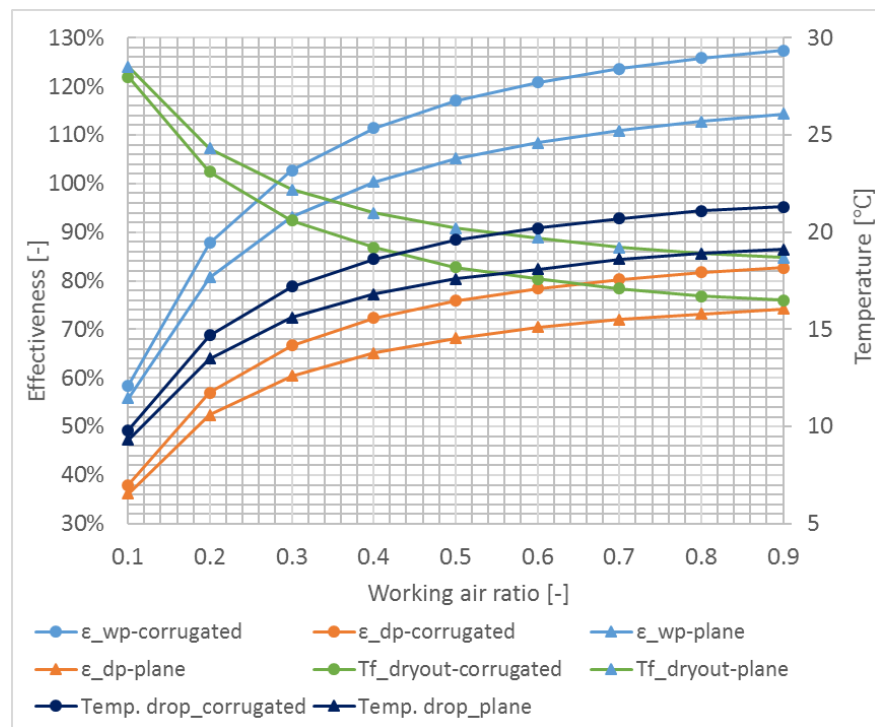


Fig. 3-20(b): Cooling effectiveness and PA temperature.

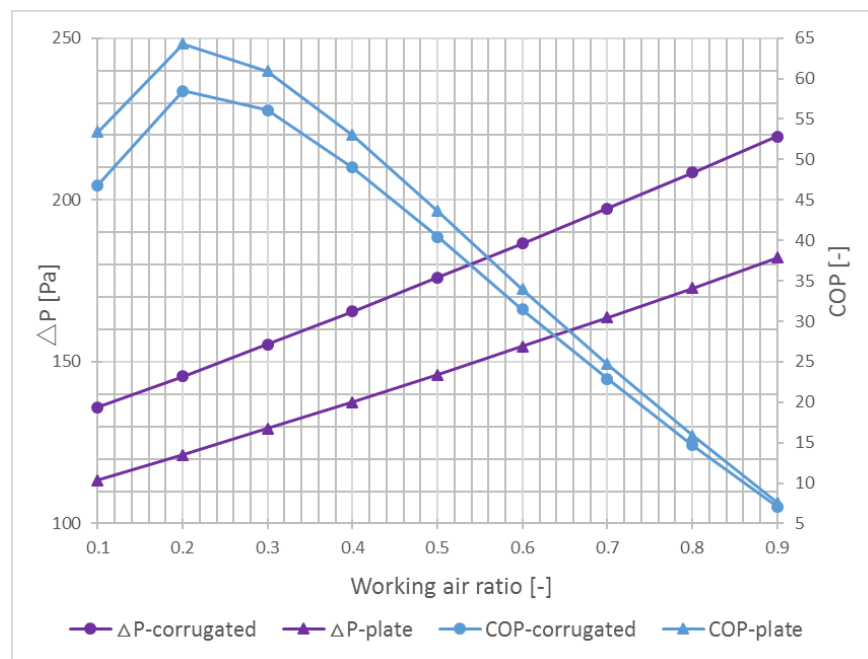


Fig. 3-20(c): Pressure drop and COP.

Fig. 3-21: Variation of performance with working air ratio.

It is found that the performance of both the irregular and plane-plate HMXs shows similar variation trend when the working air ratio varies. For the both exchangers, **Fig. 3-20(a)** shows that the highest cooling capacities appear at the working air ratio of 0.3. **Fig. 3-20(b)** indicates that the air temperature drop as well as cooling effectiveness rises with the increase of the working air ratio; while the PA temperature shows an opposite trend of the variation. However, these variations gradually slow down with the increase of the working air ratio.

As shown in **Fig. 3-20(a)**, with the increase of working air ratio, the PA flow rate keeps reducing. The fact that the cooling capacity could keep growing when working air ratio less than 0.3 implies that the effect of temperature drop is prior to the shrink of PA volume. **Fig. 3-20(c)** shows that the air pressure drop through the channel increases linearly with the rise of the working air ratio and the biggest COP value appears at working air ratio of around 0.2. Based on these findings, it is concluded that the optimum working air ratio would be around 0.3.

(2) Impact of the water temperature

During operation, water is circulated from a water container fitted beneath the wet channel outlet to the top of the wet channel by a pump. The water evaporates along the wet channel and excess water falls downward to the water container. The temperature of the inlet water is therefore determined by the temperature and amount of the water falling into the container and the feeding water from the main supply. The modelling work was carried out to investigate the effect of the inlet water temperature on the performance of the two types HMXs.

As per the proposed scheme of water supply, the water flow rate is set constant at 18 L/hr. With fixed temperatures of inlet water at various level from 10°C to 35°C, **Fig. 3-21(a)** shows the variation of the COP and cooling capacity and **Fig. 3-21(b)** shows the variation of cooling effectiveness and PA temperature. The flat curves indicate the effect of the circulating water temperature on the cooling performance of the HMXs is minor. **Fig. 3-21(c)** shows the outlet water temperature maintains at about 29°C despite of the various inlet water temperatures. It manifests again the minor impact of the inlet water temperature at such flow rate.

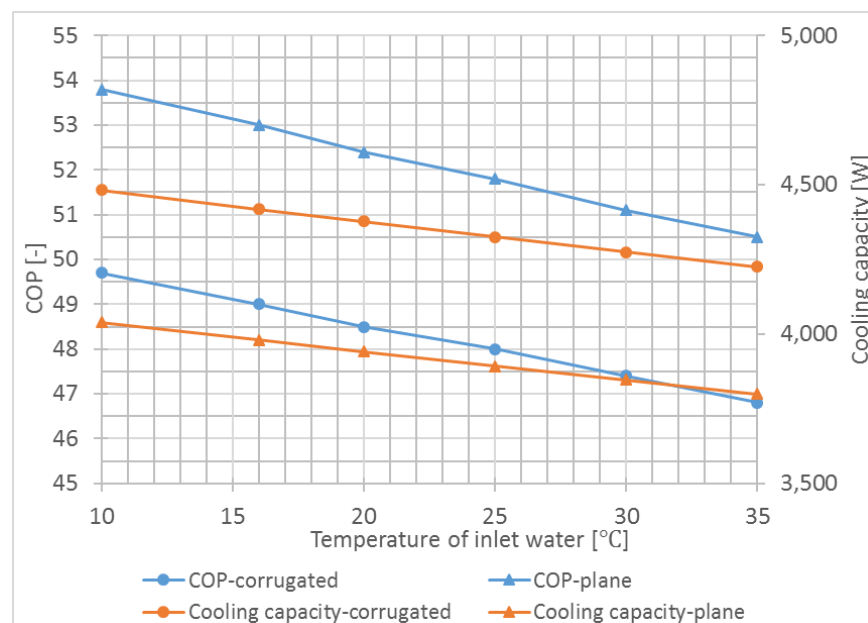


Fig. 3-21(a): Cooling capacity and COP.

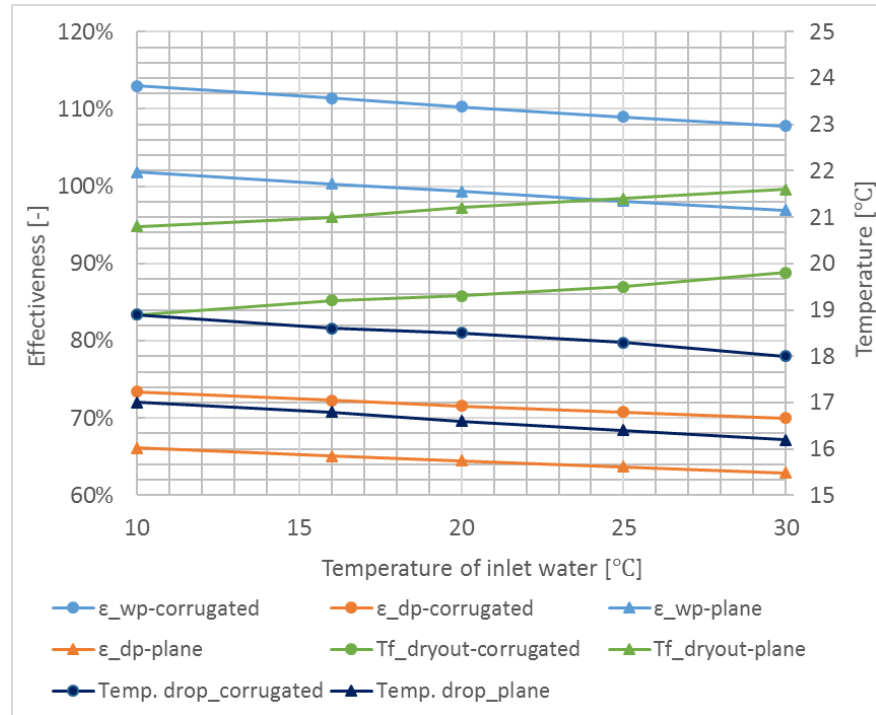


Fig. 3-21(b): Cooling effectiveness and PA temperature.

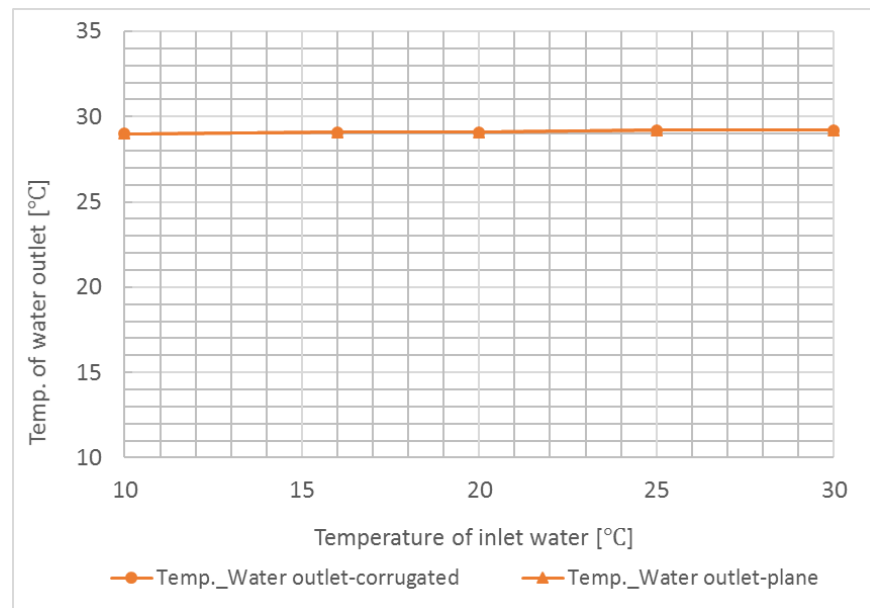


Fig. 3-21(c): Outlet water Temperature.

Fig. 3-22: Variation of performance with the temperature of inlet water.

(3) Impact of the effective evaporating area

Most of the existing common evaporative coolers fail in full wetting of the evaporating surface, thus leading to large volume of noneffective circulating water to make up. On contrary, the proposed application of fibrous fabric and the corrugated sheets are able to enlarge the acting area of water evaporation. It is necessary to clarify the impact of the effective evaporating area on the cooling performance.

Various factors from 0.1 to 10 is multiplied to the area performing water evaporation in the simulation routines and the results are shown in **Fig. 3-22**.

Fig. 3-22(a) and **(b)** both show that the effective evaporating area or the wet surface wettability is essential especially within the range of the pure smooth exchanging sheet surface. It also implies the importance of the wettability of the wet surface. For example, the cooling capacity improves by 13% (from 3832 W to 4330 W) with the increase of wettability coefficient from 0.3 to 1.0. If the effective evaporating area could enlarge by 3 times e.g. by means of porous surface, the cooling capacity (**Fig. 3-22(b)**) would increase by 4.2% (from 4330 W to 4514 W). Further improvement of the evaporating area contributes very tiny to the cooling performance under the set conditions. Nevertheless, more evaporating area definitely benefits to rationally reducing the channel length.

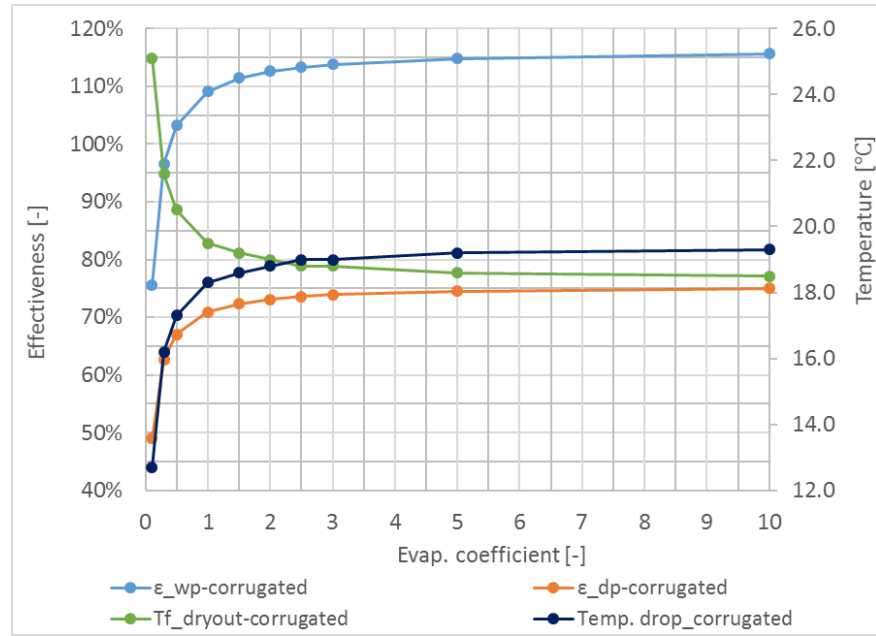


Fig. 3-22(a): Cooling effectiveness and product air temperature.

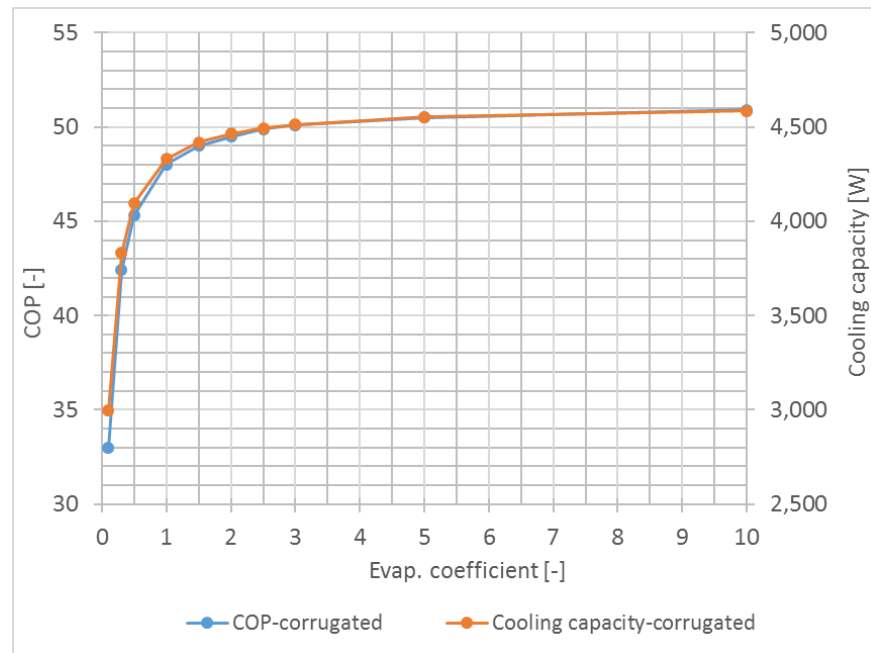


Fig. 3-22(b): Cooling capacity and COP.

Fig. 3-23: Variation of performance with the temperature of inlet water.

3.9 Chapter Summary

This chapter introduced the working principle of the system and identified its main components, i.e. heat and mass exchanger (HMX), water distributor, fans, pump and water sink. The distinct features of the proposed dew point cooler lie in: (1) the original irregular heat exchanging sheet with corrugation in an aluminium unibody structure; (2) the unique airflow organization among the stacked exchanging sheets; (3) the application of moisture-wicking and quick-drying fabric as the wet surface of the heat and mass exchanging sheet; (4) a patented water distributor to distribute water evenly and efficiently onto the fabric media; (5) the controlled intermittent water supply scheme.

Theoretical analysis of the heat and mass transfer in the HMX was performed and dedicated simulation routines were developed, see [Appendix 2], to predict the performance of the proposed dew point cooler. The computer simulation tool was validated with the published experimental and numerical results under the extremely identical boundary and initial conditions and the results met with high accuracy under the intake air temperature in range of 25°C-45°C and humidity ratio of 6.9-26.4 g/kg. More than cooling parameters for common plane-plate HMX in other published papers, the established simulation tool also aimed to rationally predict the cooling performance of the whole cooler, e.g. COP, for both common and the proposed irregular HMX, which will be further double validated by the following experimental research.

The dynamic process of heat and mass exchange in the HMX was investigated with the established simulation model and well proved by the theoretical analysis.

Performance study of the proposed irregular HMX was then carried out with the validated numerical model to further explore for assisting the prototype design. The impacts of intake air parameters, channel dimensions and operational

parameters were studied in detail to offer useful information for the following experiment and application research. The main conclusions from the parametric research list as follow.

(1) Cooling capacity increases substantially with the IA temperature, i.e. the higher the outdoor temperature, the better the cooling performance. For the proposed dew point cooler, in the IA temperature range of 25°C-40°C, the variation of PA temperature could be controlled within 3.1°C, i.e. 16.4°C-19.5°C based on equal airflow rate.

(2) Higher air velocity helps to improve the cooling capacity whilst it is detrimental to the COP. By comparison, it implies more feasible for the proposed irregular HMX to boost cooling capacity by increasing airflow rate in practice. A balanced air velocity is suggested at around 2 m/s.

(3) Humidity ratio impacts the cooling performance greatly. Other than the other performance indicative parameters, e.g. cooling capacity and COP, the cooling effectiveness depends closely on the IA conditions besides the cooler performance. Lower temperature and higher humidity ratio means worse cooling effect, but leads to a higher value of cooling effectiveness.

(4) Undersized channel interval results in small airflow rate, cooling capacity and large flow resistance, power consumption. Oversized channel interval leads to worse cooling effect, i.e. higher PA temperature, and bulky profile. The selection in the proposed range of 5-7 mm may depend on which leads, design or performance.

(5) Longer channel length means more heat and mass exchange but the consequent augment of flow resistance and power consumption. Increase of material cost should also be considered during the trade-off of channel length.

(6) In terms of corrugation form, longer wave length based on certain chord means more shape deformation besides more effective exchanging area. Mechanical behaviour of materials in exchanging sheet forming plays essential role. For the wave length from theoretical view, the longer, the better.

(7) In numerical modelling, geometric similarity for the computational element is as important as initial and boundary conditions. In this case, 15 times of the bench chord for the establishment of computational element could be considered reliable to keep the geometric similarity with the real entity.

(8) Working air ratio is an essential parameter in operation and prototype design and 0.3 could be a valuable reference for the balance between cooling capacity and power consumption.

(9) The impact of inlet water temperature on latent cooling may be negligible for controlled water volume. Large quantity of water flow may result in sensible cooling more than evaporative cooling.

(10) Porous surface and excellent wettability could help water evaporation and reduce the channel length.

The findings in this part of theoretical and numerical study will be employed to help determine the specific parameters in prototype design and manufacture in **Chapter 4**. Also, the adaptive improvements as per the experimental prototype will be made and validated with the following experiment results and finally applied in a case study in **Chapter 7**.

CHAPTER 4: PROTOTYPE DESIGN AND CONSTRUCTION

4.1 Chapter Introduction

Based on the established conceptual design and simulation investigation, this chapter reports the manufacturing process of a 4-kW rated prototype to realize all the set objectives. As a core component, the material selection and trial in fabrication process of the HMX constitute a major part of the entire manufacturing process of the cooler prototype. Other than the fans, pump and control components which are commercial products, the HMX and water distributor are innovative and original. The concept realization needs repeated careful tests from material selection to process trial. The major works completed in this chapter are presented as follows.

- (1) Detailed design of the proposed DPC prototype.
- (2) Performance test and selection of the HMX material, such as the proper aluminium plate meeting the requirement of mechanical process, fibrous material for evaporation medium on the wet surface and suitable adhesive to form the sandwich structure of the exchanging sheet.
- (3) Manufacturing process of the HMX.
- (4) Assembly of the cooler prototype.

4.2 Design of the Heat and Mass eXchanger (HMX)

The exchanger, which is stacked by a certain amount of irregularly shaped exchanging sheets to form dry and wet channels alternatively, is the core component of the cooler to perform water evaporation and heat and mass transfer. The expected performance of the novel dew point cooler (DPC) is above all guaranteed by reliable system and components design. To demonstrate its

advantage in performance, the well-known commercial product of *Coolerado*® M30 with patented and multi-award winning HMX was selected as a comparable rival in design and experiment stages.

4.2.1 Design Conditions

The proposed DPC aims to offer 4-kW cooling capacity under the identical test conditions with *Coolerado*® M30, i.e. basically the intake air at $T_{db}=37.8^{\circ}\text{C}$ and $T_{wb}=21.1^{\circ}\text{C}$ with supply airflow of $750\text{ m}^3/\text{h}$.

The achievement of cooling capacity is basically guaranteed by sufficient water evaporation and efficient heat transfer, e.g. the adequate area of heat and transfer. The total heat and mass transfer area comes from the stack of amounts of exchanging sheets. Compactness in configuration requires a high efficiency HMX design.

For indirect evaporative air coolers, the cooling output comes totally from the sensible air temperature drop. Therefore, the PA dry-bulb temperature can be deduced by the energy equation [4-1].

$$Q = c \cdot \rho_a \cdot V \cdot (T_1 - T_2) \quad [4-1]$$

Where,

Q - Cooling power, here 4 kW;

c - Specific heat of the air, $1.016\text{ kJ}/(\text{kg}\cdot^{\circ}\text{C})$;

ρ_a - Air density, $1.17\text{ kg}/\text{m}^3$;

V - Product air flow rate, $750\text{ m}^3/\text{h}$;

T_1 - Temperature of intake air, 37.8°C ;

T_2 - Temperature of product air, $^{\circ}\text{C}$.

With the calculated PA dry-bulb temperature of 21.6°C, the PA state can be determined at the psychrometric chart, e.g. RH=55.2%, as point **P2** shown in **Fig. 4-1**.

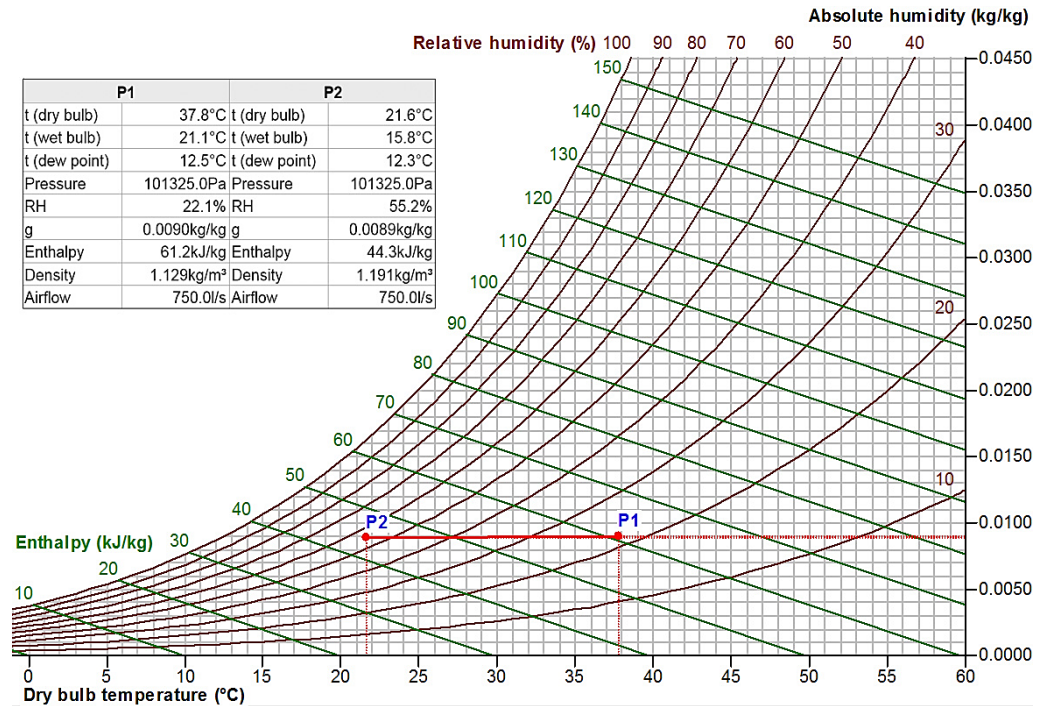


Fig. 4-1: Design state variation of primary air at psychrometric chart.

The state of the exhaust air depends on the working air ratio which initially also referred to the *Coolerado*® M30 of 0.441. (working air 592 m³/h and total intake air 1342 m³/h). Saturation efficiency in wet channels is assumed at 98%, the mean value of the test results of *Coolerado Cooler*™ [4.1].

Regarding the whole HMX as an adiabatic system, the incoming items include IA enthalpy and the evaporated water enthalpy and the output items include PA enthalpy and EA enthalpy. Thus, the energy equilibrium equation shows as [4-2], with neglect of excess circulating water due to its small contribution in sensible heat.

$$i_1 + i_w = i_{1'} + i_2$$

[4-2]

Where,

i_1 - Intake air enthalpy, kJ/kg;

i_w - Evaporated water enthalpy, kJ/kg;

$i_{1'}$ - Exhaust air enthalpy, kJ/kg;

i_2 - Product air enthalpy, kJ/kg.

4.2.2 Heat and Mass Exchanging Sheets

Structure

To enlarge the efficient exchanging area, the main portion of the exchanging sheet is shaped into a corrugated geometry, as shown in **Fig. 4.2**. Instead of the supporting guides between the sheets existing in former products, the corrugated sheet keeps the shape by its own rigidity, thereby to reduce the flow resistance inside the air channels.

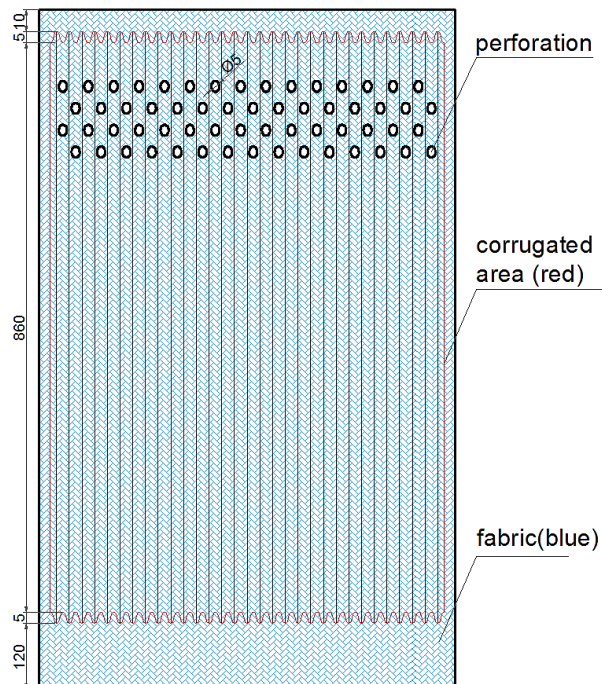


Fig. 4-2 (a): Front view.

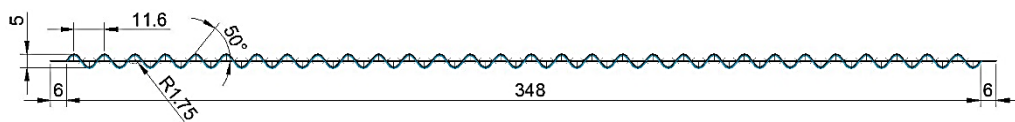


Fig. 4-2(b): Top view.

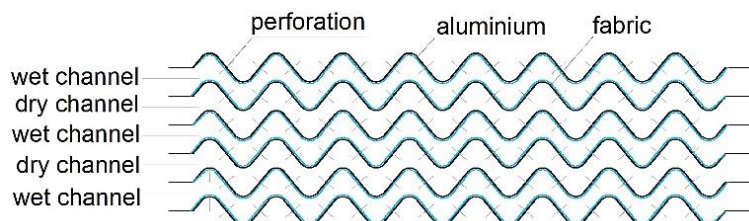


Fig. 4-2(c): Air channels formed with the exchanging sheets.

Fig. 4-2: Schematic drawing of the heat and mass exchanging sheet. (Unit: mm)

The schematic and the corrugation details are shown in **Fig. 4-2(a)** and **(b)**. **Fig. 4-2(c)** demonstrates the stack structure of the sheets to form the alternative dry and wet air channels. For each heat exchanging sheet, its inlet and outlet portions are made into the flat geometry for convenience of air and water distribution within the channel space; while its main portion is made into the corrugated geometry for increasing the heat transfer area between the two parts of air.

Integrating the machining property, heat transfer property and corrosion resistance, aluminium was selected to form the exchanging sheet base. One side of the sheet is bare aluminium and the other side is treated to be hydrophilic, moisture wicking and large specific surface area facilitating water evaporation. A sort of moisture-wicking and quick-drying fibrous fabric is bonded by marine adhesive to constitute a sandwich structure with the aluminium base, as shown in **Fig. 4-3** thus to form the wet channel wall and perform water evaporation.

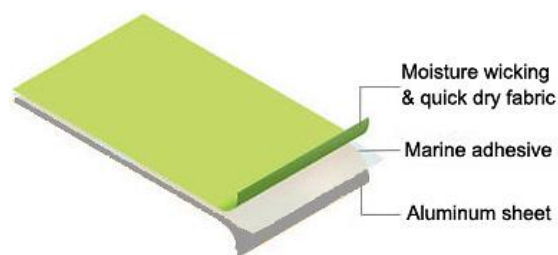


Fig. 4-3: Sandwich structure of the exchanging sheet.

More than 10 fibrous materials, e.g. *Coolmax*®, *Cooldry*®, *Coolplus*®, have been selected and the final selection of the materials will be determined by the following dedicated testing.

Dimension

As shown in **Fig. 4-4**, the heat and mass exchanger has the dimensions of 1000 mm (H) × 360 mm (L) × 800 mm (W) with the internal interval of 5 mm between the sheets. Along the 1000 mm length of the exchanging sheet, the lengths of the inlet & outlet flat planes and corrugated section are 120 mm, 10 mm and 860 mm with two 5 mm transitional regions up and down respectively. At the top side of each exchanging sheet, numerous perforated holes with diameter of 5 mm are opened to allow part of the dry channel air to be diverted to the neighbourhood wet channels, thus enabling the heat transfer between the two parts of airstreams and cooling of the dry channel air.

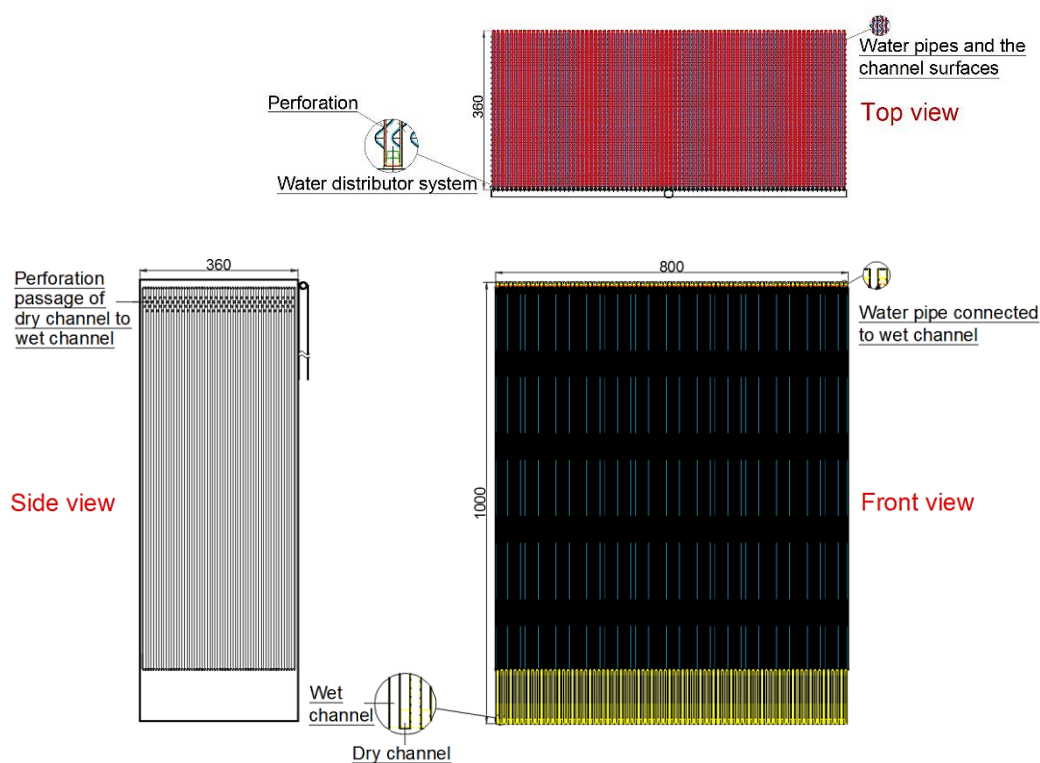


Fig. 4-4: 3-view drawing of the heat and mass exchanger. (Unit: mm)

Based on the configuration design, the area of corrugated section is 341032 mm^2 , lower plane section 41760 mm^2 and the perforation area 2316 mm^2 per sheet. The effective heat and mass transfer area includes the corrugated section and the lower plane plate. Accordingly, the effective heat transfer and evaporation area results in 380479 mm^2 , i.e. 0.38 m^2 , and there is a promotion of 12.3% in effective exchanging area comparing to the totally plane plate area of 338724 mm^2 .

4.3 Design of the Water Distributor, Water Sink and Control Strategy

4.3.1 Water Distributor

A dedicated water supplier/distributor was designed and patented (ZL2016-2-0563598.X [4.3]). This configuration, as shown in Fig. 4-5, comprises a main water supply pipe, a horizontal water header and numerous small-sized water

distribution tubes, all of which are appropriately jointed together to form an integrated unit.

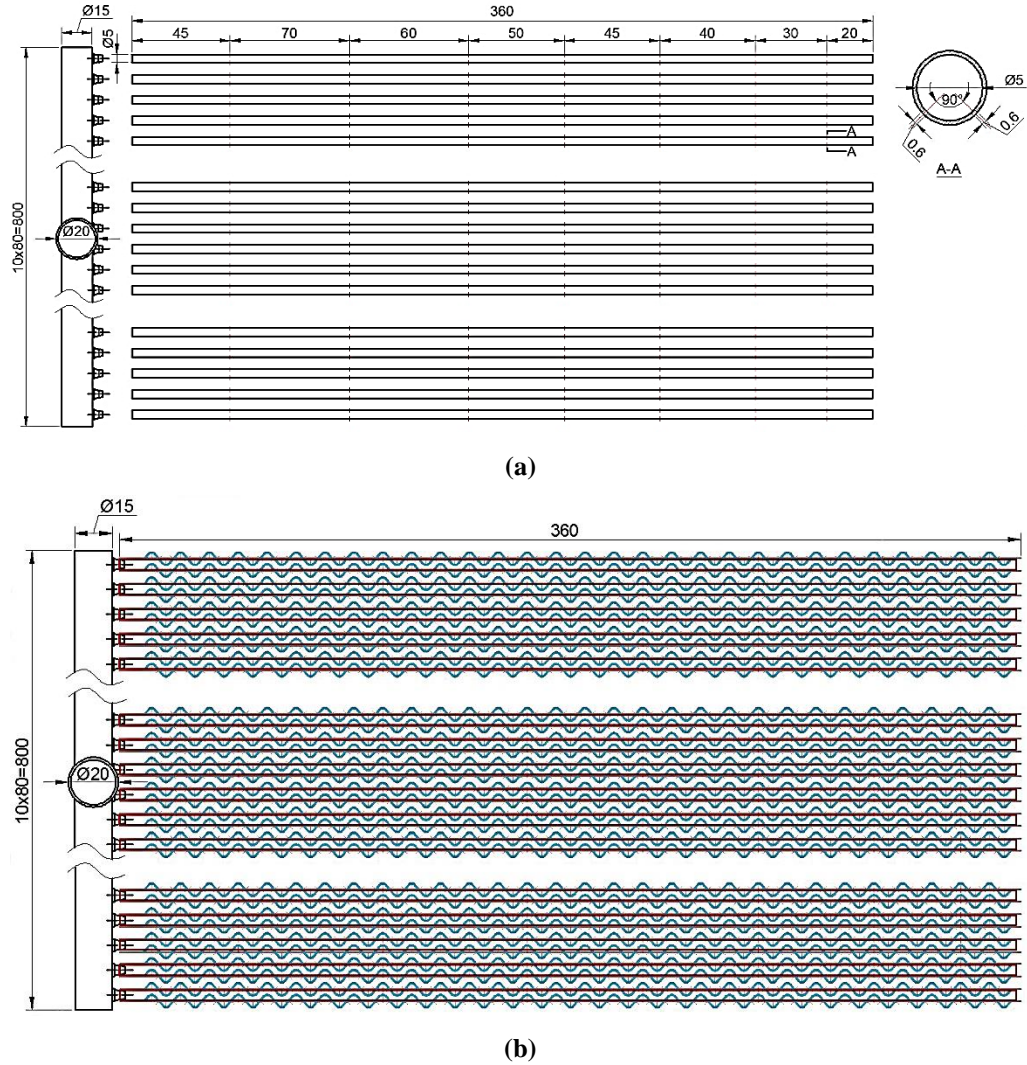


Fig. 4-5: Water distributor. (Unit: mm)

(a) design details; (b) assembled and positioned between the exchanging sheets

4.3.2 Water Sink

The lower water sink collects water dripping along the walls of wet channels and accommodates water to realize the intermittent action of the circulating pump. Two water detectors located at high and low levels, along with a dedicated control logic, are responsible for the control of pump operation. Besides the outlet of circulating water, there are overflow and drain openings as well, shown

as **Fig. 4-6**. The plenum between the exchanger and water sink, which is under negative pressure due to the action of exhaust fans, should be well sealed around.

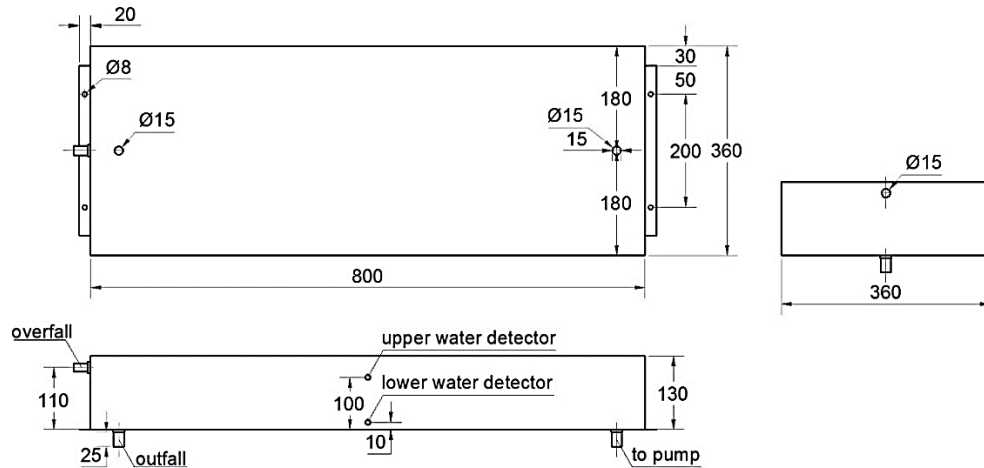


Fig. 4-6: Design of the water sink. (Unit: mm)

4.3.3 Control Strategy

Water route

The high absorption capacity of the fibre layer enables it to hold significant amount of water for a relatively longer period. This creates an opportunity to implement the intermittent water supply scheme that can minimize the water usage and water pump power consumption. During operation, the main water supply pipe, connecting to a circulating pump or an in-house tap, receives the water during the designed time interval. This amount of water is then delivered to the horizontal water header that can balance the pressure of water and distribute it to each water distribution tube. It should be noted that each single distribution tube is drilled with numerous tiny openings (0.5 mm in diameter and diminishing gaps between the two adjacent openings as per the change of water flow rate along each branch pipe) and inserted into a wet channel of the heat and mass exchanger (**Fig. 4-5(b)**). This allows the water to be delivered into each wet channel with equal flow rate and even water distribution across the wet surface.

Further, the water is delivered intermittently with the scheme as below (**Fig. 4-7**): (1) if the bottom water tank is not full, the water supply pipe is connected to an in-house tap, running 15 seconds for every 10-minute interval with the flow rate of 6.85 litre per minute; (2) when the bottom water tank is full, the water supply pipe will be switched to the circulating pump, running 60 seconds for every 10-minute interval with the flow rate of 2.45 litres per minute. To realise this operational scheme, two sensors are installed into the water tank that can detect the lower and upper levels of the water within the tank and instruct the action of the solenoid valve fitted into the water supply system of the unit. The control circuit is demonstrated in **Fig. 4-8**.

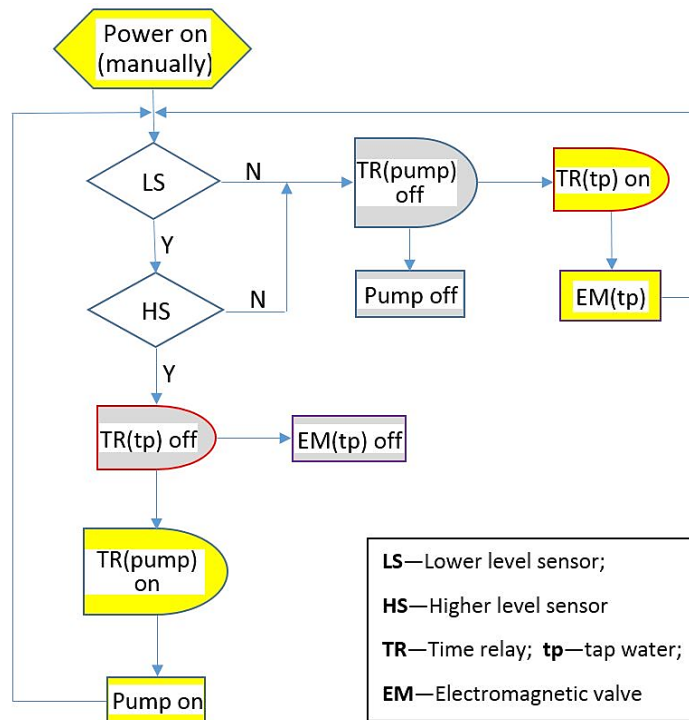


Fig. 4-7: Control logic of water supply.

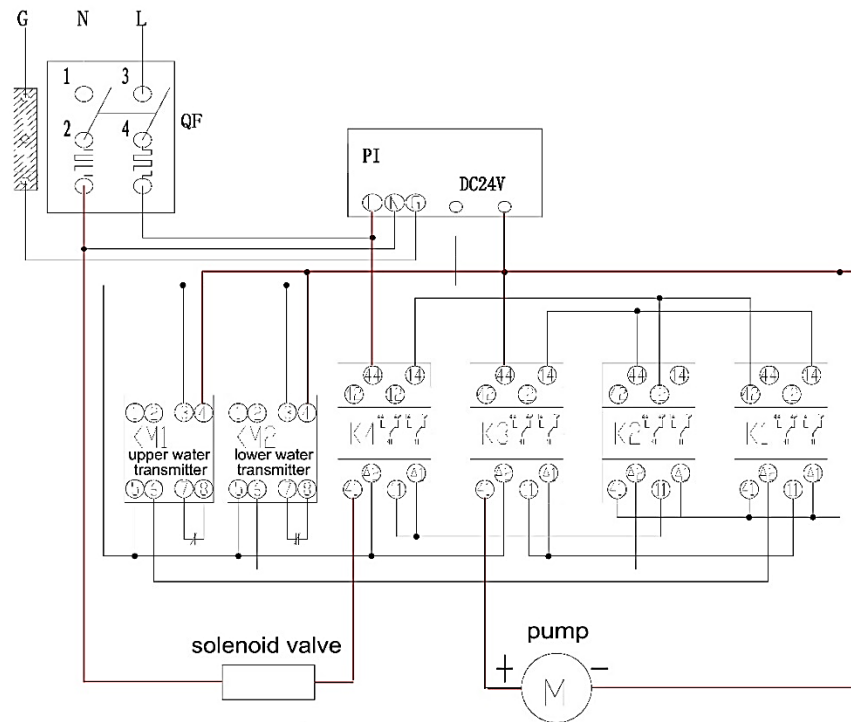


Fig. 4-8: Control circuit for water circulation.

Air route

Airflow is co-driven by the supply and exhaust fans. Two manual fan controllers are assigned to the supply and exhaust fans respectively. It is convenient to adjust the vanes rotate speed to achieve the desirable airflow rate and the working air ratio. The control circuit for airflow is shown in **Fig. 4-9**.

Besides the simple control procedure to facilitate manually adjusting the input parameters in lab test stage, a full function automatic control programme for independent demonstration has been developed in **C** programming language, which is listed in **Appendix 1**.

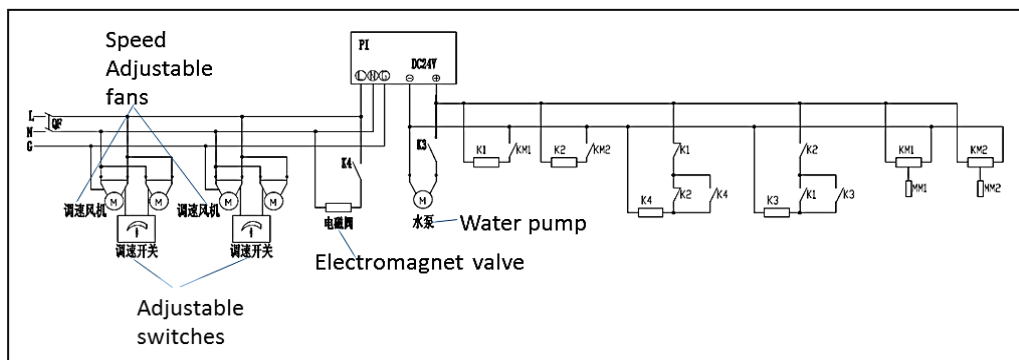


Fig. 4-9: Control circuit for airflow.

4.4 Selection of the Fans and Pump

4.4.1 Fans

Fans layout

The airflow is driven by the joint action of the upper supply fans and lower exhaust fans. Considering the size of HMX and the uniformity of air distribution, two supply fans and two exhaust fans are spaced respectively at upper and lower sides of the prototype. To facilitate the deployment of air inlet and outlet, the damp air from the wet channels is exhausted from one lateral side while intake/product air in/out by the back/front side, as shown in **Fig. 3-1** and **Fig. 3-2**.

CFD method was employed to identify the distribution effect of the air entering from just back side other than both back and front sides. As shown in **Fig. 4-10**, at various flow rate, air distributes evenly in wet channels.

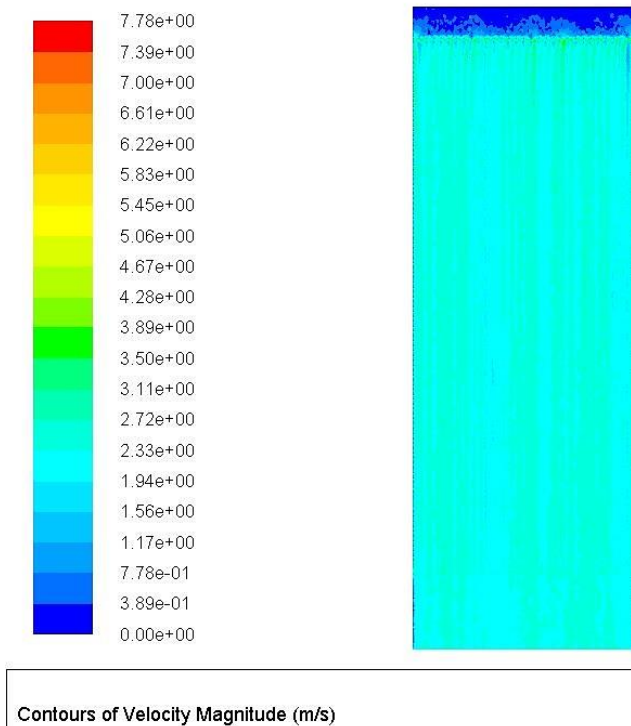


Fig. 4-10: Velocity distribution in wet channel at airflow rate of 1128 m³/h.

There will be a backflow area above the IA inlet in the dry channel, which enlarges with the increase of airflow rate. The backflow of intake air would heavily affect the heat convection between the airflow and the HMX sheet. At the volume flow rate of 1128 m³/h, the backflow area in the velocity contours appears obvious and when the flowrate arrives at 2257 m³/h, the backflow area expands to nearly one thirds of the total HMX sheet. The variation of the backflow area with airflow rate is illustrated in **Fig. 4-11**.

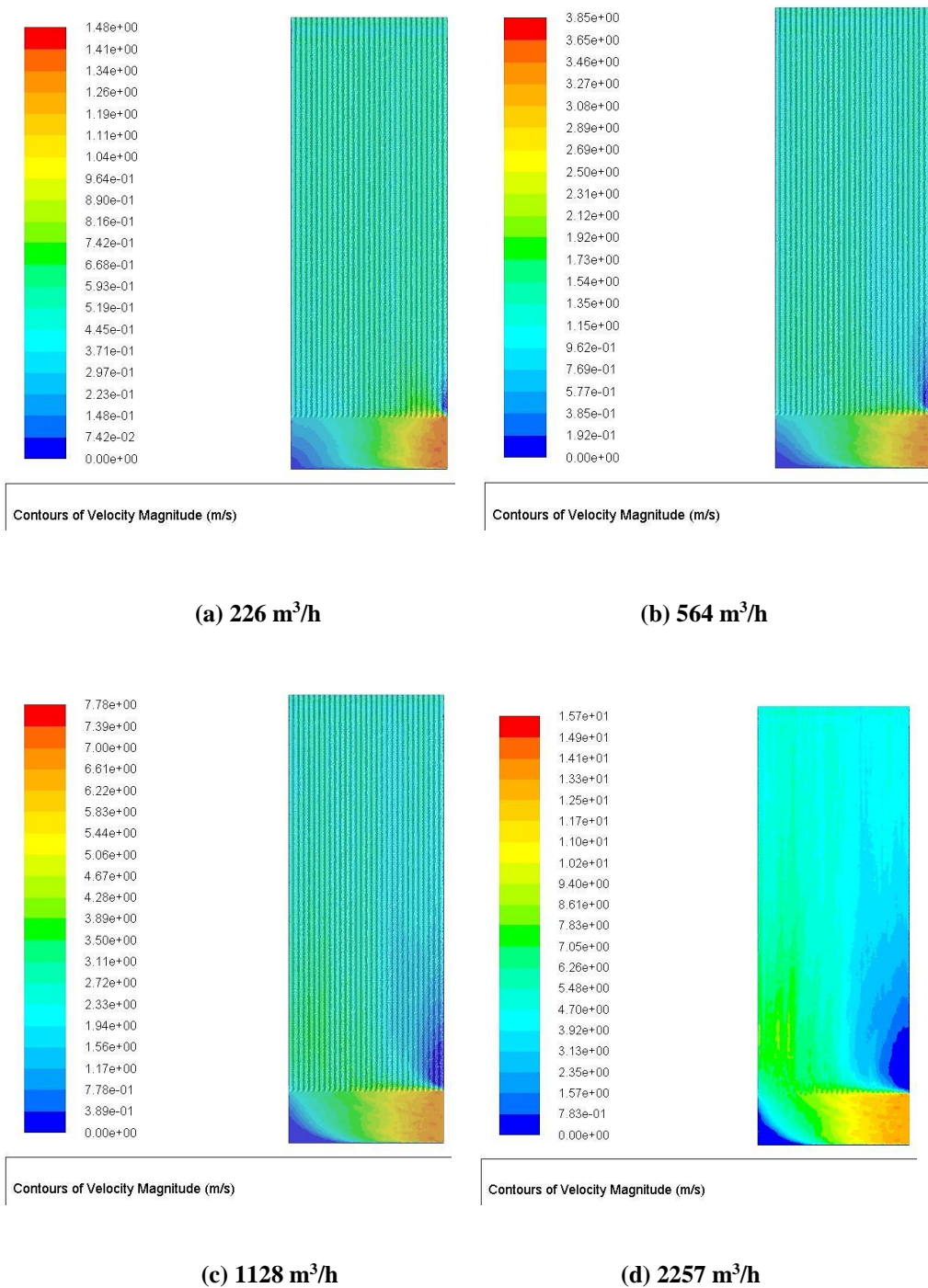


Fig. 4-11: Velocity distribution in dry channel at various airflow rate.

To simplify the air organization and the prototype configuration, one air inlet at back side, which is adopted in the final design scheme, is considered reasonable as per the design entering airflow rate.

Fans selection

The air flows against both the on-way resistance along the channels and local resistance existing in the channel inlet, outlet and the perforations connecting dry and wet channels. With assistance by CFD simulation, 300 Pa was taken as the nominal design pressure drop for fans selection.

The supply and exhaust fans act in parallel to draw the airflow from the inlet to the top of the dry channel where the air splits through perforations and enters the wet channel or continues into the plenum above the heat exchanger. The shared load could be determined to carefully select the fans.

The maximum design flow rate of the supply fans is 1250 m³/h with a maximum pressure requirement of 350 Pa. Two 160 mm backward curved *ebm-papst*TM centrifugal fans with part number *K3G225-RE07-03* were selected to use in parallel. These fit the space envelope well and in addition could improve the air distribution across the width of the heat exchanger. The specification of the fans is listed in **Table 4-1**.

Table 4-1: Specification of the selected fan

Nominal data						
Type	K3G225-RE07-03					
Motor	M3G055-DF					
Phase		1~				
Nominal voltage	VAC	230				
Nominal voltage range	VAC	200 .. 240				
Frequency	Hz	50/60				
Type of data definition		ml				
Speed	min ⁻¹	2860				
Power input	W	170				
Current draw	A	1.4				
Min. ambient temperature	°C	-25				
Max. ambient temperature	°C	60				
<small>ml = Max. load · me = Max. efficiency · fa = Running at free air · cs = Customer specs · cu = Customer unit Subject to alterations</small>						
Data according to ErP directive						
		Actual	Request 2015			
01 Overall efficiency η_{es}	%	61.7	43.1	09 Power input P_{ed}	kW	0.16
02 Measurement category		A		09 Air flow q_v	m ³ /h	705
03 Efficiency category		Static		09 Pressure increase p_{fs}	Pa	458
04 Efficiency grade N		80.6	62	10 Speed n	min ⁻¹	2865
05 Variable speed drive		Yes		11 Specific ratio*		1.00
<small>Data definition with optimum efficiency. The ErP data is determined using a motor-impeller combination in a standardised measurement configuration.</small>				<small>* Specific ratio = $1 + p_s / 100\,000\text{ Pa}$</small>		

The output of each fan would be half of the total IA flow rate, i.e. 625 m³/h. **Fig. 4-12** shows a selection at 625 m³/h and 207 Pa. There is sufficient capacity to increase the fan speed to exceed the estimated dirty filter condition of 625 m³/h at 350 Pa.

The maximum design flow rate and pressure of the exhaust fans is 1000 m³/h at 360 Pa. Similarly, two same fans work in parallel to meet this duty and each handles 500 m³/h. The fan could be set each side of the plenum between the heat exchanger and the water tank.

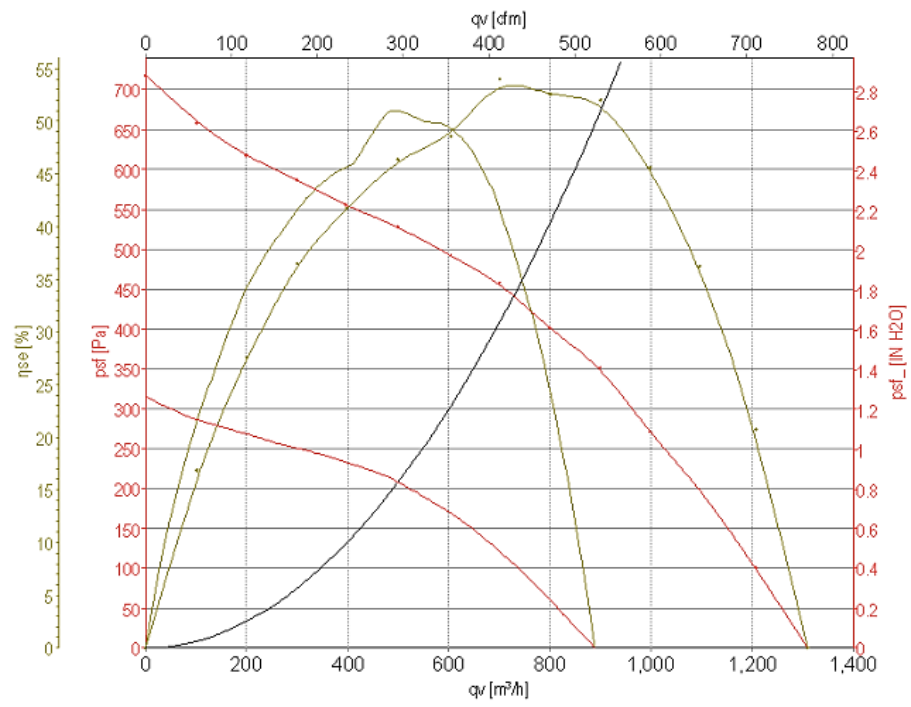


Fig. 4-12: Performance of *K3G225-RE07-03* at a duty point of 625 m³/h at 207 Pa.

Fig. 4-13 illustrates the installation of the two upper supply fans and the two lower exhaust fans.

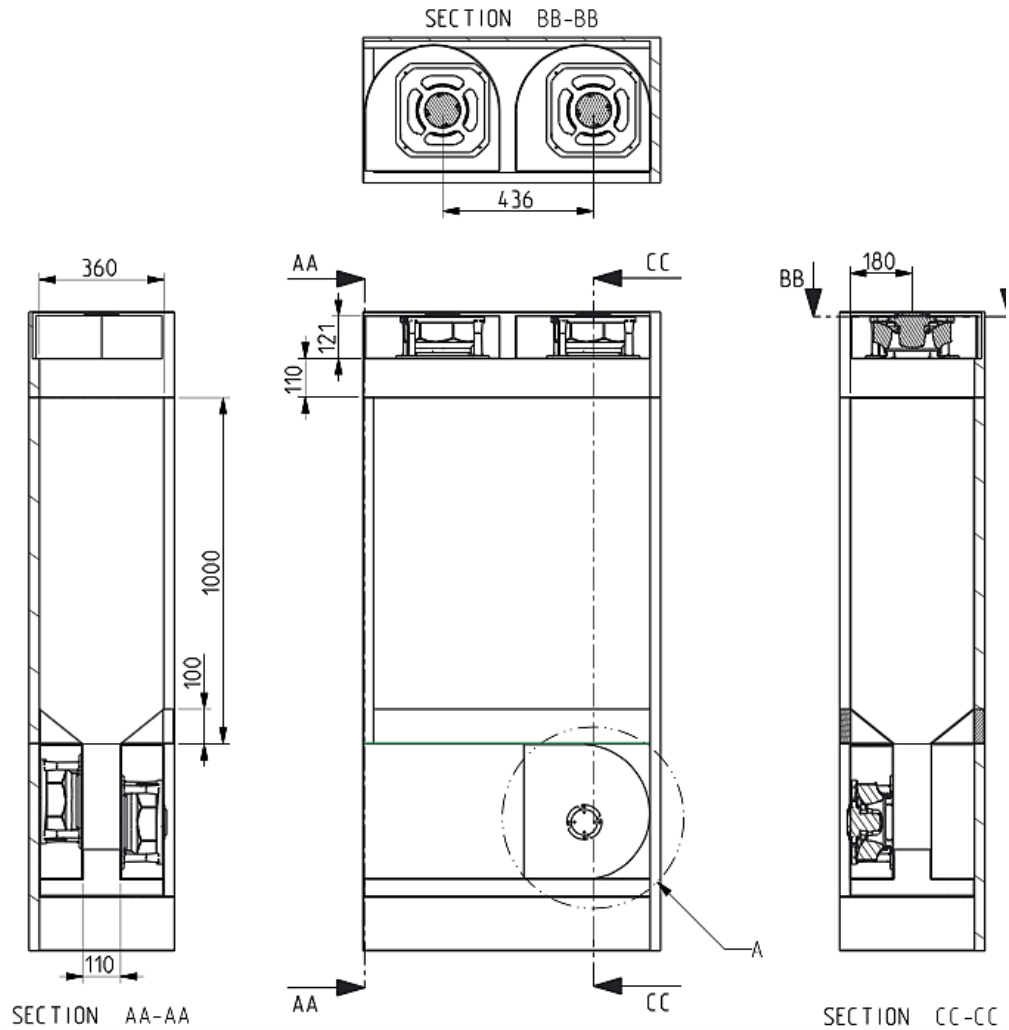


Fig. 4-13: The fit of the supply fans and exhaust fans in the prototype. (Unit: mm)

4.4.2 Circulating pump

Water feeds from the main supply. To ensure the evaporating surface being all over wetted, extra water is needed. The pump circulates water from the lower water sink just when the excess water accumulates to a certain level. As per the water evaporation rate of 1.5 L/kWh(cooling), the 4-kW rated prototype consumes 6 L water per hour. Considering the cooling taken away by the exhaust air, 3 times (comparing 20-30 times of like products [4.4]) extra water, as low as 18 L/hr, is accepted as the required circulating water flow rate. The water route is open and the pump head is required to lift water to a height of around 1.6 m, overcome the corresponding on-way resistance and keep certain static pressure

to pray through the numerous pinholes at the water distributor. Overall, the required pump head is as low as no more than 2 m water column.

A small 24V/1.2A DC pump with output of 6.5 mH₂O and 360 L/h was selected and a plumbing valve was employed to adjust the feeding water pressure. The specification of the circulating pump is listed in **Table 4-2**.

Table 4-2: Specification of the circulating pump

Circulating water pump	DH40H-24110, Shenzhen Zhongke Century Technology Ltd, 24V/1.2A DC, 11 mH ₂ O, 360 L/hr	
产品型号: DC40H-1265		
	电 流 Current	1.2A
	电 压 Voltage	直流12V
	最大流量 Maximum flow	360L/H(6升/分钟)
	最大扬程 Lift	6.5M
	工作温度 Working temperature	≤60°
	出水口径 Outlet diameter	8mm
	进水口径 Inlet diameter	11mm
	重 量 The weight of the	220克
	功 耗 Power consumption	14.4W
	防水等级 Waterproof level	IP68
	驱动方式 Drive way	直流无刷 磁力驱动
工作寿命 The working life	大于20000小时	

4.5 Material Selection, Performance and Process Testing in HMX fabrication

The exchanging sheet is designed as a sandwich structure of base plate/adhesive/fibrous material (refer to **Fig. 4-2**). The base panel is required to be a good thermal conductor, impervious to water, rust prevention, easy to process, self-supported and shape preserving when standing. The adhesive should be able to work and last long in soggy circumstances. Fibrous material used as evaporating surface is expected to be superb in performance of moisture wicking and quick drying. Moreover, it is essential to be able to realize all the requirements in the actual mechanical process.

4.5.1 Aluminium Plate and Moulding Process

As per the requirements for the base panel, aluminium may be the proper material due to its high strength and good ductility in forming and anticorrosive property in operation. Since large area of aluminium plate is needed to form the HMX, reducing the self-weight while keeping shape becomes an issue to be considered. As for the mixed irregular shape of the corrugation, plane and transition sections, integrated mould forge and press could be a feasible choice regarding aluminium's property of ductility.

Firstly, a small-scale mould was produced based on the original design to validate the feasibility. Unfortunately, fractures occurred even if careful consideration had been taken in the selection of specified aluminium series as per their mechanical properties.



Fig. 4-14: Trial mould pair.



Fig. 4-15: Fractures after mould pressing.

To solve the crack problem, plenty of subsequent trials were conducted from two aspects, i.e. adjusting the corrugation design to reduce the deformation stress and enlarging the option of the aluminium alloy by special mechanical properties and plate thickness.

More than 10 small-scale moulds, as partially shown in **Fig. 4-16**, were generated to adopt for the corrugation adjustment. Various aluminium series, e.g. 1060, 3003, 5052 and 5005, were tested. Numerous failures were experienced

and fractures diminished gradually as shown in **Fig. 4-17**. Progress was made step by step and finally the optimal portfolio was found. The final corrugation alteration is shown and compared with the original design in **Fig. 4-18** and the wave shape is demonstrated in **Fig. 4-19** in side view. The aluminium series of 5005 which can farthest adopt for the deformation at plate thickness of 0.27 mm was eventually selected. The specifications and the test certificate of the selected aluminium sheet are shown in **Table 4-3**. Comparing to the original design, the final wave height diminished from 5 mm to 2.8 mm and accordingly the heat and mass exchanging area is reduced by 16.7%. All the lost exchanging area will be compensated by increasing the amount of the exchanging sheets.



Fig. 4-16: Some of the small-scale sheet moulds for trial.

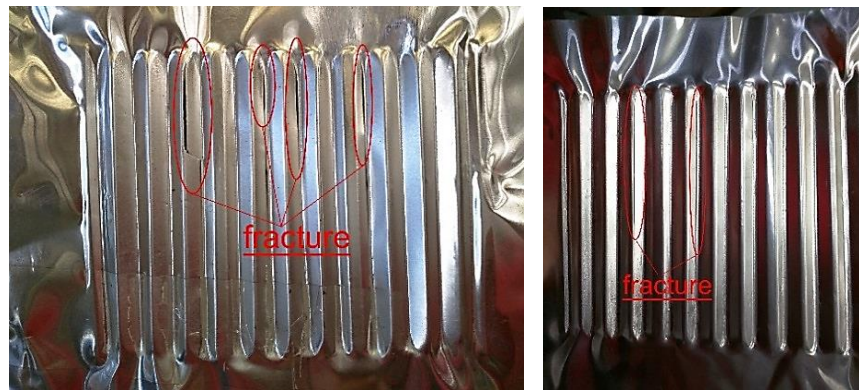


Fig. 4-17: Various failure of fracture.

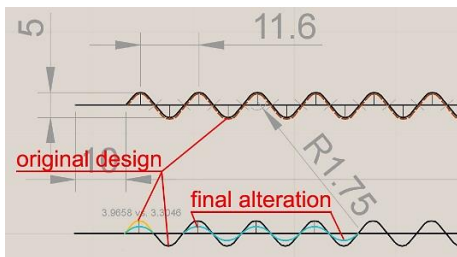


Fig. 4-18: Change of the corrugation form. Fig. 4-19: Final wave form in side view.

Table 4-3: Specification and test certificate of the selected aluminium sheet

华商(天津)铝业有限公司
HuaShang(Tianjin)Aluminum Co.,Ltd
质量证明书
TEST CERTIFICATE

收货单位: 山西中绿环保集团有限公司 日期:

品名 PRODUCT	批号 NO	规格 SPECIFICATION	牌号 SPEC	状态 ESTATE	净重 N.W	化学成分(%) CHEMICAL ANALYSIS								机械性能 M. T. R		
						Fe	Si	Cu	Mn	Mg	Zn	Cr	Ti	抗拉强度 T.S.(Mpa)	屈服强度	延伸率 E.L.(%)
铝卷	RA19127	0.27*1050*C	5005	O	440kg	0.395	0.076	0.039	0.113	6.7.8	<0.005	0.066	0.0248	111	98	34

执行标准: GB/T3880-2006 GB/T3190-2008

审核: 王秋娟 检验员: 01

The final real-size punching and forge moulds and the associated components were developed from raw steel billets after the process of cutting, polishing and milling as shown in Fig. 4-20.



(a) Raw steel billets



(b) Polishing process

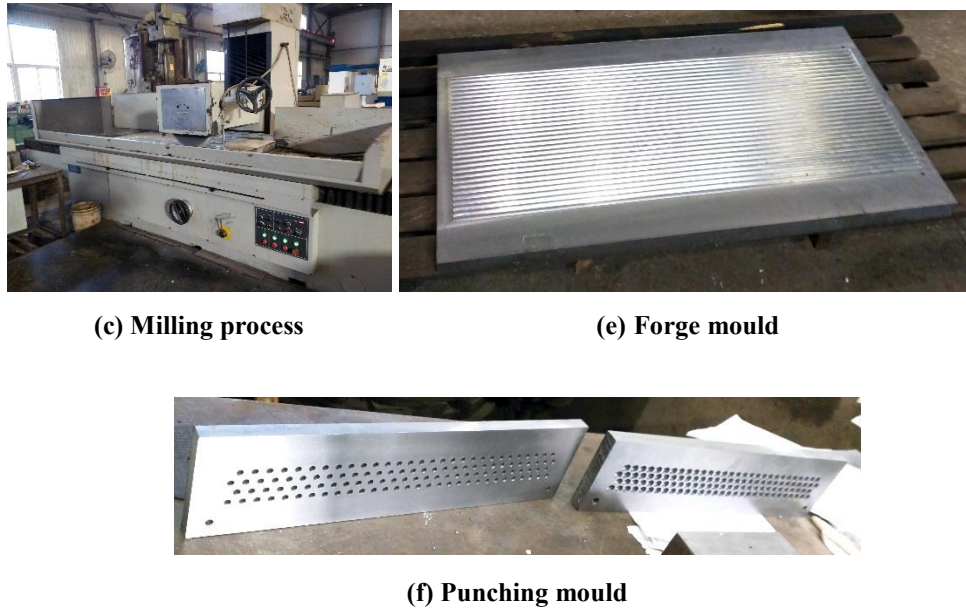


Fig. 4-20: Manufacturing process of the forge and punching moulds.

4.5.2 Fibrous Fabric

The performance of water evaporation from the wet surface, which greatly depends on the effective evaporating area and the surface tension on the evaporating media, is of importance for an evaporative cooler. Finding the appropriate material with superb performance of moisture wicking and quick drying is one of the key tasks of the whole project.

Some functional fibres with irregular section or non-smooth surface applied in sportswear present excellent performance to help transfer the moisture from the human skin to the outer surface of the fabric and quickly evaporate it into the ambient air. Besides the well-known *Coolmax*® fibres developed in 1986 by *DuPont Textiles and Interiors*TM (now *Invista*TM), many other fibres, e.g. *Cooldry*®, *Coolpass*® and blended fabrics, have been springing up in the textile markets. In this section, six fibrous fabrics along with Kraft paper as a reference, which had been extensively used in conventional evaporative coolers, were selected to test as for their performance in moisture wicking, water diffusivity and water evaporation.

The specifications of the material under test are listed in **Table 4-4** with the images, fabric brand, weaving, weight and breadth information. Orders are assigned to each sample for convenience of description. “Fabric brand” indicates the material used to weave the fabric and “Weaving” indicates the weaving method. Both sides of each fabric are shown in each image if they are different. The costs of the textile fabrics in retail market are listed in **Table 4-5**.

Table 4-4: Specifications of the fabrics under test

Sample No.	Photo of the fabric	Specification			
		Fabric brand	Weaving	Weight	Breadth
1		Coolbass®	bird eye mesh fabric 100D*72F	170 gsm	180 cm
2		Kraft paper	-	117 gsm	32 cm
3		Bamboo charcoal + Coolmax® active	75D	150 gsm	155 cm
4		Coolbass®	knitted (double) pique mesh 75D*72F	150 gsm	170 cm
5		Topcool® spandex	single jersey 88/12	170 gsm	165 cm
6		320D Supplex® +3M®	70D* (160D+160D)	130 gsm	150 cm
7		228T Supplex® +3M®	75D*160D	103 gsm	150 cm

Table 4-5: Costs of the textile fabrics.

Sample No.	1	3	4	5	6	7
Cost per kilogram in Chinese currency (Yuan)	¥36/kg	¥75/kg	¥30/kg	¥50/kg	¥19.5/m	¥17.5/m
Minimum order	200 kg	1000 kg	200 kg	500 kg	1000 m	1000 m

Methodology and testing rig

Fig. 4-21 shows the testing rig, in which major parts include a high resolution (1920×1080 pixels) camera, a ruler, a burette with drop flow controller, a hygromograph and computer. The high resolution *Logitech®* HD Pro webcam c910 with *Carl Zeiss®* optics autofocus facility was used to record the dynamic movement of the liquid over the fabric surface. The camera is mounted on a support stand, equipped with a LED light, and connected to the computer via a USB port. The distance between the camera and fabric sample was maintained at a fixed distance.

Fig. 4-21(a) shows the vertical moisture wicking test. The several different sample strips of 20 cm × 2 cm were suspended vertically with their lower ends (2.5 cm) immersed in a water reservoir. A ruler adjacent to the strips was used to measure the wicking height. To track the water movement at a regular time interval, a video of the wicking process was taken with the camera. The video shown in the computer enabled the variation of wicking height with time to be assessed, by stopping the video at a certain time for image capture. The camera was compatible with image analysis software, hence the captured image was processed with *Adobe Photoshop*, which facilitated measurement of wicking height from the ruler within the image.

The test was carried out in a laboratory environment with ambient temperature of 22°C-24°C and relative humidity of 36%-40%. The ambient humidity and temperature were monitored with a hygromograph during the testing period, as shown in **Fig. 4-21(a)**.

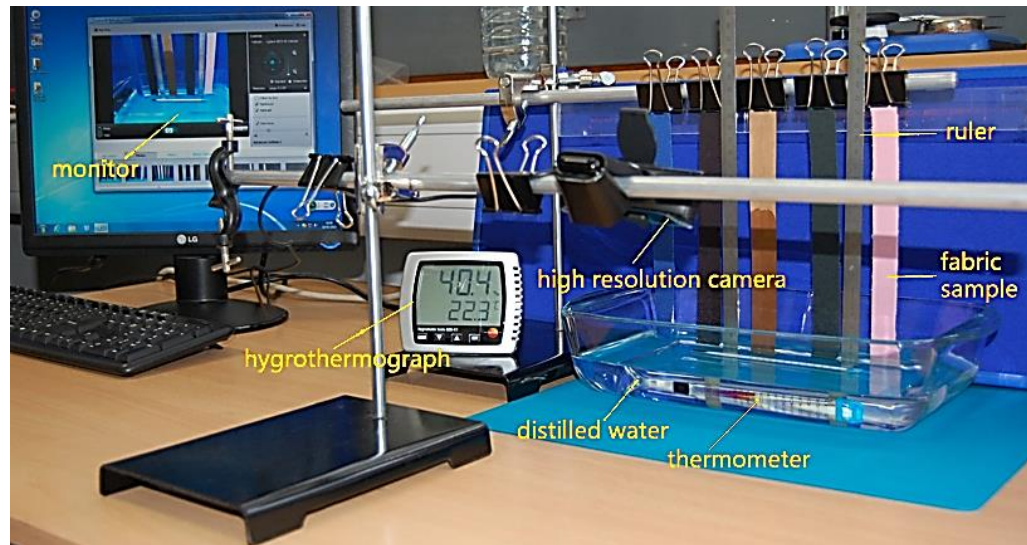


Fig. 4-21(a): Moisture wicking test.

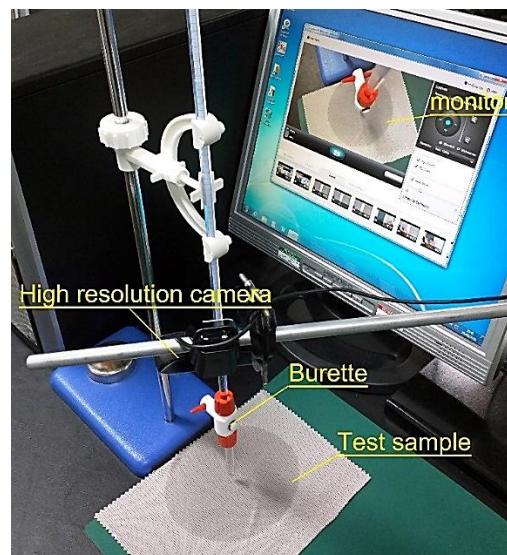


Fig. 4-21(b): Diffusivity and evaporation test.

Fig. 4-21: Experimental testing rig set up.

Fig. 4-21(b) shows the moisture diffusivity and evaporation test rig. The fabric (15 cm × 15 cm) was laid on a flat metal surface horizontally, which was fixed on a vibration-free bench. Ten water drops (0.5 mL in total) were dropped onto the centre of the fabric surface using a burette with drop flow controller, which was positioned 5 mm above the fabric. The moisture diffusivity/evaporation process was taken as a video with the camera.

Fig. 4-22 shows an image of the moisture diffusivity/evaporation on Kraft paper with the reference area. The video fed to the computer enabled the moisture spread and evaporation processes to be assessed by stopping the video at a certain time and capturing the image. *Photoshop* software was used to process the image to determine the pixel count of both the wetted region and the reference area, which could then be compared to determine the area of the wetted region of the fabric [4.5].

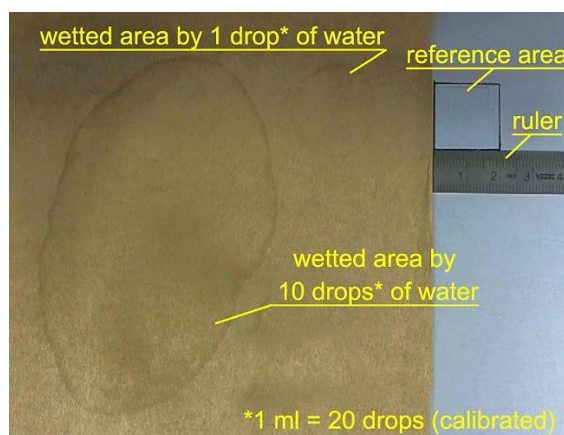


Fig. 4-22: Wetted area on Kraft paper compared with the reference area.

A schematic diagram of the commercial image processing method is shown in **Fig. 4-23**. Before starting a new test, the position of the camera above the fabric surface is calibrated. A square ($2\text{ cm} \times 2\text{ cm}$) reference area (i.e. 4 cm^2) is drawn on the back paper and placed adjacent to the sample. The captured image is transferred into *Photoshop* and the image resolution is changed into 15 pixels/cm. Then the area of the square is found in terms of pixels. The total pixels are compared with the calculated value (4 cm^2), and the camera height is repeatedly adjusted to produce new images until the total *Photoshop* pixel count matches the calculated result.

Details of the *Photoshop* measurement are described as follows. Firstly, the required raw image (**Fig. 4-23**) is opened to find the reference area in the image processing software. Then, the image quality is adjusted by correcting brightness

and contrast. Needless area is removed by cropping the image. The image is then calibrated by changing the image resolution value into 15 pixels/cm. The wetted area is selected using the magic wand selection tool, assisted with the tolerance properties facility. After exact selection of the wetted area, the histogram option is finally used to determine the number of pixels in the selected (wetted) area.

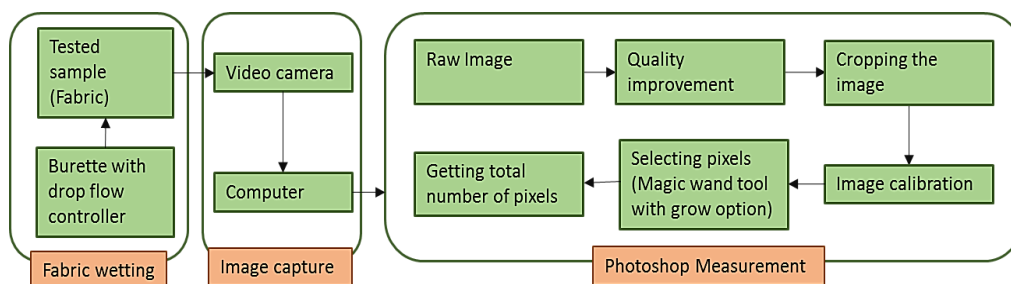


Fig. 4-23: Schematic diagram of the commercial image processing method.

Test results and the selection

(1) Wicking height

The wicking height tests were carried out for 15 minutes. The results are listed in **Table 4-6** and shown in **Figs. 4-24, 4-25** and **4-26**. **Fig. 4-24** shows variation of the wicking height with time for the seven different fabric samples. It is seen that the wicking heights of **Samples 1, 3 and 4** increased faster and demonstrated higher vertical wicking ability than **Samples 2, 5, 6, and 7**. **Sample 2** (Kraft paper) showed the lowest vertical wicking ability.

Table 4-6: Wicking height variation with time

Sample No.	Wicking height, cm					
	0.5 minute	1 minute	3 minutes	5 minutes	10 minutes	15 minutes
1	6.1	7.5	10.7	12.7	15.8	17.5
2	1.0	1.5	3.1	3.6	5.2	6.2
3	5.5	6.9	9.9	11.8	14.9	16.8
4	4.3	5.7	8.6	10.3	13.5	15.9
5	3.7	4.3	5.5	6.3	7.1	7.6
6	3.6	4.0	5.2	6.3	7.3	7.7
7	1.9	2.5	4.2	5.2	6.1	6.6

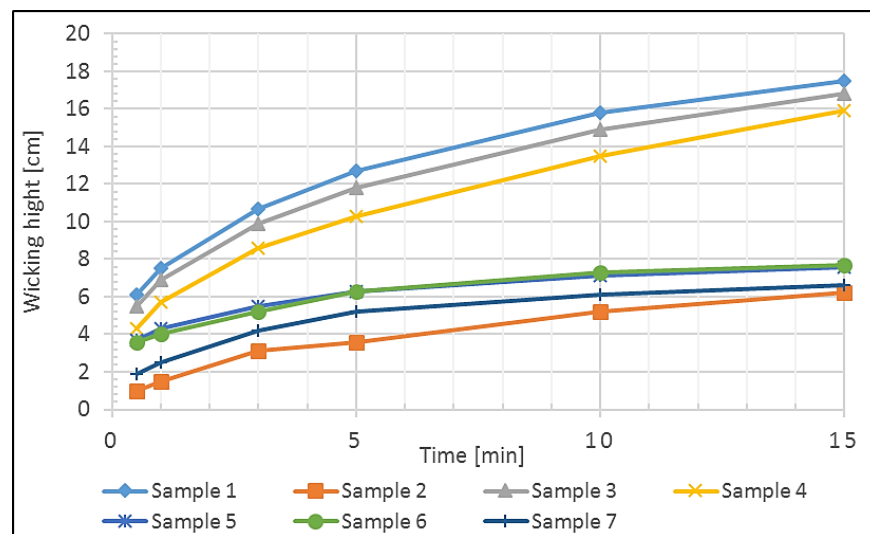
**Fig. 4-24: Variation of the wicking height with time.**

Fig. 4-25 shows variation of the wicking height growth rate with time. It is seen that Samples **1**, **3** and **4** perform generally higher wicking height rate than Sample **2**, **5**, **6** and **7**. For all the samples the wicking height growth rate reduces quickly in the first three minutes, and the growth rate continues to reduce with time. **Fig. 4-25** shows that the wicking height growth rates of Samples **2**, **5**, **6**, and **7** are close to zero at the end of the test, which indicates that their wicking heights have almost reached their highest positions after 15 minutes. However, the growth rates of Samples **1**, **3** and **4** are still at a lower rates of 0.34 cm/min, 0.38 cm/min and 0.48 cm/min respectively after 15 minutes.

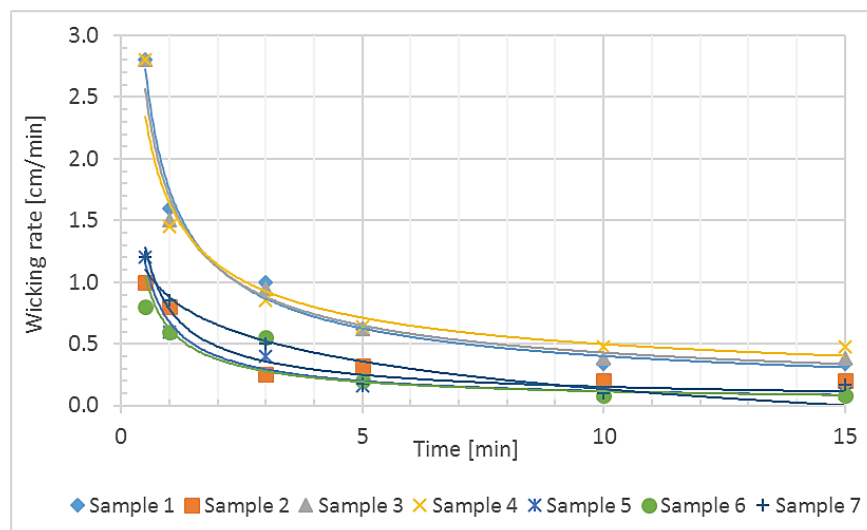


Fig. 4-25: Variation of wicking height growing rate with time.

The comparison of wicking heights after 15 minutes for the seven fabrics is shown in **Fig. 4-26**. It is seen that Samples **1**, **3** and **4** achieve the highest wicking heights of 17.5 cm, 16.8 cm and 15.9 cm respectively and the lowest height of 6.2 cm is observed with Sample **2** (Kraft paper). In summary, the test demonstrates that all the cloth fabrics give better wicking heights when compared with the conventionally used Kraft paper and Samples **1**, **3** and **4** show excellent wicking height performance among the tested cloth fabrics.

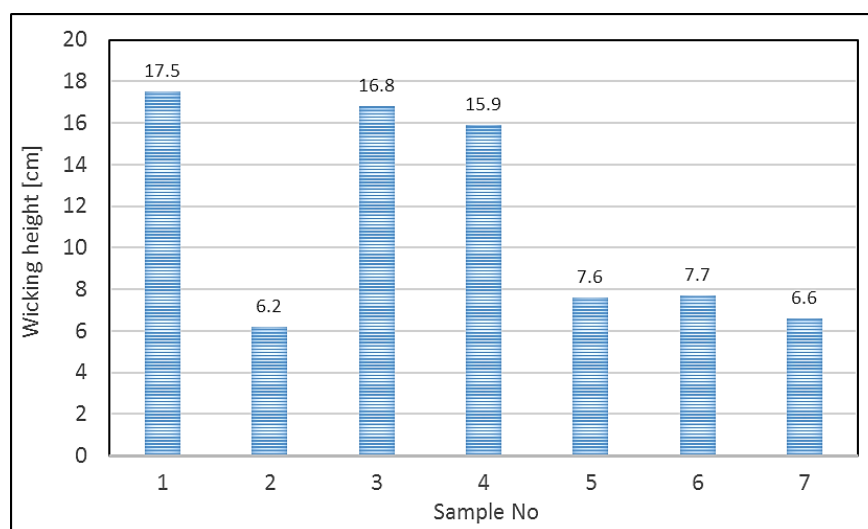


Fig. 4-26: Wicking height after 15 minutes.

(2) Diffusivity and evaporation ability

An preliminary evaluation of moisture diffusivity/evaporation characteristics was carried out by visual assessment for each of the fabrics. Water drops (total of 0.5 mL) were applied onto each fabric positioned horizontally on a flat backboard with a burette. It was observed that unlike other samples in which the water drops could naturally diffuse immediately (within 1 second), the drops on Samples 4 and 5 tended to retain their droplet shapes and did not appear to diffuse within a few seconds (see **Fig. 4-27**), although they diffused eventually. Usually, the wet surfaces in an indirect evaporative cooler are positioned vertically. Thus, if droplets cannot diffuse immediately, they would directly flow downwards under gravity instead of wetting the surround area. Therefore, Samples 4 and 5 were omitted and no further diffusivity/evaporation tests were conducted for these two samples.



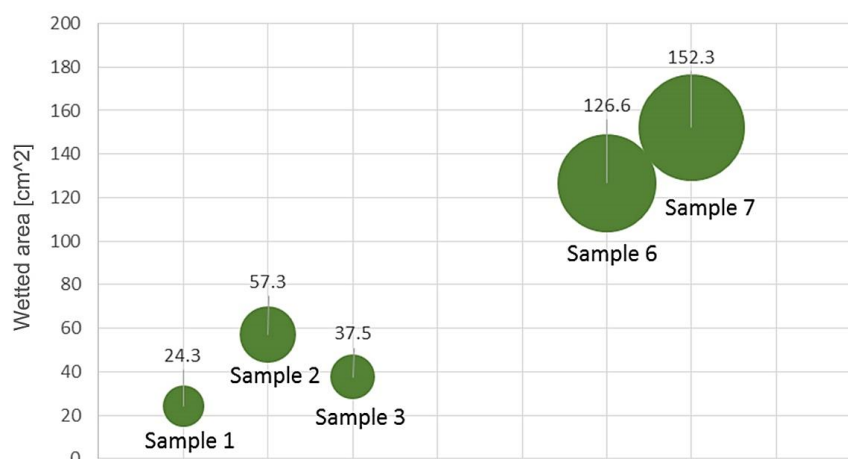
Fig. 4-27: Water drop on the fabric.

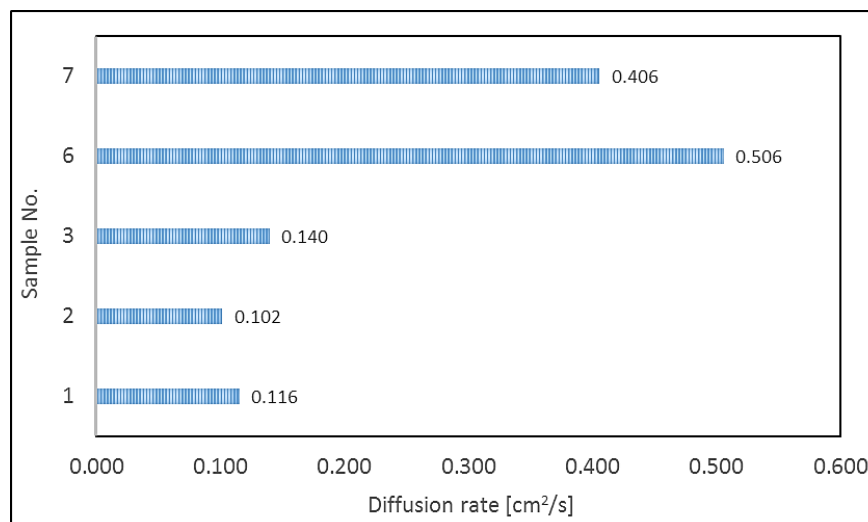
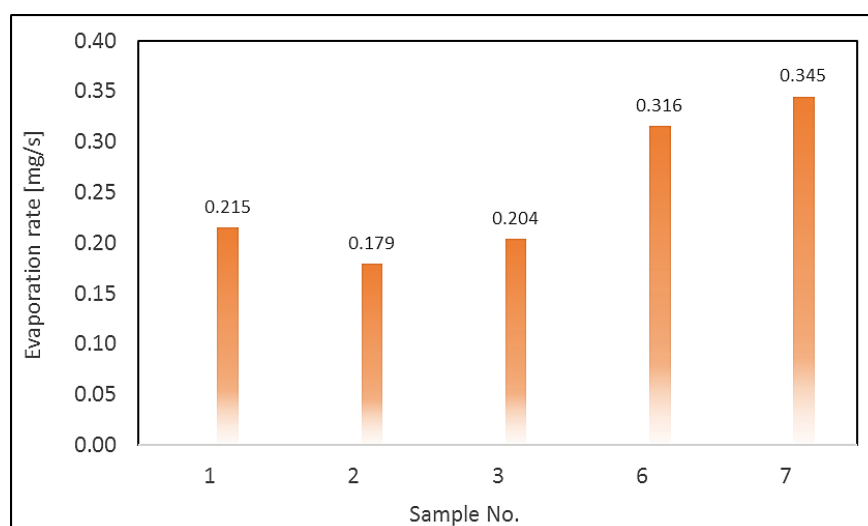
Then, testing for the remaining samples, i.e. Samples 1, 2, 3, 6 and 7, were performed with 10 drops of water (totally 0.5 ml) dropped by the burette. The results are listed in **Table 4-7** and shown in **Figs. 4-28, 4-29** and **4-30**. **Table 4-7** lists the final wetted area and related diffusion time for each sample. The evaporation time for each sample was the time required for the wetted area to become completely dry, based on the direct observation.

Table 4-7: Moisture diffusion and evaporation testing results

Sample No.	Wetted area (cm ²)	Diffusion time (s)	Mean diffusion rate (cm ² /s)	Evaporation time (s)	Mean evaporation rate (mg/s)
1	24.3	210	0.116	2330	0.215
2	57.3	560	0.102	2800	0.179
3	37.5	268	0.140	2450	0.204
6	126.6	250	0.506	1580	0.316
7	152.3	375	0.406	1450	0.345

Fig. 4-28 shows the final wetted area on each fabric resulting from the diffusion process. It is seen that for the same amount of water drops (totally 0.5 ml) the final wetted area of the tested samples are different and this can be attributed to differences in sample thickness. Thicker materials absorbed more water, resulting in a reduced spread area. Since thinner materials can achieve larger wetted areas, this can promote more efficient. As shown in **Fig. 4-28**, Samples **6** and **7** achieve larger wetted areas of 126.6 cm² and 152.3 cm² respectively. Samples **1**, **2** and **3** achieved smaller wetted areas of 24.3 cm², 57.3 cm² and 37.5 cm² respectively.

**Fig. 4-28: Wetted area.**

**Fig. 4-29: Diffusion rates.****Fig. 4-30: Evaporation rates.**

Among the remaining five fabrics, Samples **6** and **7** presented outstanding general performance in terms of final wetted area (126.6 cm² and 152.3 cm² respectively), average diffusion rates (0.506 cm²/s and 0.406 cm²/s respectively) and also average evaporation rates (0.316 mg/s and 0.345 mg/s respectively). However, further studies on their performance when they were bonded onto a heat exchanging sheet (aluminium) with water-resistant adhesive found Samples **6** and **7** became distorted after being wetted (see **Fig. 4-31**), which could affect

heat transfer within the HMX. Although the above adhesive method is difficult to realize for such thin materials as Samples 6 and 7, other methods, such as thermal bonding [4.6], could be applied to allow these materials to be used as a high-performance wet surface.



Fig. 4-31: Images of distorted fabrics. (a) sample 6; (b) sample 7

As shown in Figs. 4-28, 4-29 and 4-30, within Samples 1, 2, and 3, Sample 2, i.e. the Kraft paper, gives the lowest evaporation rate of 0.179 mg/s and the lowest diffusion rate of 0.102 cm²/s, although it has a slightly larger final wetted area of 57.3 cm². However, the result of 57.3 cm² was obtained with only 10 drops of water (0.5 ml). In practice, usually a much higher density of water drops are continually sprayed onto the wet surface, which would provide the increased wetted area. Therefore, the difference between the final wetted area among the three fabrics is less important than diffusion rate and evaporation rate. A higher diffusion rate can prevent the formation of continuous water film on the wet surface, which is detrimental to the water evaporation. Higher evaporation rate can, no doubt, provide a higher cooling efficiency. Therefore, Samples 1 and 3, which have relatively higher diffusion rates of 0.116 cm²/s and 0.140 cm²/s respectively and evaporation rates of 0.215 mg/s and 0.204 mg/s respectively, are considered to have general better performance than Sample 2, i.e. Kraft paper. It was also found that Samples 1, 2 and 3 demonstrated good mechanical

performance when they were bonded onto an aluminium sheet with water-resistant adhesive.

(3) Evaluation of the results from the tested fabrics

Based on the above experimental work, a summary of the performance of the tested fabrics is shown in **Table 4-8**.

Table 4-8: Summary of the performance of the tested fabrics.

Sample No.	Performance				Suitability
	Vertical wicking	Diffusion	Evaporation	Mechanical	
1	higher	higher	higher	good	suitable with higher performance
2	lowest	lowest	lowest	good	suitable with lower performance
3	higher	higher	higher	good	suitable with higher performance
4	higher	Immediate natural diffusion is not good			not suitable
5	lower	Immediate natural diffusion is not good			not suitable
6	lower	highest diffusion	highest evaporation	Adhered surface distorted	Suitable with higher performance (not good for adhesive)
7	lower	highest diffusion	highest evaporation	Adhered surface distorted	Suitable with higher performance (not good for adhesive)

As shown in **Table 4-8**, Samples **4** and **5** are not desirable choices to be used as wetted media within evaporative coolers due to their poor characteristics of immediate natural diffusion. Samples **6** and **7** are too thin to be bonded with the exchanging sheet with adhesive, but other bonding approaches might work. Except for Samples **4** and **5**, other samples (**1**, **3**, **6** and **7**) showed better performance regarding to their wicking, diffusion and evaporation ability, compared to Kraft paper. The results showed that the cloth fabrics, i.e. Samples **1**, **3**, **6** and **7**, have great potential in terms of achieving more efficient water evaporation. The percentage increase in fabric performance compared to Kraft paper is shown in **Table 4-9**.

Table 4-9: Percentage increase in performance relative to Kraft paper.

Performance	Vertical wicking rate	Diffusion rate	Evaporation rate
Sample 1	182%	14%	20%
Sample 3	171%	37%	14%
Sample 6	24%	396%	77%
Sample 7	7%	298%	93%

For large scale indirect evaporative coolers, appropriate fabric adhered to rigid supportive sheet has been found the most effective and simple way to construct a wet channel wall. For this reason, it is considered that Samples **1** and **3** are the most suitable materials for this application and will offer great potential to enhance the efficiency of dew point cooling system.

(4) Final selection

As per the test results, the knitted (double) pique mesh *Coolmax*® fabric (100% *Coolmax*® fibre) was finally selected to be applied to the prototype.

4.5.3 Adhesive

In the sandwich structure, adhesive is responsible for bonding the aluminium plate and the *Coolmax*® fabric tightly together and transfer heat through. The work condition includes contacting with water all the time. Superior to other adhesives ever tried e.g. silicone glue in bond strength, no-blocking fabric and ease to process, a kind of marine adhesive, i.e. *Sikaflex*®291i shown in **Fig. 4-32**, was tested and finally selected to implement in the prototype fabrication.

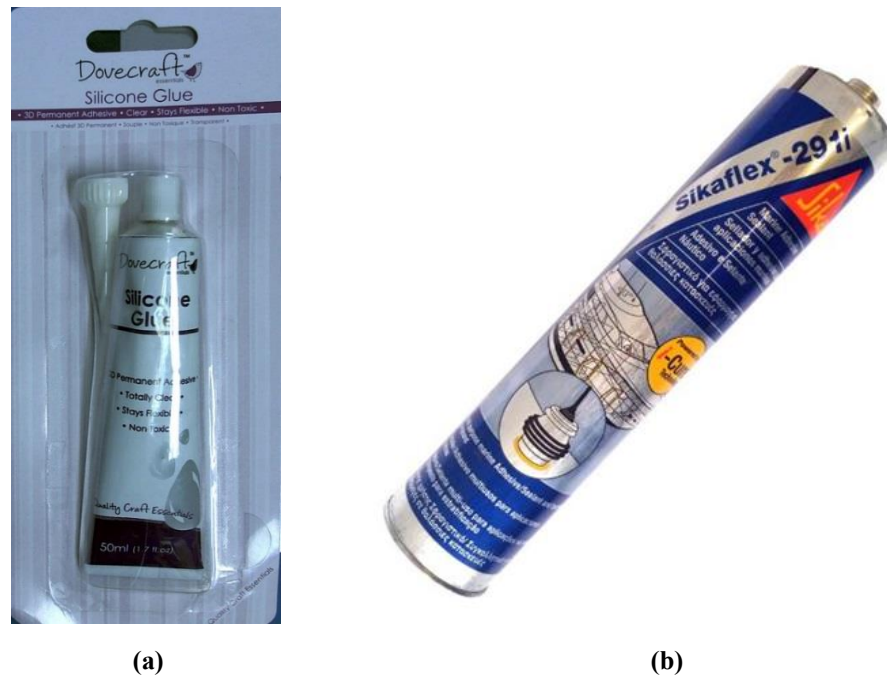


Fig. 4-32: Adhesive. (a) Silicone glue; (b) Sikaflex®291i

Sikaflex®291i is a non-sag 1-C polyurethane sealant specifically developed for the marine market, which cures on exposure to atmospheric moisture and forms a durable elastomer. It benefits in single component (1-C), highly elastic to be able to resist the following mechanical formation process, non-corrosive, low odour and VOC and emission free.

Sikaflex®-291i is mainly a multipurpose product used in marine constructions. It is suitable for making elastic, vibration-resistant joint seals, and can also be used for a variety of interior and exterior sealing applications. *Sikaflex®-291i* is resistant to fresh water, seawater, limewater, sewage effluent, diluted acids and caustic solutions; temporarily resistant to fuels, mineral oils, vegetable and animal fats and oils; not resistant to organic acids, alcohol, concentrated mineral acids and caustic solutions or solvents.

Some of the properties of *Sikaflex®291i* is listed in **Table 4-10**.

Table 4-10: Properties of Sikaflex®291i.

Chemical base	1-C polyurethane
Colour (CQP ¹ 001-1)	White, grey, black, brown
Cure mechanism	Moisture-curing
Density (uncured) (CQP 006-4)	(depending on colour) 1.3 kg/l approx.
Non-sag properties	Good
Application temperature	ambient 10 - 40°C (50 - 105°F)
Tack free time ² (CQP 019-1)	60 min. approx.
Open time ² (CQP 526-1)	45 min. approx.
Curing speed (CQP 049-1)	(see diagram)
Shrinkage (CQP 014-1)	2% approx.
Shore A-hardness (CQP 023-1 / ISO 868)	40 approx.
Tensile strength (CQP 036-1 / ISO 37)	1.8 MPa approx
Elongation at break (CQP 036-1 / ISO 37)	500% approx.
Tear propagation resistance (CQP 045-1/ ISO 34)	7 N/mm approx
Glass transition temperature (CQP 509 -1/ ISO 4663)	-45°C (-50°F) approx.
Service temperature (CQP 513-1)	-40 - 90°C (-40 - 195°F)
Short term	4 hours 120°C (250°F) 1 hour 140°C (285°F)
Shelf life (storage below 25°C) (CQP 016-1)	12 months

¹⁾ CQP= Corporate Quality Procedure ²⁾ 23°C / 50% r.h.

4.6 HMX Fabrication and Prototype Assembly

4.6.1 HMX

HMX plates fabrication

The HMX plate fabrication follows the process schematic in **Fig. 4-33**.

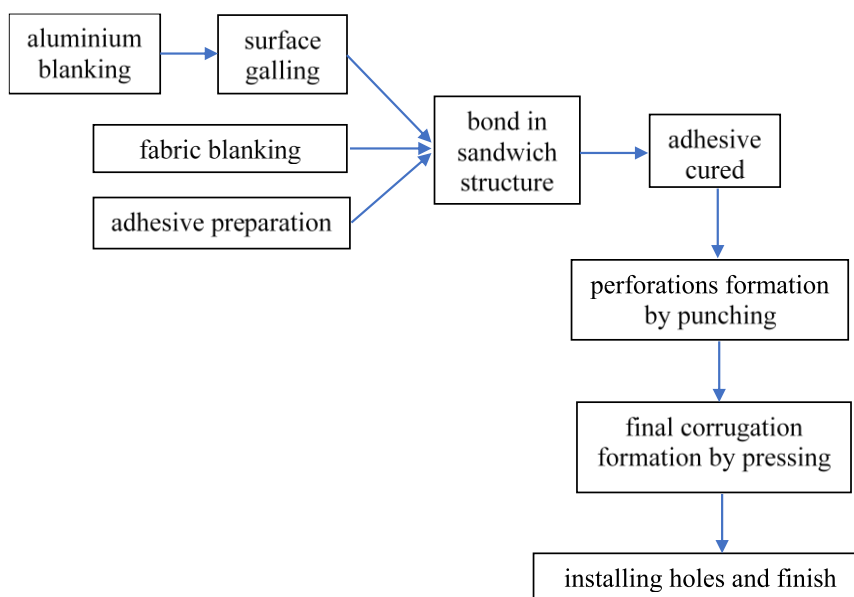


Fig. 4-33: HMX plates fabrication process.

The preparation of the fabric/adhesive/aluminium sandwich plate, including aluminium and fabric blanking, surface treatment, bonding and curing process, was conducted manually in a workshop. **Fig. 4-34** shows the material preparation in workshop for the following mechanical process.

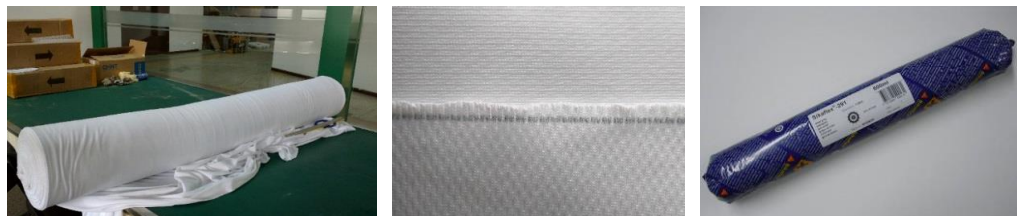
Coolmax® fabric and aluminium rolls were cut into the required sizes. One of the aluminium smooth surfaces was roughened by electric grinder manually. The marine adhesive was smeared evenly onto the roughened surface and covered by the *Coolmax*® fabric. Keeping the compound sheets under an even pressure for over 10 hours then the fabric and aluminium sheet can be integrated tightly.



(a) Aluminium plate blank

(b) Surface galling

(c) Roughened surface

(d) *Coolmax*® fabric roll

(e) Fabric detail (both sides)

(f) *Sikaflex*®-291i adhesive

(g) Spreading the adhesive

(h) Fabric to aluminium bonding

Fig. 4-34: Material preparation in workshop.

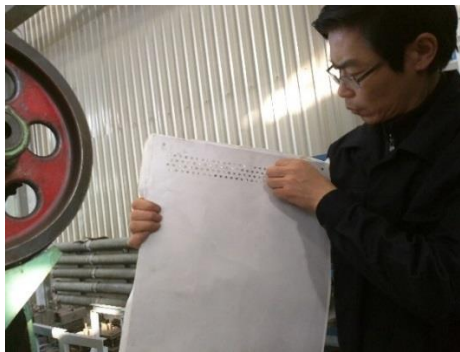
The cured sandwich plane sheets were punched and pressed successively with the pre-prepared moulds and finished with edge cutting and install holes opening manually piece by piece. **Fig. 4-35** shows the formation process of the irregular shape exchanging sheets.



(a) Punching mould in position



(b) A sandwich sheet ready to be punched



(c) Perforations formation



(d) Pressing mould in position



(e) A punched sheet ready for pressed

Fig. 4-35: Formation process of the irregular shape exchanging sheets.

Fig. 4-36 presents a finished irregular shape exchanging sheet with local details.



(a) A finished exchanging sheet



(b) Fabric (wet) side detail



(c) Aluminium (dry) side detail

Fig. 4-36: A finished irregular shape exchanging sheet.

HMX Assembly

The exchanging sheets were stacked together with 16 long threaded rods through the mounting holes. The stacked sheets form the alternative dry and wet channels with a controlled uniform interval of 5 mm by gaskets. The gaps between two exchanging sheets were filled with rubber strips on the edge and the outsides

were waterproofed with marine glue. The top side of wet channels and bottom sides of dry channels were treated in the same way.

The final HMX is composed of 200 corrugated sheets, which was divided into 10 groups, i.e. each group of 20 sheets. For assembly, the individual group of sheets was assembled firstly to produce a sub-unit. Then the 10 sub-units were assembled to constitute the final heat exchanger.

Fig. 4-37 presents the alternative dry and wet channels of the assembled HMX in bottom view.



(a) The complete assembled HMX in bottom view

(b) Detail of the channels

Fig. 4-37: Assembled HMX.

4.6.2 Water Distributor

The quality of water distribution affects the evaporation performance greatly. As per the patented design [4.3], firstly, a water distributor was trial-manufactured and tested to validate the performance. **Fig. 4-38** shows the water distributor under test. Then the water distributor was carefully produced with copper for the cooler prototype. **Fig. 4-39** presents the finished water distributor and **Fig. 4-40** shows the water distributor in assembly with the stacked exchanging sheets. The test of water distributing indicated that the fabric surface could be infiltrated evenly under controlled minimum static water pressure of about 3.0 kPa.

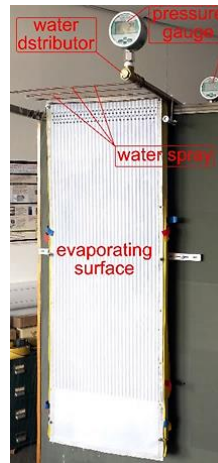


Fig. 4-38: Test and demonstration system of water distributing.

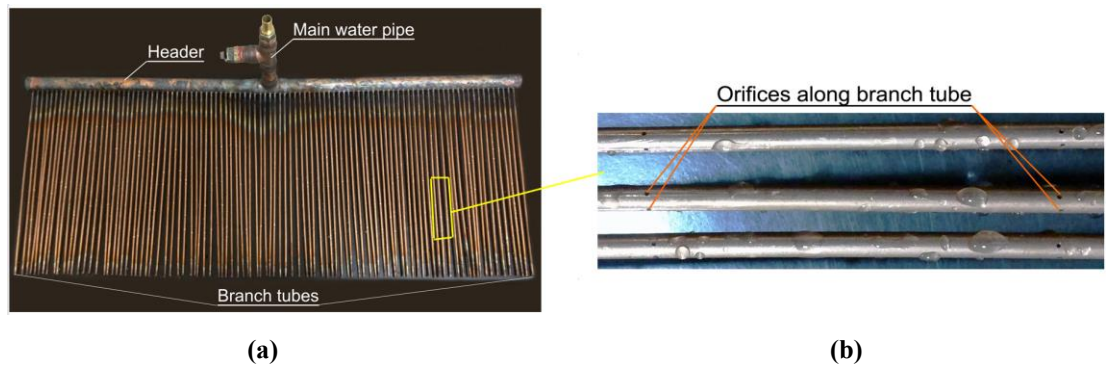


Fig. 4-39: Structural view of the Water distributing system.
 (a) water distributor; (b) openings setting on the distribution pipes

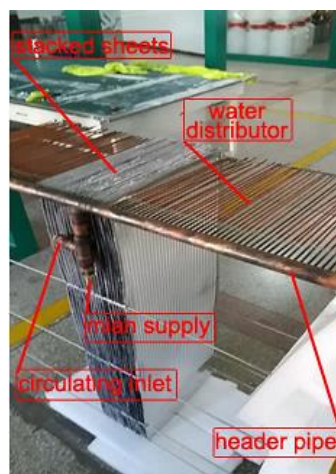


Fig. 4-40: Water distributor in assembly.

The configuration, as shown in **Fig. 5-39(a)**, comprises a main water supply pipe, a horizontal water header and numerous small-sized water distribution tubes, all of which were appropriately jointed together to form an integrated unit. A single distribution tube is drilled with numerous tiny openings (0.5 mm in diameter and diminishing gaps between the two adjacent openings as per the change of water flow rate along each branch pipe, refer to **Fig. 4-39(b)**) and inserted into a wet channel of the heat and mass exchanger (**Fig. 4-40**). This allows the water to be delivered into each wet channel with the equal flow rate and even water distribution across its wet surface.

4.6.3 Fan housing, Louvres and Water Sink

The selected backward curved centrifugal fans, *ebm-papst*® K3G225-RE07-03, can exhaust air full 360° circumference of the impeller without a scroll around the wheel. A simple housing, shown in **Fig. 4-41**, was produced and fitted around the impeller to guide the air in one direction. In addition, the half scroll can be applied to slightly improve the flow around the inside of the box which has four sides and acts as a plenum. The fan exhausts the air into the plenum and the air turns right angles to exhaust out.



Fig. 4-41: Fan and housing.

To prevent the suction of dripping water around the inlet of the lower exhaust fans, louvres were installed as shown in **Fig. 4-42**.



Fig. 4-42: Louvres on the fan housing.

A Propene Polymer (PP) water sink equipped with water detectors was produced and fitted closely beneath the fan housings, shown in **Fig. 4-43**.

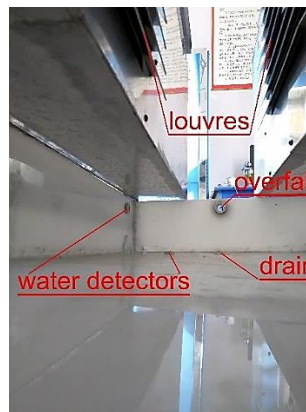


Fig. 4-43: Water sink in position.

4.6.4 Fans, Pump and Control Components

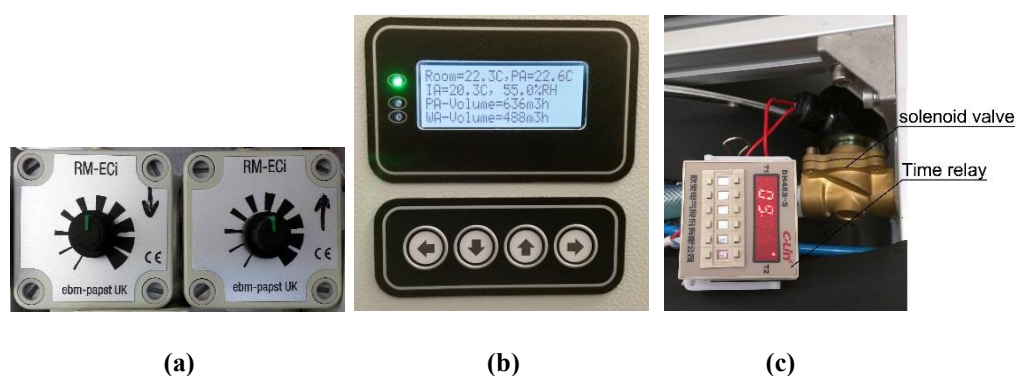
Four energy efficient fans, two for the supply air and the other two for the exhaust air, and one circulating pump, were selected. To enable the timely alteration between the selected operating schemes, the dedicated fan and pump controllers were selected and their technical specifications are presented in **Table 4-11**.

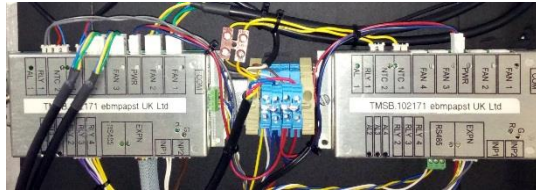
Table 4-11: Specification of fans, pump and controllers

Component	Specification	Quantity
Supply air fan	R3G225-RE07-03, <i>ebm-papst Ltd</i> , fan speed 2865/min, 705m ³ /hr, 458 Pa, 160W	2
Exhaust air fan	R3G225-RE07-03, <i>ebm-papst Ltd</i> , fan speed 2865/min, 705m ³ /hr, 458 Pa, 160W	2
Circulating water pump	DH40H-24110, <i>Shenzhen Zhongke Century Technology Ltd</i> , 24V/ 1.2A DC, 11mH ₂ O, 450L/hr	1
Fan controller	980-CAS11007 - TMS Controller, <i>ebm-papst Ltd</i>	1
Pump controller	DH48S-S, <i>Xinling Electrical Co. Ltd</i>	1

The rotation speeds of the supply and exhaust fans were manually adjustable by two assorted *RM-ECi* fan controllers (shown in **Fig. 4-44(a)**) at lab testing stage and finished by panel display and input (as shown in **Fig. 4-44(b)**) at demonstration stage.

The running of the circulating water pump is time controlled by a time relay (shown in **Fig. 4-44(c)**) and the on-off of main water supply is under the control of a solenoid valve (shown in **Fig. 4-44(c)**) as per the dedicated control logic described in **Chapter 3**. The control of feeding water pressure depends on a pipeline valve along with the monitor by a pressure gauge (shown in **Fig. 4-44(e)**). The water detectors/transducers (**Fig. 4-44(f)**), air differential pressure sensors (**Fig. 4-44(g)**) and the system controller (**Fig. 4-44(d)**) combine to make the water system and air system run in order.





(d)



(e)



(f)



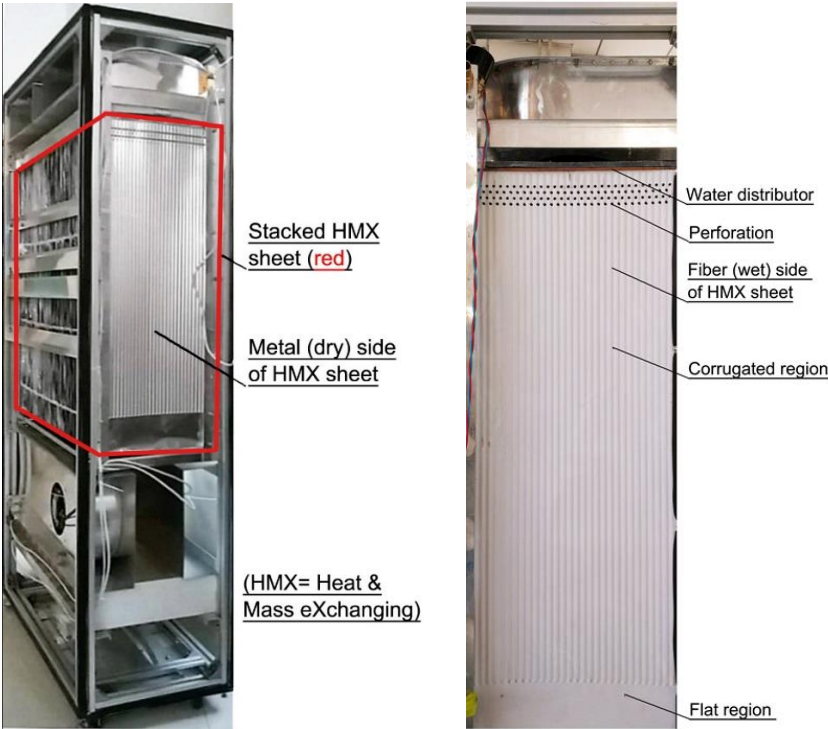
(g)

Fig. 4-44: components for fan and pump control.

(a) fan controller; (b) control panel; (c) solenoid valve and time relay;
 (d) system controller; (e) water pressure gauge and regulating valve;
 (f) transducers; (g) differential pressure sensor.

4.6.5 Prototype Assembly

All the pre-prepared components, i.e. fan units, HMX and water distributor etc., were fitted into a customized frame, insulated and equipped with pipes, electric circuits and controllers. The assembly process is demonstrated in **Fig. 4-45** and **Fig. 4-46**.



(a) HMX in position

(b) HMX detail



(c) Assembly in place

(d) Waterproof and insulation of the HMX

Fig. 4-45: Prototype assembly in progress.

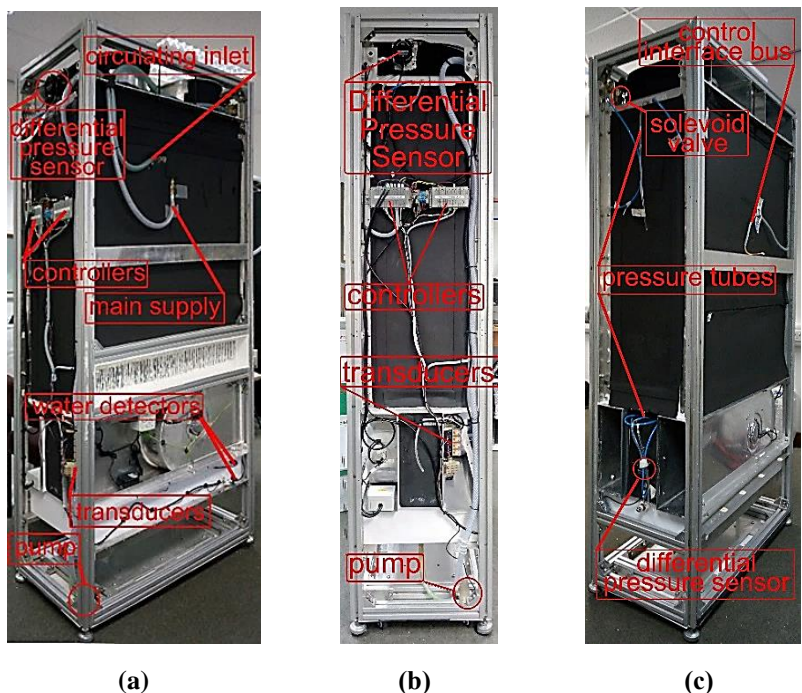


Fig. 4-46: Prototype equipped with accessories in 3-side view.

Finally, the unit was well covered with solid steel casing as shown in **Fig. 4-47**. **Fig. 4-46** presents the main components layout inside the casing from around 3-side view.

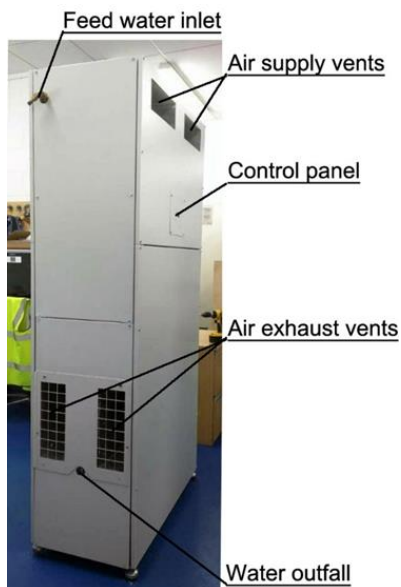


Fig. 4-47: Finishing air cooler prototype.

4.7 Chapter Summary

This chapter described the complete manufacturing process of the proposed DPC prototype, including detailed configuration design, material and manufacturing process trial, design/ selection of the main components, development of control logic and assembly of the whole system.

The fibrous material used as the evaporating medium on wet channel wall significantly influences the cooling performance. Seven commercial fibres were tested and finally one of the *Coolmax*® fabric extruded either in water diffusivity or moisture evaporation.

Mechanical forming of the irregular corrugated exchanging sheet is another key problem to realize the HMX design. Numerous trials were conducted to compromise between the material properties and the three-dimensional profile, by both changing the material and adjusting the design. As per the mechanical process trials, a little modification was made to the waved shape of the exchanging sheet in the final product. However, the lost exchanging area has been compensated by increasing the amount of exchanging sheets and eventually the entire exchanging area was maintained same with the original design.

A practical sandwich structure being able to bond the fabric and aluminium panel together and resist the mechanical deformation during the manufacturing process was developed to realize the design of the HMX.

Two sets of control system were developed. One was easy to manually adjust at the testing stage, and the other was later developed in C-language for demonstration with panel or external computer input and display.

Equipped with the dedicated water distributor, fans, circulating pump, water sink and control system, a novel DPC prototype, which realized all the

aforementioned innovative design and could almost be commoditized, was well constructed, waterproofed and insulated. Continuous improvement has been made during the entire process and the final pilot run indicated that it could run in proper conditions with cooler air delivery. It was ready to face the serious performance tests under various climatic and operational conditions in the following experimental investigation.

CHAPTER 5: TESTING IMPLEMENTION, RESULTS ANALYSIS AND VALIDATION/UPDATE OF THE COMPUTER MODEL

5.1 Chapter Introduction

This chapter introduces the development of the dedicated testing rigs for climatic conditions simulating and cooler performance evaluation. Ducting systems were designed to allow the full development of the airflow. An intake air regulating system was constructed to be able to supply the intake airflow at required conditions. The sensors and measuring instruments of temperature, humidity, pressure, flow rate, power meter etc., were fitted in position to enable the accurate parametrical measurement and data record.

Laboratory experiments were carried out under various climate conditions to evaluate the performance, e.g. wet-bulb and dew-point cooling effectiveness, cooling capacity, COP, and explore the performance potential of the innovative cooler. The cooling performance was also parallelly compared with the current product counterpart and the experimental results were discussed.

Based on the experimental results, dedicated update was applied to the self-developed general simulation tool, making it better reflect the technical innovation of the proposed DPC and predict the cooling effects more accurately.

The main work in this chapter is listed as follows.

- (1) Design and construct a testing rig for cooling performance evaluation.
- (2) Implement the systematic performance tests under standard inlet conditions and identify the optimum working air ratio of the prototype.

- (3) Parallely compare the cooling performance with the product M30 dew point cooler (*Coolerado*[®] USA) under various intake air conditions.
- (4) Conduct performance tests under various inlet conditions at the optimum working air ratio.
- (5) Validate and update the simulation model established in **Chapter 3** with the experimental results.

As a result, the prototype system was proven to have super cooling performance, especially in energy efficiency, under appropriate climatic conditions. The dedicated simulation model was thus regarded reliable in predicting the system annual performance for the socio-economic analysis in **chapter 6**.

5.2 Design of the Testing Rig

To comprehensively evaluate the cooler prototype, various input parameters and operating conditions should be included. The testing platform is such a system that facilitates to realize the required test conditions and accurate parameters measurement. A high-power electric heater is designed to increase the intake air temperature, humidifier/dehumidifier for air moisture control, mixer selector valves help to further adjust the air parameters. For fully developed airflow and accurate measurement of the air parameters, adequate straight pipe length prior to and after the gauge point is maintained, e.g. 10/5 times distance of the pipe diameter prior to/after the gauge point. The layout of the piping system in a 40 m² exclusive lab is shown as **Fig. 5-1**. The details of the accessories at the inlet air treatment section are shown in **Fig. 5-2**. The organization of the air and water flow and the deploy of measure point is shown in **Fig. 5-3**.

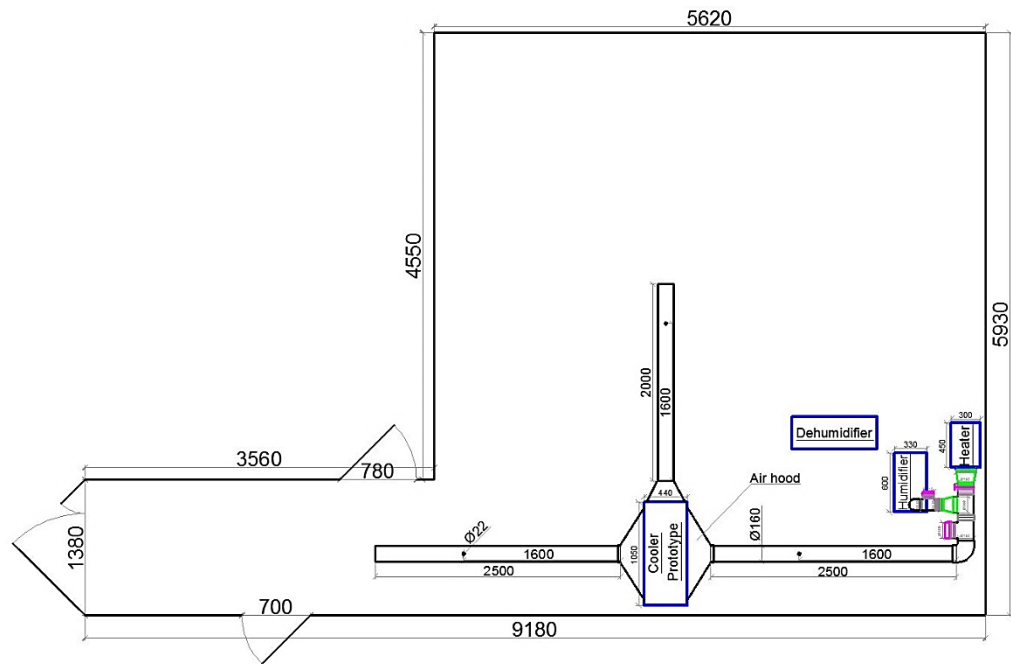


Fig. 5-1: Layout of the piping system in the lab.

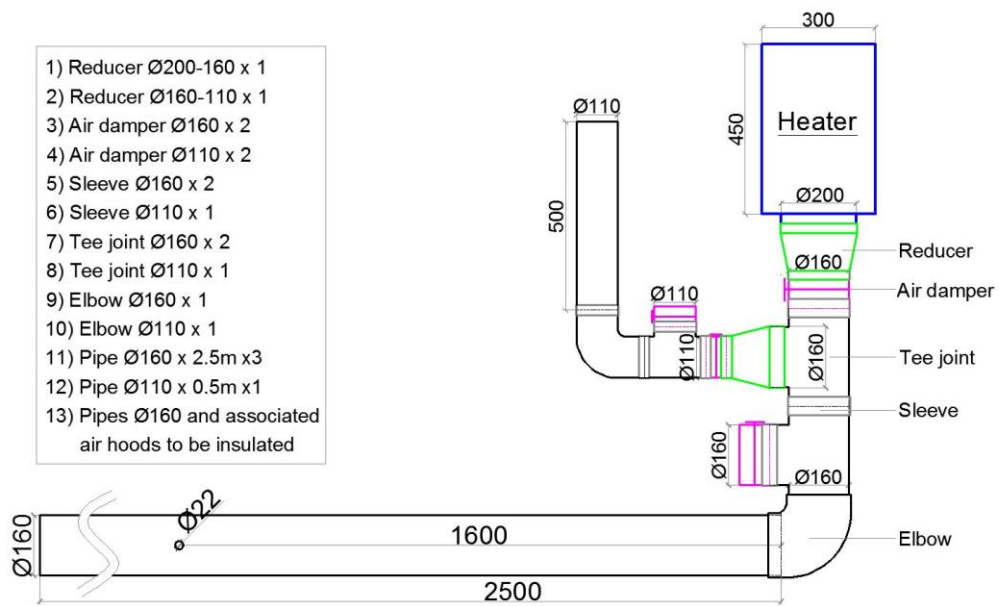


Fig. 5-2: Airflow regulation system prior to the entrance.

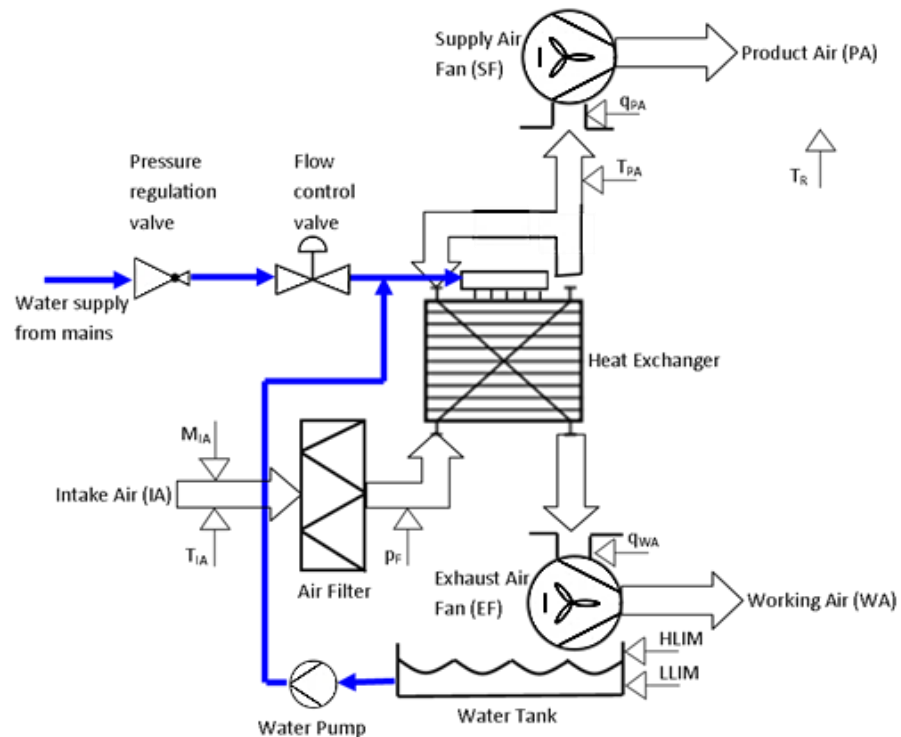


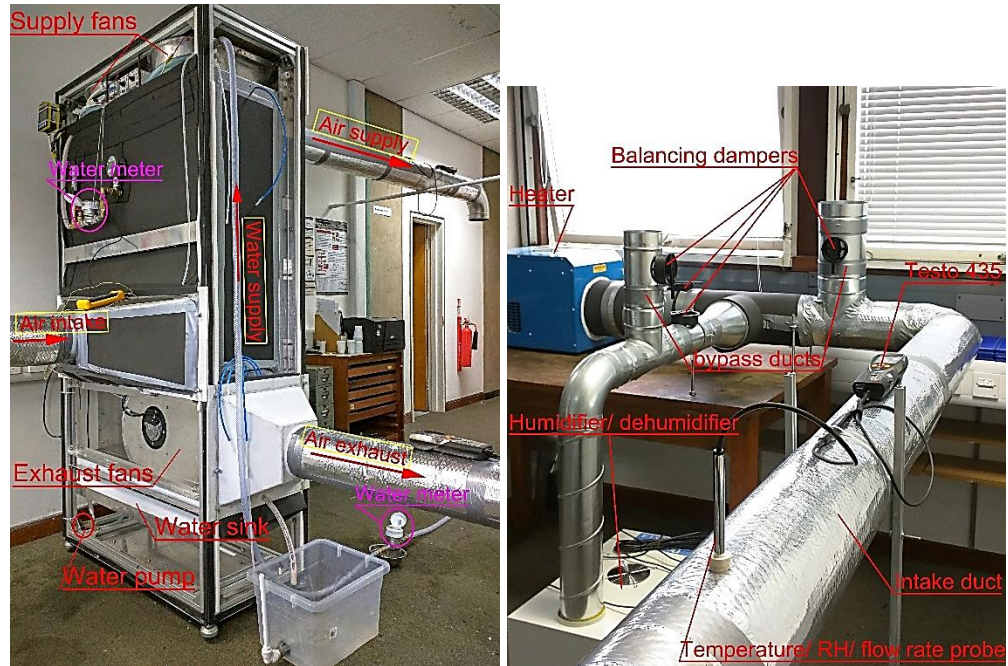
Fig. 5-3: Organization of the air and water flow and measure points deployment.

5.3 Experimental Instruments and Testing System

5.3.1 Intake Air Regulating System

To enable the accurate parametrical measurement of the 4-kW rated prototype dew point air cooler, a dedicated test rig was constructed. This rig, as shown in **Fig. 5-4**, comprises an intake air regulating system, discharging and supply air ducting systems, as well as associated measurement instruments that were fitted into the appropriate positions of the duct lines and the cooler interior. The intake air regulating system comprises a high-power electrical heater (**Fig. 5-5(a)**), a humidifier (**Fig. 5-5(b)**), a dehumidifier (**Fig. 5-5(c)**), ducts and dampers (**Fig. 5-4(b)**), all of which were integrated into a dedicated fan and ducting system to

provide a variety of intake air parameters that can simulate the different climatic conditions across the world.



(a) Prototype system

(b) Intake air regulation system

Fig. 5-4: Testing system.



(a) Electric air heater



(b) Humidifier

(c) Dehumidifier

Fig. 5-5: Auxiliary equipment to help create required air conditions.

The technical specifications of the individual components of the intake air regulating system are presented in **Table 5-1**.

Table 5-1: Major components in the intake air regulation system.

Component	Specification	Quantity
Electric heater/ auxiliary fan	FF13T-13 electric heater 13.9kW, 16 amps, 415v, 3-phase/ airflow rate 1017m ³ /hr, 400 Pa ₂	1
Humidifier	DRS-06A 600W, 6kg/hr	1
Dehumidifier	Igenix IG9805 Portable Dehumidifier R-410A, 740W - 50L/day (30 and 80 % RH)	1
Ducting/ fittings	Spiral steel ducts ϕ 160, couplings, pressed tees, reducers with thermal insulation	10m
Dampers	Manual balancing dampers with single round blade and 23 adjustable levels	6

5.3.2 Parameters Measurement System

The layout of the measurement instruments is demonstrated in **Fig. 5-4** and **Fig. 5-6**.



Fig. 5-6: Layout of the measurement instruments and control elements.

Similar to the intake air regulating system, the combined ducting and auxiliary fan systems were also connected to the supply and discharging air vents of the prototype dew point air cooler. These systems were dedicatedly configured to enable the accurate measurement of the temperature, humidity, and air velocity of the two air streams, by creating a stabilised airflow states at the measurement sections. In particular, the auxiliary fans installed in the two systems were dedicated to compensating the pressure losses resulted from the ducting systems, thus creating the zero-pressure conditions at the outlets of the discharge and supply air vents. The technical specifications of the individual components of the measuring system are presented in **Table 5-2**.

Table 5-2: Individual components in the supply and discharge air delivery system.

Component	Specification	Quantity
Ducting/ fittings	Spiral steel ducts $\phi 160$, couplings, pressed tees, reducers with thermal insulation	8m each
Fan	EBM-Papst DC axial fan – 6314N/2 TDHHP, 970 m ³ /h	1 each
Dampers	Manual balancing dampers with single round blade and 23 adjustable levels	1 each

Further, the dedicated multi-functional measurement instruments, namely *Testo*® 435-2-multi-function instrument for VAC (Ventilation and Air Conditioning) & IAQ (Indoor Air Quality) shown in **Fig. 5-7(a)**, were installed on the supply, discharge and intake air duct lines for measurement of the temperature and humidity (**Fig. 5-7(b)**). The installation positions were 10 times the duct diameter away from the vents and other local fittings that allowed the establishment of the steady airflows at the measurement sections for purpose of the accurate reading. Thermal couples (**Fig. 5-7(c) and (d)**) were positioned at the outlet of dry channels to double check the PA temperature delivered by *Testo*® 435. *Testo*® resistance thermometer sensors (**Fig. 5-7(e)**) were used to measure the water temperature at the inlet of the water distributor and outlet of wet channels.

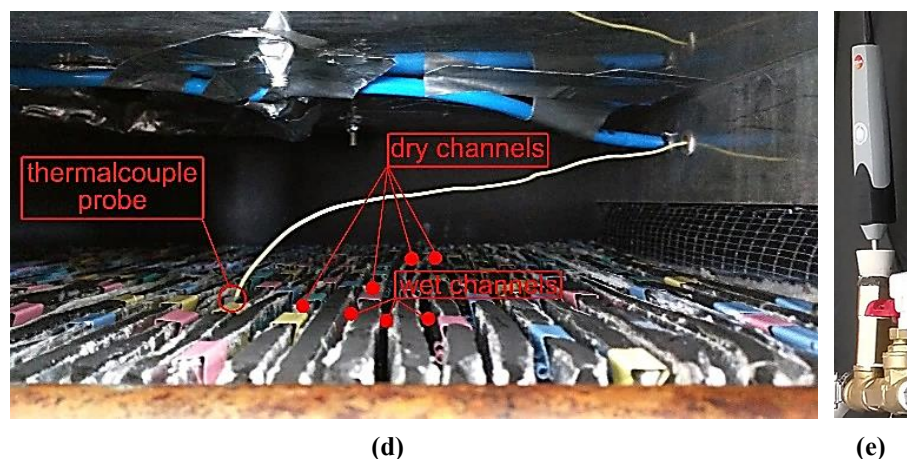
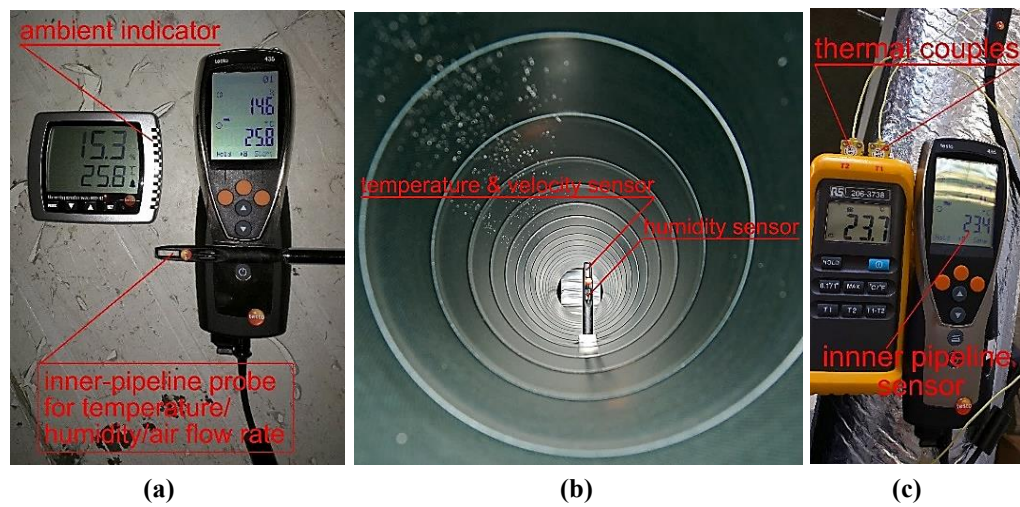


Fig. 5-7: Temperature measuring instruments.

- (a) *Testo*® 435 and ambient indicator;
- (b) *Testo*® temperature/humidity/airflow rate probe positioned in the test duct;
- (c) *Testo*® 435 and thermocouple data processor;
- (d) thermocouple in position;
- (e) *Testo*® resistance thermometer for water temperature

The micro manometers *DPM*® ST650 and auxiliary sample rings were installed at the inlets of the fans to measure the airflow rates [5.1], as shown in **Fig. 5-8**.

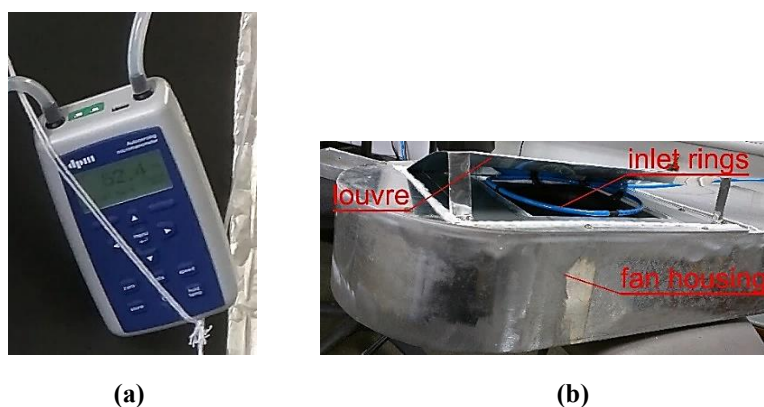


Fig. 5-8: Pressure and airflow rate measuring instruments.
 (a) manometers *DPM*® ST650; (b) pressure sampling system

Meanwhile, an *ABB*® power meter (**Fig. 5-9(a)**) was used to measure the fan power consumption and a variable DC power supply (**Fig. 5-9(b)**) was applied to measure the power consumption by the water pump.

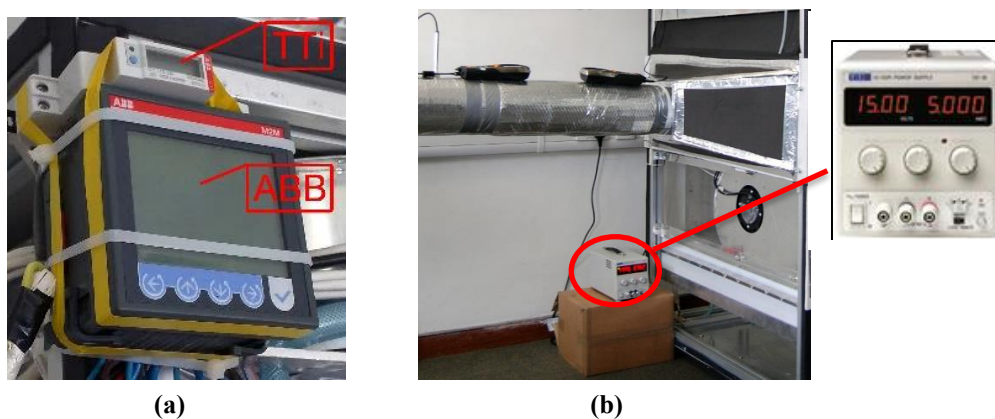


Fig. 5-9: Power meters.
 (a) *ABB*® power meter for fans; (b) variable DC power supply and meter for pump

Two water meters (**Fig. 5-4(a)** and **Fig. 5-6**) were connected to the piping loop to measure the water flow rate supplied to the wet channels of the heat and mass

exchanger and the total water consumption by evaporation function. A pressure gauge (**Fig. 4-44(e)** and **Fig. 5-6**) installed at the inlet of the water supplier/distributor was used to monitor water pressure to ensure achieving the optimum pressure of 3.0 kPa for the even water distribution across the wet surfaces.

All the measuring instruments were calibrated prior to their experimental usage (**Fig. 5-7(a)** and **(c)**). Further, the fan controllers (**Fig. 4-44(a)** and **(b)**) were used to adjust the fan speed to obtain different working air ratios and varying cooling capacities. The major instruments for measurement are listed in **Table 5-3**.

Table 5-3: Specification of the major measurement instruments.

Instrument	Specification	Quantity
Temperature/humidity/air flow rate probe	Testo, thermal velocity probes with built-in temperature and humidity measurement, ± 0.3 °C, ± 2 %RH (+2 to +98 %RH), $\pm (0.03$ m/s +4% of mv)	3
Instrument used with probe	Testo 435-2/4-multi-function instrument for VAC & IAQ, Accuracy ± 1 digit, ± 0.02 hPa (0 to +2 hPa), $\pm 1\%$ of mv (remaining range) ; Resolution 0.1 %RH, 0.01 hPa / 200 hPa	3
Air pressure meter	DPM, ST650 micromanometer, Accuracy: ± 2 counts (Readings < 100 counts); $\pm 1\%$ of reading ± 1 count (Readings > 100 counts)	2
Water pressure gauge	Hangzhou Asmik Sensor Technology Co. Ltd, MIK-Y190, digital pressure gauge, 0.4%fs	1
Fan power meter	ABB, M2M LCD digital power meter, 1 Phase, Accuracy ± 0.5 %	1
Pump power meter	TTi, EL 155R DC Power supply, 15V 5A, Resolution: 10mV, 1mA; Accuracy: 0.3% of reading ± 3 digits (Voltage Meter), 0.5% of reading ± 3 digits (Current Meter)	1
Water meter	Ningbo Amico Inc., LYH-8, 600L/hr, resolution 0.005L	2



Fig. 5-10: Piping system.

Fig. 5-10 presents an overview of the piping system from two perspectives. **Fig. 5-11** demonstrates the system in demo operation with process parameters being projected onto a large wall-mounted screen real-timely via the dedicatedly developed control and data acquisition program in C-language (**Appendix 1**).



Fig. 5-11: The proposed dew point air cooler prototype in demo operation.

5.4 Implementation of the Systematic Testing

During operation, the electric heater, humidifier (or dehumidifier) and dampers in combination created the required temperature and humidity of the intake air, by mixing up the two parts of air (one from the heater and the other from the humidifier (or dehumidifier)) at the proper volume flow rate proportion. Meanwhile, the auxiliary fan and ducting system were applied to deliver the conditioned air into the cooler and maintained its zero static-pressure status at the inlet of the cooling unit. Various intake air conditions, reflecting the hot & dry, warm & dry, warm & humid and moderate climatic characteristics, were created as per the test requirements.

According to the difficulty of adjustment in practice, the entire experiments were carried out at different parametric levels. Firstly, the tests were performed at a fixed intake airflow rate, which was realized with the upper supply fans. Under each intake airflow rate, secondly to vary the lower exhaust fans to get series of working-to-intake air ratio. Under a set of intake airflow rate and working air ratio, thirdly to adjust the electric air heater to achieve various intake air temperature. Finally, with the fixed intake airflow rate, working air ratio and intake air temperature, to realize the required humidity with the humidifier/dehumidifier.

The main results were attained by strictly following the test procedure below.

- (1) Power on the prototype and set the upper supply fans at a pre-set airflow rate.
- (2) Adjust the lower exhaust fans to make a rough pre-set working air ratio.
- (3) Carefully tune the supply fans and exhaust fans simultaneously to eliminate the coupling effects in between to realize the required intake airflow rate and working air ratio.
- (4) Connect the prototype to the ducting systems equipped with measuring instruments and adjust the auxiliary fans to realize zero static-pressure status at each inlet and outlet of the cooling unit to remove the flow resistance brought by the ducting systems.
- (5) Regulate the electric air heater to achieve the pre-set intake air temperature.
- (6) Vary the humidifier or dehumidifier to get series of humidity states of intake air and record the measuring data under each set of intake air condition.

Alter the intake air parameters in reverse order, i.e. temperature and then working air ratio, to acquire the entire performance data under a certain intake

airflow rate. Repeat the operation under serial intake airflow rate to complete the performance test under various inlet conditions of temperature, humidity and airflow rate.

Besides, the impacts of water temperature and flow rate were also observed under certain testing conditions.

It is worth mentioning that all the final results were obtained from five sets of testing, each taking 5-minute long at least and average values of the testing data being recorded at steady states.

5.5 Performance Testing and Results Discussion

5.5.1 Performance Testing under Various Climates at Working Air Ratio of 0.44 (Test 1)

The tests being carried out at the working air ratio of around 0.44 ratio based on the competitor's design state, created identical operational conditions between the proposed cooler and an M30 (*Coolerado*® USA) dew point cooler (DPC) for convenience of the performance comparison.

During the series of test, the product airflow rate was aimed to adjust to around 750 m³/h (for designed 4-kW cooling rate) and exhaust airflow rate to around 600 m³/h, thus yielding the pre-set working air ratio of 0.44. However, in practice, due to the inevitable fluctuation of the devices' output from the fans, heater, humidifier etc., although the variations were controlled in limited ranges, it was impossible to exactly fix the working condition at a specific point for a while. To acquire relatively accurate results, the final data under each experimental condition presented in this thesis were the mean values of five independent

measurements during a consecutive period of steady operation. The error bar at each point is included in the following corresponding figures. [5.2]

The tests covered six intake air conditions which represented the design outdoor summer parameters for the cities of Riyadh (Saudi Arabia), Las Vegas (US), Kashi (China), London (UK) and Beijing (China) [5.3, 5.4], as well as the *Coolerado*® M30 testing conditions [3.14, 4.1]. Four different climate characters as per *Köppen* climate classification [5.5], i.e. hot dry, warm dry, warm humid and moderate, were referred to as shown in **Fig. 5-12**. These data and the pre-set product/exhaust/working air flow rates are presented in **Table 5-4**.

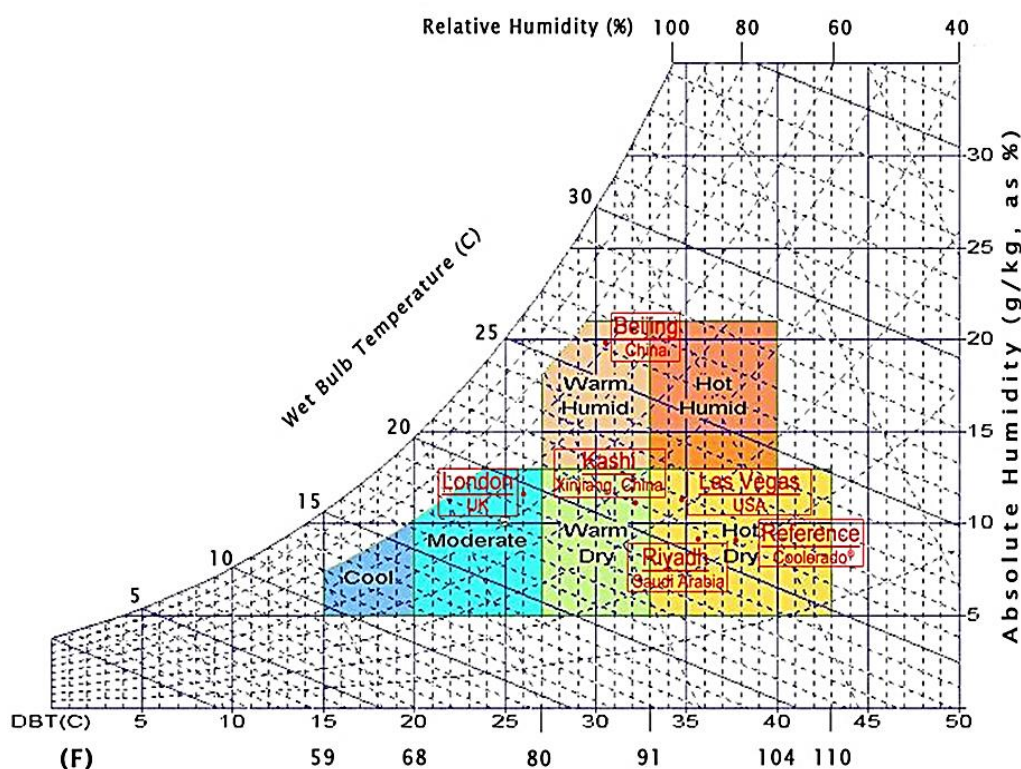


Fig. 5-12: Climate characters at the psychrometric chart.

Table 5-4: Testing conditions (Test 1)

Location	External design conditions			PA	EA	Working air ratio
	DB (°C)	WB (°C)	RH (%)	Flow rate (m ³ /h)		
Coolerado® M30 (US)	37.8	21.1	21.7	750	600	0.44
Riyadh, Saudi Arabia	35.6	20.6	25			
Las Vegas, US	34.8	21.9	32.2			
Kashi, China	32.1	21	36.9			
London, UK	26	19.6	55.5			
Beijing, China	30.5	26.2	71.5			
DB—Dry bulb temperature, °C; WB—Wet bulb temperature, °C; RH—Relative humidity, %;						
PA—Product air; EA—Exhaust air; Working air ratio—Working-to-intake air ratio.						

The test results are shown in **Table 5-5** and **Fig. 5-13**. **Table 5-5** lists the parametrical data, including product air (PA) temperature, air temperature drop, cooling capacity, COP, cooling effectiveness, exhaust air (EA) relative humidity (RH) as well as the system power consumption. It was found that for all sets of tests, the wet-bulb cooling effectiveness (WBE) was in the range 100%-109.8% and the dew-point cooling effectiveness (DPE) was in the range 67%-76.3%, while the exhaust air RH was as high as 90.7%-94.3%, indicating that the water evaporation within the wet channels was efficient to reach the approximate EA saturation [5.6].

Fig. 5-13 shows the comparison of the testing results (COP, cooling capacity and temperature drop) under six simulated intake air (IA) conditions that represent six aforementioned climates. It is clear that dryer intake air with lower relative humidity leads to higher temperature drop of the air, as well as higher cooling output and COP. The order of cooling performance from high to low is the *Coolerado*® M30 testing condition, followed by those for Riyadh, Las Vegas, Kashi, London and Beijing, as shown in **Table 5-5**. The highest performance, i.e. that under the *Coolerado*® M30 testing condition, gave a temperature drop of 17.1°C, cooling capacity of 4.2 kW and COP of 37.4; while the lowest

performance was found to occur under Beijing climate, with a temperature drop of 4.5°C, cooling capacity of 1.1 kW and COP of 9.7.

Table 5-5: Test results (Test 1)

	Tp	Td	Cooling capacity	COP	Wet _{eff}	Dew _{eff}	Fans power	RH of EA	Pump power
Location	(°C)	(°C)	(kW)	(-)	(-)	(-)	(W)	(-)	(W)
Coolerado®	20.8	17.1	4.25	37.4	102.4%	67.1%	112	94.3%	1.56
Riyadh	20.7	14.9	3.66	32.2	107.2%	72.0%	112	92.2%	
Las Vegas	20.4	14.5	3.56	31.3	109.8%	74.4%	112	92.9%	
Kashi	20.3	11.8	2.89	25.5	106.3%	71.1%	112	91.0%	
London	19.8	6.1	1.5	13.2	100.0%	67.0%	112	90.7%	
Beijing	26.0	4.5	1.1	9.7	102.3%	76.3%	112	92.0%	

Tp—product air temperature; Td—temperature drop;
Wet_{eff}—Wet bulb effectiveness; Dew_{eff}—Dew point effectiveness.

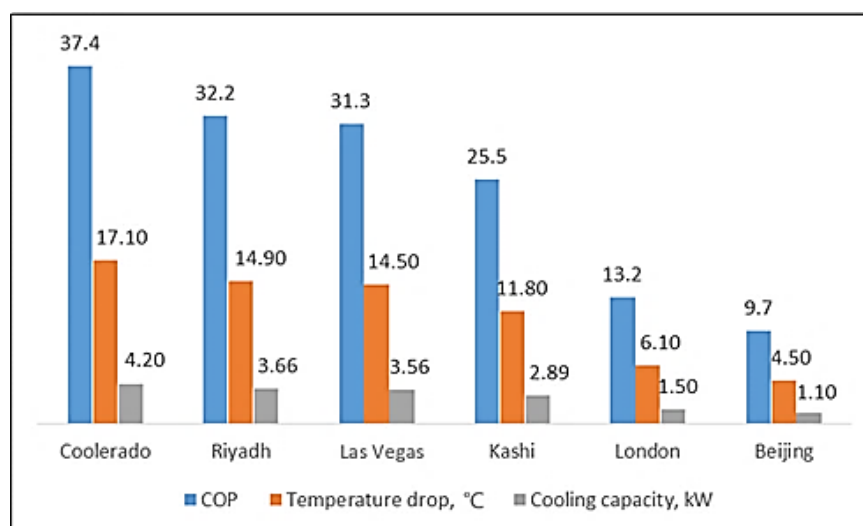


Fig. 5-13: Cooling performance under various climates (Test 1-working air ratio of 0.44).

5.5.2 Identification of the Optimum Working Air Ratio (Test 2)

The working air ratio represents the percentage of the exhaust air relative to the total intake air. The increased working air ratio leads to the decreased product airflow rate and increased temperature drop of the intake air. Since the cooling capacity of an air cooler is proportional to the product of the air temperature drop and corresponding flow rate, an optimum working air ratio would assume to be in existence that allows the highest cooling output to be achieved.

Series of tests were dedicated to identifying the optimum working air ratio of the prototype cooler. The IA conditions for the tests were set to exact the same as those for the *Coolerado*® M30 testing [5.7], i.e. 37.8°C of dry-bulb temperature and coincident wet-bulb temperature of 21.1°C.

With the fixed PA flow rate of 750 m³/h, a range of working airflow rates were generated to make different working air ratios. The comparison among the test results under different working air ratios was undertaken, suggesting an optimum working air ratio of 0.364, under which the cooler achieved the highest cooling output.

Fig. 5-14 shows the variation of the temperature drop and cooling capacity of the cooler under different working air ratios. It is found that at the optimum working air ratio of 0.364, the cooler achieves the maximum temperature drop of 19.1°C and cooling capacity of 4.75 kW. With the working air ratio increasing from 0.364 to 0.445, the temperature drop keeps falling. Inversely, with the working air ratio increasing from 0.268 to 0.364, the temperature drop continues to grow. This indicates that at the optimum working air ratio of 0.364, the water evaporation within the wet channels achieves the maximum that results in the best cooling effect of the cooler. As shown in **Fig. 5-15**, increasing the working air ratio leads to the decrease of the exhaust air RH, which confirms that the optimum working air ratio is 0.364 and further improving the working air ratio is hard to promote the EA saturation.

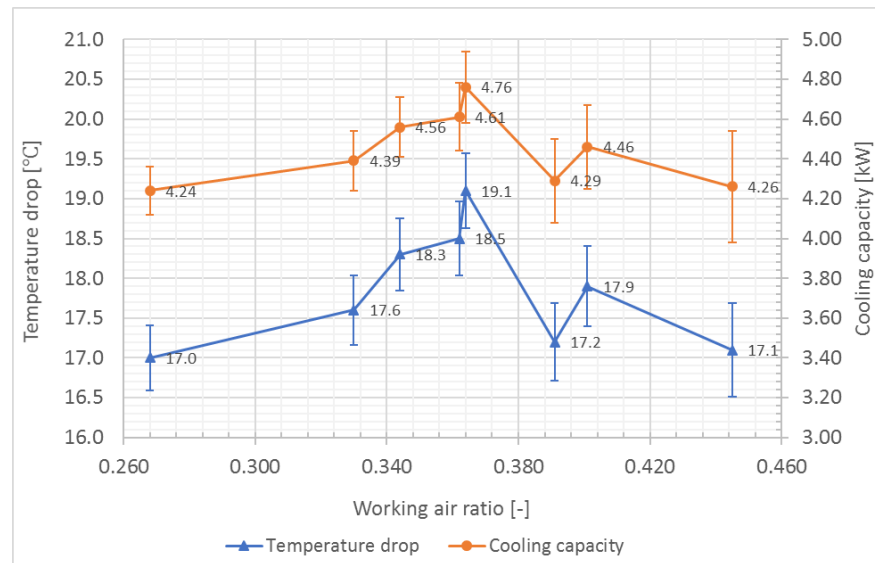


Fig. 5-14: Variation of the temperature drop and cooling capacity with working air ratio.

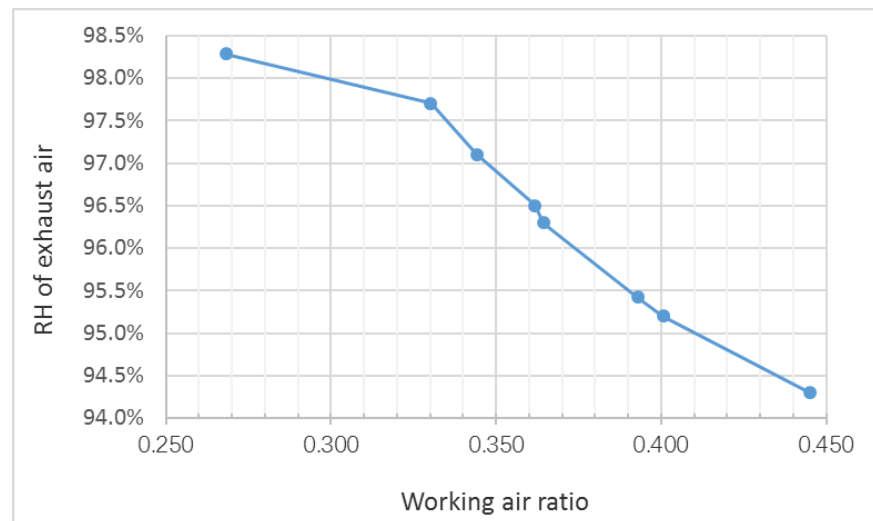


Fig. 5-15: RH of exhaust air under different working air ratio.

5.5.3 Performance Comparison between the Prototype and the M30 DPC (Test 3)

Based on the above tests, a comparison between the prototype's performance data and those of the M30 (*Coolerado*[®], US) is presented in **Table 5-6**. It is seen that under the *Coolerado*[®] M30 IA conditions (i.e., dry bulb-temperature of 37.8°C and coincident wet-bulb temperature of 21.1°C) and working air ratio of 0.44, the prototype cooler achieved lower product air temperature (20.8°C vs. 21.5°C), higher COP (37.4 vs. 18.4) and higher wet-bulb cooling effectiveness

(102.4% vs. 93%). The cooling output of the prototype cooler is also slightly higher (4.25 kW vs. 4.15 kW) despite its PA flow rate (750 m³/h) is slightly lower than that of the M30 (765 m³/h).

Table 5-6: Comparison of the prototype system with the M30.

	PA flow rate	Working air ratio	Cooling capacity	PA temperature	COP	Dew _{eff}	Fan power	Pump power
Cooler	(m ³ /h)	(-)	(kW)	(°C)	(-)	(-)	(W)	(W)
M30	765	0.441	4.15	21.5	18.4	93.0%	450	1.56
Prototype	750	0.441	4.25	20.8	37.4	102.4%	112	
		0.364	4.75	18.8	52.5	114.4%	89	
Testing conditions: DB-37.8°C; WB-21.1°C (same as Coolerado® M30)								

Comparison between the two different working air ratios (i.e. 0.364 and 0.441) indicates that the working air ratio of 0.364 is more favourable for achieving higher cooling output and COP. At this ratio, the lower PA temperature (i.e. 18.8°C), higher wet-bulb cooling effectiveness (i.e. 114.4%) and higher cooling capacity (i.e. 4.75 kW) were achieved. It should be particularly noted that the prototype cooler achieved an extremely high COP (52.5), largely owing to the lower energy consuming fan (89 W under the specified operational condition).

5.5.4 Performance Testing under Various Intake Air conditions at the Optimum Working Air Ratio of 0.364 (Test 4)

After the optimum working air ratio (i.e. 0.364) was identified by the experimental investigation, further tests were carried out under various IA conditions in order to assess the climatic adaptability of the cooler. The working air ratio of 0.364 corresponds to the EA flow rate of 429 m³/h for the designed PA flow rate of 750 m³/h. The other conditions for these tests are the same as those in Test 1 (see **Table 5-4**). The test results, as presented in **Table 5-7**, are compared with those obtained from Test 1 which are based on the working air ratio of 0.44. It is found that all the results at the ratio of 0.364, including temperature drop, cooling capacity, COP and cooling effectiveness, are superior

to those at ratio of 0.44. During these tests, a smaller fan power (i.e. 89W) was required comparing to that at the ratio of 0.44 (i.e. 112W), owing to the decreased EA flow rate. The increased cooling output and decreased fan power consumption resulted in the significantly higher COP compared to those at the working air ratio of 0.44.

Table 5-7: Performance under various climatic conditions.

	Temp. drop		Cooling output		COP		Wet _{eff}		Dew _{eff}		Fan power	
	(°C)		(kW)		(-)		(-)		(-)		(W)	
Working air ratio	0.44	0.364	0.44	0.364	0.44	0.364	0.44	0.364	0.44	0.364	0.44	0.364
Coolerado® M30	17.1	19.1	4.3	4.8	37.4	52.5	102	114	67	75	112	89
Riyadh	14.9	16.6	3.7	4.2	32.2	46.2	107	114	72	75		
Las Vegas	14.5	14.6	3.6	3.7	31.3	40	110	112	74	76		
Kashi	11.8	12.7	2.9	3.2	25.5	35.3	106	115	71	77		
London	6.1	6.3	1.5	1.8	13.2	18.1	100	104	67	69		
Beijing	4.5	5.9	1.1	1.5	9.7	16.5	102	128	76	95		

5.5.5 Cases for Different Cooling Outputs at the Optimum Working Air Ratio of 0.364 (Test 5)

Under each set of IA condition (i.e., those for *Coolerado*® M30, Riyadh, Las Vegas, Kashi, London and Beijing), tests were carried out in a range of PA flow rates from 510-760 m³/h to obtain the cooling outputs at the optimum working air ratio of 0.364. The results indicated that under all the selected climates, the cooling capacity increased with the PA flow rate, while other performance parameters, including temperature drop, COP and cooling effectiveness, varied in opposite direction. A range of test results, under the climates of Riyadh (Saudi Arabia, hot & dry), Kashi (China, warm & dry) and London (UK, moderate), are discussed as follows.

Riyadh, Saudi Arabia (hot and dry)

The design summer outdoor air condition for Riyadh is 35.6°C of dry-bulb temperature and coincident wet-bulb temperature of 20.6°C. Under this intake air condition, the variation of the temperature drop and cooling capacity against the PA flow rate was observed and the results are shown in **Fig. 5-16**. It is found

that when the PA flow rate rise from 513 m³/h to 758 m³/h, the cooling capacity of the prototype cooler increases from 3.0 kW to 4.2 kW and the temperature drop falls from 17.8°C to 16.6°C. The variation of the COP and cooling effectiveness is shown in **Fig. 5-17**, indicating that when the PA flow rate increases from 513 m³/h to 758 m³/h, the COP presents a quick fall, i.e. from 69.3 to 46.2, while the WBE and DPE values have just slight falls, i.e., from 120.5% to 114.0% and from 78.7% to 75.1% respectively.

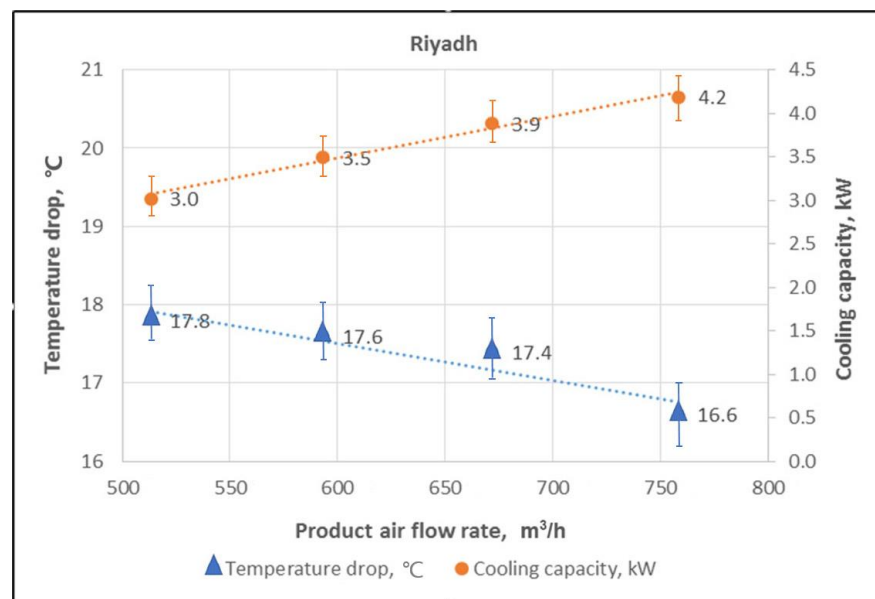


Fig. 5-16: Temperature and cooling capacity vs PA flow rate (Riyadh).

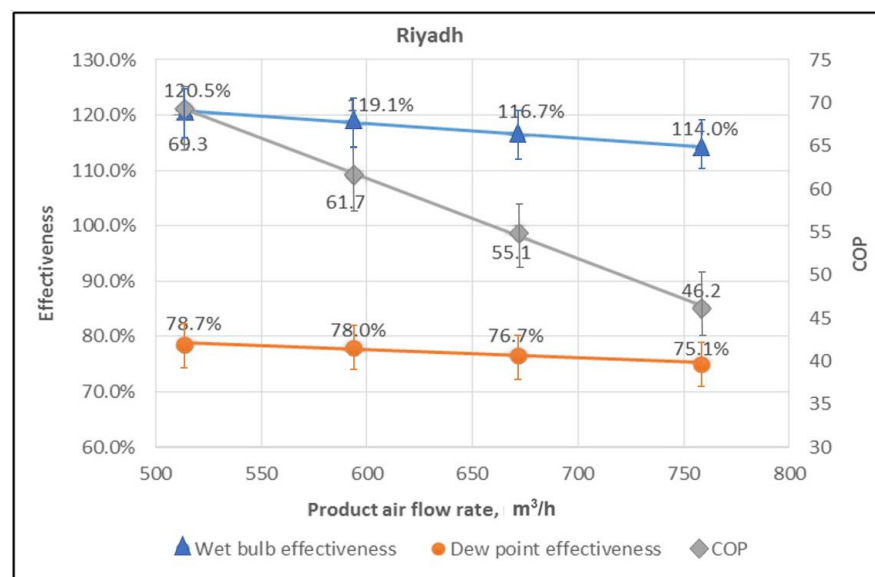


Fig. 5-17: Effectiveness and COP vs PA flow rate (Riyadh).

Kashi, China (warm and dry)

The design summer outdoor air condition for Kashi is 32.1°C of dry-bulb temperature and coincident wet-bulb temperature of 21.0°C. Under this IA condition, the variation of the temperature drop and cooling capacity against the PA flow rate was experimentally investigated and the results are shown in **Fig. 5-18**. It is found that when the PA flow rate increases from 512 m³/h to 756 m³/h, the cooling capacity increases from 2.3 kW to 3.2 kW and the temperature drop falls slightly from 13.3°C to 12.7°C. The variation of the COP and cooling effectiveness is shown in **Fig. 5-19**. When the PA flow rate increases from 512 m³/h to 756 m³/h, the COP gives a significant fall, i.e. from 52.1 to 35.3, while the WBE and DPE values have just slight fall, i.e. from 119.7% to 114.7% and from 80.6% to 77.0% respectively.

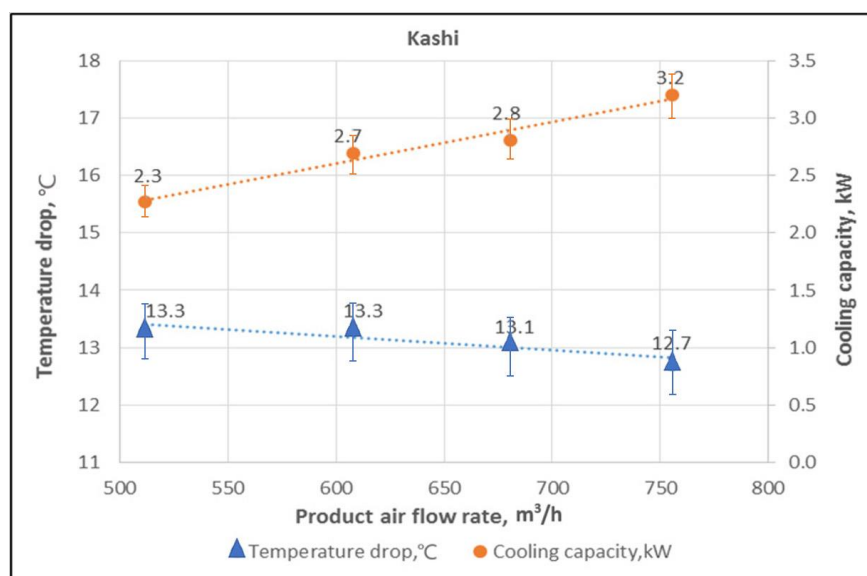


Fig. 5-18: Temperature and cooling capacity vs PA flow rate (Kashi).

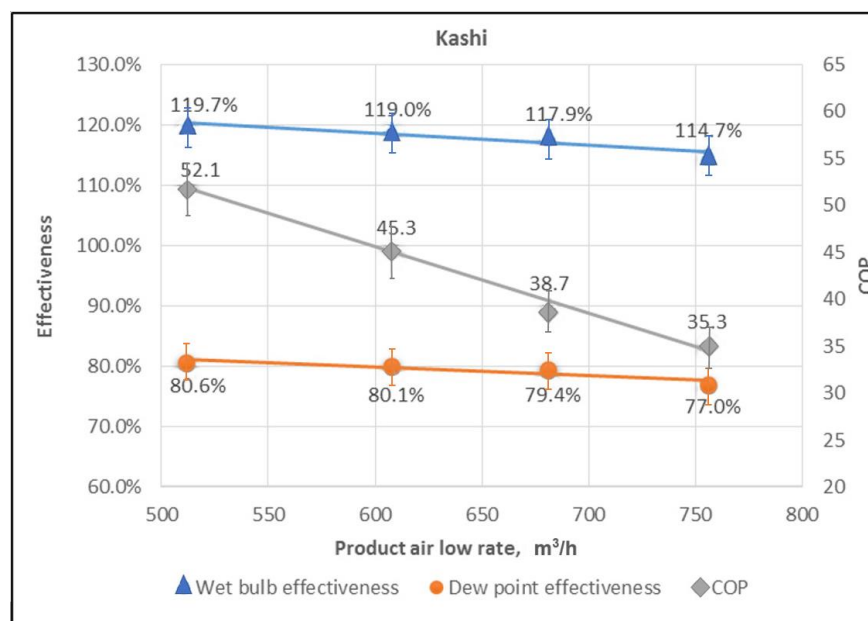


Fig. 5-19: Effectiveness and COP vs PA flow rate (Kashi).

London, UK (moderate)

The design summer outdoor air condition for London is 26°C of dry-bulb temperature and coincident wet-bulb temperature of 19.6°C. Under this IA air condition, the variation of the temperature drop and cooling capacity against the PA flow rate was experimentally investigated and the results are shown in **Fig. 5-20**. It is found that when the PA flow rate increases from 526 m³/h to 750 m³/h the cooling capacity has a measurable growth, i.e. from 1.4 kW to 1.8 kW, while the temperature drop presents a slight fall, i.e. from 7.7°C to 6.3°C. The variation of the COP and cooling effectiveness against the PA flow rate is shown in **Fig. 5-21**. When the PA flow rate increases from 526 m³/h to 750 m³/h, the COP gives a significant fall, i.e. from 29.7 to 18.1, while the WBE and DPE values show small falls, i.e. from 119.5% to 104.0% and from 79.4% to 69.0%, respectively.

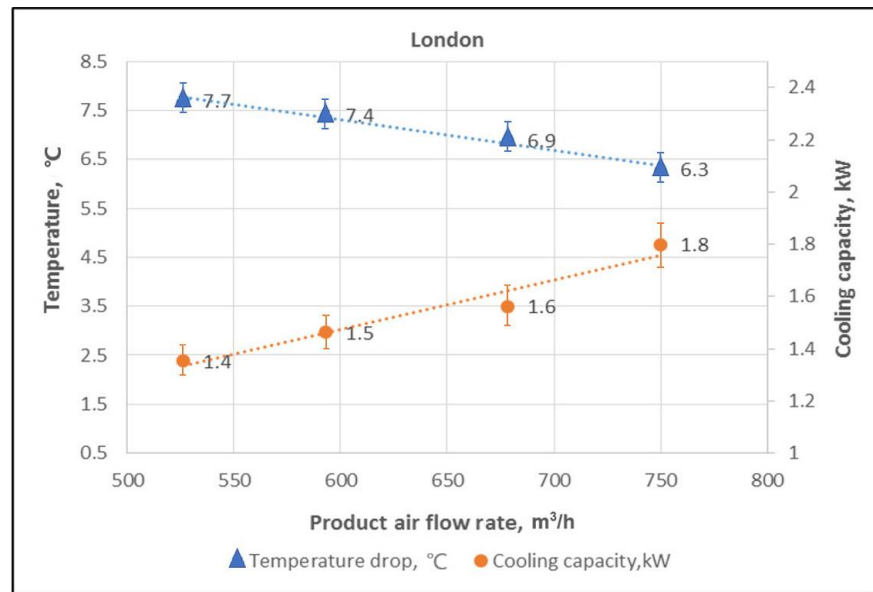


Fig. 5-20: Temperature and cooling capacity vs PA flow rate (London).

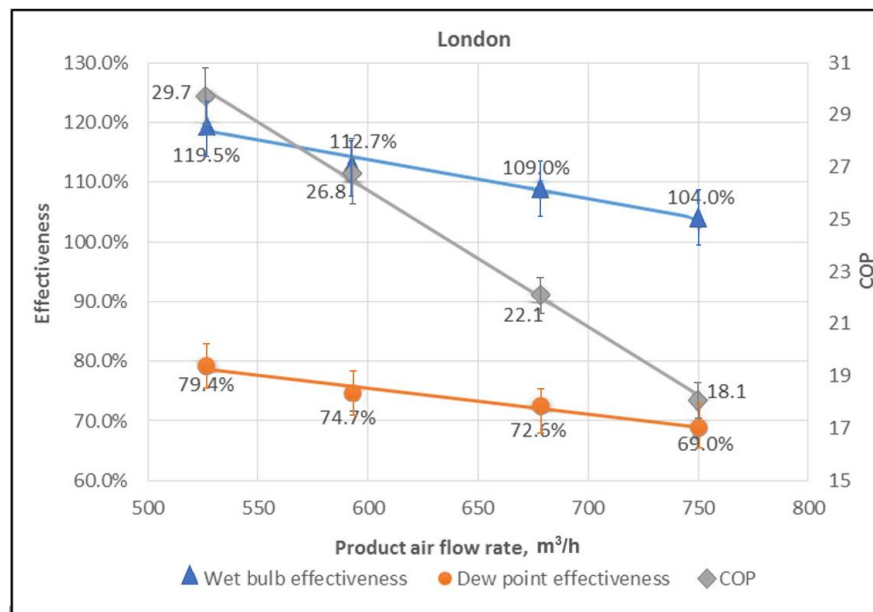


Fig. 5-21: Effectiveness and COP vs PA flow rate (London).

It is clear that under dryer IA conditions the cooler demonstrated higher cooling and energy performance. Among the simulated IA conditions that represent the climates of six different cities in the world, the prototype cooler presented the best energy performance at Riyadh (hot & dry climate), followed by Kashi (warm & dry climate) and London (moderate climate).

The prototype cooler presented the worst cooling performance under the warm and humid climate in Beijing. As a case study, the application feasibility of the proposed cooler in Beijing will be further investigated in much more details in **Chapter 6**.

5.6 Validation and Update of the Simulation Tool

Although the aforementioned self-developed simulation tool has been validated under identical conditions with the published experimental results, and been successful in assisting theoretical analysis and optimizing the HMX and system design, some innovative aspects were not well reflected for the exact established cooler prototype in technical details as follows.

- (1) Contribution to water evaporation by the application of moisture-wicking and quick-drying fabric.
- (2) Impact of the properties of aluminium sheet and fabric on heat transfer.
- (3) Impact of the specific channel dimension on the geometric similarity in the set-up of computational elements.
- (4) Airflow resistance characteristics and actual fan power consumption in practice.
- (6) The selection of optimal operation parameters, e.g. working air ratio and airflow velocity.

The reason for such treatment of simplifying the initial simulation model is partly from the consideration to avoid too complicated theoretical models of heat and mass transfer, e.g. the heat transfer through the sandwich exchanging sheet

with irregular dimensional shape and the impact of fabric surface properties on moisture evaporation, and partly form the unknown, undetermined or unforeseen characteristics of the material, structure, facilities and operational state, e.g. the detailed specifications of the fabric for heat and mass transfer and flow resistance computation and the performance of the fans under coupled working conditions.

With the series of experimental data under various working conditions, empirical correction factors could be introduced to help improve the predictive veracity of the pre-proved theoretical model. The adaptive improvements for the exact established dew pointer cooler mainly existed in the following aspects.

(1) The dimension of the computational element, which was proved to be essential in simulation in **Chapter 3**, was determined by the actual size of the air channels, i.e. wave length of 0.396 m based on a chord of 0.348 m.

(2) A factor of 1.16 was applied to the theoretical dynamic heat transfer coefficient due to the unknown details in heat transfer through the sandwich exchanging sheet.

(3) A variable factor was introduced to correct the dynamic mass transfer coefficient as per the range of PA flow rate, i.e. 0.5 for the PA flow rate below 712 m³/hr, 1.5 for PA flow rate beyond 817 m³/hr and 1.0 for the mid-range, due to the impact of unstable air distribution in the channels on moisture evaporation.

(4) A factor of 1.5 was applied to the evaporating area to compensate the increase of effective area owing to the fabric's porous surface.

(5) A factor of 1.5 was used to make up the unforeseen items in airflow resistance calculation.

(6) The comprehensive efficiency value of the fans was corrected to 0.55 based on the test results.

(7) Circulating water flow rate was fixed at 18 kg/hr with fixed temperature of 16 °C by the aforementioned control logic of interment operation mode.

(8) Working air ratio was fixed at 0.364, which had been proved by the experimental investigation to be the optimal value for the cooler prototype.

(9) The channel length was fixed at 1.0 m due to the material availability in the manufacturing process.

(10) 200 sandwich-structure exchanging sheets were employed to form 100 wet channels and 99 dry channels in the finished heat and mass exchanger and the related parameters were fixed in the simulation routines.

The dedicated improvements for the established cooler prototype were validated with abundant experiment data under various operation conditions. **Table 5-8** presents the typical test data at various PA flow rate, i.e. different air velocity in the channels, under the reference *Coolerado*® air conditions which is suggested by Australian Standard [5.7], and the simulation results under the identical set values. The comparison between the parallel performance parameters proved the high reliability of the simulation results under such initial and operational conditions.

Table 5-8: Validation with test results under various PA flow rate.

No.	Ref. initial conditions			Remark	WA-FR (m ³ /hr)	PA-FR (m ³ /hr)	Velocity (m/s)	WAR (-)	IA Temp. (°C)	IA-RH	IA-HR	PA Temp.	
	WBT (°C)	DBT (°C)	Location									Temp. (°C)	error
1	21.1	37.8	Coolerado®, Ref.	Exp.	429.3	748.8		0.364	37.9	21.8%	8.95	18.8	2.1%
				Sim.		749.0	1.880	0.364	37.9	21.8%	8.95	19.2	
2				Exp.	388.1	674.5		0.365	37.6	24.5%	9.92	19.1	1.0%
				Sim.		674.2	1.695	0.365	37.6	24.5%	9.92	19.3	
3				Exp.	343.4	603.7		0.363	38.0	22.9%	9.50	18.7	-1.1%
				Sim.		603.7	1.513	0.363	38.0	22.9%	9.50	18.5	
4				Exp.	334.6	586.0		0.364	37.6	24.5%	10.14	18.6	1.6%
				Sim.		586.0	1.471	0.364	37.6	24.5%	10.14	18.9	
5				Exp.	294.5	521.0		0.361	37.9	23.8%	9.83	18.5	-2.7%
				Sim.		520.8	1.301	0.361	37.9	23.8%	9.83	18.0	

No.	EA Temp.		EA-RH	Temp. drop		Cooling capacity		COP		WBE		DPE	
	Temp. (°C)	error		Temp. (°C)	error	Cooling (kW)	error	COP	error	WBE	error	DPE	error
1	28.6	-3.1%	96.0%	19.1	-2.1%	4.751	-3.6%	52.5	2.2%	114.4%	-1.7%	74.9%	-2.0%
	27.7		100.0%	18.7		4.582		53.6		112.4%		73.4%	
2	28.3	-1.1%	96.6%	18.5	-1.1%	4.152	-3.0%	58.8	-0.6%	117.2%	-1.0%	78.1%	-1.1%
	28.0		100.0%	18.3		4.028		58.5		116.0%		77.2%	
3	28.1	0.6%	98.3%	19.3	1.0%	3.874	-0.5%	69.7	1.9%	117.8%	1.4%	77.8%	1.2%
	28.3		100.0%	19.5		3.853		71.0		119.4%		78.8%	
4	27.7	2.8%	98.8%	19.0	-1.6%	3.704	-1.1%	69.2	3.3%	120.3%	0.1%	80.2%	0.5%
	28.5		100.0%	18.7		3.665		71.5		120.5%		80.6%	
5	28.1	1.7%	98.8%	19.4	2.6%	3.362	0.6%	85.0	0.0%	120.5%	2.6%	80.2%	2.5%
	28.6		100.0%	19.9		3.381		85.0		123.7%		82.2%	

DBT-dry bulb temperature; **WBT**-wet bulb temperature; **WA**-working air; **PA**-product air;
EA-exhaust air; **IA**-intake air; **FR**-flow rate; **WAR**-working air ratio; **RH**-relative humidity;
HR-humidity ratio; **WBE**-wet bulb cooling effectiveness; **DPE**-dew point cooling effectiveness;
Temp.-temperature; **Ref.**-reference; **Exp.**-experimental data; **Sim.**-simulation results.

Table 5-9 compares the typical test data under various climatic conditions and simulation results under the same conditions. The relative error values validate once more the aforementioned improvements to the original simulation routines.

Table 5-9: Validation with test results under various climatic conditions.

No.	Ref. initial conditions			Remark	WA-FR (m ³ /hr)	PA-FR (m ³ /hr)	Velocity (m/s)	WAR (-)	IA Temp. (°C)	IA-RH	IA-HR	PA Temp.	
	WBT (°C)	DBT (°C)	Location									Temp. (°C)	error
1	21.1	37.8	Coolerado®, Ref.	Exp.	388.1	674.5		0.365	37.6	24.5%	9.92	19.1	1.0%
				Sim.		676.2	1.700	0.365	37.6	24.5%	9.92	19.3	
2	21.9	34.8	Las Vegas, USA	Exp.	393.5	688.4		0.364	34.9	32.1%	11.23	19.8	1.0%
				Sim.		689.2	1.730	0.364	34.9	32.1%	11.23	20.0	
3	20.6	35.6	Suaudi Arabia	Exp.	389.7	671.7		0.367	35.9	25.7%	9.47	18.5	1.1%
				Sim.		670.1	1.690	0.367	35.9	25.7%	9.47	18.7	
4	21.0	32.1	Kashi, China	Exp.	395.4	680.9		0.367	32.3	37.1%	11.22	19.2	1.6%
				Sim.		678.0	1.710	0.367	32.3	37.1%	11.22	19.5	
5	19.6	26.0	London, UK	Exp.	388.5	678.3		0.364	25.9	55.8%	11.67	19.0	-1.6%
				Sim.		677.3	1.700	0.364	25.9	55.8%	11.67	18.7	
6	26.2	30.5	Beijing, China	Exp.	388.4	685.5		0.362	30.6	69.6%	19.36	24.7	1.2%
				Sim.		685.4	1.715	0.362	30.6	69.6%	19.36	25.0	

No.	EA Temp.		EA-RH	Temp. drop		Cooling capacity		COP		WBE		DPE	
	Temp. (°C)	error		Temp. (°C)	error	Cooling (kW)	error	COP	error	WBE	error	DPE	error
1	28.3	-1.1%	96.6%	18.5	-1.1%	4.152	-2.8%	58.8	-0.9%	117.2%	-1.1%	78.1%	-1.1%
	28.0		100.0%	18.3		4.037		58.3		115.9%		77.2%	
2	27.3	-0.7%	97.1%	15.1	-1.3%	3.467	-3.4%	46.5	0.4%	116.6%	-1.3%	79.1%	-1.5%
	27.1		100.0%	14.9		3.348		46.7		115.1%		77.9%	
3	27.1	-0.4%	97.7%	17.4	-1.1%	3.886	-2.9%	55.1	0.1%	116.7%	-0.8%	76.7%	-0.9%
	27.0		100.0%	17.2		3.774		55.1		115.8%		76.0%	
4	25.5	0.8%	98.8%	13.1	-2.3%	2.808	0.7%	39.8	1.5%	117.9%	-2.4%	79.4%	-2.5%
	25.7		100.0%	12.8		2.827		40.4		115.1%		77.4%	
5	23.1	-2.6%	94.1%	6.9	4.3%	1.562	1.7%	22.8	1.8%	109.0%	4.3%	72.6%	4.1%
	22.5		100.0%	7.2		1.589		23.2		113.7%		75.6%	
6	27.9	-1.4%	98.3%	5.9	-5.1%	1.300	-3.9%	17.9	-1.1%	127.5%	-5.2%	95.2%	-5.5%
	27.5		100.0%	5.6		1.249		17.7		120.8%		90.0%	

The above comparison between the test data and corresponding simulation results suggests that the updated simulation tool could achieve high reliability in predicting the cooling performance of the proposed dew point cooler under certain airflow conditions. The following case study will focus on the PA temperature, cooling capacity and power consumption. It is no doubt that the simulation tool would be qualified for the job.

5.7 Chapter Summary

To create the required testing environment, an intake air regulating system, along with the supply and exhaust air ducting systems, were constructed. The intake air regulating system consisted of a high-power electric heater, a humidifier, a dehumidifier, ducts and dampers, all of which were integrated into a dedicated fan and ducting system to provide a variety of intake air parameters that can simulate various climatic conditions across the world. The lab test system was equipped with sorts of sensors and measuring instruments to enable the accurate parametrical measurements of the prototype DPC under various operational conditions.

Series of laboratory tests to evaluate the performance and explore the potential of the cooler prototype were carried out. Six intake air conditions, which represented the climates of standard lab testing condition (*Coolerado*®), hot & dry (Riyadh, Saudi Arabia and Las Vegas, US), warm & dry (Kashi, China), moderate (London, UK) and warm & humid (Beijing, China), were selected to conduct performance test under the controllable laboratory environment.

Parallel tests were carried out under identical conditions to compare the cooling performance and energy efficiency with the referenced commercial product in same sizes, i.e. *Coolerado*® M30 which stands for the advanced technology of evaporative cooling. The test results under various climatic conditions manifested the superiority of the cooler prototype in cooling performance and energy use.

Optimum working air ratio of the prototype was identified and adopted to explore the applied potential under various climatic conditions. Test results including error information were presented, discussed and finally employed to validate and improve the dedicated simulation tool.

With improvement in details, the exclusive simulation software could give high reliable simulation results under various applied circumstances and will be employed in the following case study in **Chapter 6**.

CHAPTER 6: ENERGY SAVING, ECONOMIC, AND ENVIRONMENTAL PERFORMANCE ANALYSES

6.1 Chapter Introduction

In this chapter, a case study of the proposed dew point cooler (DPC) applied in Beijing, China is carried out, including an hourly cooling performance analysis in a typical cooling day, annual energy performance prediction, economic analysis and environmental sustainability assessment based on the adaptively improved simulation tool. The main works involved in this chapter are given as follows.

- (1) The hourly cooling performance of the prototype cooler in a typical cooling day in summer was analysed to illustrate the possible operation conditions using the dedicated simulation model which was validated in **chapter 5**.
- (2) Annual energy performance based on hourly analysis was presented in comparison with conventional packaged air conditioner (PAC).
- (3) Based on life-cycle assessment methods, including the cost payback period, cost saving and CO₂ emission reduction across the whole life span of the proposed DPC, were analysed.

This part of research presents the cooling performance and energy issues of the proposed DPC in real climatic conditions, including hourly climatic data all over a meteorological year in Beijing, a great city with huge demands for cooling in summer time but generally being considered not that suitable for the application of existing evaporative cooling technologies owing to its warm but humid climate. Although it is a challenge for the application in such a warm and humid climate, the results proved its feasibility based on hourly performance analysis all year round with the validated simulation tool. The socio-economic analysis

can predict the energy saving, economic and environmental benefits of the proposed DPC. The success in application of the proposed DPC in the warm and humid region promises more opportunities of the dew point cooling technology.

6.2 Annual Operational Performance

Owing to the high reliability of the previously validated simulation model in calculating the cooling parameters, including PA temperature, cooling capacity, COP and cooling effectiveness, in certain temperature and humidity ranges, it is appropriate for predicting the day and annual operational performance of the proposed DPC based on hourly weather data.

6.2.1 Application Conditions for Evaluation

The following feasibility, energy saving and environmental evaluation are intended to be applied in the possible application in Beijing (39.8°E, 116.5°N), China, where the summer climate is warm and humid and is generally considered not that suitable for normal evaporative cooling technologies. It is a challenge for the application of the proposed DPC. However, if it could success in the application in such regions with warm and humid climate, it presents superiorities itself in cooling performance and adaptation over the existing evaporative cooling technologies.

Considering the features of high airflow rate and moderate temperature difference of supply air of evaporative cooling technologies, the application is positioned in the scenarios where large fresh airflow rate is required e.g. high occupancy public buildings like libraries or waiting rooms. In view of the influence on comfort owing to the higher supply air velocity, the required indoor design temperature could be moderately lowered comparing to the application

of the conventional mechanical cooling technologies. Based on these considerations, the following applied case will be based on a room located in Beijing with 15-20 occupiers. (the commonly required fresh air of 28.8 m³/person·hr as per the British standard [6.1], and 30 m³/person·hr for Chinese standard [6.2]). Based on the local design codes [6.2], the indoor design conditions are set at indoor temperature of 26°C and coincident RH of 50%.

Exhaustive meteorological parameters, including hourly, various day and monthly average weather data etc in the typical meteorological year, are given by *China Standard Weather Data for Analysing Building Thermal Conditions*, which is published by China Meteorological Bureau, Climate Information Centre, Climate Data Office and Tsinghua University, Department of Building Science and Technology [6.3]. In the following sections, the weather data will be analysed for the DPC application.

The profile of the proposed HMX is 1 m × 1 m × 0.35 m (Height × Width × Thickness), stacked by 200 irregularly corrugated sandwich sheets with 5 mm interval. The cooling performance and energy issues have been both numerically and experimentally validated with high reliability in previous chapters.

6.2.2 Weather Profiles and Operational Conditions

Hourly weather parameters including outdoor temperature, humidity ratio and relative humidity, during the whole cooling season (1st June – 30th September) in typical meteorological (for design) year (1999) are plotted in **Figs. 6-1**.

As per the pre-set design indoor conditions, i.e. temperature of 26°C, RH of 50% and coincident humidity ratio of 10.54 g/kg, **Fig. 6-1(a)** presents the following facts that 1) in most time of the four general cooling months the outdoor temperature is under 26°C and space cooling could be considered being replaced by ventilation; 2) the time demanding for air cooling intensively distributes

during the period from 7 am.- 11 pm., which is in accordance with the general application scenario for an university library; 3) The dispersion of outdoor temperature in June is obviously great with the appearance of both highest and lowest temperature; 4) during most time of September, there could be no demand for cooling; 5) July and August are in great and steady demand for air cooling in Beijing; 6) associating above 3)-5), it is easy to understand that the cooling demand concentrates in the middle stage of the cooling season, while at the entering stage in June and leaving stage in September, the cooling demand is weak.

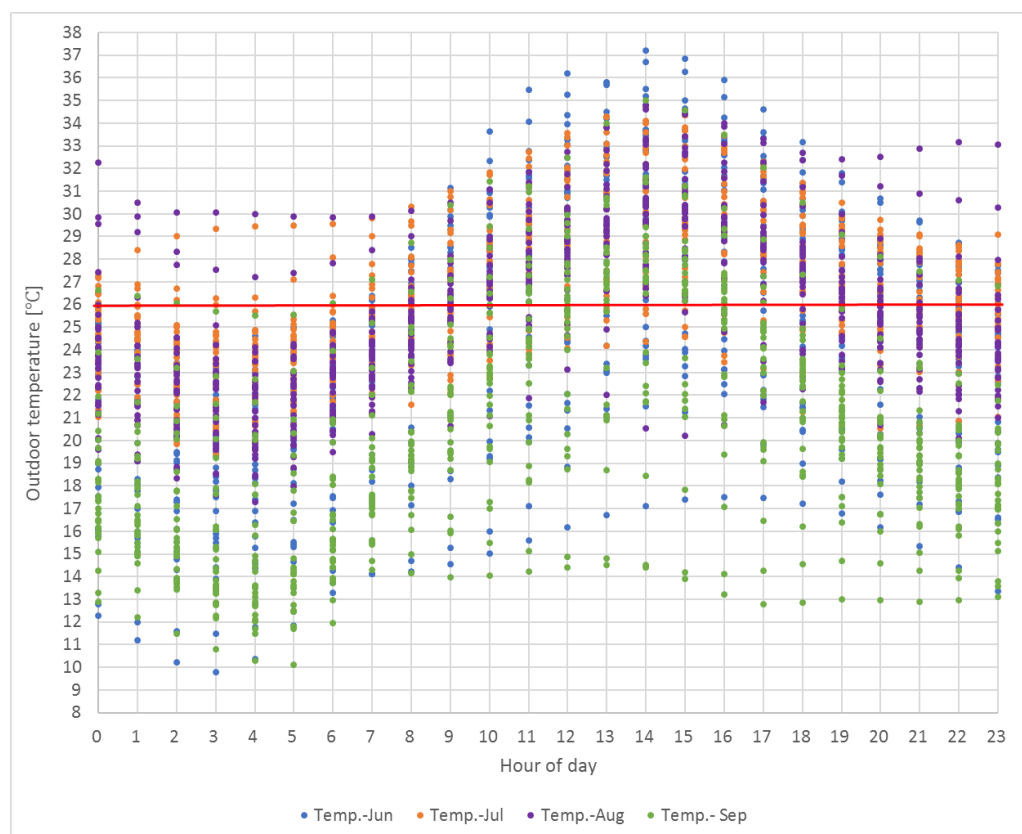


Fig. 6-1(a): Outdoor temperature distribution in the cooling season.

Fig. 6-1(b) shows the similarity of the humidity distribution in the months. Moreover, dehumidification is a must for nearly all through July and August while a relatively very weak demand appears in September. The maximum

dispersion in humidity ratio exists likewise in June. It is worth mentioning now that dehumidification is a must to meet the indoor comfort requirement, the superiority of evaporative cooling technology would be prominent comparing to the conventional mechanical cooling.

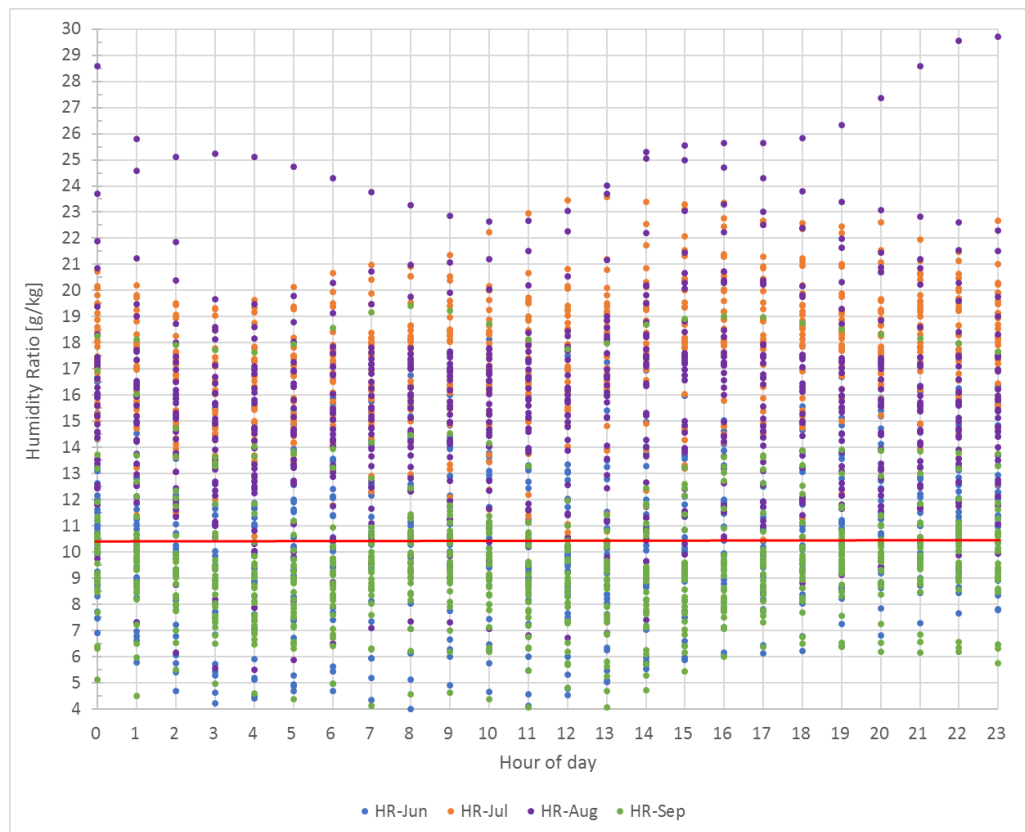


Fig. 6-1(b): Humidity ratio in the cooling season.

Fig. 6-1(c) shows the RH distribution during the whole cooling season. It witnesses the humid climate feature in Beijing in summer.

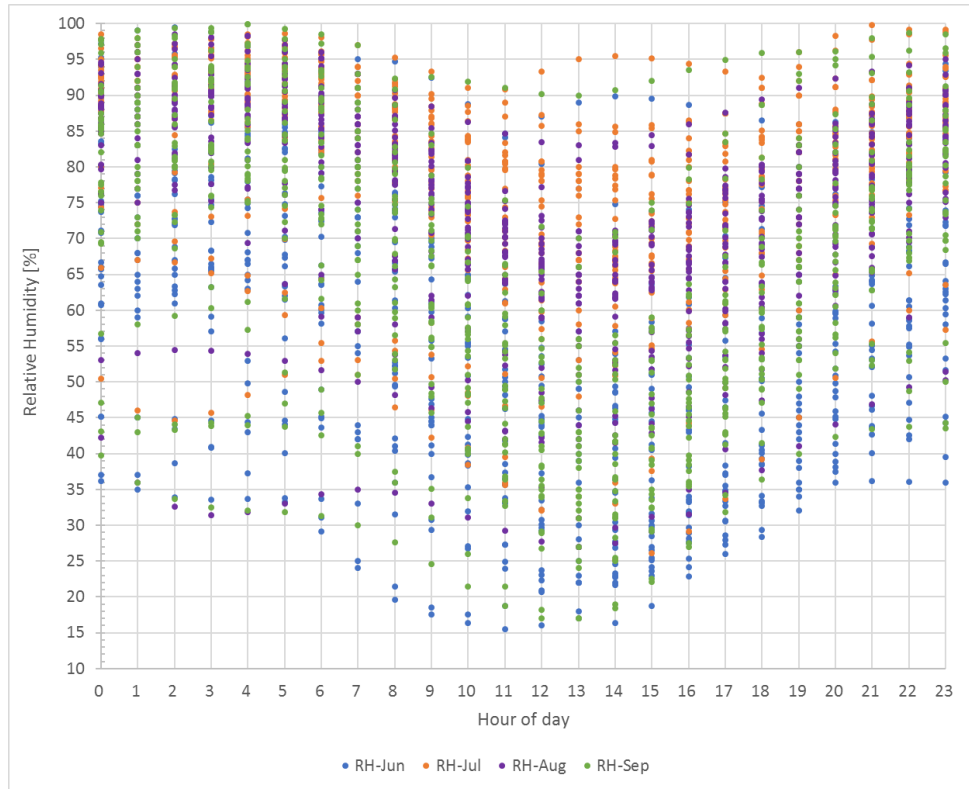


Fig. 6-1(c): Relative humidity in the cooling season.

Fig. 6-1: Hourly weather profiles in the cooling season.

Hourly weather profiles in two typical cooling days in the cooling season in typical meteorological (for design) year are presented in **Fig. 6-2** and will be following as bases to perform evaluation of cooling performance for example.

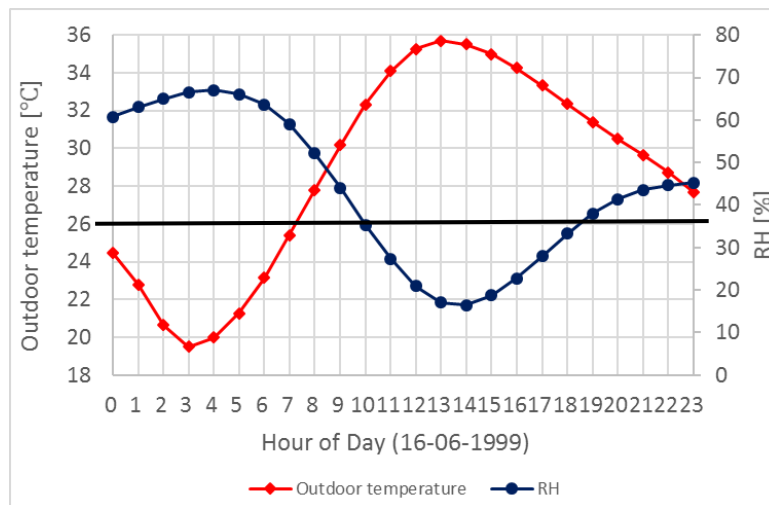


Fig. 6-2(a): Hourly weather profiles on 16th June

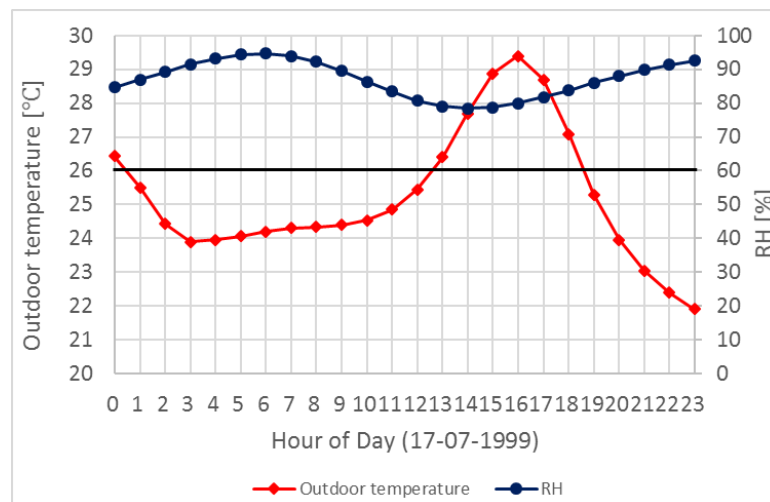


Fig. 6-2(b): Hourly weather profiles on 17th July

Fig. 6-2: Hourly weather profile in two typical cooling days in Beijing, China.

The weather profile on 6th June plotted in **Fig. 6-2(a)** could be a most common case in summer days. The outdoor temperature waves roughly following a sine curve and the temperature above 26°C presents during the period between 7 am. and 11 pm. and accordingly the relative humidity varies with a reverse trend. Higher temperature and lower relative humidity appear at noon, which would just offer more desirable cooling performance for higher cooling demands. The other one on 17th July plotted in **Fig. 6-2(b)** could be a sample of other common meteorological days when the daily mean relative humidity is above 80% although the temperature might not be that high.

6.2.3 Hourly Energy-Saving Potential for Summer Cooling Days in Beijing

Fig. 6-3(a) shows profiles of hourly building cooling load and cooling capacity provided by the DPC on the summer design day (16th June) in Beijing. The figure also depicts power consumption of the DPC unit and a stand-alone PAC unit which is used to generate the same cooling. It is obvious that the cooling capacity provided by the proposed DPC is higher than the cooling load all day long,

therefore during this period the DPC is able to provide the whole cooling independently.

As for the practical period between 7 am. and 11 pm. in default working mode, the power consumption by the DPC unit keeps constant at around 70 W and far below that by the conventional PAC unit while offers more cooling capacity. The all-day bonus cooling during the working period is the difference between the DPC cooling capacity and the time integral of cooling load, i.e. 26.3 kWh, which is highlighted in green in **Fig. 6-3(a)**. From 0 am. to 7 am., the cooling load has negative values due to the lower outdoor air temperature (under indoor design temperature). In this case, outdoor fresh air could be directly introduced into the building to replace the indoor stale air at less cost if necessary.

Table 6-1 gives the details of the hourly cooling load, cooling capacity and power consumption of both the proposed DPC and conventional PAC, which associate with **Fig. 6-1(a)**.

Table 6-1: Hourly cooling load and power consumption (16th June 1999).

Time	Outdoor temp.	RH	HR	PA temp.	Temp. drop	Cooling capacity	COP	Power (DPC)	DPE	WBE	Cooling load	COP (PAC)	Power (PAC)
[-]	[°C]	[%]	[g/kg]	[°C]	[°C]	[W]	[-]	[W]	[-]	[-]	[W]	[-]	[W]
0	24.5	60.7%	11.8	18.5	6.0	1345	19.1	0	74.9%	112.9%	-337.8	0	0
1	22.8	63.0%	11.1	17.5	5.3	1196	17.1	0	72.2%	111.2%	-716.0	0	0
2	20.6	65.0%	10.0	16.0	4.6	1033	14.8	0	67.9%	108.1%	-1201.5	0	0
3	19.5	66.5%	9.5	15.4	4.1	926.2	13.3	0	65.9%	106.4%	-1454.3	0	0
4	20.0	67.0%	9.9	15.8	4.2	948	13.6	0	67.1%	107.4%	-1346.9	0	0
5	21.3	66.1%	10.6	16.7	4.6	1034	14.8	0	70.0%	109.6%	-1058.3	0	0
6	23.1	63.6%	11.4	17.8	5.3	1177	16.8	0	73.3%	111.9%	-637.7	0	0
7	25.4	59.0%	12.2	18.9	6.5	1458	20.7	0	75.8%	113.5%	-134.2	0	0
8	27.8	52.2%	12.4	19.5	8.3	1855	26.3	70.5	77.1%	114.2%	402.7	3.1	129.9
9	30.2	44.0%	12.0	19.7	10.5	2354	33.3	70.7	77.3%	114.5%	933.0	3.0	315.8
10	32.3	35.3%	10.9	19.1	13.2	2958	41.9	70.6	75.9%	114.4%	1414.0	2.8	500.9
11	34.1	27.3%	9.3	18.1	16.0	3573	50.5	70.8	73.8%	114.3%	1807.8	2.7	665.8
12	35.3	20.9%	7.5	17.1	18.2	4077	57.7	70.7	71.1%	114.1%	2071.8	2.6	783.9
13	35.7	17.0%	6.3	16.1	19.6	4396	62.2	70.7	68.2%	113.8%	2170.3	2.6	829.6
14	35.5	16.4%	6.0	15.7	19.8	4441	62.9	70.6	66.9%	113.5%	2127.7	2.6	809.7
15	35.0	18.7%	6.6	16.3	18.7	4177	59.1	70.7	69.0%	113.7%	2013.6	2.7	757.3
16	34.3	22.8%	7.8	17.1	17.2	3841	54.4	70.6	71.2%	113.9%	1845.8	2.7	682.4
17	33.3	27.9%	9.1	17.9	15.4	3438	48.7	70.6	73.2%	114.0%	1642.2	2.8	594.9
18	32.4	33.3%	10.3	18.7	13.7	3075	43.5	70.7	75.0%	114.1%	1423.0	2.8	504.5
19	31.4	38.0%	11.1	19.2	12.2	2732	38.7	70.6	76.2%	114.3%	1208.2	2.9	419.6
20	30.5	41.4%	11.5	19.3	11.2	2517	35.7	70.5	76.3%	114.2%	1009.1	2.9	343.9
21	29.6	43.6%	11.5	19.3	10.3	2314	32.8	70.5	76.4%	114.1%	814.4	3.0	272.6
22	28.7	44.7%	11.2	18.8	9.9	2209	31.4	70.4	75.4%	113.6%	610.8	3.0	200.7
23	27.7	45.2%	10.7	18.1	9.6	2143	30.4	70.5	73.6%	112.8%	380.4	3.1	122.5

RH-relative Humidity; **HR**-Humidity Ratio; **PA**-Product Air; **DPC**-Dew Point Cooler; **DPE**-Dew Point cooling Effectiveness; **WBE**-Wet-Bulb cooling Effectiveness; **PUA**-conventional Packaged Unit Air

In case of warm and humid days e.g. 17th July presented in **Fig. 6-2(b)**, high humidity ratio restricts the cooling performance of the DPC. As shown in **Fig. 6-3(b)**, the cooling demands just exist during the time from 12:30 to 18:30 in the day. The cooling capacity of the DPC could cover all the cooling demands for fresh air and save 1.84 kW power in comparison to the mechanical PAC in all day use.

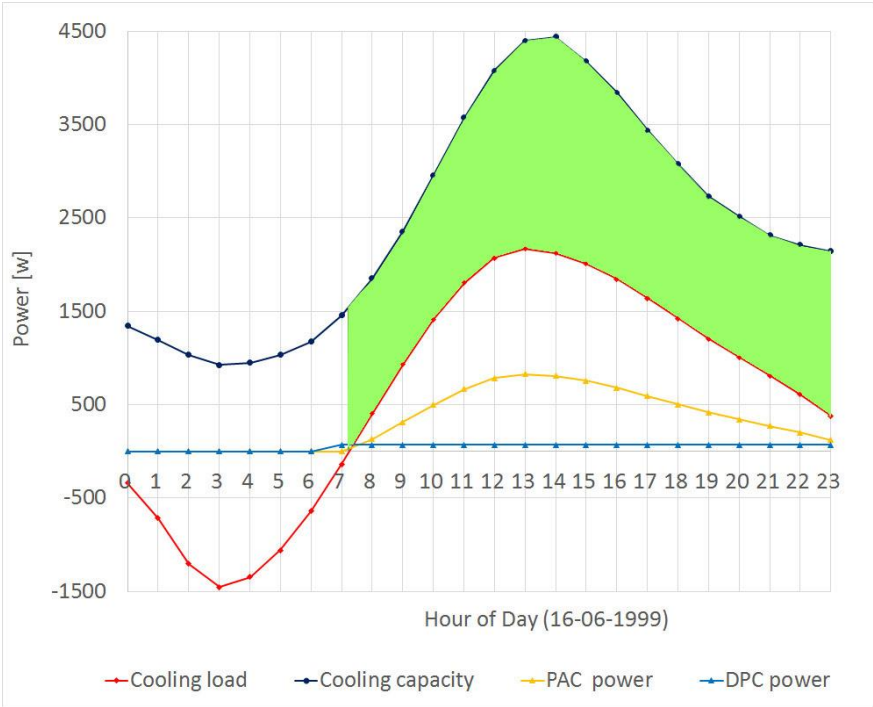


Fig. 6-3(a): Required cooling load/ power and available cooling capacity on 16th June.

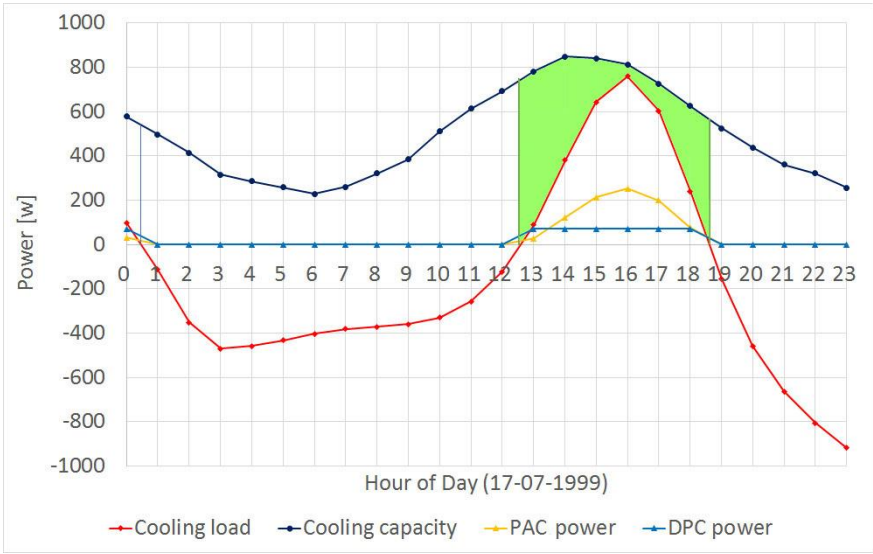


Fig. 6-3(b): Required cooling load/ power and available cooling capacity on 17th July.

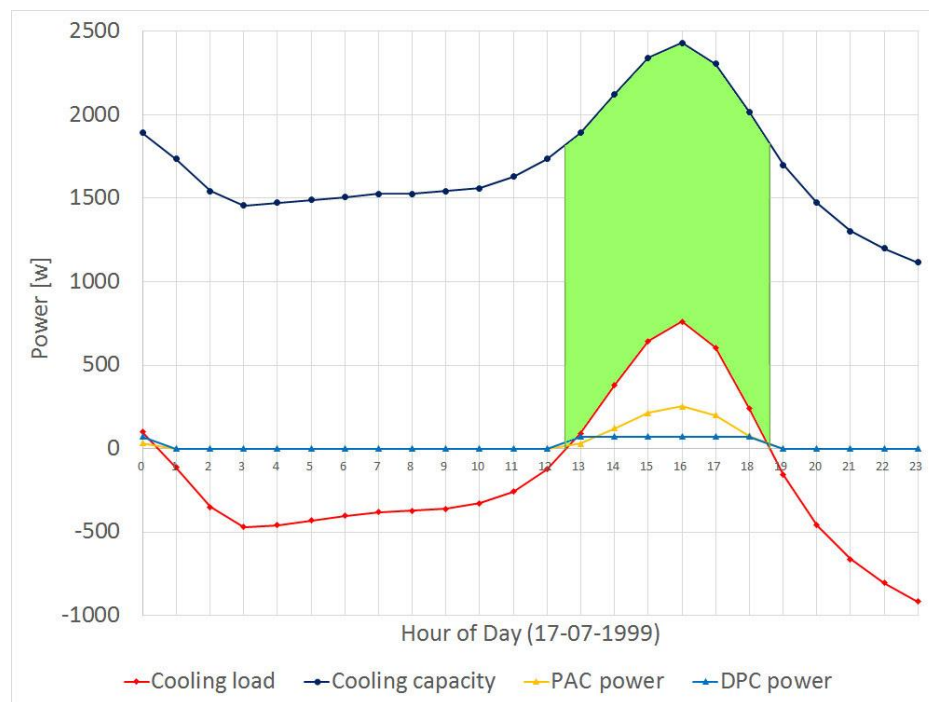


Fig. 6-3(c): Promotion of cooling capacity with pre-dehumidified process on 17th July.

Fig. 6-3: Hourly cooling demands and cooling capacity in typical cooling days.

Fig. 6-3(c) illustrates the change of cooling capacity of the DPC with IA pre-dehumidification. The energy saving in operation period of 9.19 kW, which is highlighted in **Fig. 6-3(c)** in green, could be integrated for the cooling capacity curve. In contrast with the energy saving of 1.84 kW without dehumidification process, the effect of power saving by pretreatment of dehumidification is notable.

From the detailed parameters listed in **Table 6-2**, it is noticeable that the humidity ratio in outdoor air, with day mean value of 18.0 g/kg, is far more than the required indoor level of 10.5 g/kg and the average RH level over 80% makes the COP value just stay at around 10 in the operation period. Now that dehumidification is a must to meet the indoor comfort requirement for air humidity, the cooling performance of the DPC would get a great lift with the pre-dehumidification process. **Table 6-3** gives the details of the cooling performance promotion by pre-dehumidifying the intake air to the design level of HR=10.5 g/kg.

Table 6-2: Hourly cooling load and power consumption (17th July 1999).

Time	Outdoor temp.	RH	HR	PA temp.	Temp. drop	Cooling capacity	COP	Power (DPC)	DPE	WBE	Cooling load	COP (PAC)	Power (PAC)
[-]	[°C]	[%]	[g/kg]	[°C]	[°C]	[W]	[-]	[W]	[-]	[-]	[W]	[-]	[W]
0	23.8	84.6%	18.9	23.8	2.6	578.9	8.2	71	94.9%	129.3%	98.4	3.2	30.9
1	23.3	87.0%	18.3	23.3	2.2	497	7	0	95.5%	131.3%	-111.9	0	0
2	22.5	89.3%	17.6	22.5	1.9	415	5.9	0	96.0%	133.4%	-351.3	0	0
3	22.5	91.5%	17.5	22.5	1.4	315.6	4.5	0	102.2%	142.0%	-469.9	0	0
4	22.7	93.2%	17.9	22.7	1.3	286.8	4.1	0	106.6%	147.5%	-458.7	0	0
5	22.9	94.4%	18.2	22.9	1.2	258	3.7	0	112.3%	154.9%	-431.8	0	0
6	23.2	94.7%	18.4	23.2	1.0	229.2	3.3	0	120.1%	162.1%	-402.7	0	0
7	23.1	94.0%	18.4	23.1	1.2	260.5	3.7	0	113.2%	155.7%	-380.4	0	0
8	22.9	92.2%	18.1	22.9	1.4	321.3	4.6	0	103.7%	143.3%	-371.4	0	0
9	22.7	89.5%	17.6	22.7	1.7	384.1	5.5	0	98.2%	136.1%	-360.2	0	0
10	22.2	86.4%	17.2	22.2	2.3	510.6	7.2	0	91.4%	127.7%	-328.9	0	0
11	22.2	83.4%	16.9	22.2	2.7	614.5	8.7	0	89.0%	124.5%	-257.3	0	0
12	22.4	80.8%	17.0	22.4	3.1	693.5	9.8	0	88.5%	123.4%	-123.1	0	0
13	22.9	79.0%	17.6	22.9	3.5	782.5	11.1	70.5	88.8%	122.8%	89.5	3.2	28.1
14	23.9	78.4%	18.9	23.9	3.8	849	12	70.8	90.6%	123.4%	380.4	3.1	122.5
15	25.1	78.8%	20.4	25.1	3.8	840.1	11.9	70.6	93.6%	125.2%	644.4	3.0	212.4
16	25.8	80.0%	21.3	25.8	3.6	813.6	11.5	70.7	95.3%	126.4%	760.7	3.0	253.4
17	25.5	81.8%	20.9	25.5	3.2	726.5	10.3	70.5	96.0%	127.9%	604.1	3.0	198.4
18	24.3	83.8%	19.4	24.3	2.8	625.8	8.9	70.3	95.1%	128.8%	241.6	3.1	76.9
19	23.0	86.0%	17.9	23.0	2.3	525.7	7.5	0	93.5%	129.1%	-156.6	0	0
20	22.0	88.0%	16.9	22.0	2.0	439.1	6.2	0	92.9%	130.2%	-458.7	0	0
21	21.4	89.8%	16.3	21.4	1.6	361.4	5.1	0	93.4%	132.2%	-662.3	0	0
22	21.0	91.4%	15.9	21.0	1.4	322.1	4.6	0	93.4%	133.1%	-805.5	0	0
23	20.8	92.6%	15.6	20.8	1.1	257.1	3.7	0	9710.0%	138.8%	-917.3	0	0

Table 6-3: Hourly cooling load and power consumption (17th July 1999).

Time	Outdoor temp.	RH	HR	PA temp.	Temp. drop	Cooling capacity	COP	Power (DPC)	DPE	WBE	Cooling load	COP (PAC)	Power (PAC)
[-]	[°C]	[%]	[g/kg]	[°C]	[°C]	[W]	[-]	[W]	[-]	[-]	[W]	[-]	[W]
0	23.8	49.0%	10.54	17.9	8.5	1893	26.9	70	73.2%	112.4%	98.4	3.2	30.9
1	23.3	51.7%	10.54	17.7	7.8	1735	24.7	0	72.7%	112.0%	-111.9	0	0
2	22.5	55.2%	10.54	17.5	6.9	1543	22.0	0	72.2%	111.5%	-351.3	0	0
3	22.5	56.9%	10.54	17.4	6.5	1457	20.8	0	71.9%	111.2%	-469.9	0	0
4	22.7	56.6%	10.54	17.4	6.6	1474	21.0	0	71.9%	111.3%	-458.7	0	0
5	22.9	56.2%	10.54	17.4	6.7	1491	21.3	0	72.0%	111.3%	-431.8	0	0
6	23.2	55.9%	10.54	17.5	6.7	1508	21.5	0	72.0%	111.4%	-402.7	0	0
7	23.1	55.6%	10.54	17.5	6.8	1526	21.7	0	72.1%	111.4%	-380.4	0	0
8	22.9	55.6%	10.54	17.5	6.8	1526	21.7	0	72.1%	111.4%	-371.4	0	0
9	22.7	55.2%	10.54	17.5	6.9	1543	22.0	0	72.2%	111.5%	-360.2	0	0
10	22.2	54.9%	10.54	17.5	7.0	1560	22.2	0	72.2%	111.5%	-328.9	0	0
11	22.2	53.6%	10.54	17.6	7.3	1630	23.2	0	72.4%	111.7%	-257.3	0	0
12	22.4	51.7%	10.54	17.7	7.8	1735	24.7	0	72.7%	112.0%	-123.1	0	0
13	22.9	49.0%	10.54	17.9	8.5	1893	26.9	70.4	73.2%	112.4%	89.5	3.2	28.1
14	23.9	45.4%	10.54	18.2	9.5	2125	30.2	70.4	73.8%	112.9%	380.4	3.1	122.5
15	25.1	42.4%	10.54	18.4	10.5	2341	33.2	70.5	74.4%	113.3%	644.4	3.0	212.4
16	25.8	41.2%	10.54	18.5	10.9	2431	34.5	70.5	74.6%	113.5%	760.7	3.0	253.4
17	25.5	42.9%	10.54	18.4	10.3	2305	32.7	70.5	74.3%	113.2%	604.1	3.0	198.4
18	24.3	47.1%	10.54	18.1	9.0	2018	28.7	70.3	73.6%	112.6%	241.6	3.1	76.9
19	23.0	52.3%	10.54	17.7	7.6	1700	24.2	0	72.6%	111.9%	-156.6	0	0
20	22.0	56.6%	10.54	17.4	6.6	1474	21.0	0	71.9%	111.3%	-458.7	0	0
21	21.4	60.1%	10.54	17.2	5.8	1302	18.6	0	71.3%	110.8%	-662.3	0	0
22	21.0	62.3%	10.54	17.0	5.4	1200	17.1	0	71.0%	110.4%	-805.5	0	0
23	20.8	64.2%	10.54	16.9	5.0	1116	15.9	0	70.7%	110.1%	-917.3	0	0

Comparing the figures in **Table 6-2** and **Table 6-3**, it could be found that the cooling performance of the DPC achieves great promotion with COP from a mean value of 11.0 to 31.0 and temperature drop from 3.4°C to 9.8°C owing to the pre-dehumidification process while keeping the humidity ratio at 10.54 g/kg as per the design indoor condition.

6.2.4 Annual Energy-Saving Potential

As per the pre-set design indoor temperature, the outdoor temperatures above 26°C are screened out and plotted by hour, as shown in **Fig. 6-4**. There are totally 1045 hours when the outdoor temperature is above 26°C all year round, including 47 hours appearing out of service time, i.e. 0:0-7:00. Therefore, the annual service time for coolers amounts to 998 hours.

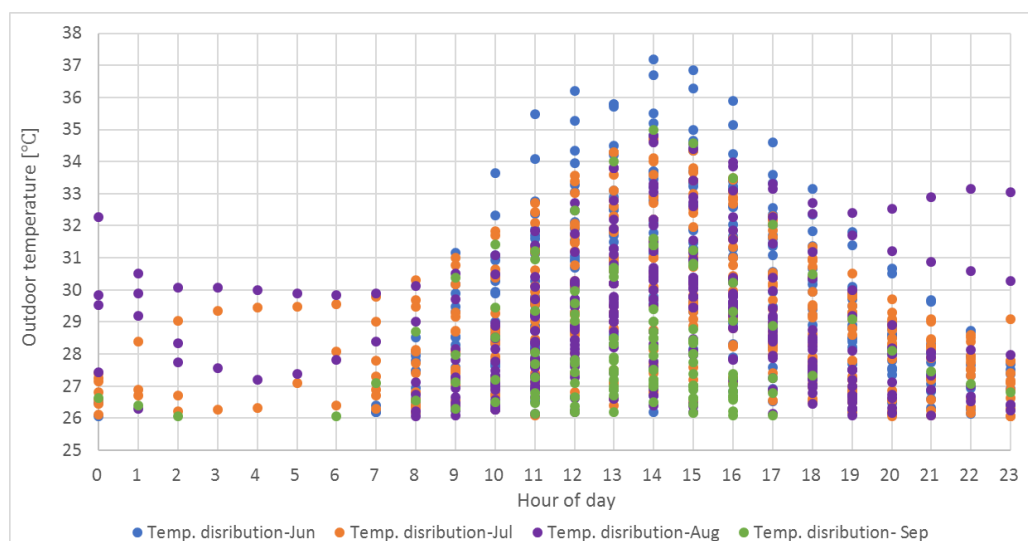


Fig. 6-4: Annual cooling time by hour.

To evaluate the annual energy saving potential, the cooling performance of the proposed DPC is calculated as per the hourly outdoor air temperature with fixed humidity ratio of 10.54 g/kg, which corresponds to the design indoor condition. To simply the calculation, the median of each temperature range is set as calculation value with error evaluation detailed in **Table 6-4**. It can be seen that each deviation of all the computed parameters is less than 5%. Therefore, the calculation by range media is rational and reliable and will be used in the following evaluation of annual cooling performance.

Table 6-4: Validation of the calculating temperature and summary of service hourage.

Calculating Temp. (°C)	Temp. range (°C)	Hourage (7:00-23:00) (hour)	Hourage (0:00-7:00) (hour)	PA temp. deviation (-)	CC deviation (-)	COP deviation (-)	DPE deviation (-)	WBE deviation (-)
26.5	26-27	160	18	0.6%	4.8%	5.0%	0.4%	0.2%
27.5	27-28	184	10	0.6%	4.5%	4.2%	0.4%	0.2%
28.5	28-29	164	3	0.5%	4.1%	3.9%	0.4%	0.2%
29.5	29-30	138	11	0.5%	3.9%	3.9%	0.4%	0.2%
30.5	30-31	109	4	0.5%	3.6%	3.6%	0.3%	0.2%
31.5	31-32	95	0	0.5%	3.4%	3.4%	0.3%	0.2%
32.5	32-33	56	1	0.5%	3.2%	3.2%	0.4%	0.2%
33.5	33-34	50	0	0.5%	3.0%	3.0%	0.3%	0.1%
34.5	34-35	26	0	0.5%	2.9%	2.8%	0.3%	0.1%
35.5	35-36	11	0	0.5%	2.7%	2.7%	0.3%	0.1%
36.5	36-37	4	0	0.5%	2.6%	2.7%	0.3%	0.1%
37.2	37-38	1	0	0.0%	0.0%	0.0%	0.0%	0.0%
Sub-total:		998	47					

* **Deviation** means the max. deviation within the temp. range. **CC** - Cooling Capacity. * **Temp. range** means greater than or equal to the lower range and less than the upper range.

Fig. 6-5 shows the cooling load for fresh air and cooling capacity of the proposed DPC by supplying same amount of fresh air. It is clear a great deal of bonus cooling is offered along with the fresh air supply. Corresponding to the relatively steady supply air temperature, seen in **Table 6-5**, the bonus cooling is between 1384 W and 1799 W in the IA temperature range of 26.5°C to 37.5°C. In **Fig. 6-5**, with the rise of outdoor air temperature, the PAC power consumption for cooling the fresh intake air increases linearly while the power demand by the proposed DPC stays steadily at the lower level of 70 W.

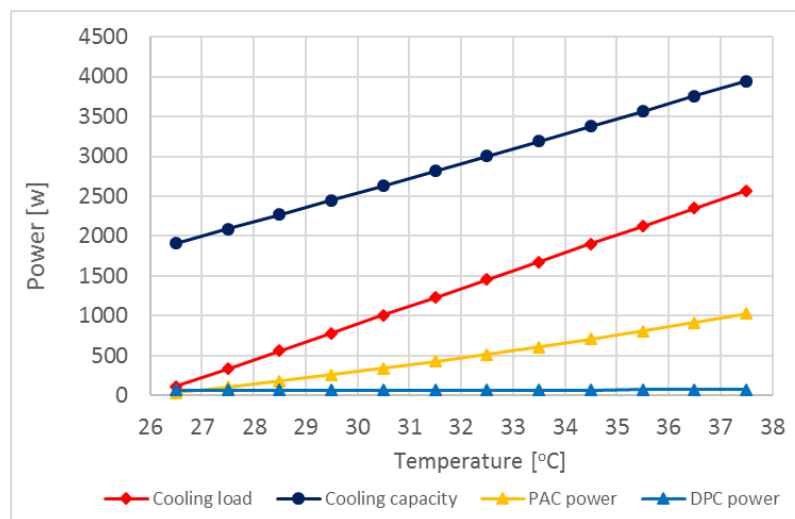


Fig. 6-5: Cooling load and power consumption with outdoor air temperature.

Table 6-5 gives the parameters in detail. Within the whole working temperature range, the proposed DPC could supply fresh air of 685.2 m³/hr at relatively steady temperature level, i.e. 18.0°C -19.8°C and cooling effectiveness (DPE between 73.3% and 77.8%; WBE between 112.4% and 115.4%). Another bonus is the self-adaptability of cooling capacity. With the rise of outdoor temperature and cooling load, the cooling capacity of the proposed DPC greatly improves accordingly rather than going downward like the conventional PAC.

Table 6-5: Cooling performance and power consumption under various outdoor temperature.

No.	Outdoor temp.	RH	PA temp.	temp. drop	COP	DPC Power	DPE	WBE	Cooling capacity
	(°C)	(-)	(°C)	(°C)	(-)	(W)	(-)	(-)	(W)
1	26.5	48.7%	18.0	8.5	27.2	70.3	73.3%	112.4%	1911
2	27.5	46.0%	18.2	9.3	29.7	70.3	73.7%	112.8%	2089
3	28.5	43.4%	18.4	10.1	32.2	70.4	74.2%	113.2%	2268
4	29.5	40.9%	18.6	10.9	34.7	70.6	74.7%	113.5%	2450
5	30.5	38.6%	18.7	11.8	37.3	70.6	75.1%	113.8%	2632
6	31.5	36.5%	18.9	12.6	39.9	70.6	75.5%	114.1%	2816
7	32.5	34.5%	19.1	13.4	42.5	70.6	76.0%	114.4%	3002
8	33.5	32.6%	19.3	14.2	45.1	70.7	76.4%	114.7%	3188
9	34.5	30.8%	19.4	15.1	47.7	70.8	76.8%	114.9%	3377
10	35.5	29.2%	19.6	15.9	50.3	70.9	77.1%	115.2%	3566
11	36.5	27.6%	19.7	16.8	53.0	70.9	77.5%	115.4%	3756
12	37.2	26.6%	19.8	17.4	54.9	70.9	77.8%	115.5%	3890

No.	Cooling load	PUA COP	PAC power	eq. PAC power	Annual cooling load	Annual DPC cooling	Annual PAC power	Annual DPC power	Annual eq. PAC power
	(W)	(-)	(W)	(W)	(kW)	(kW)	(kW)	(kW)	(kW)
1	111.9	3.18	35.2	601.1	17.9	305.8	5.6	11.2	96.2
2	335.6	3.12	107.6	670.0	61.8	384.4	19.8	12.9	123.3
3	559.3	3.06	183.0	742.0	91.7	372.0	30.0	11.6	121.7
4	783.1	3.00	261.4	817.9	108.1	338.1	36.1	9.7	112.9
5	1006.8	2.93	343.1	896.9	109.7	286.9	37.4	7.7	97.8
6	1230.6	2.87	428.3	980.1	116.9	267.5	40.7	6.7	93.1
7	1454.3	2.81	517.2	1067.6	81.4	168.1	29.0	4.0	59.8
8	1678.0	2.75	610.0	1158.9	83.9	159.4	30.5	3.5	57.9
9	1901.8	2.69	707.1	1255.6	49.4	87.8	18.4	1.8	32.6
10	2125.5	2.63	808.7	1356.7	23.4	39.2	8.9	0.8	14.9
11	2349.3	2.57	915.1	1463.1	9.4	15.0	3.7	0.3	5.9
12	2505.9	2.52	992.7	1541.0	2.5	3.9	1.0	0.1	1.5
Total:					756.2	2428.1	261.0	70.3	817.6

eq. = equivalent, means to generated cooling as much as DPC does.

To match the bonus cooling with fresh intake air by the proposed DPC, more power is required for the conventional PAC. The total power consumption to match the cooling supplied by DPC is the equivalent PAC power consumption in **Table 6-5**. The value of annual energy saving could be attained by multiplying the respective power consumption at each computing temperature and the counted hourage in **Table 6-4**.

Fig. 6-6 compares the power consumption by the proposed DPC and conventional PAC at the same cooling capacity and various outdoor air temperature. It is clear the energy-saving effect greatly improves with the rise of outdoor air temperature. The comparison of annual power consumption between DPC and PAC in **Fig. 6-7** illustrates the great difference. To meet the pre-set requirement for fresh air, the annual power demand for the conventional PAC will be 817.6 kW, seen **Table 6-5**, while just 70.3 kW for the proposed DPC. It means a energy-saving rate of 91.4%.

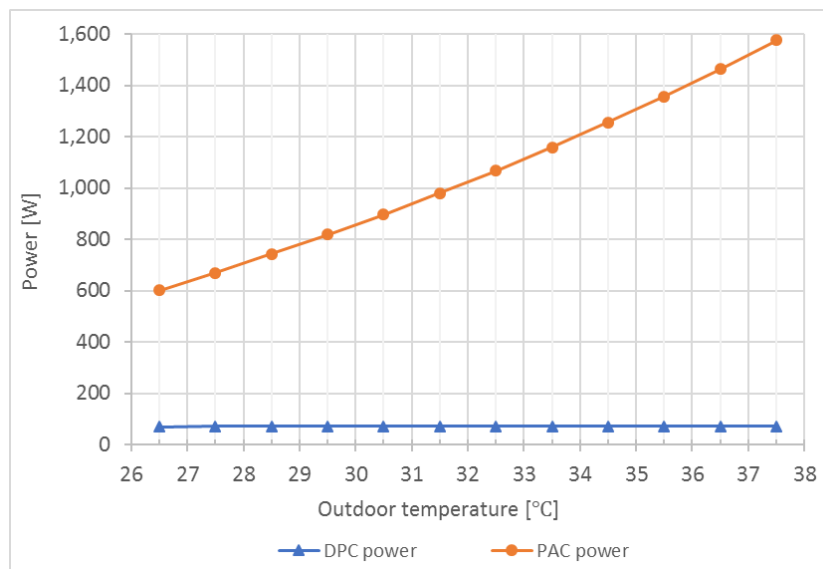


Fig. 6-6: Power consumption by DPC and PAC at same cooling capacity.

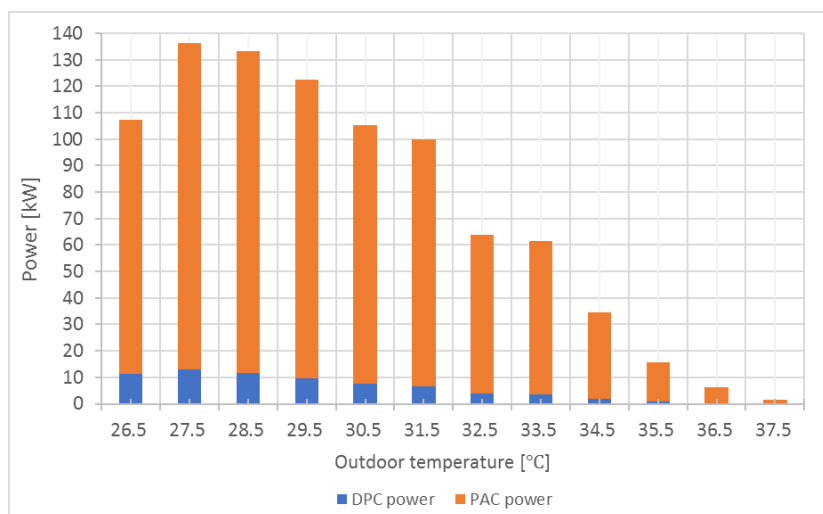


Fig. 6-7: Comparison of annual power consumption between DPC and PAC.

6.3 Life-cycle Economic Analysis

6.3.1 Capital Cost

The capital cost of the prototype DPC is estimated by adding together the individual prices of all the components. The prototype was fabricated in China and most of the components were purchased in local markets, excluding the fans from the UK for GBP 115 each (equivalent to CNY 1080). **Table 6-6** provides a list of cost breakdown and indicates that the initial cost of such a unit is CNY 8756 equal to around GBP 1000. For batch purchase, the cost might get a 30% reduction and lower to about GBP 700. Furthermore, the cost details of the various system components are presented in **Fig. 6-8**. The fans are the most expensive in the system components, accounting for 49.3% of the total system cost.

Table 6-6: Capital cost breakdown of the prototype DPC.

No.	Item	Description	Quantity	Price per unit (VAT included)	Line total
1	Fabric for wet channel	Coolmax, double pique, 170gsm	67.9 m ²	¥20.1/ m ²	¥1,365
2	Aluminum coil	0.27(thickness)*1050(width)*C	67.9 m ²	¥13.2/ m ²	¥896
3	Marine adhesive	Sikaflex-291i	4	¥123	¥492
4	Water distributor	4/3+32/24	34m+0.8m	-	¥220
5	Fan	Ebm- R3G225-RE07-03	4	¥1,080	¥4,320
6	DC water pump	24V, Hydraulic head 11m, 450L/hr	1	¥134	¥134
7	Inner frame and outer casing	Aluminum frame and steel casing	1	¥800	¥800
8	Water sink	800*360*10, PP	1	¥50	¥50
9	Insulation board	10mm (thickness)	8m	¥70	¥35
10	Rubber Seal strip	5mm(thickness)10mm(width)	1	¥86	¥86
11	Gasket	5mm (thickness)	1950	¥0.08	¥156
12	Silicon sealant	-	6	¥2	¥12
13	Water level sensor	-	2	¥20	¥40
14	Electromagnetic valve	220VAC	1	¥50	¥50
15	Time relay	DH48S-S, 220VAC , 0.1s-990h	1	¥100	¥100
				Total	¥8,756

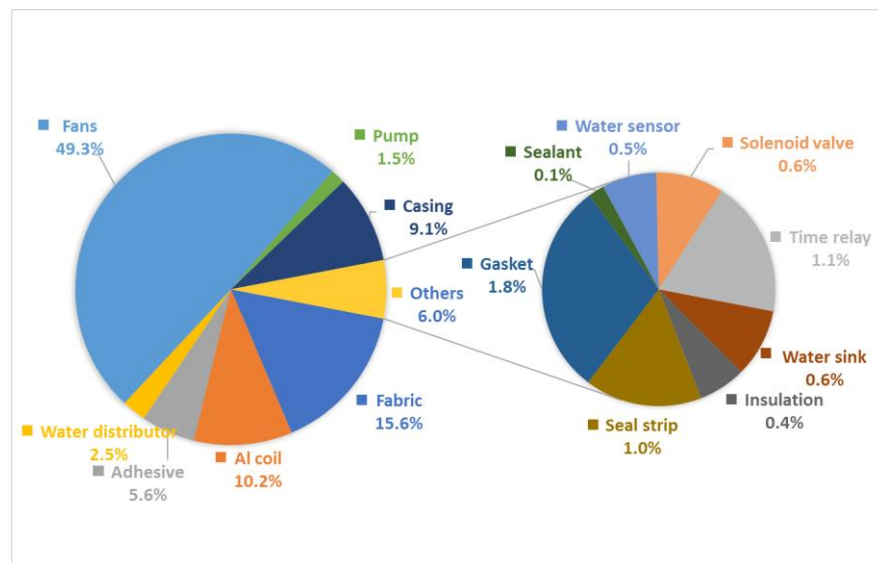


Fig. 6-8: Cost breakdown of the proposed DPC prototype.

6.3.2 Annual Operational Cost and Saving

The operational cooling performance is evaluated under the relatively adverse working condition in warm and humid climate, i.e. the real hourly weather parameters in 1999 which is recommended as the typical meteorological year (for design) by China Meteorological Bureau, Climate Information Centre, Climate Data Office [6-3].

The annual operational energy cost was calculated by the hourly weather data based on the validated simulation tool by detailed experimental research. The proposed DPC was pre-set to supply cooling fresh air in service time from 7:00 to 23:00. The design indoor temperature was set at 26°C and coincident RH of 50%. Accordingly, the outdoor air must be dehumidified to meet the humidity requirement in most of the cooling hours either for the proposed DPC or any other cooling technologies. Therefore, the following analysis of operational energy saving is based on the dehumidified air, i.e. the design humidity ratio of 10.54 g/kg.

Table 6-7 gives the annual power demand of 70.3 kW for the proposed DPC and 817.6 kW for the compared conventional PAC supplying the same amount of cooling of 2428.1 kW. Thus, 747.3 kW electricity could be saved by the replacement of PAC with the proposed DPC. As per the local power tariff for commercial use of CNY 0.7625 [6.4], the annual operational energy cost saving would be CNY 570.

The annual power cost breakdown is listed in **Table 6-8**. It is notable that with the rise of outdoor temperature, i.e. the cooling load, the cooling output of the DPC greatly improves whilst the PAC goes down. It contributes to shaving the power peak load for cooling. This is more significant for the economy of the power grid, regarding the potential saving of 91.4% power demand by air conditioning.

Table 6-7: Annual operating costs of DPC and PAC.

	Service hourage	Power consumption	Power tariff*	power cost
	(h)	(kWh)	(¥/kWh)	(¥)
PAC	998	817.6	0.7625	623.42
DPC	998	70.3	0.7625	53.60

* Local power tariff for commercial use.

6.3.3 Annual Maintenance Cost

The maintenance of the DPC system mainly exists in the water system. As water evaporates, it leaves behind dissolved salts and other impurities, concentration of which will gradually rise in the water remaining in the system. This leads to blocking of the evaporation medium and reduced cooling performance. Consequently, the sump water needs to be dumped off regularly. The amount of water bled/dumped off is dependent on the bleeding method used and the quality of feeding water. There are three bleeding/dumping systems commonly

employed, i.e. constant bleed off, salinity level monitoring, and periodic/timed drain off systems [6.5].

Therefore, the water consumption of the proposed DPC includes the water evaporated to provide the cooling effect and the water dumped off for the purpose of cleaning and avoiding high salt concentration. Based on the extensive investigation, it is reported that the total water consumption is largely dominated by the moisture evaporation for common cases [6.5].

There are two methods to calculate the water evaporated. One is by means of latent heat of evaporation. It should be noted that the cooling effect by water evaporation is not only for product air but also for exhaust air. The other is by means of HR increment in exhaust air. The latter is adopted to evaluate the annual water consumption. In this case, the PA flow rate is 685.2 m³/h with working air ratio at 0.364. It means the exhaust air flow rate is 392.2 m³/h.

Table 6-8 presents the details to evaluate the volume of evaporated water all year round. The exhaust air is assumed at saturated state and intake air being pre-treated to the design HR level of 10.54 g/kg. The EA temperature at various outdoor air temperature could be figured out by the dedicated simulation software. The total EA flow rate could be attained with the service hourage at flow rate of 392.2 m³/h. Accordingly, the final calculated result of the annual evaporated volume is 3335.5 kg.

Table 6-8: The volume of evaporated water all year round.

No.	Outdoor temp.	HR	EA temp.	saturation HR	Service hourage	HR increment	Evap. Amount
	(°C)	(g/kg)	(°C)	(g/kg)	(hour)	(g/kg)	(kg)
1	26.5	10.54	22.5	17.27	160	6.73	422.3
2	27.5	10.54	23.0	17.82	184	7.28	525.4
3	28.5	10.54	23.6	18.49	164	7.95	511.4
4	29.5	10.54	24.1	19.08	138	8.54	462.2
5	30.5	10.54	24.7	19.80	109	9.26	395.9
6	31.5	10.54	25.2	20.41	95	9.87	367.7
7	32.5	10.54	25.7	21.05	56	10.51	230.8
8	33.5	10.54	26.2	21.70	50	11.16	218.8
9	34.5	10.54	26.7	22.38	26	11.84	120.7
10	35.5	10.54	27.2	23.07	11	12.53	54.1
11	36.5	10.54	27.7	23.78	4	13.24	20.8
12	37.2	10.54	28.0	24.22	1	13.68	5.4
				Total:	998		3335.5

On the other hand, the water being dehumidified from the outdoor air in the pre-treatment process could be also calculated with the hourly HR data given by [6.3] within the service hours. The statistical result presents the total volume of dehumidified water in the annual service time is 3061.2 kg.

The difference between the water evaporated to perform cooling and the water pre-dehumidified from the intake air is only 0.27 t per year. It is such a small figure that could be neglected in view of year-round.

Thus, it is concluded that the annual maintenance cost could be negligible.

6.3.4 Cost Payback Period and Life-cycle Net Cost Saving

The cost payback period for operating such a DPC under warm and humid climate e.g. in Beijing, to replace a conventional PAC can be estimated by Eq. [6-1].

$$PP_{DPC} = \frac{C_{c,DPC} - C_{c,PUA}}{(C_{o,PUA} + C_{m,PUA}) - (C_{o,DPC} + C_{m,DPC})} \quad [6-1]$$

where, PP_{DPC} is the payback period of the DPC unit (year); $C_{c,DPC}$ and $C_{c,PAC}$ is the capital cost (CNY); C_o and C_m are respectively the annual operational and maintenance costs (CNY).

The capital cost CNY 6129 of the proposed DPC is calculated with 30% off the prototype total costs due to the cost reduction by batch purchase. The price CNY ¥4000 of a 4 kW-rated conventional PAC is based on the general local marked information. Regardless of the difference in maintenance costs due to the aforementioned insignificance, the payback period would be 3.7 years to replace a 4-kW rated conventional PAC by the proposed DPC under the warm and humid climate in Beijing area.

As per the local regulation, a conventional PAC is considered to have a life span up to 12 years [6.6]. The expected life span of the proposed DPC mainly depends on the fans, which covers nearly half of the total initial cost, due to its specific configuration. Generally, the bearing life expectancy determines that of the fan and thereinto the lubricating grease is the limiting factor. As per the manufacture' information [**appendix 3**], the lubricant life expectancy would be 85810 hours, which covers 86-year normal service in view of the aforementioned scenario in Beijing.

The heat exchanger, which accounts for less than 30% of the total capital cost, is consumable and replaceable in view of the sandwich-structure exchanging sheet and the operating condition. A life expectancy of 10,000 hours for the heat exchanger, i.e. 10-year active service, is conservatively estimated based on the preliminary lab endurance test. In general, an overall static life span of the proposed DPC is estimated by 30 years.

The life-cycle net cost saving, CS_{DPC} (CNY), of this proposed DPC in energy bills can be determined by

$$CS_{DPC} = (30 - PP_{DPC}) \left[(C_{o,PAC} + C_{m,PAC}) - (C_{o,DPC} + C_{m,DPC}) \right] \quad [6-2]$$

The breakdown of life-cycle cost saving is listed in **Table 6-9**.

Table 6-9: Cost payback period and life-cycle net cost saving.

	Power consumption	Annual maintenance cost	Annual operational cost	Capital cost	Payback period	Life-cycle cost saving
	(kWh)	(¥)	(¥)	(¥)	(year)	(¥)
PAC	817.6	0	623.42	4000	3.7	14991
DPC	70.3	0	53.60	6129		

6.4 Life-Cycle Environmental Benefits

6.4.1 Greenhouse Gas (GHG) Emission

Environmental benefits can be estimated easily by using the annual CO₂ emission factor when operating this DPC to replace a conventional PAC [6.7].

This is given by

$$CR_{DPC} = f_{co_2} (Q_{PAC} - Q_{DPC}) \quad [6-3]$$

where, CR_{DPC} is the carbon reduction of the proposed DPC (kg); f_{co_2} is the CO₂ emission factor for electricity consumption; Q_{PAC} and Q_{DPC} are the annual electricity consumption by the PAC and DPC respectively (kWh).

The local CO₂ emission factor in Beijing is 0.7757 kg/kWh due to the efficiencies of the regional power grid [6.8], published by the Department of Climate Change, China National Development and Reform Commission.

6.4.2 Water Use Issues

One of the common criticisms of the common evaporative cooling is large scale use of water to perform cooling, especially in hot and dry climate and water-deficient area. Owing to the efficient water distribution control and utilization, as previously discussed, the annual water consumption for a proposed nominal 4-kW rated DPC applied in Beijing is only 0.27 t per year, including the water extracted in the pre-humidification process.

What should not be ignored is a significant amount of water is also used in thermal electric power plants to generate the electricity required to power a conventional PAC. Reducing the amount of electrical energy consumed for cooling thus also means reducing water consumption in the power plant. From this point of view, electricity saving means water conservation.

The referenced target value of local water consumption for thermal power generation in Beijing is 2.5 m³/MWh [6.8]. Accordingly, the water saving could be calculated by

$$WS_{DPC} = (Q_{PAC} - Q_{DPC}) \times 2.5 \times 10^{-3} - WC \quad [6-4]$$

where, WS_{DPC} is the water reduction of the proposed DPC (m³) per year; WC means water consumed (m³). The value of WC equals to the difference between the water evaporated to perform cooling and the water extracted in the pre-dehumidification process. In this case, the WC value is 0.27 m³.

Table 6-10 lists the life-cycle environmental benefits in terms of carbon reduction and water conservation.

Table 6-10: Environmental benefits of the proposed DPC.

Environmental benefits	Location: Beijing, China	
	CO ₂	CO ₂ emission factor (kg CO ₂ /kWh) [7.8]
CO ₂ emission reduction (kg)		579.7
Life cycle CO ₂ emission reduction (t)		17.4
Water	Thermal power factor (m ³ /MWh) [7.9]	2.5
	Water saving (m ³)	1.60
	Life cycle water saving (m ³)	48
*Power saving per year: 747.3 kWh; Life expectancy: 30 years.		

6.5 Chapter Summary

This chapter provided a feasibility study for the use of the proposed dew point cooler in Beijing, a representative city in warm and humid climate. The overall analysis included a prediction of the annual operational performance, economic rewards, and associated environmental benefits.

Hourly prediction of cooling performance in service hours (7:00-23:00) in Beijing was conducted and the results indicate that the dew-point cooling effectiveness is in the range of 73.3% (outdoor temperature of 26.5°C) to 77.8% (outdoor temperature of 37.2°C) and 112.4%-115.5% for wet-bulb cooling effectiveness. With the rise of cooling demand, i.e. outdoor temperature from 26.5°C to 37.2°C, the cooling capacity keeps increasing from 1911 W to 3890 W along with the value of COP from 27.2 to 54.9. The product air temperature could remain in the range of 18.0°C to 19.8°C with the outdoor air temperature varying from 26.5°C to 37.2°C.

Calculating the cooling performance hour by hour in year-round service time with the validated simulation tool, the results show that the annual power consumption is only 70.3 kWh to offer 2428.1 kWh cooling capacity, excluding

the power demand for dehumidification. Thus, the annual mean value of COP is 34.5.

Comparing to the conventional PAC under the same conditions, 91.4% of annual power demand could be saved. Moreover, most of the saved electricity power comes from the daily peak demand hour. This means the application of the proposed DPC contributes to reducing the stress of power grid by peak shaving.

Taking account of the water harvested by air pre-dehumidification, the annual water consumption is less than 0.3 t to provide the cooling of 2428.1 kWh.

To replace a typical PAC, the capital cost will increase by about CNY 2000 while the annual operational cost could get a reduction about CNY 570. Thus, the payback period would be less than 4 years. During its life span of 30 years, the total cost saving would be CNY 14991 comparing to the PAC.

The proposed DPC could achieve the highest life-cycle CO₂ emission reduction of about 17.4 t in Beijing when using it to replace the widely used PAC.

CHAPTER 7: CONCLUSIONS AND FURTHER WORK

7.1 Conclusions

The research has presented an in-depth investigation of a novel dew point air cooler (DPC) that was undertaken through a critical literature review, optimal concept design, theoretical analysis, development of dedicated simulation programme, prototype construction, laboratory-controlled tests, validation of the simulation models, and socio-technical acceptance analysis.

The major achievements are: (1) a full range of computer simulation models based on heat and mass transfer analysis, which were validated by published results of peer researchers and own independent experiments; (2) a 4-kW rated prototype DPC undergone severe lab tests; and (3) a socio-economic assessment method to analyse energy saving, economic and environmental benefits for the proposed DPC relative to the conventional mechanical vapour compression air conditioners.

The major conclusions derived from the PhD research are given below.

7.1.1 Application of New Materials and New Processes

(1) The application of moisture-wicking and quick-drying fibrous material helps distribute moisture efficiently across the evaporating area, promote moisture evaporation within its porous surface and reduce the circulating water flow rate that consequently leads to the reduced pump power consumption. Test results show that the circulating water flow rate could be controlled at about 3 times of the water evaporation volume, which is significantly lower compared to those applied in existing dew point air coolers, i.e. 20-30 times. This leads to significant power saving in water pump operation and reduced water use, which

is particularly meaningful for its application in water-scarce and hot & dry climate regions.

(2) The use of the aluminium/fibre based corrugated heat and mass exchanging sheets, as the replacement to the existing flat-plate sheets, leads to increased heat transfer and decreased air flow resistance, owing to the increased heat transfer area and removal of the tri-angular supporting guides that are commonly used in the flat-plate heat exchanger. Compared to the non-metallic exchanging sheets which are the common choice for the existing evaporative coolers, aluminium based heat exchanger has a better heat transfer performance, owing to the enhanced thermal conductivity of the thin aluminium panel.

(3) An effective binding skill involving roughing treatment to the metal surface and applying a marine adhesive enables a firm combination between the two material layers, thus creating long life-cycle and better-performance heat exchanging sheets.

7.1.2 Computer-Aided Design, Optimization and Prediction Tool

A dedicated numerical simulation software with friendly GUI (graphical user interface) was developed, validated and applied in the structural optimization of the heat and mass exchanger (HMX) and performance prediction in case study for socio-economic evaluation. The programme was developed in EES (Engineering Equation Solver) environment, involving the professional analysis of heat/mass transfer and fluid dynamics. By simply changing the setup of structural parameters, the programme could also be used for the conventional plane-plate HMX simulation. The simulation results under various conditions were proved to be effective with an accuracy of less than 4% in practical application.

7.1.3 Numerical Investigation

With the validated simulation tool, the dynamic process of heat and mass exchange in the HMX and impacts of intake air parameters, channel dimensions and operational parameters on cooling performance were investigated and the results were well explained with the theoretical analysis. The main conclusions from the parametrical study are listed below.

(1) Cooling capacity increases substantially with the intake air temperature, i.e. the higher the outdoor temperature, the better the cooling performance. For the proposed DPC, in the IA temperature range of 25°C to 40°C, the variation of PA temperature could be controlled to a level of 3.1°C, i.e. 16.4°C-19.5°C, at the same airflow rate.

(2) Higher IA velocity helps improve the cooling capacity whilst it has a negative impact on COP of the unit. The suggested IA velocity should be around 2 m/s.

(3) Humidity ratio imposes a great impact on the cooling performance of the unit.

(4) Unlike other performance indicative parameters, e.g. cooling capacity and COP, the cooling effectiveness is directly related to the IA conditions. Lower temperature and higher humidity ratio, referring to the unfavourable operational condition, lead to a higher cooling effectiveness.

(5) Small-size channel gaps lead to the reduced airflow rate, low cooling capacity and increased airflow resistance and pump power consumption, while large-size channel gaps lead to the reduced cooling effectiveness, increased PA temperature and large unit size.

(6) Increased channel length leads to the growing heat exchange rate and consequently, the unit suffers from the larger airflow resistance and higher power consumption.

(6) Geometric similarity between the computational element and the real entity is as important as initial and boundary conditions in numerical modelling. In this case, 15-time length of the bench corrugation could be considered reliable to keep the geometric similarity with the real entity.

(7) Working air ratio is an essential parameter in operation.

(8) The impact of inlet water temperature on the latent cooling may be negligible for controlled water volume.

7.1.4 Laboratory Testing

Series of tests were carried out under the controllable laboratory environment. Initial tests were conducted under six typical IA conditions to compare the cooling performance with the high-efficiency commercial like product, i.e. *Coolerado*® M30. The comparison, i.e. PA temperature (20.8°C vs. 21.5°C), wet-bulb cooling effectiveness (102.4% vs. 93%) and COP (37.4 vs. 18.4), manifests the huge superiority and potential of the proposed DPC in cooling performance, especially in energy use.

Following tests identified the optimal working air ratio of 0.364 for the prototype cooler. Under the standard test condition, i.e. dry-bulb temperature of 37.8°C and coincident wet-bulb temperature of 21.1°C, the prototype cooler achieved the wet-bulb cooling effectiveness of 114% and dew-point cooling effectiveness of 75%, yielding a significantly high energy efficiency (COP) of 52.5 at the optimal working air ratio. Compared to the conventional mechanical vapour compression air conditioners which have the COP of around 3, the new DPC had 17.5 times higher COP, leading to the reduction in electrical power consumption by about 91%.

Experimental tests under various climatic conditions manifested the climate adaptability of the proposed DPC and further indicated that the lower IA relative humidity led to a higher cooling efficiency, while the lower cooling output helped increase COP and cooling effectiveness of the proposed cooler.

7.1.5 Socio-Economic Assessment

A case study of the proposed DPC applied in warm and humid climate in Beijing (China) was carried out, including an hourly cooling performance analysis in a typical cooling day, annual energy performance prediction, economic analysis and environmental sustainability assessment based on the adaptively improved simulation tool with the exclusive experimental results.

It is found by hourly calculation of the cooling performance that with the rise of cooling demand, i.e. outdoor temperature in a day, the cooling capacity as well as the value of COP keeps increasing, and vice versa. The PA temperature could remain in the range of 18.0°C to 19.8°C when the outdoor air temperature varying from 26.5°C to 37.2°C at constant air supply rate.

Hourly cooling performance in year-round service shows that the annual power consumption is only 70.3 kWh to offer 2428.1 kWh cooling, excluding the power demand for dehumidification. The annual mean value of COP is 34.5. Comparing to the conventional packaged air conditioner (PAC) under the same conditions, 91.4% of annual power demand could be saved. Taking account of the water harvested by air pre-dehumidification, the annual water consumption is less than 0.3 ton to provide the cooling of 2428.1 kWh.

To replace a typical mechanical PAC, the capital cost will increase by about CNY 2000. However, the payback period would be less than 4 years. During its life span of 30 years, the proposed DPC could achieve a total cost saving of CNY

14991 and CO₂ emission reduction of about 17.4 ton in Beijing when using it to replace the widely used PAC.

The significant leap forward in the dew point air cooling technology will open up enormous global business in the near future, thus bringing about enormous economic, environmental and sustainability benefits worldwide. The research created an opportunity to develop a novel dew point air cooler with significantly enhanced energy efficiency, greatly reduced power use and much smaller unit size and would contribute to the realisation of the global energy saving and carbon reduction targets, and bring about the enormous economic, environmental and sustainability benefits to the world.

7.2 Problems and Further Opportunities

Although such achievements have been made and validated in theoretical investigation and laboratory tests, there are still many problems and works that need further exploration.

7.2.1 Cooler Structure and Manufacture

(1) Due to the aforementioned problem of material fracture during mould pressing, the corrugated shape of the exchanging sheet has been greatly limited. Further exploration for proper material adapting to the mechanical deformation would help enlarge the effective area for heat and mass exchange and make the configuration more compact.

(2) There are two main problems existing in the adopted sandwich structure to bond the functional fabric and aluminium baseboard with marine adhesive. One relates to the cost of the special adhesive, and the other is the manufacture quality

of the sandwich sheet is hard to guaranteed due to the laborious and boring handwork. Attempt for a new process of thermal pressing [4.6], has been made to remove the use of adhesive and associate manual work.

(3) Considering the cost and weight of the qualified aluminium sheet, light-weight plastic material and related moulding process could be tried to replace the metal sheet for large-scale commercial production and evaluated on heat transfer performance.

(4) The detailed configuration of the HMX could be further optimized in the layout and dimension of the perforations on the exchanging sheet and the size of the air entrance.

7.2.2 Numerical Simulation

The calculation of moisture evaporation is based on the universal correlation between the heat and mass transfer. Although the simulation programme could give final results with high reliability under the practical range of entry conditions, the monitoring process parameter of relative humidity along the wet channel was found easy to approach the saturated state, commonly within the distance of 40 cm. It manifests the calculated evaporating rate is bigger than the actual value. Although a proper correction factor was found based on experience and applied to the coefficient of mass transfer, the intrinsic mechanism is still undiscovered.

The study on impacts of temperature, air velocity and partial vapour pressure on evaporating rate would help develop a more reliable model to numerically simulate the evaporation process along the wet channel.

7.2.3 Experimental Investigation

(1) Due to the limitation of the laboratory condition, the cooling performance test under high humidity environment, i.e. humidity ratio beyond 20 g/kg and relative humidity over 70%, was not conducted. It would be interesting to explore the difference if possible.

(2) The moisture distribution across the fabric at the standing-up state of the exchanging sheet was only observed by sight. In-depth investigation of the moisture diffusion with dynamic evaporation would help for a more accurate water supply scheme.

(3) During adjustment of the fans' output, it was found the variation of the upper supply fans and the lower exhaust fans coupled. Imbalance between the exhaust air and product air would lead to sharp rise of power consumption. The actual overall efficiency of the fan in operation was usually at the level of about 55%. All these implies there is still potential to further reduce the power consumption by optimizing fan selection and layout.

(4) For the specific configuration of the prototype, the plenum above the water sink is under negative pressure condition due to the operation of the exhaust fans. There is a fair chance for air suction not only from the surroundings but more seriously from the intake air. More comprehensive scheme against air leakage should be paid more attention in the further development.

(5) Experimental investigation on the temperature variation along the channel would help make sure of the heat and mass exchanging process under the specific boundary conditions and further validate the theoretical analysis and numerical simulation.

7.2.4 Case Study

(1) It is obvious to meet the indoor comfort requirement, dehumidification is a must for air conditioning system in application in humid climate. The study of the combined operation mode with dehumidification process may approaches more to the real applied scenario.

(2) A potential applied scenario of warm and humid climate (Beijing, China) was selected to be studied and manifested the climatic adaptability of the proposed DPC. More case in various climates may help present the technical and socio-economic superiorities more intuitively.

7.2.5 Aware but Uncovered

(1) Stale smell appeared in the exhaust air during the experiment, especially after a long idle time. It is always damp in the narrow and long wet channels. The quality of the circulating water and the microorganism breeding are of great concern and should be studied carefully.

(2) The problem of performance decrease after long time running due to the contamination of the wet surface performing evaporation, e.g. scale and impurities, should be noted. Related research could help develop effective bleeding/dumping schemes to keep the cooler running always efficiently.

7.2.6 Ideal Cooler

The ideal dew point cooler is expected to be a modular product with removable low-cost HMX. It should also be easy to jointly work to adapt to various applied environment and be ease of maintenance.

REFERENCES

References for Chapter 1

- [1.1]. BP Energy Outlook 2016,
- [1.2]. United Nations Framework Convention on Climate Change, Kyoto Protocol to the United Nations Framework Convention on Climate Change,
<http://unfccc.int/resource/docs/convkp/kpeng.pdf>
- [1.3]. United Nations Framework Convention on Climate Change, Report of the Conference of the Parties on its twenty-first session, held in Paris from 30 November to 13 December 2015. Addendum. Part two: action taken by the Conference of the Parties at its twenty-first session. 2016.
https://unfccc.int/documentation/documents/advanced_search/items/6911.php?prire=600008865
- [1.4]. United Nations Framework Convention on Climate Change, Adoption of the Paris Agreement. <https://unfccc.int/resource/docs/2015/cop21/eng/109r01.pdf>
- [1.5]. IEA, Key World Energy Statistics 2016,
<https://www.iea.org/publications/freepublications/publication/KeyWorld2016.pdf>
- [1.6]. L. Pérez-Lombard, J. Ortiz, C. Pout, A review on buildings energy consumption information, *Energy Build*, 40 (2008), pp. 394–398
- [1.7]. A. Costa, M.M. Keane, J.I. Torrens, E. Corry. Building operation and energy performance: monitoring, analysis and optimisation toolkit, *Applied Energy*, 101 (2013), pp. 310–316
- [1.8]. Department for Business, Energy & Industrial Strategy, Energy Consumption in the UK (2016), <https://www.gov.uk/government/statistics/energy-consumption-in-the-uk>
- [1.9]. Pérez-Lombard, L., J. Ortiz, et al., A review on buildings energy consumption information, *Energy and Buildings*, vol. 40 (2008), pp. 394-398.

-
- [1.10]. Jiang, Y., Chinese building energy consumption situation and energy efficiency strategy, *New Architecture* (in Chinese) (2008).
- [1.11]. U.S. Energy Information Administration, *Annual Energy Review 2011*, U.S. Energy Information Administration, Washington, DC (2012) (September 27)
- [1.12]. <http://www.datacentermap.com/western-europe/>, accessed on 25/11/2016.
- [1.13]. Tianwen Li, In-depth analysis of 2013 data centre efficiency situation, *The World of Power Supply*, 6(2013) 7-8.
- [1.14]. China Data Centre Industry Development Alliance, *Development Plan for National Green Data Centre in China*, 18th March 2015.
- [1.15]. Renewable Energy Unit, Institute for Energy, Directorate-general joint research centre, European Commission, *The European Code of Conduct on Data Centre Energy Efficiency*, version 3.0, 2015
- [1.16]. Digital Realty Trust Inc, *Europe Campos Survey Results*, Jan 2013.
- [1.17]. J.G. Koomey. Worldwide electricity used in data centres, *Environ. Res. Lett.*, 3 (2008), p.3
- [1.18]. Targets elaborated within the document E2B Impact Assessment, Version 2, February 2009.
- [1.19]. Zhang, L.Z., Energy performance of independent air dehumidification systems with energy recovery measures. *Energy*, 2006. 31(8–9): p. 1228-1242.
- [1.20]. K. Daou, R.Z. Wang, Z.Z. Xia. Desiccant cooling air conditioning: a review. *Renewable and Sustainable Energy Reviews*, 2006. 10(2): p. 55-77.
- [1.21]. Chen, Q., Pan, Ning., Guo, Zeng-Yuan., A new approach to analysis and optimization of evaporative cooling system II: Applications. *Energy*, 2011. 36(5): p. 2890-2898.
- [1.22]. Goshayshi, H.R., Missenden, J. F., Tozer, R., Cooling tower—an energy conservation resource. *Applied Thermal Engineering*, 1999. 19(11): p. 1223-1235.

-
- [1.23]. Z Duan, et al, Indirect evaporative cooling: Past, present and future potentials, *Renewable and Sustainable Energy Reviews* 16 (2012) 6823-6850.
- [1.24]. Alfonso Oliva, BSRIA Market Research - BSRIA in the US and AC Trends, Air Conditioning USA 2014 AHR EXPO, 2014, www.slideshare.net/BSRIA/air-conditioning-usa-2014-ahr-expo-edited-market-research?utm_source=slideshow02&utm_medium=ssemail&utm_campaign=share_slideshow_loggedout
- [1.25]. D. Weitzel, Efficient Techniques for Estimating Baseline and Market Shares Projections from Market Transformation Interventions, Panel 6 of the 2004 ACEEE Summer Study on Energy Efficiency in Buildings, Pacific Grove, CA, 2004
- [1.26]. Zhan C. et al., Comparative study of the performance of the M-cycle counter-flow and cross-flow heat exchangers for indirect evaporative cooling – paving the path toward sustainable cooling of buildings. *Energy* 36(2011) 6790 – 6805.
- [1.27]. Davis Energy Group, Advanced evaporative cooling white paper, California Energy Commission, March 2004
- [1.28]. Zhao X, Li JM, Riffat SB. Numerical study of a novel counter-flow heat and mass exchanger for dew point evaporative cooling. *Applied Thermal Engineering* 2008; 28(14-15):1942-51.
- [1.29]. M. Jradi, S. Riffat, Experimental and numerical investigation of a dew-point cooling system for thermal comfort in buildings, *Applied Energy* 132 (2014) 524-535.
- [1.30]. C. Ren, H. Yang, An analytical model for the heat and mass transfer processes in indirect evaporative cooling with parallel/counter flow configurations, *Int. J. Heat Mass Transfer* 49 (2006) 617-627.
- [1.31]. Joohyun Lee, Dae-Young Lee, Experimental study of a counter flow regenerative evaporative cooler with finned channels, *International Journal of Heat and Mass Transfer* 65 (2013) 173-179.

-
- [1.32]. Suoying He, Zhiqiang Guan, et al., Experimental study of film media used for evaporative pre-cooling of air, *Energy Conversion and Management* 87 (2014) 874-884.
- [1.33]. Afonso, C. F. A., Recent advances in building air conditioning systems, *Applied Thermal Engineering*, vol. 26 (2006), pp. 1961-1971
- [1.34]. Z. Duan, Investigation of a Novel Dew Point Indirect Evaporative Air Conditioning System for Buildings, PhD thesis, University of Nottingham, September 2011

References for Chapter 2

- [2.1]. John Watt. *Evaporative air conditioning handbook* 2nd. Springer Science & Business Media, 2012, p5.
- [2.2]. ASHRAE. *ASHRAE handbook Fundamentals Volume: SI edition*, American Society of Heating, Refrigerating and Air -Conditioning Engineers, 2009, Chapter 33, p33.2.
- [2.3]. Huber, M.L., McLinden, M.O., Thermodynamic Properties of R134a (1,1,1,2-tetrafluoroethane) (1992). International Refrigeration and Air Conditioning Conference. Paper 184. <http://docs.lib.purdue.edu/iracc/184>
- [2.4]. Xiaoyun Xie, Yi Jiang. Comparison of Two Kinds of Indirect Evaporative Cooling System: To Produce Cold Water and To Produce Cooling Air. *Procedia Engineering* 121 (2015) 881 – 890
- [2.5]. *Evaporative Cooling Basics*, Western Environmental Services Corporation., <http://www.wescorhvac.com/Evaporative%20cooling%20white%20paper.htm>
- [2.6]. Renato Lazzarin. *Evaporative Cooling*. 27th Informatory Note on Refrigeration Technologies / January 2015.
- [2.7]. Stoitchkov, N.J., Dimitrov, G. I., Effectiveness of crossflow plate heat exchanger for indirect evaporative cooling: Efficacité des échangeurs thermiques à plaques, à courants croisés pour refroidissement indirect évaporatif. *International Journal of Refrigeration*, 1998. 21(6): p. 463-471.

-
- [2.8]. Duan Z. (Supervised by Zhao X.), Investigation of a novel dew point indirect evaporative air conditioning system for buildings. PhD thesis, University of Nottingham, Nov. 2011, 61-82, 84-95, 108-117, 145-149.
- [2.9]. Maisotsenko, V. and Gillan, L, Maisotsenko cycle for air desiccant cooling, Proceeding of the 2003 4th International Symposium on HVAC. Beijing, China. October 2003, Pages 1011-1020
- [2.10]. Elberling L., Laboratory Evaluation of the Coolerado Cooler-Indirect Evaporative Cooling Unit. Pacific Gas and Electric Company; 2006.
- [2.11]. Will Lintner, Steven A. Parker, Robi Robichaud. Coolerado Cooler Helps to Save Cooling Energy and Dollars. Technology Installation Review. U.S. Department of Energy, Energy Efficiency and Renewable Energy, by the National Renewable Energy Laboratory, DOE/GO-102007-2325. June 2007. Internet: www.eere.energy.gov/femp/
- [2.12]. K.J. Chua, S.K. Chou, W.M. Yang, J. Yan. Achieving better energy-efficient air conditioning – A review of technologies and strategies. Applied Energy 104 (2013) 87–104
- [2.13]. Bureau of Indian Standards. IS 3315-1974 Evaporative air coolers [S],1974
- [2.14]. Canadian Standards Association International. C22.2 No 104: Humidifiers and evaporative coolers [S],1983
- [2.15]. Standards Australia International Ltd. AS 2913-1987 Evaporative air conditioning equipment [S]. 1987
- [2.16]. Saudi Arabian Standards Organization. SASO 35 Evaporative air coolers [S].1997
- [2.17]. ISIRI 4514. Methods for Performance Testing of Water Cooling Tower (Wet Type). Institute of Standards and Industrial Research of Iran. Tehran, 1998.
- [2.18]. ANSI/ASHRAE Standard 143-2000 Method of Testing Direct Evaporative Air Coolers. 2001
- [2.19]. ANSI/ASHRAE Standard 133-2001 Method of Test for Rating Indirect Evaporative Coolers. 2002

-
- [2.20]. China General Administration of Quality Supervision, Inspection and Quarantine, General Administration of Quality Supervision Inspection and Quarantine. GB-T25860-2010 Evaporative air cooler. 2011
- [2.21]. Australian Greenhouse Office. Analysis of potential for minimum energy performance standards for evaporative air conditioners[R], 2001
- [2.22]. ANSI/ASHRAE Standard 143-2015 Method of Test for Rating Indirect Evaporative Coolers. 2015
- [2.23]. ASHRAE. ASHRAE handbook Fundamentals Volume: SI edition, American Society of Heating, Refrigerating and Air -Conditioning Engineers. 2009, Chapter 2, p2.3.
- [2.24]. Maisotsenko, V. and I. Reyzin, The Maisotsenko cycle for electronics cooling, Proceedings of the ASME/Pacific Rim Technical Conference and Exhibition on Integration and Packaging of MEMS, NEMS, and Electronic Systems: Advances in Electronic Packaging, San Francisco, CA, U.S. (2005), pp. 415-424.
- [2.25]. Zhiyin Duan, Changhong Zhan, Xingxing Zhang, Mahmud Mustafa, Xudong Zhao. Indirect evaporative cooling: Past, present and future potentials. Renewable and Sustainable Energy Reviews 16 (2012) 6823–6850.
- [2.26]. K.J. Chua, S.K. Chou, W.M. Yang, J. Yan. Achieving better energy-efficient air conditioning – A review of technologies and strategies. Applied Energy 104 (2013) 87–104.
- [2.27]. Hafiz M. Daraghme, Chi-Chuan Wang. A review of current status of free cooling in datacenters. Applied Thermal Engineering 114 (2017) 1224–1239.
- [2.28]. Vahid Vakiloroay, Bijan Samali, Ahmad Fakhar, Kambiz Pishghadam. A review of different strategies for HVAC energy saving. Energy Conversion and Management 77 (2014) 738–754.
- [2.29]. Bogdan Porumb, Paula Ungureșan, Lucian Fechete Tutunaru, Alexandru Șerban, Mugur Bălan. A review of indirect evaporative cooling operating conditions and performances. Energy Procedia 85 (2016) 452 – 460.

-
- [2.30]. Bogdan Porumb, Paula Ungureșan, Lucian Fechete Tutunaru, Alexandru Șerban, Mugur Bălan. A review of indirect evaporative cooling technology. *Energy Procedia* 85 (2016) 461 – 471.
- [2.31]. O. Amer, R. Boukhanouf, and H. G. Ibrahim. A Review of Evaporative Cooling Technologies. *International Journal of Environmental Science and Development*, Vol. 6, No. 2, February 2015.
- [2.32]. Yu Huang, Jian-lei Niu. A review of the advance of HVAC technologies as witnessed in ENB publications in the period from 1987 to 2014. *Energy and Buildings* 130 (2016) 33–45.
- [2.33]. R. Best, W. Rivera. A review of thermal cooling systems. *Applied Thermal Engineering* xxx (2014) 1-14.
- [2.34]. Ana Tejero-González, Manuel Andrés-Chicote, Paola García-Ibáñez, Eloy Velasco-Gómez, Francisco Javier Rey-Martínez. Assessing the applicability of passive cooling and heating techniques through climate factors: An overview. *Renewable and Sustainable Energy Reviews* 65(2016)727–742.
- [2.35]. Y.M. Xuan, F. Xiao, X.F. Niu, X. Huang, S.W. Wang. Research and application of evaporative cooling in China: A review (I) – Research. *Renewable and Sustainable Energy Reviews* 16 (2012) 3535– 3546.
- [2.36]. Y.M. Xuan, F. Xiao, X.F. Niu, X. Huang, S.W. Wang. Research and applications of evaporative cooling in China: A review (II)—Systems and equipment. *Renewable and Sustainable Energy Reviews* 16 (2012) 3523– 3534
- [2.37]. U.V.Kongre, N.T.Neware, P.A.Bagade, N.P.Ingale. Review on Two Stage Evaporative Cooler. *International Journal of Engineering and Technical Research (IJETR)*. Volume-3, Issue-1, January 2015
- [2.38]. Qun Chen, Kangding Yang, Moran Wang. A new approach to analysis and optimization of evaporative cooling system I: Theory. *Energy* 35 (2010) 2448-2454
- [2.39]. Qun Chen, Ning Pan, Zeng-Yuan Guo. A new approach to analysis and optimization of

- evaporative cooling system II: Applications. *Energy* 36 (2011) 2890-2898
- [2.40]. Fang Yuan, Qun Chen. A global optimization method for evaporative cooling systems based on the entransy theory. *Energy* 42 (2012) 181-191
- [2.41]. J.C. Santosa, G.D.T. Barros, J.M. Gurgel, F. Marcondes. Energy and exergy analysis applied to the evaporative cooling process in air washers. *International journal of refrigeration* 36(2013) 1154-1161
- [2.42]. M. Farmahini-Farahani, S. Delfani, J. Esmaeliani. Exergy analysis of evaporative cooling to select the optimum system in diverse climates. *Energy* 40 (2012) 250-257
- [2.43]. Hakan Caliskan, Ibrahim Dincer, Arif Hepbasli. Exergetic and sustainability performance comparison of novel and conventional air cooling systems for building applications. *Energy and Buildings* 43 (2011) 1461–1472
- [2.44]. Tao Zhang, Xiaohua Liua, Haida Tang, Jun Liu, Yi Jiang. Exergy and entransy analyses in air-conditioning system part1—Similarity and distinction. *Energy and Buildings* 128 (2016) 876–885
- [2.45]. Tao Zhang, Xiaohua Liua, Jun Liu, Haida Tang, Yi Jiang. Exergy and entransy analyses in air-conditioning system part2—Humid air handling process. *Energy and Buildings* 139 (2017) 10–21
- [2.46]. Tao Zhang, Xiaohua Liu, HaidaTang, Jun Liu, Yi Jiang. Performance investigation of terminal handling process in air-conditioning system from the perspective of entransy dissipation. *Energy and Buildings* Volume 137, 15 February 2017, Pages 27–37.
- [2.47]. M. Mahmood, M. Sultan, T. Miyazaki, S. Koyama, V. Maisotsenko. Overview of the Maisotsenko cycle – A way towards dew point evaporative cooling. *Renewable and Sustainable Energy Reviews* 66 (2016) 537–555
- [2.48]. Coolerado cooler helps to save cooling energy and dollars: new cooling technology target speak load reduction. United States: U.S. Department of Energy, Energy Efficiency & Renewable Energy, Federal Energy Management Program (FEMP), Report no. DOE/GO-102007-2325, (<http://www.osti.gov/scitech/biblio/908968>); 2007.

-
- [2.49]. Yi Jiang and Xiaoyun Xie. Theoretical and testing performance of an innovative indirect evaporative chiller. *Solar Energy* 84 (2010) 2041–2055
- [2.50]. R. Armbruster, J. Mitrovic. Evaporative cooling of a falling water on horizontal tubes. *Experimental Thermal and Fluid Science* 18 (1998) 183-194
- [2.51]. Rey Martinez, F.J., Velasco Gomez, E., Herrero Martin, R., Martinez Gutierrez, J., Varela Diez, F. Comparative study of two different evaporative systems: an evaporative cooler and a semi-indirect evaporative cooler. *Energy and Buildings* 36 (2004) 696–708.
- [2.52]. Velasco Gomez E, et al. Description and experimental results of a semi-indirect ceramic evaporative cooler. *International Journal of Refrigeration* 2005;28(5):654–62.
- [2.53]. K.J. Chua, S.K. Chou, W.M. Yang, J. Yan. Achieving better energy-efficient air conditioning – A review of technologies and strategies. *Applied Energy* 104 (2013) 87–104
- [2.54]. Vahid Vakiloroaya, Bijan Samali, Ahmad Fakhar, Kambiz Pishghadam. A review of different strategies for HVAC energy saving. *Energy Conversion and Management* 77 (2014) 738–754
- [2.55]. Yu Huang, Jian-lei Niu. A review of the advance of HVAC technologies as witnessed in ENB publications in the period from 1987 to 2014. *Energy and Buildings* 130 (2016) 33–45.
- [2.56]. R. Best, W. Rivera. A review of thermal cooling systems. *Applied Thermal Engineering* xxx (2014) 1-14.
- [2.57]. Ana Tejero-González, Manuel Andrés-Chicote, Paola García-Ibáñez, Eloy Velasco-Gómez, Francisco Javier Rey-Martínez. Assessing the applicability of passive cooling and heating techniques through climate factors: An overview. *Renewable and Sustainable Energy Reviews* 65 (2016) 727–742.
- [2.58]. S. D. Suryawanshi, Tarup M. Chordia, Nikita Nenwani, Harish Bawaskar, Suraj Yambal. Efficient Technique of Air-Conditioning. *Proceedings of the World Congress on Engineering 2011 Vol III, WCE 2011, July 6 - 8, 2011, London, U.K.*

-
- [2.59]. E R. Pacheco, J. Ordóñez*, G. Martínez. Energy efficient design of building: A review. *Renewable and Sustainable Energy Reviews* 16 (2012) 3559– 3573.
- [2.60]. Farah Kojok, Farouk Fardoun, Rafic Younes, Rachid Outbib. Hybrid cooling systems: A review and an optimized selection scheme. *Renewable and Sustainable Energy Reviews* 65(2016)57–80.
- [2.61]. Hafiz M. Daraghme, Chi-Chuan Wang. A review of current status of free cooling in data centres. *Applied Thermal Engineering* 114 (2017) 1224–1239
- [2.62]. M. Mujahid Rafique, P. Gandhidasan, Shafiqur Rehman, Luai M. Al-Hadhrami. A review on desiccant based evaporative cooling systems. *Renewable and Sustainable Energy Reviews* 45 (2015) 145–159
- [2.63]. Farah Kojok, Farouk Fardoun, Rafic Younes, Rachid Outbib. Hybrid cooling systems: A review and an optimized selection scheme. *Renewable and Sustainable Energy Reviews* 65 (2016) 57–80
- [2.64]. Zongwei Han, Yanqing Zhang, Xin Meng. Simulation study on the operating characteristics of the heat pipe for combined evaporative cooling of computer room air-conditioning system. *Energy* 98 (2016) 15-25
- [2.65]. Riffat SB, Zhu Jie. Mathematical model of indirect evaporative cooler using porous ceramic and heat pipe. *Applied Thermal Engineering* 2004, 24(4):457–470.
- [2.66]. Yousef S.H. Najjar, Ahmad M. Abubaker. Indirect evaporative combined inlet air cooling with gas turbines for green power technology. *International Journal of Refrigeration* 59(2015) 235–250.
- [2.67]. Moien Farmahini-Farahani, Ghassem Heidarinejad. Increasing effectiveness of evaporative cooling by pre-cooling using nocturnally stored water. *Applied Thermal Engineering* 38 (2012) 117-123.
- [2.68]. Claudio Cianfrini, Massimo Corcione, Emanuele Habib, Alessandro Quintino. Energy performance of air-conditioning systems using an indirect evaporative cooling combined with a cooling/reheating treatment. *Energy and Buildings* 69 (2014) 490–497.

-
- [2.69]. Kang Zhao, Xiao-Hua Liu, Tao Zhang, Yi Jiang. Performance of temperature and humidity independent control air-conditioning system in an office building. *Energy and Buildings* 43 (2011) 1895–1903
- [2.70]. X.J. Zhang, F. Xiao, S. Li. Performance study of a constant temperature and humidity air-conditioning system with temperature and humidity independent control device. *Energy and Buildings* 49 (2012) 640–646
- [2.71]. Y. Jiang, T.S. Ge, R.Z. Wang, Y. Huang. Experimental investigation on a novel temperature and humidity independent control air conditioning system e Part I: Cooling condition. *Applied Thermal Engineering* 73 (2014) 784-793
- [2.72]. Y. Jiang, T.S. Ge, R.Z. Wang, Y. Huang. Experimental investigation on a novel temperature and humidity independent control air conditioning system e Part II: Heating condition. *Applied Thermal Engineering* 73 (2014) 775-783.
- [2.73]. Tao Zhang, Xiaohua Liu, Yi Jiang. Development of temperature and humidity independent control (THIC) air-conditioning systems in China—A review. *Renewable and Sustainable Energy Reviews* 29 (2014) 793–803
- [2.74]. Tingting Chen, Yonggao Yina, Xiaosong Zhang. Applicability and energy efficiency of temperature and humidity independent control systems based on dual cooling sources. *Energy and Buildings* 121 (2016) 22–31
- [2.75]. H. T. EL-DESSOUKY, H. M. ETTOUNEY and W. BOUHAMRA. A novel air conditioning system-Membrane Air Drying and Evaporative Cooling. *Trans IChemE*, Vol. 78, Part A, October 2000.
- [2.76]. Si-Min Huang, Li-ZhiZhang. Researches and trends in membrane-based liquid desiccant air dehumidification. *Renewable and Sustainable Energy Reviews* 28 (2013) 425–440
- [2.77]. Ziwei Chen, Jie Zhu, Hongyu Bai, Yuying Yan, Lizhi Zhang. Experimental study of a membrane-based dehumidification cooling system. *Applied Thermal Engineering* xxx (2016) xxx–xxx.
- [2.78]. Omar Labban, Tianyi Chen, Ahmed F. Ghoniem, John H. Lienhard V, Leslie K. Norford.

- Next-generation HVAC: Prospects for and limitations of desiccant and membrane-based dehumidification and cooling. *Applied Energy* 200 (2017) 330–346.
- [2.79]. Bo Yang, Weixing Yuan, Yonghong Shang, Jing Wang, Bin Wei. Numerical and experimental study of a novel three-fluid membrane dehumidification method applied to spacecraft humidity control. *Journal of Membrane Science* 530 (2017) 112–124.
- [2.80]. D.B. Jani, Manish Mishra, P.K. Sahoo. Solid desiccant air conditioning – A state of the art review. *Renewable and Sustainable Energy Reviews* 60 (2016) 1451–1469.
- [2.81]. Kishor S. Rambhad, Pramod V. Walke, D.J. Tidke. Solid desiccant dehumidification and regeneration methods —A review. *Renewable and Sustainable Energy Reviews* 59 (2016) 73–83.
- [2.82]. Lorenzo Pistocchini, Silvia Garone, Mario Motta. Air dehumidification by cooled adsorption in silica gel grains. Part I: Experimental development of a prototype. *Applied Thermal Engineering* 107 (2016) 888–897.
- [2.83]. Lorenzo Pistocchini, Silvia Garone, Mario Motta. Air dehumidification by cooled adsorption in silica gel grains. Part II: Theoretical analysis of the prototype testing results. *Applied Thermal Engineering* 110 (2017) 1682–1689.
- [2.84]. Jason Woods, Eric Kozubal. A desiccant-enhanced evaporative air conditioner: Numerical model and experiments. *Energy Conversion and Management* 65 (2013) 208–220.
- [2.85]. Abdulrahman Th. Mohammad, Sohif Bin Mat, M.Y. Sulaiman, K. Sopiana, Abduljalil A. Al-abidi. Historical review of liquid desiccant evaporation cooling technology. *Energy and Buildings* 67 (2013) 22–33.
- [2.86]. Min-Hwi Kim, Joon-Young Park, Sang-Woo Ham, Jae-Weon Jeong. Energy conservation benefit of water-side free cooling in a liquid desiccant and evaporative cooling-assisted 100% outdoor air system. *Energy and Buildings* 104 (2015) 302–315.
- [2.87]. Mahmut Sami Buker, Blaise Mempoou, Saffa B. Riffat. Experimental investigation of a building integrated photovoltaic/thermal roof collector combined with a liquid desiccant

-
- enhanced indirect evaporative cooling system. *Energy Conversion and Management* 101 (2015) 239–254.
- [2.88]. Ahmed H. Abdel-Salam, Carey J. Simonson. State-of-the-art in liquid desiccant air conditioning equipment and systems. *Renewable and Sustainable Energy Reviews* 58 (2016) 1152–1183
- [2.89]. Farbod Fakhrabadi, Farshad Kowsary. Optimal design of a hybrid liquid desiccant-regenerative evaporative air conditioner. *Energy and Buildings* 133 (2016) 141–154.
- [2.90]. Hui-Jeong Kim, Sung-Joon Lee, Sang-Hyeon Cho, Jae-Weon Jeong. Energy benefit of a dedicated outdoor air system over a desiccant-enhanced evaporative air conditioner. *Applied Thermal Engineering* 108 (2016) 804–815.
- [2.91]. Min-Hwi Kim, Hae-Won Dong, Joon-Young Park, Jae-Weon Jeong. Primary energy savings in desiccant and evaporative cooling-assisted 100% outdoor air system combined with a fuel cell. *Applied Energy* 180 (2016) 446–456.
- [2.92]. Xiaohui She, Yonggao Yin, Yaming Dong, Xiaosong Zhang. Investigation on air flow patterns of evaporative cooling and dehumidification process for a hybrid refrigeration system. *Applied Thermal Engineering* 95 (2016) 79–94.
- [2.93]. X. Cui, M.R. Islam, B. Mohan, K.J. Chua. Theoretical analysis of a liquid desiccant based indirect evaporative cooling system. *Energy* 95 (2016) 303–312.
- [2.94]. Jae Hyun Lee, Gu Hyun Ro, Yong Tae Kang, Young Soo Chang, Seon Chang Kim, Young Lyoul Kim. Combined heat and mass transfer analysis for LiCl dehumidification process in a plate type heat exchanger. *Applied Thermal Engineering* 96 (2016) 250–257.
- [2.95]. Sung-Joon Lee, Hui-Jeong Kim, Hye-Won Dong, Jae-Weon Jeong. Energy saving assessment of a desiccant-enhanced evaporative cooling system in variable air volume applications. *Applied Thermal Engineering* 117 (2017) 94–108.
- [2.96]. Hye-Won Dong, Sung-Joon Lee, Dong-Seob Yoon, Joon-Young Park, Jae-Weon Jeong. Impact of district heat source on primary energy savings of a desiccant-enhanced evaporative cooling system. *Energy* 123 (2017) 432–444.

-
- [2.97]. Fan Zhang, Yonggao Yin, Xiaosong Zhang. Performance analysis of a novel liquid desiccant evaporative cooling fresh air conditioning system with solution recirculation. *Building and Environment* 117 (2017) 218-229.
- [2.98]. F. Bruno, On-site experimental testing of a novel dew point evaporative cooler, *Energy Build.* 43 (2011) 3475-3483.
- [2.99]. E. Velasco Gomez, A. Tejero Gonzalez, F.J. Rey Martinez, Experimental characterisation of an indirect evaporative cooling prototype in two operating modes, *Appl. Energy* 97 (0) (2012) 340-346.
- [2.100]. X. Zhao, Liu Shuli, S.B. Riffat, Comparative study of heat and mass exchanging materials for indirect evaporative cooling systems, *Build. Environ.* 43 (2008) 1902-1911.
- [2.101]. Rajesh Maurya, Nitin Shrivastava, Vipin Shrivastava, Performance evaluation of alternative evaporative cooling media, *Int. J. Sci. Eng. Res.* 5 (10) (October-2014).
- [2.102]. R.K. Kulkarni, S.P.S. Rajput, Comparative performance analysis of evaporative cooling pads of Alternative configurations and materials, *Int. J. Adv. Eng. Technol.* (Sept. 2013). ISSN: 22311963.
- [2.103]. Nitipong Soponpongpipat, Sukum Kositchaimongkol, Recycled high-density polyethylene and rice husk as a wetted pad in evaporative cooling system, *Am. J. Appl. Sci.* 8 (2) (2011) 186-191.
- [2.104]. Faleh A. Al-Sulaiman, Evaluation of the performance of local fibers in evaporative cooling, *Energy Convers. Manag.* 43 (16) (November 2002) 2267-2273.
- [2.105]. Banyat Niyomvasa, Bunjerd Potakarat, Performance study of cooling pads, *Adv. Mater. Res.* 664 (2013) 931-935.
- [2.106]. L. Elberling. Laboratory evaluation of the Coolerado cooler-indirect evaporative cooling unit. Pacific Gas and Electric Company; 2006.
- [2.107]. B. Riangvilaikul, S. Kumar. An experimental study of a novel dew point evaporative cooling system. *Energy and Buildings* 42 (2010) 637-44.

-
- [2.108]. Yi Chen, Hongxing Yang, Yimo Luo. Experimental study of plate type air cooler performances under four operating modes. *Building and Environment* 104 (2016) 296-310
- [2.109]. S. De Antonellisa, C. M. Joppolo, P. Liberati, S. Milania, L. Molinaroli. Experimental analysis of a cross flow indirect evaporative cooling system. *Energy and Buildings* 121 (2016) 130–138.
- [2.110]. T. Tulsidasani, R.L. Sawhney, S.P. Singh, M.S. Sodha. Recent research on an indirect evaporative cooler (IEC) part 1: optimization of the COP. *International Journal of Energy Research* 1997, 21(12) 1099-1108.
- [2.111]. X. C. Guo and T. S. Zhao. A parametric study of an indirect evaporative air cooler. *Int. Comm. Heat Mass Transfer*. Vol. 25, No. 2, pp. 217-226, 1998
- [2.112]. X. Zhao, J.M. Li, S.B. Riffat. Numerical study of a novel counter-flow heat and mass exchanger for dew point evaporative cooling. *Applied Thermal Engineering* 28 (2008) 1942–51.
- [2.113]. C. Zhan, Z. Duan, X. Zhao. Comparative study of the performance of the M-cycle counter-flow and cross-flow heat exchangers for indirect evaporative cooling – Paving the path toward sustainable cooling of buildings. *Energy* 36 (2011) 6790-6805.
- [2.114]. C. Zhan, X. Zhao. Numerical study of an M-cycle cross-flow heat exchanger for indirect evaporative cooling. *Building and Environment* 46 (2011) 657-668.
- [2.115]. Ala Hasan. Going below the wet-bulb temperature by indirect evaporative cooling: Analysis using a modified e-NTU method. *Applied Energy* 89 (2012) 237–245.
- [2.116]. X. Cui, K.J. Chua, W.M. Yang. Numerical simulation of a novel energy efficient dew point evaporative air cooler. *Applied Energy* 136 (2014) 979–988.
- [2.117]. X. Cui, K.J. Chua, M.R. Islam, W.M. Yang. Fundamental formulation of a modified LMTD method to study indirect evaporative heat exchangers. *Energy Conversion & Management* 88 (2014) 372–381.
- [2.118]. Yi Chen, Yimo Luo, Hongxing Yang. A simplified analytical model for indirect

- evaporative cooling considering condensation from fresh air: Development and application. *Energy and Buildings* 108 (2015) 387–400
- [2.119]. J. Lin, K. Thu, T. Bui, R. Wang, K. C. Ng, K.J. Chua. Study on dew point evaporative cooling system with counter-flow configuration. *Energy Conversion and Management* 109 (2016) 153–165.
- [2.120]. S. Moshari, G. Heidarinejad. Numerical study of regenerative evaporative coolers for sub-wet bulb cooling with cross- and counter-flow configuration. *Applied Thermal Engineering* 89 (2015) 669–683.
- [2.121]. S. Moshari, G. Heidarinejad. Numerical investigation of wet-bulb effectiveness and water consumption in one- and two-stage indirect evaporative coolers. *Energy Conversion and Management* 108 (2016) 309–32.
- [2.122]. A. Sohani, H. Sayyaadi, S. Hoseinpoori. Modeling and multi-objective optimization of an M-cycle cross-flow indirect evaporative cooler using the GMDH type neural network. *International journal of refrigeration* 69 (2016) 186–204.
- [2.123]. Pandelidis, S. Anisimov. Numerical analysis of the heat and mass transfer processes in selected M-Cycle heat exchangers for the dew point evaporative cooling. *Energy Conversion and Management* 90 (2015) 62–83.
- [2.124]. D. Pandelidis, S. Anisimov. Numerical study and optimization of the cross-flow Maisotsenko cycle indirect evaporative air cooler. *International Journal of Heat and Mass Transfer* 103 (2016) 1029–1041.
- [2.125]. B. Riangvilaikul, S. Kumar. Numerical study of a novel dew point evaporative cooling system. *Energy Build* 2010; 42: 2241–50.
- [2.126]. A.E. Kabeel, M. Abdelgaied. Numerical and experimental investigation of a novel configuration of indirect evaporative cooler with internal baffles. *Energy Conversion and Management* 126 (2016) 526–536.
- [2.127]. J. Lin, K. Thu, T.D. Bui, R.Z. Wang, K.C. Ng, M. Kumja, K.J. Chua. Unsteady-state analysis of a counter-flow dew point evaporative cooling system. *Energy* 113 (2016) 172–

185.

- [2.128]. Bellemo, L., Elmegaard, B., Reinholdt, L. O., & Kærn, M. R. (2013). Modelling of a regenerative indirect evaporative cooler for a desiccant cooling system. Paper presented at 4th IIR Conference on Thermophysical Properties and Transfer Processes of Refrigerants, Delft, Netherlands.
- [2.129]. Emmanuel D. Rogdakis, Irene P. Koronaki, Dimitrios Nik. Tertipis. Experimental and computational evaluation of a Maisotsenko evaporative cooler at Greek climate. *Energy and Buildings* 70 (2014) 497–506.
- [2.130]. M. Jradi, S. Riffat. Experimental and numerical investigation of a dew-point cooling system for thermal comfort in buildings. *Applied Energy* 132 (2014) 524–535.
- [2.131]. X. Cui, K.J. Chua, W.M. Yang, K.C. Ng, K. Thu, V.T. Nguyen. Studying the performance of an improved dew-point evaporative design for cooling application. *Applied Thermal Engineering* 63 (2014) 624-633.
- [2.132]. Sergey Anisimov, Demis Pandelidis, Jan Danielewicz. Numerical analysis of selected evaporative exchangers with the Maisotsenko cycle. *Energy Conversion and Management* 88 (2014) 426–441.
- [2.133]. Sergey Anisimov, Demis Pandelidis. Numerical study of the Maisotsenko cycle heat and mass exchanger. *International Journal of Heat and Mass Transfer* 75 (2014) 75–96.
- [2.134]. Sergey Anisimov, Demis Pandelidis, Andrzej Jedlikowski, Vitaliy Polushkin. Performance investigation of a M (Maisotsenko)-cycle cross-flow heat exchanger used for indirect evaporative cooling. *Energy* 76 (2014) 593-606.
- [2.135]. Demis Pandelidis, Sergey Anisimov, William M. Worek. Comparison study of the counter-flow regenerative evaporative heat exchangers with numerical methods. *Applied Thermal Engineering* 84 (2015) 211-224
- [2.136]. Demis Pandelidis, Sergey Anisimov. Numerical analysis of the selected operational and geometrical aspects of the M-cycle heat and mass exchanger. *Energy and Buildings* 87 (2015) 413–424.

-
- [2.137]. Sergey Anisimov, Demis Pandelidis, Jan Danielewicz. Numerical study and optimization of the combined indirect evaporative air cooler for air-conditioning systems. *Energy* 80 (2015) 452-464.
- [2.138]. Hamoon Jafarian, Hoseyn Sayyaadi, Farschad Torabi. Modeling and optimization of dew-point evaporative coolers based on a developed GMDH-type neural network. *Energy Conversion and Management* 143 (2017) 49–65.
- [2.139]. Sang-Woo Ham, Jae-Weon Jeong. DPHX (dew point evaporative heat exchanger): System design and performance analysis. *Energy* 101 (2016) 132-145.
- [2.140]. Omar Khalid, Muzaffar Ali, Nadeem Ahmed Sheikh, Hafiz M. Ali, M. Shehryar. Experimental analysis of an improved Maisotsenko cycle design under low velocity conditions. *Applied Thermal Engineering* 95 (2016) 288–295.
- [2.141]. Emmanuel D. Rogdakis, Irene P. Koronaki, Dimitrios Nik. Tertipis, Alexandros C. Mustafa. An Energy Evaluation of a Maisotsenko Evaporative Cooler Based on Cylinder Geometry. *World Academy of Science, Engineering and Technology* 82 2013.
- [2.142]. Hui-Jeong Kim, Sang-Woo Ham, Dong-Seob Yoon, Jae-Weon Jeong. Cooling performance measurement of two cross-flow indirect evaporative coolers in general and regenerative operation modes. *Applied Energy* 195 (2017) 268–277.
- [2.143]. Zhiyin Duan, Changhong Zhan, Xudong Zhao, Xuelin Dong. Experimental study of a counter-flow regenerative evaporative cooler. *Building and Environment* 104 (2016) 47-58.
- [2.144]. Zhiyin Duan, Xudong Zhao, Changhong Zhan, Xuelin Dong, Hongbing Chen. Energy saving potential of a counter-flow regenerative evaporative cooler for various climates of China: Experiment-based evaluation. *Energy and Buildings* 148 (2017) 199–210.
- [2.145]. Ala Hasan. Indirect evaporative cooling of air to a sub-wet bulb temperature. *Applied Thermal Engineering* 30 (2010) 2460-2468.
- [2.146]. J. Lin, R.Z. Wang, M. Kumja, T.D. Bui, K.J. Chua. Modelling and experimental investigation of the cross-flow dew point evaporative cooler with and without dehumidification. *Applied Thermal Engineering* 121 (2017) 1–13.

-
- [2.147]. Min-Hwi Kim, Jun-Seok Park, Jae-Weon Jeong. Energy saving potential of liquid desiccant in evaporative cooling-assisted 100% outdoor air system. *Energy* 59 (2013) 726-736.
- [2.148]. Min-Hwi Kim, Dong-Seop Yoon, Hui-Jeong Kim, Jae-Weon Jeong. Retrofit of a liquid desiccant and evaporative cooling-assisted 100% outdoor air system for enhancing energy saving potential. *Applied Thermal Engineering* 96 (2016) 441–453.
- [2.149]. Yi Chen, Yimo Luo, Hongxing Yang. Energy saving potential of hybrid liquid desiccant and evaporative cooling air-conditioning system in Hong Kong. *Energy Procedia* 105 (2017) 2125 – 2130.
- [2.150]. Samar Jaber. An assessment of the economic and environmental feasibility of evaporative cooling unit. *Applied Thermal Engineering* 103 (2016) 564–571.
- [2.151]. Hakan Caliskan, Arif Hepbasli, Ibrahim Dincer, Valeriy Maisotsenko. Maisotsenko cycle. *International Journal of Refrigeration* 34 (2011) 980-990.

References for Chapter 3

- [3.1]. X. Zhao, P. Xu, et al. Heat exchanger apparatus. GB1617362.7. 13 October 2016. <https://www.ipo.gov.uk/p-psum/Case/ApplicationNumber/GB1617362.7>
- [3.2]. Reference data- CIBSE Guide C. London: Chartered Institution of Building Services Engineers, 2007
- [3.3]. Zhao X, Liu S, Riffat SB. Comparative study of heat and mass exchanging materials for indirect evaporative cooling systems. *Building and Environment*, 2008; 43:1902-10.
- [3.4]. P.K.NAG. Heat and mass transfer, 3th edition, Tata McGraw-Hill, 2011, pp569.
- [3.5]. F. P. Incropera, D.P.Dewitt. Fundamentals of heat and mass transfer, 6th edition, New York: John Wiley & Sons, 2007, pp288-289.
- [3.6]. ASHRAE. ASHRAE handbook Fundamentals Volume: SI edition, American Society of Heating, Refrigerating and Air -Conditioning Engineers, 2009, Chapter 4, pp 4.18.

-
- [3.7]. F. M. White. Fluid mechanics, New York. McGraw-Hill, 1979, 353-356.
- [3.8]. M. Jradi, S. Riffat. Experimental and numerical investigation of a dew-point cooling system for thermal comfort in buildings. *Applied Energy* 132 (2014) 524-535.
- [3.9]. ASHRAE. ANSI/ASHRAE Standard 143-2000, Method of test for rating indirect evaporative coolers. American Society of Heating, Refrigerating and Air-Conditioning Engineers, Inc. GA 30329, 2000.
- [3.10]. ANSI/ASHRAE Standard 143-2015. Method of Test for Rating Indirect Evaporative Coolers. American Society of Heating, Refrigerating and Air-Conditioning Engineers, Inc. GA 30329, 2015.
- [3.11]. S. Klein, G. Nellis. Mastering EES, F-Chart Software. October 2014.
- [3.12]. F.E.Cellier, E.Kofman. Continuous system simulation, Springer, 2006, pp415-419.
- [3.13]. Rianguvilaikul B, Kumar S. An experimental study of a novel dew point evaporative cooling system. *Energy Build* 2010; 42:637-44.
- [3.14]. Zhan C, Duan Z, Zhao X. Comparative study of the performance of the M-cycle counter-flow and cross-flow heat exchangers for indirect evaporative cooling - paving the path toward sustainable cooling of buildings. *Energy* 2011; 36:6790-805.
- [3.15]. Australian Standard AS 2913-2000. Evaporative Air Conditioning Equipment. 2000.
- [3.16]. X. Dong, X. Huang, etc. Test and Analysis of an Evaporative Cooling Chiller's Water Consumption. *Power Generation & Air Condition*. 2095-3429 (2014) 06-0079-04
- [3.17]. Jiang Y. Temperature and humidity independent control air-conditioning system. Beijing: China Architecture & Building Press; 2006 [In Chinese].

References for Chapter 4

- [4.1]. Robert A. Davis. Laboratory Evaluation of the Coolerado Cooler™ Indirect Evaporative Cooling Unit. PY2005 Emerging Technologies Program. Pacific Gas and Electric Company, 1st March 2006

-
- [4.2]. P. Xu, X. Ma, X. Zhao, K. Fancey. Experimental investigation on performance of fabrics for indirect evaporative cooling applications. *Building and Environment* 110 (2016) 104-114
- [4.3]. H. Bai, X. Ding, P. Xu. Even liquid distribution of intensive formula. CN205718642U. <http://www.pss-system.gov.cn/sipublicsearch/patentsearch/showViewList-jumpToView.shtml>
- [4.4]. X. Dong, X. Huang, etc. Test and Analysis of an Evaporative Cooling Chiller's Water Consumption. *Power Generation & Air Condition*. 2095-3429 (2014) 06-0079-04 [In Chinese]
- [4.5]. D Raja1, G Ramakrishnan, V Ramesh Babu, M Senthilkumar and MB Sampath. Comparison of different methods to measure the transverse wicking behaviour of fabrics. *Journal of industrial textiles*, 2014, Vol 43(3) 366–382.1
- [4.6]. B. Wang, K.S. Fancey. Feasibility study on cooling efficiency of fabric/aluminium panels for indirect evaporative cooling systems: towards the next generation; Internal Report, School of Engineering & Computer Science, January 2017.

References for Chapter 5

- [5.1]. ISO 5801. Industrial Fans—Performance Testing Using Standardized Airways. 2007.
- [5.2]. J. P. Holman. *Experimental Methods for Engineers*, Eighth Edition. McGraw-Hill Education, New York, 2012. pp. 60-96
- [5.3]. Environmental design - CIBSE Guide A. The Yale Press Ltd, page 2-28 to 2-23.
- [5.4]. H. Xuan, B. Ford. The application of passive draught evaporative cooling in hot and dry climate of China. Proceedings of 27th Conference on Passive and Low Energy Architecture, Louvain-La-Neuve, Belgium, 13-15, July 2011, pp745.
- [5.5]. <https://www.britannica.com/science/Koppen-climate-classification>

[5.6]. Heating Ventilation Air Conditioning - CIBSE Guide B. The Yale Press Ltd, Appendix 2. A2.

[5.7]. Australian Standard AS 2913-2000. Evaporative Air Conditioning Equipment. 2000.

References for Chapter 6

[6.1]. Heating Ventilation Air Conditioning - CIBSE Guide B. The Yale Press Ltd, 1-9, Table1.4

[6.2]. GB 50736-2012 Design code for heating ventilation and air conditioning of civil buildings (in Chinese). Ministry of Housing and Urban-Rural Construction of China. October 2012, p.7

[6.3]. China Meteorological Bureau, Climate Information Centre, Climate Data Office and Tsinghua University, Department of Building Science and Technology. China Standard Weather Data for Analysing Building Thermal Conditions (in Chinese). China Architecture & Building Press. April 2005. Beijing: China Building Industry Publishing House, ISBN 7-112-07273-3 (13228).

[6.4]. Electricity price (in Chinese). Beijing Municipal Commission of Development and Reform.
<http://www.bjpc.gov.cn/cxfw/jgsfcx/jzjg/201208/t9779303.htm>;
<http://www.yda.gov.cn/upload/files/2008090276611723.doc>

[6.5]. Wasim Sama, Frank Bruno, Ming Liu. Technical background research on evaporative air conditioners and feasibility of rating their water consumption. the Water Efficiency Labelling and Standards (WELS) Scheme, Department of the Environment, Water, Heritage and the Arts. September 2009

[6.6]. Scrapped criterion for domestic appliance (in Chinese). Ministry of Electric Power Industry of China. September1996

[6.7]. Intergovernmental Panel on Climate Change. 2006 IPCC Guidelines for National Greenhouse Gas Inventories. the Institute for Global Environmental Strategies (IGES), Hayama, Japan. 2006

- [6.8]. Carbon dioxide emission accounting method and data verification table (in Chinese).
Department of Climate Change, China National Development and Reform Commission.
<http://www.qhs.ndrc.gov.cn/zcfg/201605/W020160525509544574361.pdf>
- [6.9]. J. Feng, Y. Li. Water conservation analysis in Beijing electric power industry. *Advances in Science and Technology of Water Resource* (in Chinese). Vol. 25 Supplement No. 2, 12.2005

**APPENDIX 1: PROGRAMME for SYSTEM CONTROL in C-
LANGUAGE**

```
// DPC_calc_ep.c
// part of TMS Controller code.
// Dew Point Cooler control system - University of Hull& ebmp-UK Ltd
2016

#include "modbus_master/modbus_master.h"
#include "modbus_master_ep.h"

#include "TMS_ep.h"//The #defines & the function prototypes go in here

#include <string.h>// for strcpy, for LCD
#include <math.h>// sqrt()

#include "i2c_ep.h"// for writing directly to LCD - cursor etc

// defines are all in DPC_ep.h

extern volatile MISC_FLAGS_1 MISC_FLAGS_1bits;// stored in EEPROM
extern volatile MISC_FLAGS_2 MISC_FLAGS_2bits;//
extern volatile MISC_FLAGS_3 MISC_FLAGS_3bits;//
extern volatile I2C_KEYPAD_LATCH I2C_KEYPAD_LATCHbits;// where I
traditionally store the Keypad state

int mains_voltage_V_AC;
double mains_current_mA_AC;
int mains_power_W;
double mains_energy_kWh;

double cooling_capacity;
double coefficient_of_performance;
double wet_bulb_effectiveness;
double dew_point_effectiveness;

double Tdc;// Temperature, Dew point, centigrade
double Wbc;// Wet Bulb temperature, centigrade
```

```
void generate_LCD_text_Cooling_Capacity(char * string_pointer)
{
if (full_RS485_message_received)
{
char i_to_a_buffer[40];

sprintf(i_to_a_buffer, "%1.0f" , cooling_capacity);// using sprintf to
convert double to ascii
strcpy((char*)string_pointer, "Cooling Cap=");//
strcat((char*)string_pointer, (char*)i_to_a_buffer);// append the ascii
characters to the existing text
strcat((char*)string_pointer, "W" );//
}
else
{
strcpy((char*)string_pointer, "FAULT - No TMS2 Comm");// start at the
beginning of the buffer
}
}

void calculate_cooling_capacity(void)// store calc in cooling_capacity
{
double total_volume_PA_m3s;
total_volume_PA_m3s = get_total_volume_PA_m3h();// volume per hour
total_volume_PA_m3s = total_volume_PA_m3s/3600;// volume per second

double PA_temperature;
PA_temperature = get_averaged_temp_as_a_double(NTC_PA);

double IA_temperature = get_IA_temperature();
double temperature_diff_in_to_out;
temperature_diff_in_to_out = IA_temperature - PA_temperature;

double density_of_air = DEFAULT_DENSITY_OF_AIR;
double specific_heat_capacity_of_air_cp =
DEFAULT_SPECIFIC_HEAT_CAPACITY_OF_AIR_CP;

cooling_capacity = density_of_air * total_volume_PA_m3s *
temperature_diff_in_to_out * specific_heat_capacity_of_air_cp;
}
```

```
void generate_LCD_text_Coefficient_of_Performance(char * string_pointer)
{
char i_to_a_buffer[40];

if (mains_power_W < 0)
{
strcpy((char*)string_pointer, "#POWER METER COMMS#");//
}
else if (mains_power_W == 0)
{
strcpy((char*)string_pointer, "#POWER VALUE FAULT#");//
}
else if (!full_RS485_message_received)
{
strcpy((char*)string_pointer, "FAULT - No TMS2 Comm");// start at the
beginning of the buffer
}
else
{
sprintf(i_to_a_buffer, "%1.0f" , coefficient_of_performance);// using
sprintf to convert double to ascii
strcpy((char*)string_pointer, "Coef of Perf=");//
strcat((char*)string_pointer, (char*)i_to_a_buffer);// append the ascii
characters to the existing text
strcat((char*)string_pointer, " ");// no units
}
}

void calculate_coefficient_of_performance(void)// store calc in
coefficient_of_performance
{
// if here we have a sensible vaue for the power consumption of the unit
double temp_double = mains_power_W;

coefficient_of_performance = cooling_capacity / temp_double;
}

void generate_LCD_text_Wet_Bulb_Effectiveness(char * string_pointer)
{
if (full_RS485_message_received)
```

```
{
char i_to_a_buffer[40];

sprintf(i_to_a_buffer, "%1.0f" , wet_bulb_effectiveness);// using
sprintf to convert double to ascii
strcpy((char*)string_pointer, "Wet Bulb Eff=");//
strcat((char*)string_pointer, (char*)i_to_a_buffer);// append the ascii
characters to the existing text
strcat((char*)string_pointer, "%" );
}
else
{
strcpy((char*)string_pointer, "FAULT - No TMS2 Comm");// start at the
beginning of the buffer
}
}

void calculate_wet_bulb_effectiveness(void)// store calc in
wet_bulb_effectiveness
{
double PA_temperature;
PA_temperature = get_averaged_temp_as_a_double(NTC_PA);
double IA_temperature = get_IA_temperature();
double temperature_diff_in_to_out;
temperature_diff_in_to_out = IA_temperature - PA_temperature;

wet_bulb_effectiveness = ( temperature_diff_in_to_out * 100 ) /
( IA_temperature - WbC );
}

void generate_LCD_text_Dew_Point_Effectiveness(char * string_pointer)
{
if (full_RS485_message_received)
{
char i_to_a_buffer[40];

sprintf(i_to_a_buffer, "%1.0f" , dew_point_effectiveness);// using
sprintf to convert double to ascii
strcpy((char*)string_pointer, "Dew Point Eff=");//
```

```
strcat((char*)string_pointer, (char*)i_to_a_buffer);// append the ascii
characters to the existing text
strcat((char*)string_pointer, "%" );
}
else
{
strcpy((char*)string_pointer, "FAULT - No TMS2 Comm");// start at the
beginning of the buffer
}
}
```

```
void calculate_dew_point_effectiveness(void)// store calc in
dew_point_effectiveness
{
double PA_temperature = get_averaged_temp_as_a_double(NTC_PA);
double IA_temperature = get_IA_temperature();
double temperature_diff_in_to_out;
temperature_diff_in_to_out = IA_temperature - PA_temperature;

dew_point_effectiveness = ( temperature_diff_in_to_out * 100 ) /
( IA_temperature - Tdc );
}
```

```
void get_mains_data_from_modbus_power_meter(void)// mains power etc
{
unsigned char modbus_slave_address;
unsigned char function_code;
unsigned int slave_register_address;
unsigned int number_of_registers;
unsigned int data_to_write;
```

```
double temp_double;
```

```
// this is how we get data from the Modbus Power Meter
```

```
// get VOLTS
```

```
modbus_slave_address = POWER_METER_MODBUS_ADDRESS;
function_code = COMMAND_03_HREG_R;
slave_register_address = POWER_METER_L1_VOLTS_REGISTER;
number_of_registers = 2;
data_to_write = 0;
```

```
modBusSend( modbus_slave_address, function_code,
slave_register_address, number_of_registers, data_to_write );

wait_for_slave_response();
wait_for_slave_response();

if ( modBusResponded() )
{
LED_TEST_GRN = !LED_TEST_GRN;// pulse the Green LED
LED_TEST_RED = LED_OFF;// switch off the Red LED

// returned register 1 will always be all zero so ignore
mains_voltage_V_AC = get_returned_register(2);
}
else
{
LED_TEST_RED = !LED_TEST_RED;// pulse the Red LED
LED_TEST_GRN = LED_OFF;// switch off the Green LED

mains_voltage_V_AC = -1;// use negative to indicate fail
printf ( " \n\r NO RESPONSE Powermeter V \n\r " );
}

// get CURRENT
modbus_slave_address = POWER_METER_MODBUS_ADDRESS;
function_code = COMMAND_03_HREG_R;
slave_register_address = POWER_METER_L1_mAMPS_REGISTER;
number_of_registers = 2;
data_to_write = 0;

modBusSend( modbus_slave_address, function_code,
slave_register_address, number_of_registers, data_to_write );

wait_for_slave_response();
wait_for_slave_response();

if ( modBusResponded() )
{
LED_TEST_GRN = !LED_TEST_GRN;// pulse the Green LED
LED_TEST_RED = LED_OFF;// switch off the Red LED
```

```
temp_double = get_returned_register(1); // zero - unless current exceeds
32000mA
temp_double = temp_double * 0x10000; // don't think I can left shift a
double
temp_double = temp_double + get_returned_register(2);
mains_current_mA_AC = temp_double;
}
else
{
LED_TEST_RED = !LED_TEST_RED; // pulse the Red LED
LED_TEST_GRN = LED_OFF; // switch off the Green LED

mains_current_mA_AC = -1; // use negative to indicate fail
printf (" \n\r NO RESPONSE Powermeter mA \n\r ");
}

// get POWER
modbus_slave_address = POWER_METER_MODBUS_ADDRESS;
function_code = COMMAND_03_HREG_R;
slave_register_address = POWER_METER_L1_A_POWER_REGISTER;
number_of_registers = 2;
data_to_write = 0;

modBusSend( modbus_slave_address, function_code,
slave_register_address, number_of_registers, data_to_write );

wait_for_slave_response();
wait_for_slave_response();

if ( modBusResponded() )
{
LED_TEST_GRN = !LED_TEST_GRN; // pulse the Green LED
LED_TEST_RED = LED_OFF; // switch off the Red LED

// returned register 1 will always be all zero so ignore
mains_power_W = get_returned_register(2);
}
else
{
LED_TEST_RED = !LED_TEST_RED; // pulse the Red LED
LED_TEST_GRN = LED_OFF; // switch off the Green LED
```

```
mains_power_W = -1; // use negative to indicate fail
printf ("\n\r NO RESPONSE Powermeter W \n\r");
}

// get Energy kWh
modbus_slave_address = POWER_METER_MODBUS_ADDRESS;
function_code = COMMAND_03_HREG_R;
slave_register_address = POWER_METER_L1_A_ENERGY_REGISTER;
number_of_registers = 2;
data_to_write = 0;

modBusSend( modbus_slave_address, function_code,
slave_register_address, number_of_registers, data_to_write );

wait_for_slave_response();
wait_for_slave_response();

if ( modBusResponded() )
{
LED_TEST_GRN = !LED_TEST_GRN; // pulse the Green LED
LED_TEST_RED = LED_OFF; // switch off the Red LED

temp_double = get_returned_register(1); //
temp_double = temp_double * 0x10000; // don't think I can left shift a
double
temp_double = temp_double + get_returned_register(2);
temp_double = temp_double/10; // convert to kWh
mains_energy_kWh = temp_double;
}
else
{
LED_TEST_RED = !LED_TEST_RED; // pulse the Red LED
LED_TEST_GRN = LED_OFF; // switch off the Green LED

mains_energy_kWh = -1; // use negative to indicate fail
printf ("\n\r NO RESPONSE Powermeter kWh \n\r");
}

}

void reset_modbus_power_meter(void)
{
```

```
unsigned char modbus_slave_address;
unsigned char function_code;
unsigned int slave_register_address;
unsigned int number_of_registers;
unsigned int data_to_write;

double temp_double;

modbus_slave_address = POWER_METER_MODBUS_ADDRESS;
function_code = COMMAND_16_HREGS_W;
slave_register_address = POWER_METER_L1_A_ENERGY_RESET_REGISTER;
number_of_registers = 2;
unsigned int data_to_write_array[number_of_registers];
data_to_write_array[0] = 0x11B0;
data_to_write_array[1] = 0x55AA;

modBusSendArrayRegisters(modbus_slave_address, function_code,
slave_register_address, number_of_registers, data_to_write_array);

wait_for_slave_response();
wait_for_slave_response();

if ( modBusResponded() )
{
// now read the updated kWh value
modbus_slave_address = POWER_METER_MODBUS_ADDRESS;
function_code = COMMAND_03_HREG_R;
slave_register_address = POWER_METER_L1_A_ENERGY_REGISTER;
number_of_registers = 2;
data_to_write = 0;

modBusSend( modbus_slave_address, function_code,
slave_register_address, number_of_registers, data_to_write );

wait_for_slave_response();
wait_for_slave_response();

if ( modBusResponded() )
{
LED_TEST_GRN = !LED_TEST_GRN;// pulse the Green LED
LED_TEST_RED = LED_OFF;// switch off the Red LED

temp_double = get_returned_register(1);//
```

```

temp_double = temp_double * 0x10000; // don't think I can left shift a
double
temp_double = temp_double + get_returned_register(2);
temp_double = temp_double/10; // convert to kWh
mains_energy_kWh = temp_double;
printf ("\n\r RESET Powermeter kWh \n\r");
}
else
{
LED_TEST_RED = !LED_TEST_RED; // pulse the Red LED
LED_TEST_GRN = LED_OFF; // switch off the Green LED

mains_energy_kWh = -1; // use negative to indicate fail
//printf ("\n\r NO RESPONSE Powermeter kWh. \n\r");
}

}
else
{
mains_energy_kWh = -1; // use negative to indicate fail
//printf ("\n\r NO RESPONSE Powermeter kWh .. \n\r");
}
}

void calculate_IA_dew_point(void) // store value in Tdc
{
double temp_double1;
double temp_double2;

double IA_humidity = get_IA_humidity();
double IA_temperature = get_IA_temperature();

// following formula is from here:
http://www.aprweather.com/pages/calc.htm
// Tdc = (IA_temperature - (14.55 + 0.114 * IA_temperature) * (1 - (0.01
* IA_humidity)))
// - ((2.5 + 0.007 * IA_temperature) * (1 - (0.01 * IA_humidity))) ^ 3
// - (15.9 + 0.117 * IA_temperature) * (1 - (0.01 * IA_humidity)) ^ 14);

temp_double1 = (IA_temperature - ((14.55 + (0.114 * IA_temperature)) *
(1 - (0.01 * IA_humidity))));

```

```

temp_double2 = ((2.5 + (0.007 * IA_temperature)) * (1 - (0.01 *
IA_humidity)));
//temp_double2 = temp_double2 * temp_double2 * temp_double2;
temp_double2 = powf(temp_double2, 3);
Tdc = temp_double1 - temp_double2;

// the third term (below) can be left out with very little effect on the
end result
// e.g typical terms are: Dew Point 10.91 - 5.13 - 0.04 = 5.73
//double temp_double3;
//temp_double3 = (1 - (0.01 * IA_humidity));
//temp_double3 = (15.9 + 0.117 * IA_temperature) * temp_double3 *
temp_double3 * temp_double3 * temp_double3 * temp_double3 * temp_double3
* temp_double3 *
//temp_double3 * temp_double3 * temp_double3 * temp_double3 *
temp_double3 * temp_double3 * temp_double3;
//Tdc = Tdc - temp_double3;

double temp_double3;
temp_double3 = (1 - (0.01 * IA_humidity));
temp_double3 = (15.9 + (0.117 * IA_temperature)) * powf(temp_double3,
14);
Tdc = Tdc - temp_double3;
// the third term (above) can be left out with very little effect on the
end result

//printf(" \n\r ~~~~~~ Dew Point %1.2f - %1.2f - %1.2f = %1.2f \n\r ",
temp_double1, temp_double2, temp_double3, Tdc); // PRINT CALC FOR
DEVELOPMENT TEST ONLY

}

void calculate_IA_wet_bulb_temperature(void) // store value in Wbc
{
double temp_double1;
double temp_double2;
double Pwb_E; // intermediate calculation for Wet Bulb
double Pmb = DEFAULT_Pmb; // barometric_pressure_millibars
double IA_temperature = get_IA_temperature();

```

```

// do intermediate calculation to generate term used by Wet Bulb
Calculation below
// E = (6.11 * 10 ^ (7.5 * Tdc / (237.7 + Tdc)))
// note for MPLAB, to raise number to a power we don't use the ^ symbol
because that's already used for Bit-wise invert
// instead we use "pow"
// Description: Calculates x raised to the power y.
// Include: <math.h>
// Prototype: double pow(double x, double y);
// Arguments: x the base
// y the exponent
// Return Value: Returns x raised to the power y (x^y).
// Pwb_E;// intermediate calculation for Wet Bulb

// Pwb_E = (6.11 * 10 ^ (7.5 * Tdc / (237.7 + Tdc)))

temp_double1 = ((7.5 * Tdc) / (237.7 + Tdc));

temp_double2 = powf(10, temp_double1);

Pwb_E= (6.11 * temp_double2);

//printf(" \n\r ~~~~~~ Pwb_E=%1.1f", Pwb_E);// PRINT CALC FOR
DEVELOPMENT TEST ONLY

// next do the actual Wet Buld Temperature calculation

// WbC=(((0.00066 * Pmb) * IA_temperature) + ((4098 * Pwb_E) / ((Tdc +
237.7) * (Tdc + 237.7)) * Tdc)) / ((0.00066 *Pmb) + (4098 * Pwb_E) /
((Tdc + 237.7) * (Tdc + 237.7)));

temp_double1 = (((0.00066 * Pmb) * IA_temperature) + ((4098 * Pwb_E) /
((Tdc + 237.7) * (Tdc + 237.7)) * Tdc));

temp_double2=((0.00066 * Pmb) + (4098 * Pwb_E) / ((Tdc + 237.7) * (Tdc +
237.7) ));

WbC = temp_double1 / temp_double2;

//printf(" \n\r ~~~~~~ WbC=%1.1f", WbC);// PRINT CALC FOR DEVELOPMENT
TEST ONLY
}

```

```
void generate_LCD_text_IA_dew_point_and_wet_bulb(char * string_pointer)
{
if (full_RS485_message_received)
{
char i_to_a_buffer[40];

strcpy((char*)string_pointer, "IA DP=");

sprintf(i_to_a_buffer, "%1.1f" ,Tdc); // using sprintf to convert double
to ascii
strcat((char*)string_pointer, (char*)i_to_a_buffer); // append the ascii
characters to the existing text
strcat((char*)string_pointer, "C, WB=" );

sprintf(i_to_a_buffer, "%1.1f" ,WBc); // using sprintf to convert double
to ascii
strcat((char*)string_pointer, (char*)i_to_a_buffer); // append the ascii
characters to the existing text
strcat((char*)string_pointer, "C" );
}
else
{
strcpy((char*)string_pointer, "FAULT - No TMS2 Comm"); // start at the
beginning of the buffer
}
}

int convert_ADC_0_1000_to_volume_m3h (int ADC_value_0_1000, int
pressure_at_10V, int k_factor)
{
double pressure;
double volume;

if (ADC_value_0_1000) // avoid divide_by_zero below
{
// first calculate the pressure
pressure = ADC_value_0_1000;
pressure = (pressure * pressure_at_10V);
pressure = (pressure / 1000);
```

```
// next calculate the volume
volume = sqrt(pressure);
volume = (volume * k_factor);
}
else
{
volume = 0;
}
return volume;
}

double get_mains_energy_kWh (void)
{
// doing it this way so I don't need yet another global variable
return mains_energy_kWh;
}

unsigned int get_mains_energy_kWh_int_x10 (void)
{
unsigned int mains_energy_kWh_int_x10;
mains_energy_kWh_int_x10 = mains_energy_kWh*TEN;
return mains_energy_kWh_int_x10;
}

double get_mains_current_mA_AC (void)
{
// doing it this way so I don't need yet another global variable
return mains_current_mA_AC;
}

int get_mains_voltage_V_AC (void)
{
// doing it this way so I don't need yet another global variable
return mains_voltage_V_AC;
}

int get_mains_power_W (void)
{
// doing it this way so I don't need yet another global variable
return mains_power_W;
}

int get_IA_dewpoint_times_ten(void)
{
```

```
int IA_dewpoint_times_ten;
IA_dewpoint_times_ten = Tdc*TEN;
return IA_dewpoint_times_ten;
}

int get_IA_wet_bulb_temperature_times_ten(void)
{
int IA_wet_bulb_temperature_times_ten;
IA_wet_bulb_temperature_times_ten = WbC*TEN;
return IA_wet_bulb_temperature_times_ten;
}

int get_cooling_capacity_watts(void)
{
int cooling_capacity_int;
cooling_capacity_int = cooling_capacity;// cooling_capacity stored as a
double so convert to int
return cooling_capacity_int;
}

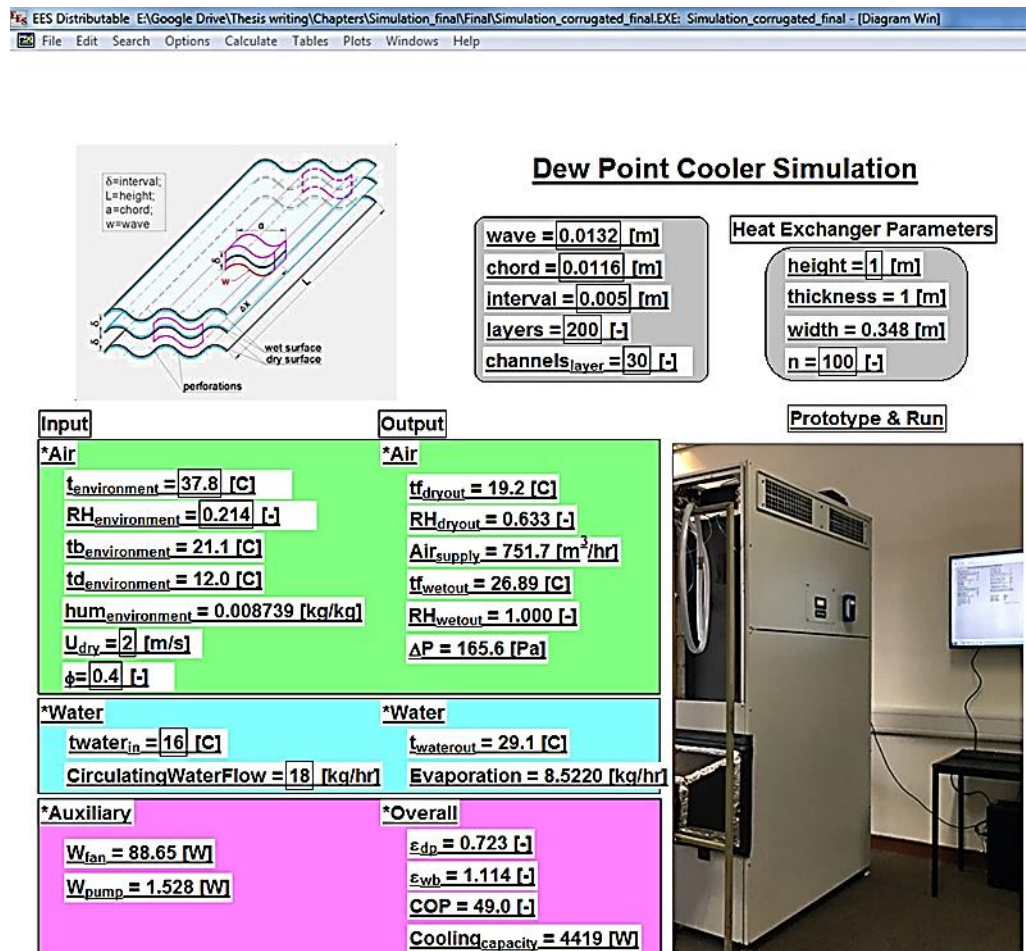
int get_coefficient_of_performance(void)
{
int coefficient_of_performance_int;
coefficient_of_performance_int = coefficient_of_performance;
return coefficient_of_performance_int;
}

int get_wet_bulb_effectiveness_times_ten(void)
{
int wet_bulb_effectiveness_times_ten;
wet_bulb_effectiveness_times_ten = wet_bulb_effectiveness*TEN;
return wet_bulb_effectiveness_times_ten;
}

int get_dew_point_effectiveness_times_ten(void)
{
int dew_point_effectiveness_times_ten;
dew_point_effectiveness_times_ten = dew_point_effectiveness*TEN;
return dew_point_effectiveness_times_ten;
}

// end of file
```

APPENDIX 2: SIMULATION PROGRAMME in EES

"Function 1"

Function h_{local}(k, h₀, l, length, number, Re, Pr, D, mu_f, mu_w, lambda)

"mu_f - dynamic viscosity of air at mean temperature of working air; mu_w - dynamic viscosity of air at mean temperature of channel wall"

If (k*length/number < l) Then

Nu₁ := 1.86 * (Re * Pr * D / (k * length / number))^(1/3) * (mu_f / mu_w)^{0.14};

h₁ := lambda * Nu₁ / D;

If (k = 1) Then

h₂ := 0

Goto 10

Endif

Nu₂ := 1.86 * (Re * Pr * D / ((k - 1) * length / number))^(1/3) * (mu_f / mu_w)^{0.14};

```

    h2:=lambda*Nu2/D;
10: h:=h1*k-h2*(k-1);
Else
If ((k-1)*length/number>l) Then
    h:=h0 "h0 -heat transfer coefficient in fully developed region"
Else
    Nu1:=1.86*(Re*Pr*D/l)^(1/3)*(mu_f/mu_w)^0.14;
    h1:=lambda*Nu1/D;
    If (k=1) Then
        h2:=0
        Goto 20
    Endif
Nu2:=1.86*(Re*Pr*D/((k-1)*length/number))^(1/3)*(mu_f/mu_w)^0.14;
    h2:=lambda*Nu2/D;
20:h3:=(h1*L-h2*(k-1)*length/number)/(l-(k-1)*length/number)
h:=(h3*(l-(k-1)*length/number)+h0*(k*length/number-l))*number/length;
Endif
Endif
    h_local:=h*1.16; "[W/m^2-C]"
End
" ....."

```

"Function 2"

```

Function q_local(tf, tw, k, h0, l, length, number, Re, Pr, D, mu_f, mu_w, lambda,
arc)

```

"tf -air temperature in dry channel; tw -wet wall temperature"

```

q_local:=h_local(k, h0, l, length, number, Re, Pr, D, mu_f, mu_w,
lambda)*(length/number)*arc*(tf-tw) "[W]"

```

```

End

```

```

" ....."

```

"Function 3"

```

Function en_air(airtemp, hum)

```

```

en_air:=1.005[kJ/kg-C]*airtemp+(2500[kJ/kg]+1.84[kJ/kg-C]*airtemp)*hum

```

"[kJ/kg]"

End

"....."

"Function 4"

Function en_water(watertemp)

en_water:=2500[kJ/kg]+1.84[kJ/kg-C]*watertemp "[kJ/kg]"

End

"....."

"Function 5"

Function

resistance_onway(Re_dry,Re_wet,l,D,u,workingair_fraction,rho_dry,rho_wet)

"frictional resistance (on-way resistance)"

lambda_f_dry:=64/Re_dry;

lambda_f_wet:=64/Re_wet;

h_f_dry:=lambda_f_dry*l*u^2/(D*2*g#);

"g# -gravitational acceleration, 9.807[m/s^2]"

h_f_wet:=lambda_f_wet*l*(u*workingair_fraction)^2/(D*2*g#);

resistance_onway_dry:=h_f_dry*rho_dry*g#;

"[Pa]";"h_f=lambda_f(length/D)*u^2/(2*g#) [m]"*

resistance_onway_wet:=h_f_wet*rho_wet*g#;

resistance_onway:=resistance_onway_dry+resistance_onway_wet;

DELTAP_f:=resistance_onway;

End

"....."

"Function 6"Function resistance_local(u1,u2,u3,u4,u5,rho_dry,rho_wet) *"local resistance"**"u1-velocity at dry channel entrance; u2-velocity in dry channels; u3-velocity at dry outlet; u4_velocity at peforations; u5-velocity in wet channel"*zeta_dryin=0.5; *"inlet sudden contraction loss" "zeta- local resistance factor"*zeta_dry=1.5; *"diversion loss"*zeta_dryout=1.0; *"outlet sudden expansion local loss of dry channel"*

```

zeta_wetin=0.9; "branch flow loss coefficient"
zeta_wet=1.5; "diversion loss coefficient zeta_dry"
zeta_wetout=1.0; "outlet sudden expansion local loss of wet channel"
resistance_local_dry=zeta_dryin*rho_dry*u1^2*0.5+zeta_dry*rho_dry*u2^2
*0.5+zeta_dryout*rho_dry*u3^2*0.5; "DELTA_P_local=zeta*rho*u^2*0.5"
resistance_local_wet=zeta_wetin*rho_wet*u4^2*0.5+(zeta_wet+zeta_wetou
t)*rho_wet*u5^2*0.5;
resistance_local=resistance_local_dry+resistance_local_wet;
DELTA_P_local:=resistance_local;
End
"....."

```

"Function 7"

```

Function w_pump(water_volume,length)
  DELTA_P_static_water=3000[Pa];
  mu_water=0.001005[Pa-s];
  rho_water=1000[kg/m^3];
  U_water=sqrt(2*DELTA_P_static_water/rho_water);
  D=0.007[m]; "pump model DC40H-24110, outlet=8mm, inner diameter=7mm;"
  water_volume_operation=60[s/min]*rho_water*U_water*3.14*D^2/
  4;
  "continuous water flow rate in water pipe"
  DELTA_P_total_water=-((11[m]/7.7[kg/min])*water_volume_operation+11[m];
  "performance curve of the selected pump, L/min"

  Re_water=U_water*D*rho_water/mu_water;
  DELTA_P_onway=0.3164/Re_water^0.25*length*U_water^2*rho_water/(D^2)
  "=h_f_water*rho_water*g#=lambda_f_water*length*U_water^2/(D^2*g#)*r
  ho_water*g#"; "turbulence Re<10^5, lambda_f=0.3164/Re^0.25""[Pa]""
  P0=101325[Pa];
  length_onway=10.34[m]*DELTA_P_onway/P0;
  length_static_water=10.34[m]*DELTA_P_static_water/P0;
  length_valve=DELTA_P_total_water-length_onway-length_static_water;

  w_pump:=28.8[W]*water_volume/60[min/hr]/water_volume_operation;

```

```

        "Nominal continuous volume=7.5L/min, corresponding power
        consumption=28.8W;
        water_volume_required/water_volume_operation=operation time ratio"
        "pump full power and meet the requirement of water_volume_operation by
        valve control"

```

```
End
```

```
"....."
```

"Function 8"

```
Function rh(tf,hum)
```

```
P0=101.325 [kPa];
```

```
If hum>humrat(AirH2O,T=tf,P=P0,R=1) Then
```

```
rh=1;
```

```
Else
```

```
rh=relhum(AirH2O,T=tf,P=P0,w=hum);
```

```
Endif
```

```
End
```

```
"....."
```

"Function 9"

```
Function hm(PA_volume,tw,lambda,rho,Cp,h)
```

```
D0=0.000022 [m^2/s];
```

```
d=D0*((tw+T_zero#)/T_zero#)^1.5;
```

```
Le=lambda/rho/(1000[W/kW]*Cp)/d;
```

```
hm=h*Le^(-2/3)/rho/(1000[W/kW]*Cp);
```

```
If PA_volume<0.712 Then
```

```
hm=0.5*hm
```

```
Else
```

```
If PA_volume>0.817 Then
```

```
hm=1.5*hm;
```

```
Endif
```

```
hm=hm;
```

```
Endif
```

```
End
```

"....."

"Main Program"

"known information"

\$ifnot DiagramWindow {These inputs will be entered from the Diagram window if it is visible.}

chord=0.396[m]; *"chord length of wave"*
 wave=0.348[m]; *"corrugatin wave length"*
 interval=0.005[m]; *"interval between sheets"*
 height=1[m];
 channels_layer=1;
 layers=200;
 n=100[-];

U_dry=2[m/s];
 phi=0.364[-]; *"phi- working air fraction"*
 t_environment=37.8[C];
 RH_environment=0.214;

twater_in=16[C];
 CirculatingWaterFlow=18;
 \$endif

thickness=interval*layers;
 width=chord* channels_layer;

"Construction geometry"

S=chord*interval/2; *"[m^2]"*
 De=4*S/(interval+2*wave); *"[m]"*

"Common parameters"

Nu0=2.47;
 P0=101.325 [kPa];
 Cp_water=4.183 [kJ/kg-C];

```

tb_environment=wetbulb(AirH2O,T=t_environment,P=P0,R=RH_environment);
                                "[C]"; "inlet air wet bulb temperature"
td_environment=dewpoint(AirH2O,T=t_environment,P=P0,B=tb_environment
);
                                "[C]"; "inlet air dew point temperature"
hum_environment=humrat(AirH2O,T=t_environment,P=P0,B=tb_environment);
                                "[kg/kg]"; "moisture content"
rho_environment=density(AirH2O,T=t_environment,P=P0,B=tb_environment);
                                "[kg/kg]";

```

"Fluid properties in the DRY channel"

```

tf_dry[0]=t_environment;
                                "tf_dry[n]- cell parameter; order reverse to wet channel, constant"
tf_dry=(tf_dry[1]+tf_dry[n])/2;
"tb_dry[0]=tb_environment;"
"td_dry[0]=td_environment;"

hum_dry=hum_environment; "constant"
Cp_dry=cp(AirH2O,T=tf_dry,P=P0,w=hum_dry);
lambda_dry=conductivity(AirH2O,T=tf_dry,P=P0,w=hum_dry);
                                "thermal conductivity"
mu_dry=viscosity(AirH2O,T=tf_dry,P=P0,w=hum_dry);
Pr_dry=prandtl(Air,T=tf_dry);
rho_dry=(rho_dry[1]+rho_dry[n])/2;
rho_dry[1]=density(AirH2O,T=tf_dry[1],P=P0,w=hum_dry);
rho_dry[n]=density(AirH2O,T=tf_dry[n],P=P0,w=hum_dry);

```

"Flow parameters in the DRY channel"

```

Re_dry=U_dry*De*rho_dry/mu_dry;
qm_dry=rho_environment*U_dry*S;
                                "[kg/s]" "constant"

l_dry=0.05*De*Re_dry*Pr_dry;
h0_dry=lambda_dry*Nu0/De;

```

"FLUID and wall PROPERTIES in WET channel"

tf_wet[n+1]=tf_dry[n];

tf_wet=(tf_wet[1]+tf_wet[n])/2;

hum_wet[n+1]=hum_dry;

hum_wet=(hum_wet[1]+hum_wet[n])/2;

rho_wet=density(AirH2O,T=tf_wet,P=P0,w=hum_wet);

Cp_wet=cp(AirH2O,T=tf_wet,P=P0,w=hum_wet);

lambda_wet=conductivity(AirH2O,T=tf_wet,P=P0,w=hum_wet);

mu_wet=viscosity(AirH2O,T=tf_wet,P=P0,w=hum_wet);

Pr_wet=prandtl(Air,T=tf_wet);

tw[n+1]=twater_in;

tw=(tw[1]+tw[n])/2;

mu_wall=viscosity(AirH2O,T=tw,P=P0,R=1);

*"mu_wall -dynamic viscosity of air at mean temperature of channel wall" " For
AirH2O (moist air), the temperature, pressure, and humidity ratio (or relative
humidity) must be supplied as arguments. "*

"Flow parameters in the WET channel"

U_wet=U_dry*phi; *"constant"*

qm_wet=qm_dry*phi; *"constant"*

Re_wet=U_wet*De*rho_wet/mu_wet;

l_wet=0.05*De*Re_wet*Pr_wet;

h0_wet=lambda_wet*Nu0/De;

"h0 -heat transfer coefficient in fully developed region"

V_water[n+1]=CirculatingWaterFlow/m/3600[s/hr]; *"kg/s"*

m=channels_layer*layers; *"m- total channel numbers";*

"....."

Duplicate j=1,n

"Fluid and wall properties in basic cell"

hum_wall[j]=humrat(AirH2O,T=tw[j],P=P0,R=1);

"Heat transfer in dry channel"

$Q_{dry[j]}=q_{local}(tf_{dry[j]}, tw[j], j, h0_{dry}, l_{dry}, height, n, Re_{dry}, Pr_{dry}, De, mu_{dry}, mu_{wall}, lambda_{dry}, wave);$ "[W]"

"Energy balance in the dry channel"

$Q_{dry[j]}=qm_{dry}*1000[W/kW]*Cp_{dry}*(tf_{dry[j-1]}-tf_{dry[j]});$ "[W]"

"Mass transfer in wet channel"

$m[j]=hm(Air_{supply}, tw[j], lambda_{wet}, rho_{wet}, Cp_{wet}, h_{local}(j, h0_{wet}, l_{wet}, height, n, Re_{wet}, Pr_{wet}, De, mu_{wet}, mu_{wall}, lambda_{wet})*(height/n)*wave*(hum_{wall[j]}-hum_{wet[j]})*rho_{wet}*1.5;$
"hm- mass transfer coefficient [m/s]" "1.5-porosity, fabric, effective evaporating area>bare surface"

$m[j]=V_{water}[j+1]-V_{water}[j];$

"V_water- water_volume, entrance parameter"

"Mass transfer balance in the wet channel"

$m[j]=qm_{wet}*(hum_{wet[j]}-hum_{wet[j+1]});$

"Heat transfer in wet channel"

$Q_{wet[j]}=-$

$q_{local}(tf_{wet[j]}, tw[j], j, h0_{wet}, l_{wet}, height, n, Re_{wet}, Pr_{wet}, De, mu_{wet}, mu_{wall}, lambda_{wet}, wave);$

"heat transfer as per bare aluminium area"

$DELTAEn_{air}[j]=qm_{wet}*1000[W/kW]*(en_{air}(tf_{wet[j]}, hum_{wet[j]})-en_{air}(tf_{wet[j+1]}, hum_{wet[j+1]}));$

"[W]"; "DELTAEn_air - enthalpy difference between inlet and outlet per second in each basic cell of wet channel"

$Q_{vap}[j]=1000[W/kW]*m[j]*en_{water}(tw[j]);$

"[W]"; "Q_vap-evaporation latent heat"

"Energy balance in the wet channel"

$DELTAEn_{air}[j]=Q_{vap}[j]+Q_{wet}[j];$ "[W]" "in function Q_loca, l always (tf-tw); tf_wet<tw"

"Total energy balance in the combined channel"

$Q_{dry[j]}=DELTAEn_{air}[j]+Cp_{water}*V_{water}[j]*(tw[j]-tw[j+1])*1000[W/kW];$

```
RH_wet[j]=rh(tf_wet[j],hum_wet[j]);
```

```
RH_dry[j]=rh(tf_dry[j],hum_dry);
```

```
DELTAx[j]=height*j/n;
```

```
End
```

```
".....End....."
```

```
epsilon_wb=(tf_dryin-tf_dryout)/(tf_dryin-tb_dryin);
```

"epsilon_wb- wet bulb effectiveness"

```
epsilon_dp=(tf_dryin-tf_dryout)/(tf_dryin-td_dryin);
```

"epsilon_dp- dew point effectiveness"

```
tf_dryin=t_environment;
```

```
tf_dryout=tf_dry[n];
```

```
tb_dryin=tb_environment;
```

```
td_dryin=td_environment;
```

```
tf_wetout=tf_wet[1];
```

```
t_waterout=tw[1];
```

"Resistance calculation"

```
Area_perforations=118*3.14*0.005[m]^2/4; "118-perforation amount"
```

```
Area_entrance=0.12[m]*interval; "12-entrance height"
```

```
Area_drychannel=S*2*channels_layer;
```

```
U_entrance=U_dry*Area_drychannel/Area_entrance;
```

```
U_perforations=U_dry*Area_drychannel/Area_perforations;
```

```
U_dryout=U_dry*(1-phi);
```

```
DELTAP=(resistance_onway(Re_dry,Re_wet,height,De,U_dry,phi,rho_dry,rho_wet)+resistance_local(U_entrance,U_dry,U_dryout,U_perforations,U_wet,rho_dry,rho_wet))*1.5;
```

"1.5- unforeseen amplification factor";

```
epsilon_fan=0.55[-];
```

"fan efficiency"

```
Vap_water=(V_water[n+1]-V_water[1]);
```

```
W_fan=U_dry*S*m*DELTAP/epsilon_fan;
```

*"poewr consumption=pressure drop*flow rate; [W]=[Pa]*[m^3/s]"*

```
W_pump=w_pump(CirculatingWaterFlow,height);
```

$Q_cooling=1005[J/kg-C]*U_dry*S*(1-phi)*1.17*rho_environment*(tf_dry[0]-tf_dry[n]);$

"cooling capacity of single elemental channel" "1.17- used in test results. for comparison"

$Q_cooling_working_air=1005[J/kg-C]*U_wet*S*rho_wet*(tf_wet[1]-tf_wet[n+1]);$

$Cooling_evaporation=Vap_water*en_water(tw)*1000[W/kW];$ *"W"*

$Cooling_water=Cp_water*1000[J/kJ]*V_water[1]*(tw[1]-tw[n+1]);$ *"W"*

$Cooling_dry=1005[J/kg-C]*U_dry*S*rho_environment*(tf_dry[0]-tf_dry[n]);$

$Cooling_capacity=Q_cooling*m;$ *"W"*

$COP=cooling_capacity/(W_fan+W_pump);$ *"epsilon_energy - COP"*

$RH_dryout=rh(tf_dry[n],hum_dry);$

$RH_wetout=rh(tf_wet[1],hum_wet[1]);$ *"W=hum_wet[1] overflow"*

"Overall Unit Parameters"

$Cooling_workingair=Q_cooling_working_air*m;$

$Evaporation=Vap_water*m*3600[s/hr];$

$Air_supply=U_dry*S*m*(1-phi)*3600[s/hr];$ *"m^3/hr"*

$Air_Working=Air_supply/(1-phi)*phi;$

